MicroRNA Regulation of Podocyte Insulin Sensitivity

Alexa Wonnacott MB BCh (Hons), MRCP, FHEA

Thesis presented for the Degree of Philosophiae Doctor

March 2020

Wales Kidney Research Unit
Division of Infection and Immunity
School of Medicine
Cardiff University
Heath Park
Cardiff, CF14 4XN

Acknowledgements

I would like to express my gratitude to my supervisors, sponsors and colleagues in their unwavering support throughout this PhD.

To *Professor Donald Fraser*, who encouraged me to apply to the Welsh Clinical Academic Training Scheme and has been a supervisor, mentor and the best possible role model to me throughout. His faith in my ability and potential, and ability to always find the positive angle when I could not, have been instrumental in my academic development.

To *Professor Richard Coward*, whose boundless energy and enthusiasm for science has been utterly contagious. Thank you for welcoming me to the Bristol Renal Unit and introducing me to so many excellent scientists who I have had the great fortune to work with, and learn from; Dr Abigail Lay, Dr Jenny Hurcombe and Dr Fern Barrington have been especially wonderful in helping me with the animal work, and maintaining my experiments when I retreat back over the bridge.

To *Dr Tim Bowen*, whose attention to detail is legendary. Thank you for always providing me with a sounding board and for all your support and encouragement over the years.

To *Dr Soma Meran* and *Professor Aled Phillips* who plucked me from foundation training and filled my head with ideas of becoming an academic nephrologist. Thank you for providing the inspiration and delivering me at Donald's door!

To *The Wellcome Trust*, for the financial support and ongoing career mentorship. Thank you to the Grant Award team who have always been incredibly helpful and informative.

And to all of the team at the *Wales Kidney Research Unit*, past and present, who have provided the learning, the logic and most importantly, the laughter. Without their friendship and support, I would certainly have faltered. Special thanks to Dr Robert Jenkins, Dr John Martin and Dr Lucy Newbury for teaching me the techniques I needed with such patience. And, of course, thanks to Dr Dan Smith for providing cake at any and every opportunity.

To *Andrew,*
For your unwavering love, patience
and support of my life decisions,
however mad they may be

To *Meredith and Rhoswen*,
The rays of sunshine who give
me the strength and reason
to succeed

&
To my amazing mother, *Deborah*
whose love makes all things possible

Thesis Summary

Diabetic Nephropathy (DN) is a devastating complication of diabetes, and is the leading cause of end stage renal failure in the UK. Uncovering mechanistic pathways in DN pathogenesis is vital in establishing new therapeutic targets to prevent its progression.

Podocyte-specific insulin resistance in mice leads to a renal injury that mimics that seen in diabetic kidney disease, indicating that podocyte insulin signalling may be of critical importance in the development of DN. MicroRNAs (miRNAs) are post-transcriptional gene regulators that demonstrate aberrant expression in multiple diabetic models, and are implicated in the development of insulin resistance in liver, fat and muscle. The aim of this work was to establish the role of miRNAs in the regulation of podocyte insulin signalling.

This thesis details the differential microRNA expression of an *in vitro* model of podocyte insulin resistance, and the subsequent validation of miR-155-5p as an important regulator of podocyte insulin sensitivity. MiR-155 was upregulated in insulin-resistant podocytes, and in the urine of patients with DN. Furthermore, overexpression of miR-155 in podocytes resulted in reduction in PI3K/Akt signalling and abrogation of glucose uptake *in vitro.* Bioinformatic analyses were used to identify putative miR-155 targets. PIK3R1 and CSF1R were confirmed to demonstrate miR-155 induced repression, hypothesised to result in podocyte insulin resistance via negative regulation of PI3K signalling.

Whole glomerular miRNA sequencing from the db/db mouse indicated that changes associated with established diabetic pathways of oxidative stress, inflammation and fibrosis are transcriptionally activated as early as 4 weeks. These findings support the hypothesis that changes in miRNA expression are an initiating insult in DN, and highlight miRNAs as potential therapeutic targets to arrest disease development.

Publications, Presentations and Awards arising from this Thesis

Peer-reviewed Publications

1. Newbury LJ, **Wonnacott A,** Simpson K, Bowen T, Fraser D. Assessment of Urinary MicroRNAs by Quantitative Polymerase Chain Reaction in Diabetic Nephropathy Patients. *Methods Mol Biol*. 2020; 2067:277–285

2. Beltrami C, Simpson K, Jesky M, **Wonnacott A,** et al. Association of Elevated Urinary miR-126, miR-155, and miR-29b with Diabetic Kidney Disease. *Am J Pathol*. 2018; 188(9): 1982–1992.

3. **Wonnacott A,** Bowen T, Fraser DJ. MicroRNAs as Biomarkers in Chronic Kidney Disease. Curr Opin Nephrol Hypertens. 2017 Nov; 26(6): 460-466

4. Simpson K, Wonnacott A**,** Fraser DJ, Bowen T. MicroRNAs in Diabetic Nephropathy: From Biomarkers to Therapy. Curr Diab Rep. 2016 Mar;16(3):35. doi: 10.1007/s11892-016-0724-

Oral presentations at Conferences

1. **Wonnacott A,** Bowen T, Coward RC, Fraser DJ. MicroRNA-155 up-regulation induces podocyte insulin resistance. Joint Association of the British Clinical Diabetologists and Renal Association Spring Meeting, (Birmingham, UK) Feb 2019.

2. **Wonnacott A,** Bowen T, Coward RC, Fraser DJ. MicroRNAs in podocyte insulin signalling: a new therapeutic target in Diabetic Nephropathy? Welsh Annual Renal Physicians meeting (Cardiff, UK) June 2018. **(Awarded Bloodworth Prize)**

3. **Wonnacott A,** Bowen T, Coward RC, Fraser DJ. MicroRNAs are differentially expressed in podocyte insulin resistance: Preliminary data.

Welsh Clinical Academic Trainees Annual Meeting. (Cardiff, UK), March 2015. **(Awarded 1st prize)**

Poster Presentations at Conferences

1. **Wonnacott A,** Lay A, Hurcombe J, Bowen T, Coward RC, Fraser DJ. MicroRNA-155 up-regulation induces podocyte insulin resistance. American Society of Nephrologists (Washington, USA) Nov 2019

2. **Wonnacott A,** Bowen T, Coward RC, Fraser DJ. MicroRNA expression changes in podocyte insulin resistance: A new therapeutic target for diabetic nephropathy? European Diabetic Nephropathy Study Group Annual Conference, (Groningen, Netherlands) May 2018

3. **Wonnacott A,** Beltarmi, C, Simpson K, Bowen T, Fraser DJ. Urinary miRNAs in Diabetic Kidney Disease. Cardiff and Vale Research and Development conference. (Cardiff, UK). March 2018. (**Awarded 3rd Prize).**

4. **Wonnacott A,** Bowen T, Coward RC, Fraser DJ. MicroRNA expression changes in podocyte insulin resistance. Wales Kidney Research Unit Annual Meeting. (Cardiff, UK). December 2017 **(Awarded 3rd Prize)**

Other Awards

1. Wellcome Trust Clinical Research Training Fellowship Award (£218,300) October 2016-March 2020

Abbreviations

ACEi	Angiotensin Converting Enzyme inhibitor
AFU	Arbitrary fluorescence units
AGE	Advanced glycation end products
AGO	Argonaute protein
AKI	Acute Kidney Disease
ANOVA	Analysis of Variance
ARB	Angiotensin II receptor blocker
BCA	bicinchoninic acid assay
BSA	Bovine Serum Albumin
C2	Podocyte cell line
CD2AP	CD2-associated protein
CDC42	Cell division control protein 42 homolog
cDNA	Complementary DNA
CKD	Chronic Kidney Disease
CPM	Counts per minute
CSFR-1	Colony stimulating factor-1 receptor
Ct	Cycle threshold
CV	Cardiovascular
DCGR8	Di-George Critical Region-8
DKD	Diabetic Kidney disease
DMEM	Dulbecco's modified Eagle's medium
DMS	Diffuse mesangial sclerosis
DMSO	Dimethyl sulfoxide
DN	Diabetic Nephropathy
dNTP	Deoxyribonucleotide triphosphate
DPM	Decay per Minute
dsDNA	Double stranded DNA
ECL	Enhanced Chemoluminecense
ECM	Extracellular matrix
EDTA	Ethylenediamine tetraacetic acid
eGFR	Estimated Glomerular Filtration Rate
EM	Electron microscopy
eNOS	Endothelial nitric oxide synthase
ER	Endoplasmic reticulum
ERK	Extracellular Receptor Kinase
ESL	Endothelial Surface Layer
ESRD	End stage Renal Disease
FACS	Fluorescence activated cell sorting
FCS	Fetal Calf Serum
FFA	Free Fatty Acid
FITC	Flourescein isothiocynate
FOX01	Forkhead box protein O1
FPMK	Fragments per kilobase of transcript per million
FSC	Forward scatter
FSGS	Focal Segmental Glomerulosclerosis
GAPDH	Glyceraldehyde 3-phosphate dehydrogenase

GBM	Glomerular Basement membrane
GDM	Gestational Diabetes Mellitus
GEnC	Glomerular Endothelial Cell
GFB	Glomerular Filtration Barrier
GFP	Green-fluorescent protein
Glc	Glucose
GLUT	Glucose transporter
GSK	Glycogen Synthase Kinase
GSV	GLUT storage vesicles
HbA1c	Haemoglobin 1Ac (glycosylated)
HBSS	Hanks' balanced salt solution
HEK293T	Human Embryonic kidney cell line
HFD	High Fat Diet
HRP	Horseradish Peroxidase
IGF-1	Insulin-like growth Factor-1
IL-6	Interleukin-6
INPP5D	Inositol Polyphosphate-5-Phosphatase D
INSR	Insulin Receptor
IPA	Ingenuity Pathway Analysis
IR	Insulin Resistant/ Insulin Receptor
IRAK	Interleukin-1 receptor-associated kinase
IRS	Insulin Receptor Substrate
Jnk	c-Jun N-terminal kinase
KO	Knock out
KRP	Krebs Ringer Phosphate
LDL	Low density Lipoproteins
LM	Light Microscopy
MAPK	Mitogen-activated protein kinase
MFI	Mean fluorescence intensity
miRNA	MicroRNA
miRseq	MicroRNA sequencing
mRNA	Messenger RNA
mTOR	Mammalian Target of Rapamycin
NA-CKD	Non-albuminuric Chronic kidney disease
NEB	New England Biolab
NGEF	Neuronal Guanine Nucleotide Exchange Factor
NGS	Next Generation Sequencing
NHS	National Health Service
NO	Nitric Oxide
Nox	NADPH oxidase
NPHS1	Nephrin
NPHS2	Podocin
NS1	Control lentiviral batch
nt	Nucleotide
NTC	Non-template control
OE	Overexpression
PBS	Phospho-buffered saline
PCA	Principal Component Analysis

PCKD	Polycystic kidney disease
PDGFRβ	Platelet-derived growth factor receptor beta
PDK4	Pyruvate Dehydrogenase Kinase 4
PECAM	Platelet endothelial cell adhesion molecule
PFA	Paraformaldehyde
PI3K	Phosphoinositide 3-kinase
PIK3R1	Phosphoinositide 3-kinase regulatory subunit-1
PODIRKO	Podocyte insulin receptor knockout
PODN	Podocan
PPAR	Peroxisome proliferator-activated receptor
PPL	Periplakin
PTEN	Phosphatase and tensin homologue
PTP1B	Protein tyrosine phosphatase-1B
RAAS	Renin-aldosterone-angiotensin system
RCC	Renal Cell Carcinoma
RhoA	Ras Homolog family member A
RIN	RNA Integrity number
RIPA	Radio Immunoprecipitation Assay
RISC	RNA-induced silencing complex
RNAseq	RNA sequencing
ROS	Reactive oxygen species
RPMI 1640	Roswell Park Memorial Institute (media)
RQ	Relative Quantification
rRNA	Ribosomal RNA
RRT	Renal Replacement Therapy
RT	Reverse Transcriptase
RT-qPCR	Real Time qualitative polymerase chain reaction
sCr	Serum Creatinine
ScSeq	Single cell sequencing
SD	Standard Deviation
SDS	Sodium Dodecyl Sulfate
SEM	Standard Error of the Mean
SGLT2	Sodium Glucose co-transporter 2
SmRNAseq	Small RNA sequencing
SOCS1	Suppressor of cytokine signalling 1
SOD	Superoxide dismutase
SSC	Side scatter
STZ	Streptozotocin
SV40	Simian Virus 40
sXBP1	Spliced X-box factor-1
T1DM	Type 1 Diabetes Mellitus
T2DM	Type 2 Diabetes Mellitus
TF control	Transfection reagents only control
TGF-β	Transforming growth factor beta
TLDA	Taqman Low Density Array
TNF-α	Tumour Necrosis factor alpha
TRAF	Tumor necrosis factor receptor-associated factor
TRPC6	Transient Receptor Potential Cation Channel Subfamily C

U6	Ubiquitin 6
uACR	Urinary albumin:creatinine ratio
UCP	Mitochondrial uncoupling protein
UTR	Untranslated region
VAMP	Vehicle associated membrane protein
VEGF	Vascular endothelial growth factor
WGP	Wales Gene Park
WKRU	Wales Kidney Research Unit
WT	Wild Type
WT1	Wilms Tumour-1
Xpo5	Exportin
"p" prefix	phosphorylated-
2-DOG	(3H)2-deoxy-D-glucose
α-SMA	Alpha Smooth Muscle Actin

Table of Contents

1 Introduction

1.1 Type 2 Diabetes Mellitus

Type 2 Diabetes Mellitus (T2DM) is a global health epidemic, with 3.8 million people diagnosed and a further 1.1 million people living with undiagnosed T2DM in the UK alone (1). The incidence of T2DM has doubled over the last decade and is causally linked with the rise in obesity The cost to NHS is estimated to be 14 billion pounds per year, equating to 10% of the entire NHS budget in England and Wales (2) . The vast majority of this health care expenditure is derived from managing complications of diabetes.

1.1.1 Macrovascular complications

Macrovascular complications of T2DM include coronary artery disease, peripheral vascular disease and stroke. The underpinning pathological mechanism is the development of atheromatous plaques, which occur in response to endothelial inflammation and the subsequent generation of foam cells: macrophages containing oxidised low-density lipoproteins (LDL). Cytokines released from foam cells incite further macrophage proliferation and T-cell chemotaxis, which induces smooth muscle proliferation, forming a fibrous cap. Hyperglycaemia initiates overproduction of reactive oxygen species (ROS), which cause endothelial cells to overexpress adhesion molecules, recruiting more leucocytes to the plaque. Rupture of these lesions results in the acute vascular infarction associated with cerebrovascular accidents (CVAs) and myocardial infarctions (MIs). Macrovascular complications are the commonest cause of death in patients with T2DM (1).

1.1.2 Microvascular complications

Microvascular complications of T2DM encompass retinal, renal and neuropathic disease. Hyperglycaemia is considered to be the principal cause of microvasculopathy, with several landmark studies demonstrating improved outcomes of microvascular, but not macrovascular complications with adherence to strict glycaemic control (3-5). One third of all patients will already have evidence of microvascular disease at the point of diagnosis (1). Retinal complications of diabetes are the leading cause of blindness worldwide, whilst the renal manifestation of diabetes, Diabetic Nephropathy (DN), is the most

common cause of end stage renal disease (ESRD) and need for renal replacement therapy (RRT) in the UK (6).

1.1.3 Pathophysiology of T2DM: Overview

T2DM is characterised by a state of hyperglycaemia that results from a combination of aberrant production and/or physiological response to the metabolic hormones responsible for regulating blood sugar: chiefly, insulin and glucagon. Genetic susceptibility, environmental triggers and related comorbidities such as hypertension and hyperlipidaemia further contribute to the pathogenesis of this complex condition. This is summarised in Figure 1.1.

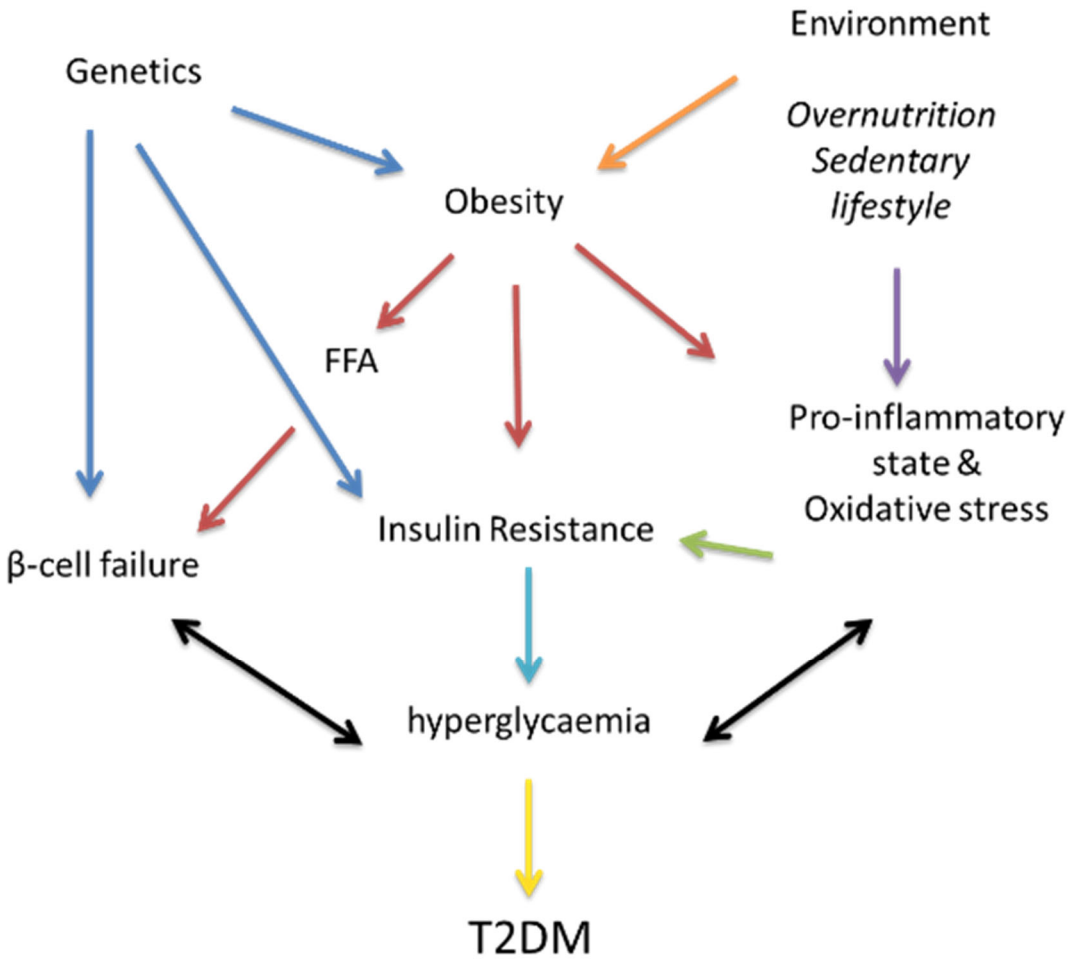

Figure 1.1 Overview of pathogenesis of T2DM. Genetics and environmental factors contribute to the development of obesity, which incites proinflammatory responses and free fatty acid (FFA) accumulation leading to insulin resistance and beta cell dysfunction, ultimately resulting in an inability to maintain normoglycaemia.

1.1.3.1 Insulin abnormalities

Insulin resistance, i.e. the requirement of higher than normal plasma insulin levels to maintain normoglycaemia, is the best predictor of T2DM (7). The development of insulin resistance is multifactorial and intrinsically linked to obesity in most cases.

In addition to insulin resistance, impairment of the insulin response to glucose by beta pancreatic cells must be present for T2DM (and hyperglycaemia) to develop (8). The precise contributions of insulin resistance and beta cell dysfunction in the development of T2DM have been the topic of considerable debate, however large studies such as the UK Prospective Diabetes Study (UKPDS) (9) and longitudinal assessments in Pima Indians (10) have concluded that progressive beta cell loss is the primary insult resulting in hyperglycaemia. Beta cell dysfunction develops as a consequence of glucotoxicity (11), free fatty acid (FFA) accumulation (12) and possibly, amyloid deposition (13), and is not merely representative of islet cell "burn-out" following prolonged hyperinsulinemia, as previously hypothesised. An impairment of insulin processing by these cells is reflected in higher proportions of proinsulin (insulin precursor) levels in T2DM patients (14)

1.1.3.2 Genetic susceptibility and environment

Whilst there is overwhelming evidence of a genetic influence in T2DM, with clear predominance in certain ethnic groups (15) and monogenic twin concordance of approximately 90% (16) , results from genome-wide association studies (GWAS) explain less than 10 per cent of the heritability of T2DM (17). Candidate genes and genetic polymorphisms associated with T2DM are summarised in Table 1.1. It is widely accepted that the "missing heritability" results from a complex interplay of polygenic susceptibility and environmental factors, such as decreased physical activity, poor diet and obesity.

Marker	Chr	Description	Gene region	Function
rs10923931	1	Intronic	NOTCH2	Transmembrane receptor implicated in pancreatic organogenesis
rs7578597	2	Missense: T1187A	THADA	Thyroid adenoma, associates with PPARγ
rs4607103	3	38kb upstream	ADAMTS9	Secreted MMP expressed in muscle/ pancreas
rs4402960	3	Intronic	IGF2BP2	Growth factor binding protein; pancreatic development
rs1801282	3	Missense: P12A	PPARG	Transcription Factor, adipocyte development
rs10010131	4	Intron-exon junction	WFS1	Endoplasmic reticulum transmembrane protein
rs7754840	6	Intronic	CDKAL1	CDK5 inhibitor, islet glucotoxicity sensor
rs864745	7	Intronic	JAZF1	Transcriptional repressor; associated with prostate cancer
rs13266634	8	Missense: R325W	SLC30A8	β-cell zinc transporter; insulin storage and secretion
rs10811661	9	125 kb upstream	CDC123-CAMK1D	Cell cycle/ protein kinase
rs7903146	10	Intronic	TCF7L2	Transcription factor; transactivates proglucgon and insulin genes
rs1111875	10	7.7 kb downstream	HHEX	Transcription factor involved in pancreatic development
rs5219	11	Missense: E23K	KCNJ11	Potassium Channel; risk allele impairs insulin secretion
rs7961581	12	Intronic	TSPAN8-LGRS	Cell surface glycoprotein implicated in GI cancers
rs8050136	16	Intronic	FTO	Alters BMI in general population
rs757210	17	Intronic	HNF1B	Transcription factor involved in pancreatic development

Table 1.1 The Genetic variants associated with Type 2 Diabetes. Genes listed demonstrate genome-wide levels of statistical significance, ordered by chromosome (Chr). Adapted from The genetics of Type 2 Diabetes: A Realistic appraisal, Florez, 2008 (18)

The obesity epidemic of recent decades has seen paralleled increases in the incidence of T2DM; indeed obesity is considered responsible for 80-85% of overall risk of developing T2DM (19). The mechanisms by which obesity induces T2DM however, are poorly understood, as not all obese individuals develop diabetes, and not all T2DM patients are obese. Pattern of fat distribution (central adiposity) (20), increased FFAs (21) and decreased adipocytokines, such as leptin and adiponectin (22), have all been hypothesised to promote insulin resistance in overweight individuals.

1.1.3.3 Inflammation

The concept of inflammation as the common denominator linking obesity, diabetes and insulin resistance has received much attention in recent years, driven by the observation of elevated levels of inflammation-associated markers such as C-reactive protein (CRP), Interleukin-6 (IL-6) and Tumour necrosis factor alpha (TNF-α) in obese, diabetic patients (23-25). Adipose tissue is highly immunologically active and metabolic homeostasis is regulated by the tight coordination of T-lymphocytes, cytokines and adipokines. Obesity is associated with an increase in adipose tissue macrophages (especially the M1 proinflammatory variant) which correlates with the development of insulin resistance (26). Uniquely, obesity-induced inflammation involves multiple organs, and a similar macrophage infiltration is observed in the liver, resulting in hepatic insulin resistance (27). The obesity-induced disruptions to the innate inflammatory regulation of fat, liver and muscle cells results in the disruption of numerous elucidated mechanistic pathways, including activation of Jnk and NF-κB pathways resulting in loss of insulin receptor/insulin receptor substrate (IRS) signalling (28), and the release of non-esterified fatty acids which impairs β-cell function (29).

The initiating trigger in obesity-induced inflammation has been proposed to be an adaptive response to overnutrition; the expanding adipose cells require increased delivery of nutrients/oxygen which necessitates angiogenesis, and therefore inflammatory cell-mediated insulin resistance my be temporarily beneficial as it protects the cells from over accumulating lipids before the tissue is able to support this new growth. However, homeostasis is not achieved in the

context of continued overnutrition, and the sustained inflammatory activation and adipose tissue expansion results in insulin resistance, cell fibrosis and necrosis (30).

1.2 Diabetic Nephropathy

1.2.1 Incidence and Risk factors

DN is a complication of both T1DM and T2DM, characterised by an increase in urinary albumin excretion in the absence of other concomitant renal disease. DN develops in 15-40% of patients with T1DM with peak incidence at approximately 15-20 years disease duration (31). The prevalence and progression of DN in T2DM is more variable, with of 5-20% of patients developing this complication. Non-modifiable risk factors for the development of DN include advancing age (partly due to age-related renal senescence, but also reflective of cumulative exposure to diabetic insults), genetic/ethnic susceptibility and female sex (although males are more likely to progress to ESRD, for undetermined reasons) (32). Modifiable risk factors include previously discussed hyperglycaemia, obesity and smoking, as well as hypertension (which, like hyperglycaemia, confers a linear increased risk of adverse renal outcomes (33)). Patients with DN are also at a greater risk of acute kidney injury (AKI) episodes, and architectural changes to the glomerulus associated with recovery and repair, particularly to the podocytes, may accelerate DN progression (34). In recent years, there has been growing interest in the concept of insulin resistance as an independent risk factor for the development of DN. This will be addressed in detail, below.

1.2.2 Diagnosis and Clinical Manifestations of DN

The diagnosis of DN is most commonly made based on the finding of persistently elevated urinary albumin:creatinine ratio (>30mg/g), and/or renal impairment (eGFR<60ml/min/1.73m^2) in a patient diagnosed with Type 2 diabetes, based on American Diabetes Association (ADA) criteria (Table 1.2). Routine annual urine and serum analysis is required to detect these asymptomatic developments in all patients with T2DM. Elevated albuminuria must be detected in 2 out of 3 samples over a 3-6 month period to control for

intra-individual daily variability in excretion and the possibility of transient albuminuria induced by physiological perturbations such as vigorous exercise, heart failure, etc. (35). Albuminuria and renal impairment are not specific to DN, and therefore clinical judgment as to the likelihood of alterative aetiologies must be employed. The presence of other microvascular diabetic complications, particularly proliferative diabetic retinopathy, is considered to be predictive of a diagnosis of DN in the context of albuminuria (36). Renal biopsy is rarely performed unless there is uncertainty over the diagnosis, such as in the presence of active urinary sediment, other systemic disease and rapid GFR/albuminuria change.

Diagnostic Criteria for Type 2 Diabetes
HbA1c ≥ 6.5%
OR
Fasting Plasma Glc ≥ 7.0 mmol/L (No caloric intake for 8 hours)
OR
2hr plasma Glc ≥ 11.1 mmol/L during Oral Glc Tolerance test (Glc load of 75g anhydrous Glc dissolved in water)
OR
Random Plasma Glc ≥ 11.1 mmol/L (In patients with classic symptoms of hyperglycaemia)

Table 1.2 American Diabetes Association Diagnostic Criteria for Type 2 diabetes. Glc = glucose. Adapted from (37)

1.2.3 Natural History and outcomes in DN

The natural history of DN has been challenged in recent years. Previously considered to be a unidirectional progression through stages of glomerular hyperfiltration, progressive albuminuria and eventual GFR decline (Figure 1.2), it is now appreciated that some patients exhibit a more variable disease course. For example, a subgroup of diabetics develop GFR decline before, or in the absence of albuminuria, coined as non-albuminuric chronic kidney disease (NA-CKD) pattern. The prevalence of NA-CKD pattern in type 2 diabetics has been reported as between 0.6-28.4% in large population based studies, as recently

reviewed by Klimontov *et al* (38). Others demonstrate non-progression of albuminuria and preserved renal function and even regression of albuminuria (39). Although the increased use of angiotensin converting enzyme inhibitors (ACEi) and sodium glucose co-transporter-2 inhibitors (SGLT2i) has undoubtedly influenced the above, there is evidence to support differences in the underlying pathophysiological mechanisms of the non-albuminuric/regressive variants. NA-CKD pattern is associated with a lower incidence of microvascular diabetic complications, non-smoking status and favourable HbA1c values (40), although cardiovascular risks and outcomes are the same in albuminuric and non-albuminuric diabetics (41). Histopathological findings in T2DM with NA-CKD include predominance of interstitial and vascular changes over the classic diabetic glomerulopathy observed in albuminuric DN (42) (see Figure 1.3). It has therefore been hypothesised that NA-CKD is reflective of a macroangiopathy associated with normal aging, hypertension and arteriosclerosis (38). This highlights the inherent heterogeneity of DN, and the challenges researchers face in identifying/showing efficacy of new biomarkers and therapeutic targets in such a diverse population.

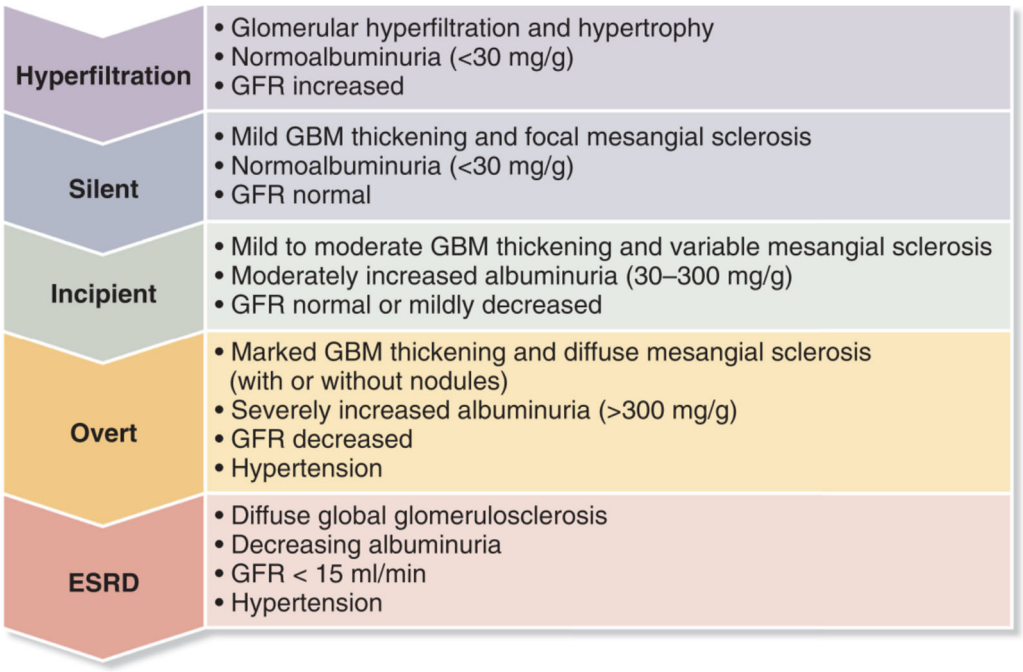

Figure 1.2 Classical stages of diabetic nephropathy (43)

1.2.4 Histopathology of DN

The classical histopathological changes of DN are demonstrated in Figure 1.3, although there may be considerable variation in findings in T2DM, as noted

above. The Renal Pathology Society published a unifying classification applicable for T1DM and T2DM, shown in Table 1.3 (44), although this has been criticised for failing to include important pathologic lesions such as focal segmental glomerulosclerosis (FSGS) and extracapillary hypercellularity (45). A typical case of DN shows diffuse mesangial matrix increase, which becomes more discretely organised into "Kimmelstiel-Wilson" nodules, glomerular basement membrane (GBM) thickening, podocyte loss and arteriolar hyalinosis. Other findings can include fibrin caps, capsular drops, and capillary microaneurysms. Extra-glomerular features of tubular fibrosis and atrophy are also evident. All of the glomerular and tubulointerstitial features listed in Table 1.3 have been correlated to adverse renal outcomes, justifying their inclusion in this classification scheme (46, 47). Non-diabetic renal lesions are also commonly seen (up to 30%) in proteinuric type 2 diabetics undergoing biopsy, skewed in part by the bias towards biopsying only those patients where diagnostic uncertainty exists (based on unusual or confounding clinical features) (48), but also reflective of the aforementioned contributions of aging, atherosclerosis and hypertension.

A.

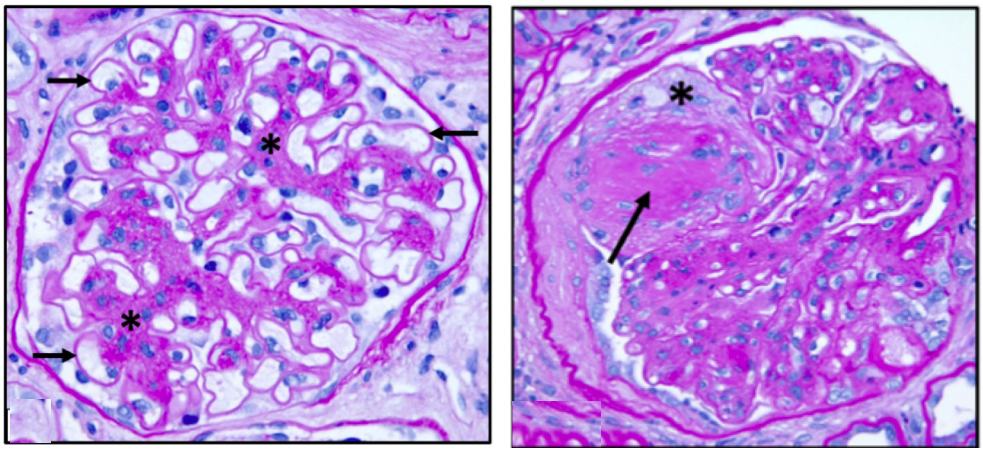

B.

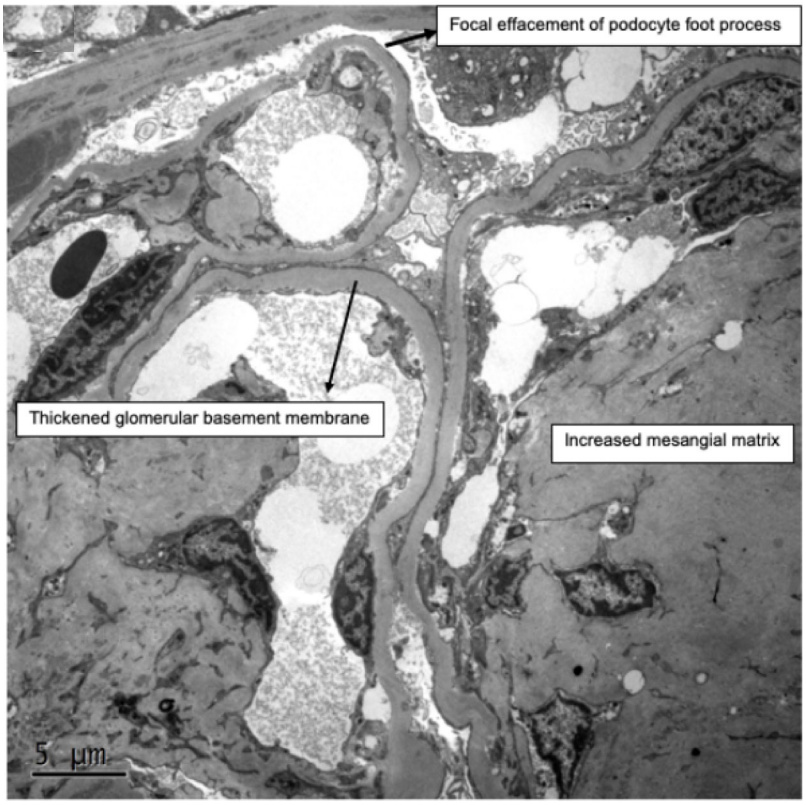

Figure 1.3A Histological findings in Diabetic Nephropathy by Light microscopy. These include diffuse mesangial sclerosis (asterixed in left hand image) and diffuse thickening of capillary loops (arrowed, left hand image). A Kimmelstiel-Wilson nodule is shown in the right hand image (arrowed), as well as a peripheral microaneurysm (asterix). Light microscopy images, Periodic Acid Schiff staining, x400 magnification. **Figure 1.3B. Histological findings in Diabetic Nephropathy by Electron microscopy.** Diffuse thickening of the glomerular basement membrane, increased mesangial matrix and podocyte effacement. Scale bar 5µm. Images reproduced from https://www.renalfellow.org/2019/05/24/kidney-biopsy-of-the-month-diabetic-nephropathy/

Class	Description	Inclusion Criteria
I	Mild/ non-specific LM changes and EM proven GBM thickening	Biopsy does not meet class II, III or IV criteria GBM >395 (female) and >430 nm (male)
IIa	Mild mesangial expansion	Biopsy does not meet class III or IV criteria Mild mesangial expansion in > 25% of mesangium
IIb	Severe mesangial expansion	Biopsy does not meet class III or IV criteria Severe mesangial expansion in > 25% mesangium
III	Nodular sclerosis	Biopsy does not meet class IV criteria At least one convincing Kimmelstiel-Wilson lesion
IV	Advanced glomerulosclerosis	Global glomerulosclerosis in >50% glomeruli Lesions from class I through III

lesion		Criteria	Score
Interstitial	Interstitial Fibrosis Tubular Atrophy (IFTA)	No IFTA	0
		<25%	1
		25-50%	2
		>50%	3
	Interstitial inflammation	Absent	0
		Only in relation to IFTA	1
		In areas without IFTA	2
Vascular	Arteriolar Hyalinosis	Absent	0
		At least one area	1
		>1 area	2
	Large vessel arteriosclerosis (score worst artery)	Presence of large vessels	Y/N
		No intimal thickening	0
		Intimal thickening < thickness of media	1
		Intimal thickening > thickness of media	2

Table 1.3. Renal Pathology Society Classification of Diabetic Nephropathy, 2010.

LM= light microscopy, EM= electron microscopy. Adapted from (44).

1.2.5 Current Management Strategies and Outcomes in DN

The cornerstone of DN management is risk factor modification to prevent disease progression. Many are measures common to the management of diabetes in general, such as blood pressure control, smoking cessation, strict glycaemic control and avoidance of obesity. Others are more directly targeted at the kidney, such as the use of ACEi and ARBs to retard albuminuric progression, which, for the last two decades, has represented the gold standard treatment in minimising loss of renal function and progression to ESRD (49, 50). However, even when renin-angiotensin-aldosterone system (RAAS) blockade is achieved, the risk of ESRD can remain high and correlates with residual levels of albuminuria (51). Resultantly, great effort has been focused on devising new treatments for DN, but randomised controlled trials of, for example, antioxidant inflammatory mediators (52) and advanced glycation end- product (AGE) inhibitors (53) have failed to translate into mainstream care due to lack of efficacy and unacceptable side effect profiles. The advent of two new glucose-lowering therapies with apparent renoprotective effects has generated considerable excitement after a long period of stagnation in DN management, however there remains no known intervention that is capable of fully reversing or "curing" DN.

1.2.5.1 Sodium Glucose co-transporter 2 inhibitors (SGLT2i)

SGLT2 is expressed in the S1 and S2 portions of the apical side of the proximal tubule, where it is connected with glucose transporter-2 (GLUT2) on the basolateral side and functions to reabsorb 90% of filtered glucose under normoglycaemic conditions. Inhibition of SGLT2 promotes renal glucose excretion (glycosuria), leading to reduced plasma glucose, weight loss and reduced blood pressure (BP). Initial cardiovascular outcome trials of SGLT2i demonstrated apparent renoprotective effects, which prompted dedicated renal phase 3 outcome studies. In April 2019, CREDENCE trial was terminated early having reached the composite primary endpoint of 30% relative risk reduction in doubling of serum creatinine (sCr), ESRD, renal death or CV death in patients who received canagliflozin versus placebo (54).

The potential mechanisms of SGLT2i- induced renoprotection continue to unfold but are hypothesised to go beyond the effects of reduction in obesity and improvement in glycaemic control. They include amelioration of oxidative stress (55), favourable systemic and glomerular haemodynamics via RAAS inhibition, altered tubuloglomerular feedback mechanism and natriuretic peptide effects (56, 57) and anti-inflammatory/anti-fibrotic effects (58, 59). SGLT2i are increasingly being used in mainstream DN therapy in those with eGFR>30ml/min/1.73m^2 (in whom proximal tubule induced glucose-lowering effect is maintained).

1.2.5.2 Incretin-based therapy

Glucagon-like peptide 1 receptor agonists (GLP-1 RA) stimulate glucose-dependent insulin release from β-cells. Unlike endogenous GLP-1, they are variably resistant to Dipeptidyl peptidase-4 (DPP-4) breakdown, and so they exert their effects for longer. Animal studies have shown reduced albuminuria and improved tubulointerstitial architecture in GLP-1 RA treated rats, associated with reduction in inflammatory and fibrotic markers such as TNF-α and fibronectin (60). GLP-1 RA have also been shown to normalise oxidative stress markers independently of glucose lowering action (61). Clinical trials have demonstrated variable but consistent reduction in albuminuria with the use of GLP-1 RA, although the mechanism for this effect is unclear. The observed beneficial cardiometabolic effects of these drugs are attributed to canonical GLP-1RA signalling, yet the expression of GLP-1R in the kidney is surprisingly scant and predominantly limited to vascular smooth muscle cells, as reviewed recently by Drucker (62). It is likely, therefore, that renoprotective effects are mediated via a combination of extra-renal haemodynamic and glucose lowering effects in combination with the GLP-1R independent effects on renal inflammation (63-66).

DPP-4 inhibitors have also been shown to confer anti-fibrotic renoprotective effects in diabetic mice models (67), and reduced albuminuria in patients with T2DM and renal dysfunction (68). Results of a recent non-inferiority trial of linagliptin versus placebo on CV and renal outcomes (CARMELINA (69))

appears to have mitigated concerns highlighted in earlier trials of saxagliptin (increased incidence of heart failure (70)), however was not designed to demonstrate renoprotective effects, and so further work is required before conclusions can be made on specific utility in DN treatment.

1.2.5.3 Other novel DN treatments

Activation of the Endothelin-A (ET_A) receptor has been implicated in glomerular inflammation, oxidative stress, podocyte damage and vasoconstriction of the afferent vessels, resulting in increased permeability to albumin, as reviewed by Anguiano *et al* (71). An initial trial of Avosentan, a non-selective ET_A antagonist, was terminated due to high incidence of fluid overload (72). In 2019, a trial of a low-dose, selective ET_A antagonist showed a 35% reduction in composite primary outcome of doubling of sCr, onset of ESRD, RRT or death from kidney failure. Unfortunately, the statistical power of the trial has been called into question as the study was terminated early (73). The treatment group also required an "enrichment period" to ascertain drug tolerability and those who developed fluid overload were excluded, suggesting that this may only be a viable treatment option in a select group (providing further evidence for the heterogeneity of DKD pathophysiology).

Mineralocorticoid receptor blockade results in additive anti-proteinuric effects in patients treated with ACEi/ARB (74), but has made limited progress as a therapeutic agent due to the consequential increase in hyperkalemia. A pilot study of novel, non-steroidal mineralocorticoid receptor antagonist, Fineronone, demonstrated a dose-dependent reduction in uACR without a significant increase in hyperkalemia, compared to placebo (75). A large, phase 3 clinical trial, FIDELIO-DKD is due to report its findings in 2020, including how any reduction in uACR translates into protection against GFR decline (76).

There is also a great deal of interest in harnessing inflammatory mediators in DN, including resident and infiltrating inflammatory cells, complement pathway activation, anti-oxidants and advanced glycation end- product (AGE) inhibitors, eloquently summarised in a recent review article by Pichler et al (77). Specific interventions, such as the targeting of overactive JAK-STAT signalling with

Barcitinib have resulted in encouraging reductions in ACR and urinary biomarkers of inflammation, but it is not known whether this will translate into reduction of DKD progression (78). Of note, inhibition of IL-1β with canakinumab has been shown to reduce major cardiovascular events in patients with CKD, thereby validating inflammation as a target to address the most significant cause of mortality in this patient population (79). Bardoxolone Methyl, a nuclear 1 factor (erythroid-derived 2)-related factor 2 (NRF2) activator and hence potent anti-oxidant is currently under re-review as a treatment in DN having previously been rejected owing to increased heart failure occurrence in the BEACON trial (80). However, re-analysis of the data has highlighted a discrepancy in pre-existing susceptibility to heart failure in the treatment group versus placebo group (81), and therefore the potential effects of preserved renal function may still hold promise as a novel treatment in DN.

It remains unclear what impact the above agents will have on the mainstream management of DN. What remains certain, however, is that new treatments that are applicable to the common core of diabetic patients are still desperately needed.

1.3 Insulin Resistance in DN

In recent years there has been a paradigm shift in recognising the importance of insulin resistance in DN, in addition to the deleterious effects of hyperglycaemia. It is now widely accepted that the effects of insulin resistance are significant not simply at a tissue-specific level, but also at a cellular-specific level.

1.3.1 Insulin Signalling in Health

The insulin signal transduction pathway (Figure 1.4) is a highly conserved pathway responsible for the regulation of cell cycle, growth and proliferation in addition to its metabolic roles in controlling glucose uptake/utilisation and fatty acid synthesis (82). Insulin is able to signal to the cell via the insulin receptor (IR), insulin-like growth factor receptor (IGF-1R) and a hybrid of the two. These tyrosine kinase receptors exhibit the usual autophosphorylation, but are unique in that they subsequently recruit a number of scaffolding proteins (insulin

receptor substrates (IRS1-4)) which act as intermediaries in recruiting downstream effectors, thereby orchestrating the differential activation of the various phosphorylation cascades (83). IRS1 and IRS2 have the longest C-terminal tail with the most phosphorylation sites, and consequently exhibit more diverse signal transduction compared to IRS3/4 (84). The 3 main pathways propagated by IRS phosphorylation are the phosphoinositide 3-kinase (PI3K) pathway, the mitogen-activated protein kinase (MAPK) pathway and the cbl-associated (c-Cbl) pathway.

The metabolic consequences of insulin resistance are most frequently associated with defects in PI3K signalling. PI3K is recruited to the cell membrane via regulatory subunit p85α, producing phosphatidylinositol-3,4,5-triphosphate (PIP_3), which, in turn, activates phosphoinositide-dependent protein-kinase 1 (PDK1). PDK1 is responsible for the phosphorylation of Akt at Thr308 (although full activation of Akt requires phosphorylation at an additional site, Ser493, performed by the RICTOR subunit of mammalian target of rapamycin complex 2 (mTORC2)) (85). Downstream substrates of Akt direct a number of critical components of glucose metabolism, such as glucose uptake (via AS160), glycogen synthesis (via Glycogen synthase 3, GSK3) and gluconeogenesis (via FOX01) (86). The PI3K/Akt pathway is additionally involved in aspects of cell growth via activation of mTORC1, although it is the MAPK pathway that predominantly regulates cell cycle progression and the determination of proliferation, differentiation and apoptosis (87). The MAPK family consists of the various isoforms of p38, ERK (extracellular-signal-regulated kinase) and JNK (c-Jun N-terminal kinase), and the pathway is initiated following binding of the small GTPases Ras, followed by Raf. This results in phosphorylation of MEK1 and MEK2 (MAPK and ERK kinases). Activated ERKs cause cell growth via promoting the expression of various transcription factors and ribosomal (translational) activators (82). Ras also binds to the p85/p110 PI3K complex, thus demonstrating the interplay between these two pathways (88).

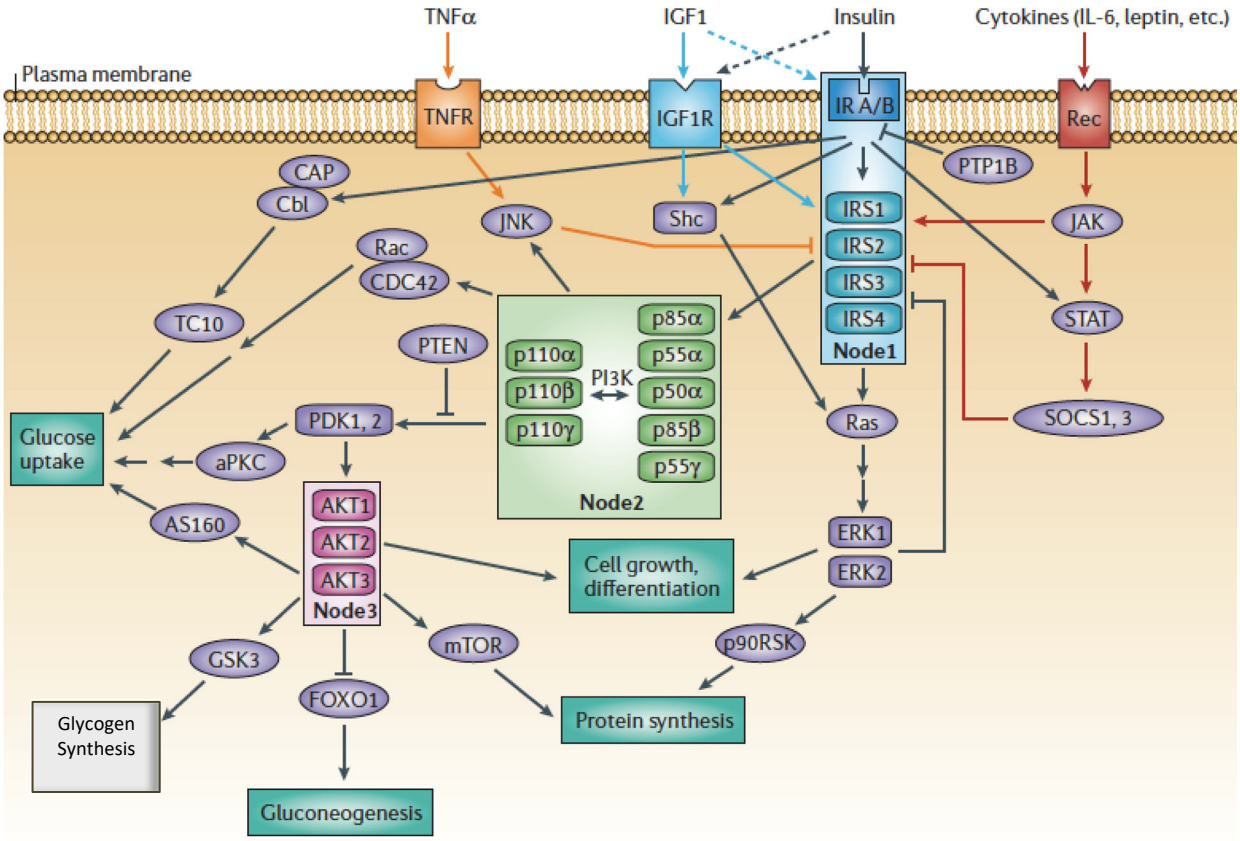

Figure 1.4 Insulin signalling cascade. Insulin can signal via the insulin receptor (IR) and the insulin-like growth factor-1 receptor (IGF-1R). Signalling pathways that are activated by cytokines such as tumour necrosis factor-α (TNFα), interleukin-6 (IL-6), and leptin interfere with insulin signalling through crosstalk (orange and red arrows). Three important nodes in the insulin pathway are the IR, the IR substrates (IRS) 1–4 (blue box), the phosphatidylinositol 3-kinase (PI3K) with its several regulatory and catalytic subunits (light green box), and the three AKT isoforms (pink box). These nodes propagate signal transduction via the PI3K, MAPK and C-cbl pathways to regulate glucose metabolism, protein synthesis and cell growth. Downstream or intermediate effectors of these critical nodes include atypical protein kinase C (aPKC), Akt substrate of 160 kDa (AS160), Cas-Br-M (murine) ecotropic retroviral transforming sequence homologue (Cbl), Cbl-associated protein (CAP), cell-division cycle 42 (CDC42), extracellular signal-regulated kinase 1 and 2 (ERK1 and ERK2), forkhead box O1 (FOXO1), glycogen synthase kinase 3 (GSK3), Janus kinase (JAK), c-Jun-N-terminal kinase (JNK), mammalian target of rapamycin (mTOR), p90 ribosomal protein S6 kinase (p90RSK), phosphoinositide-dependent kinase 1 and 2 (PDK1 and 2), phosphatase and tensin homologue (PTEN), protein tyrosine phosphatase-1B (PTP1B), Ras, Rac, Src homology- 2-containing protein (Shc), suppressor of cytokine signalling (SOCS), signal transducer and activator of transcription (STAT), and Ras homologue gene family, member Q (ARHQ; also called TC10). Dashed arrows represent an activation process with less intensity. Adapted from (82)

The *in vivo* significance of the c-Cbl signalling pathway remains unclear; although insulin receptor mediated tyrosine phosphorylation of this proto-oncogene has been described in the context of GLUT4 translocation and glucose uptake (89, 90). This pathway may therefore represent an important adjunct to PI3K signalling in regulating glucose metabolism.

Importantly, whilst the above transduction cascade described is common to most cells, the precise downstream actions of insulin signalling are largely cell-dependent. This is frequently determined by the relative expression of key signal transducers and their isoforms (such as IR-A/-B, IRS1-4, and Akt1-3), in addition to expression of interacting suppressors or enhancers.

In the kidney, insulin is able to traverse the entire nephron, being small enough (6kD) to pass freely across the glomerular filtration barrier. The cell-specific effects of insulin in the nephron are summarised in Figure 1.5.

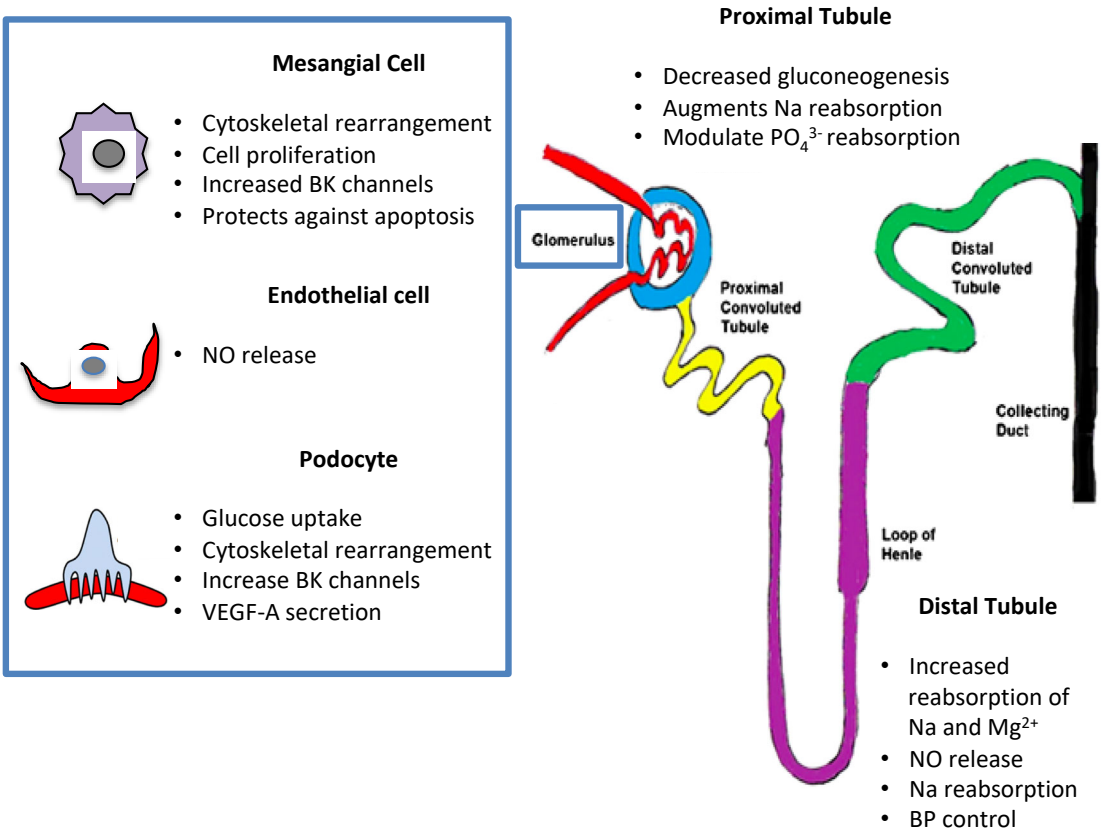

Figure 1.5 Effects of insulin on the nephron. NO= nitric oxide, VEGF= vascular endothelial growth factor, Na= sodium, PO_4^{3-}= phosphate, Mg= magnesium. Adapted from (91)

1.3.2 Clinical evidence supporting the importance of Insulin Signalling in DN

The link between insulin signalling and the glomerulus was first established in 1980 when Mogensen *et al* demonstrated that urinary albumin excretion doubled following intravenous infusion of insulin (with concomitant glucose to maintain euglycaemia) in newly diagnosed Type-1 diabetics (92). Following the hypothesis that insulin itself may be inducing increased glomerular permeability to albumin, the urinary excretion of albumin after an oral glucose load was compared in Type 1 (insulin-deficient) diabetics and healthy controls. An increase in albumin excretion was observed only in the healthy patients capable of mounting a normal insulin response to glucose, corroborating the theory that insulin, and not glucose, is responsible for the albuminuric effect (93).

Large population cohort studies have further characterised the relationship between insulin and albuminuria. Insulin resistance is associated with the development of albuminuria in non-diabetic patients (94), where it is an independent predictor of cardiovascular outcomes (95). Even insulin-deficient Type 1 diabetics develop insulin resistance, often reflected in large doses of exogenous insulin requirements, and these patients are significantly more likely to develop DN than those who maintain sensitivity to administered insulin (96). Most recently, Ahlqvist *et al* proposed an entirely novel classification of diabetes based on cluster analysis of comprehensive phenotyping which identified a subset of "severely insulin-resistant" diabetics who were significantly more likely to develop DN (97).

Hereditary influences are frequently identified in the literature, with insulin-resistant Type 1 diabetics significantly more likely to have family history of cellular insulin resistance (98). Genetic syndromes of insulin resistance present with variable renal phenotypes; congenital lipodystrophy is associated with albuminuria but only a minority have classical DN histology, Type B insulin resistance (autoimmune disease directed against the insulin receptor) leads to albuminuria in more than 50% of cases, but with a histological pattern more consistent with lupus nephritis, whilst patients with Type A insulin resistance (inherited mutation of the insulin receptor) commonly develop DN (99) . This

heterogeneity in renal phenotype may explain why findings from GWAS data have not been as helpful as anticipated in identifying a subset of susceptibility genes for DN specifically.

Whilst there is clear evidence of a link between insulin resistance, albuminuria and an increased susceptibility to DN, the precise underlying mechanism, whilst suggestive of a defect at the level of the glomerular filtration barrier (GFB), remains a subject of research interest. The role of the GFB and its constituent parts is reviewed below, with specific focus on the role of the podocyte in DN.

1.4 The Glomerular Filtration Barrier (GFB)

The GFB is a highly specialised structure that uniquely utilises size, charge and shape-selection in the ultrafiltration of blood (100). The GFB is freely permeable to water and small-to-medium sized solutes, but larger molecules, such as albumin (~67 kDa), are not filtered and are hence retained in the circulation. The identification of such molecules in the urine is indicative of a mechanical breach or malfunction in selectivity of the GFB, and is the basis of the urinary dipstick test for albuminuria in diabetes (101).

The GFB consists of three distinct layers: the endothelial cells of glomerular capillaries, the glomerular basement membrane (GBM) and specialised visceral epithelial cells called podocytes. In recent years, the physiological importance of two further "layers" has been described: the endothelial surface layer and the sub-podocyte space (102). However subdivided, it is clear that the function and maintenance of the GFB is determined by the harmonious workings of all its component parts, with evidence of cross-talk between cell types via numerous elucidated pathways (103-105).

1.4.1 Glomerular Endothelial cells (GEnC)

The glomerular endothelial cells (GEnCs) constitute the first layer of the GFB and are in direct contact with glomerular blood. GEnCs are distinguishable from endothelial cells elsewhere by the high density of large fenestrae; covering approximately 20-50% of total cell surface area (106). The fenestrae are approximately 60 nm diameter in humans (107) and as such, should not present a physical barrier to the passage of plasma proteins such as albumin (8 x 8 x 3 nm) (108). However, the fenestrae are lined with a hydrated mesh of glycocalyx, composed of negatively charged glycoproteins, glycosaminoglycans (GAGs), glycolipids and proteoglycans, which has been historically difficult to demonstrate *in vitro* (109, 110). In recent years, evidence for its contribution in preventing albumin passage, along with other important roles, has led to the proposal of its reclassification as an independently labelled layer of the GFB; the endothelial surface layer (ESL) (111). Disruption of the ESL *in vitro* and *in vivo* results in albuminuria (112-114), thus demonstrating the importance of ESL integrity.

The GEnCs themselves are responsible for regulating the ESL, with small alterations in ESL constitution being communicated to podocytes via an increase in sheer-stress sustained (115), or increased delivery of filtered macromolecules to this downstream layer of the GFB (116).

1.4.2 Glomerular Basement Membrane (GBM)

The glomerular basement membrane (GBM) is derived from the fusion of two membranes: the podocyte membrane, which makes up the outer wall (lamina rara externa) and the endothelial membrane that becomes the inner wall (lamina rara interna). Akin to all basement membranes, its key molecular components are Type IV collagen, laminin, nidogen and heparan sulfate proteoglycans which confer an anionic charge to the GBM that is (contentiously) considered to contribute to the charge selectivity of the GFB (117, 118).

The functional significance of the GBM is exemplified by the clinical syndromes that result from genetic mutations in 4 of the 9 known genes encoding critical components of the GBM, reviewed by Miner *et al* (119). Heterozygous null mutations in *COL4A3* or *COL4A4*, which encode the α3 and α4 chains of type IV collagen manifest as haematuria in the absence of progressive renal impairment (thin basement membrane disease), whilst homozygous mutations, or more commonly, X-linked inheritance of a mutated *COL4A5* allele, leads to the typical triad of clinical manifestations exhibited by patients with Alports nephropathy: ocular abnormalities (lenticonus), renal insufficiency and sensorineural deafness. A recent GWAS study of diabetic kidney disease has reaffirmed the importance of *COL4A3* and identified a minor allele (Asp326Tyr) that is significantly associated with GBM width and confers protection against development of albuminuria and ESKD (120).

1.5 Podocytes

The outermost layer of the GFB consists of podocytes; terminally differentiated, specialised epithelial cells literally translated as “cells with feet”. Although they exhibit typical epithelial cell features of apico-basal polarisation along a basement membrane, they have also been phenotypically likened to neurons with their extensile processes and secretory ability, and to contractile smooth muscle cells (121). The cytoskeletal configuration of the podocyte is uniquely complex and reflects the physiological need for dynamic remodeling to maintain the integrity of the filtration barrier under a variety of environmental stresses.

1.5.1 The Slit Diaphragm

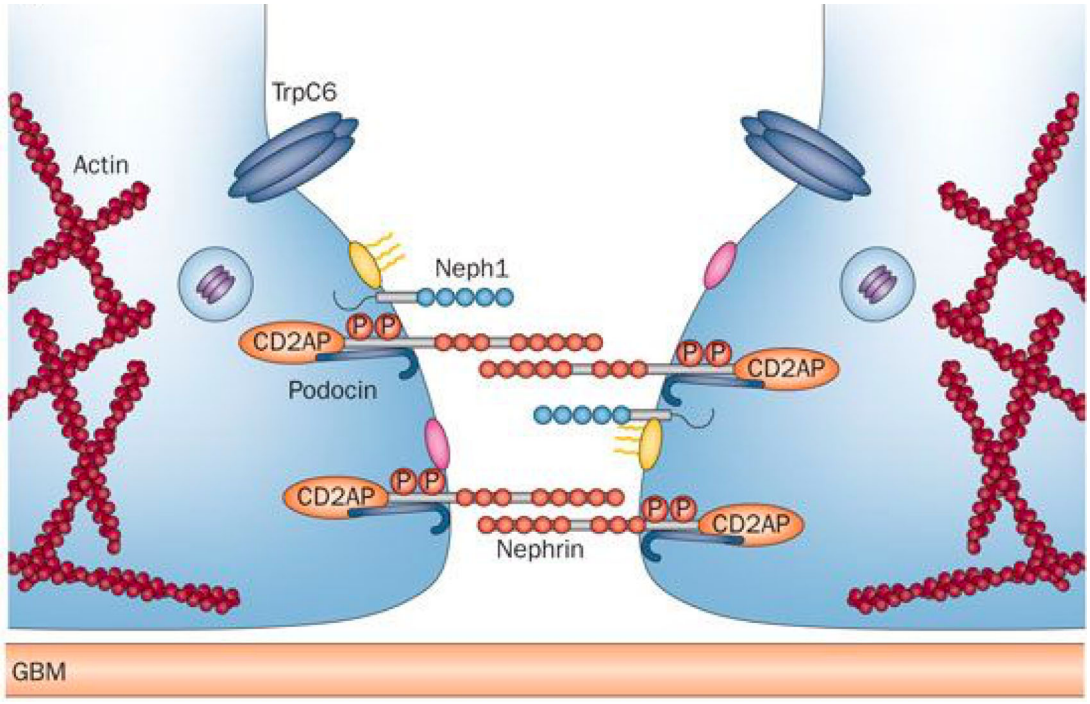

Figure 1.6 Molecular components of the podocyte slit diaphragm. During development, podocytes are initially connected via tight-junction and gap-junctions that become replaced by neuronal-junction components, nephrin, podocin and Neph1. These proteins form a zipper-like structure that is the hallmark of the mature slit diaphragm. CD2AP= CD2-associated protein; GBM= glomerular basement membrane; P= phosphorylated residues. Adapted from (122)

Podocytes consist of large cell bodies which communicate with the urinary space, and protruding foot processes which adhere to the GBM via focal adhesions and interdigitate with neigbouring podocytes via unique adherens

junctions called slit diaphragms (123). The slit diaphragms house a set of transmembrane proteins and cytosolic adapter molecules that link to the underlying actin cytoskeleton and are critical mediators of signal transduction. Much of what we understand about the significance of slit diaphragm proteins has been learnt from hereditary nephrotic conditions characterised by the loss or mutation of genes encoding them, summarised in Table 1.4.

Gene	Protein	Inheritance	Phenotype
NPHS1	Nephrin	AR	Congenital nephrotic syndrome of the Finnish type, ESRD
ACTN4	A-Actinin-4	AD	FSGS (adult onset, mild)
WT1	Wilms tumour protein	AD	Denys-Drash syndrome (DMS) Frasier syndrome (FSGS)
LMX1B	LIM homeobox transcription factor 1β	AD	Nail-patella syndrome (FSGS)
CD2AP	CD2-associated protein	AR	Congenital nephrotic syndrome
NPHS2	Podocin	AR	Steroid-resistant nephrotic syndrome (childhood)
TRPC6	Transient receptor potential cation channel, subfamily C, member 6	AD	FSGS (adolescent)
INF2	Formin	AD	FSGS (adolescent/adult onset- mild)
PLCE1	Phospholipase C, E1	AR	FSGS (childhood) and ESRD

Table 1.4 Inherited podocytopathies. Many causes of hereditary nephrotic syndromes are the result of genetic defects in important slit diaphragm proteins. AR= autosomal recessive, AD= autosomal dominant, FSGS= focal segmental glomerulosclerosis, DMS= diffuse mesangial sclerosis, ESRD= end stage renal disease. Adapted from (99) and (124)

One of the most central slit diaphragm proteins is nephrin, a member of the immunoglobulin superfamily. In the absence of nephrin, the mammalian slit diaphragm does not form (125), and congenital mutation of NPHS1 results in nephrotic syndrome of the Finnish type (126). The localisation of nephrin is dependent on its cytosolic interaction with Podocin; a stomatin protein family

member that associates with specialised lipid raft microdomains of the plasma membrane, which recruit nephrin to the slit diaphragm. A third scaffolding protein of major importance, CD2-associated protein (CD2AP), connects nephrin and podocin. The extracellular components of Nephrin, and its structural homologue NEPH1, act as a physical barrier to the passage of macromolecules. The intracellular domain has diverse roles in signal transduction, facilitated by numerous cytosolic binding proteins that determine cell polarity, calcium sensing, membrane trafficking and actin organisation, as recently reviewed by Martin *et al* (127) .

The calcium-permeable channel TRPC6 also sits within the slit diaphragm, where it plays an important role in podocyte mechano- and chemosensation (128), detecting alterations in pressure, fluid flow or filtration rate which might necessitate remodelling of the cytoskeleton and foot process contraction to maintain GFB equilibrium (129).

1.5.2 Actin dynamics

The podocyte cell body contains F-actin, intermediate filaments and microtubules. The foot process cytoskeleton is almost exclusively composed of very dense actin fibres, which extend longitudinally across its entire length (130). Actin is regulated by slit diaphragm proteins and by small GTPases, such as the Rac-1 and RhoA family. Synaptopodin is a dominant orchestrator of RhoA-mediated actin regulation (131) and can also modify the activity and localisation of TRPC6 in the slit diaphragm (132).

1.5.3 Focal adhesions

Adherence to the GBM is achieved via a number of transmembrane proteins including integrins (particularly alpha3beta1 (α3β1)), α-dystroglycan and syndecans that bind to extracellular matrix (ECM) components and collectively enable podocytes to withstand the oscillating filtration pressures within the

glomerulus. Much like the adherens junctions of the slit diaphragm, these connections are also a hub for signal transduction (133).

1.6 Podocytes in DN

The morphological changes of the diabetic podocyte have been well described and include foot process effacement (Figure 1.3C), detachment and loss (134, 135). Mechanisms of podocyte effacement include loss of nephrin and imbalance of small GTPases, mediated by the hyperglycaemic environment (136). Detachment occurs when podocytes become less stably anchored to the GBM as a result of reduction in α3β1 integrin expression, secondary to stresses such as haemodynamic-induced stretch and transforming growth factor beta (TGF-β) signalling (137). Podocyte death may be mediated by numerous pathways including direct apoptotic effects of hyperglycaemia, increased ROS and defects in podocyte autophagy (136). In an unfortunately deleterious cycle, podocyte death begets further podocyte death, with animal models demonstrating a critical threshold of 20% podocyte loss equating to irreversible glomerular damage that will progress to renal failure even in the absence of ongoing insults (138).

Histological abnormalities of podocytes are amongst the first detectable signs of DN in albuminuric human and animal models (139, 140) and podocyte loss is an established predictor of DN progression (134, 141). Podocytes express a number of paracrine factors such as VEGF-A, angiopoetins and CXCL12 that may communicate distress signals to other glomerular cells, as reviewed by Dimke *et al* (142). Podocytes that become detached from the GBM and enter the urinary space may additionally communicate with extra-glomerular parts of the nephron. This may represent a mechanism by which podocytes can initiate a deleterious cascade of pathophysiological events that results in DN, thereby explaining the prognostic significance of isolated podocyte loss. This has not yet been proven, however there is evidence that the degree of podocyturia correlates not only with active glomerular disease (143) but also with proximal tubular dysfunction (144).

1.6.1 Importance of Podocyte Insulin Responses

The importance of insulin signalling in the podocyte has become clear over the last decade. *In vitro* studies of glomerular cells demonstrated increased expression of IR and IRS1 specifically in podocytes (145). In 2008, Tejada *et al* reported that the development of albuminuria was associated with a loss of podocyte insulin responses in 12-week old db/db (T2DM) mice, with demonstrable loss of Akt phosphorylation leading to increased cell death, which led them to hypothesise that loss of podocyte insulin sensitivity may account for the podocyte depletion seen in early DN (146).

Throughout the 2000's, our Bristol group (Coward lab) published a series of papers that characterise podocyte responses to insulin in health and disease. Initial work undertaken using a conditionally immortalised human cell line showed that insulin signals to the podocyte via the insulin receptor, which predominantly activates PI3K and MAPK pathways resulting in phosphorylation of Akt and ERK1/2. This results in rapid actin cytoskeletal rearrangement to translocate glucose transporters (GLUT1 and GLUT4) from cytoplasmic GLUT-storage vesicles (GSVs) to the plasma membrane (147). This cytoskeletal remodelling is dependent on the action of small GTPases RhoA and CDC42, which specifically cause contraction and corticalisation of F-actin fibres (148). Exocytosis of glucose transporters at the cell membrane, achieved via a critical interaction between nephrin and vehicle-associated membrane protein 2 (VAMP2) (149), enables the podocyte to double its glucose concentration in response to insulin. This response is unique to (fully differentiated) podocytes and not observed in other glomerular cells (147). Following glucose uptake, the podocyte may utilise the energy source to undergo further conformational changes, which result in cellular contraction against the GBM (148). This mechanical rearrangement is facilitated by the insulin-induced translocation of BK and TRPC6 channels to the cell membrane, which generates ionic flux into the cell (150, 151). The purpose of this podocyte-specific cytoskeletal response to insulin is not fully understood, but it has been hypothesised to represent an adaptive process that "braces" the cell for the increased delivery of blood to the glomerular capillaries that occurs post-prandially as a result of generation of vasoactive metabolites such as nitric oxide, glucagon and kinins (152-154).

Insulin signalling may, therefore, be considered an important homeostatic mechanism that biologically prepares the podocyte for an increase in workload, thereby minimising repetitive biomechanical stress. As a terminally differentiated cell of extremely limited regenerative capacity, this would be of great evolutionary advantage to the cell.

The consequences of disrupted insulin signalling *in vivo* have been demonstrated using a podocyte-specific insulin receptor knock out mouse (PODIRKO). These albuminuric animals develop many of the histological hallmarks of DN, including podocyte foot process effacement, increased glomerular matrix and thickened GBM, the pivotal finding being the recapitulation of the DN phenotype under euglycaemic conditions (148). The animals did not, however, develop mesangial hypercellularity, raising the possibility that some aspects of DN may be insulin-dependent whilst others are more directly related to glucotoxicity.

Following the discovery of the podocyte as an-insulin sensitive cell, there have been a number of studies that recognise the downstream effects of podocyte-specific insulin signalling. These include the aforementioned roles of cytoskeletal regulation and calcium/potassium mobilisation as well as VEGF-A production (155), mitochondrial function (156) and ER stress responses (157), summarised in Figure 1.7. There has also been considerable interest in determining the key isoforms dictating signal divergence in podocyte insulin signalling that commit the cell to these downstream actions. For example, it is known that IRS2 is the most important IRS isoform in activating PI3K signalling in the podocyte (158) and that Akt2 is upregulated in podocytes and is critical in protecting against renal injury in CKD models (159), which may be related to its role in mediating metabolic insulin responses (160). Delineating the normal podocyte response to insulin enables a better understanding of the potential mechanisms and consequences of insulin resistance in these important cells.

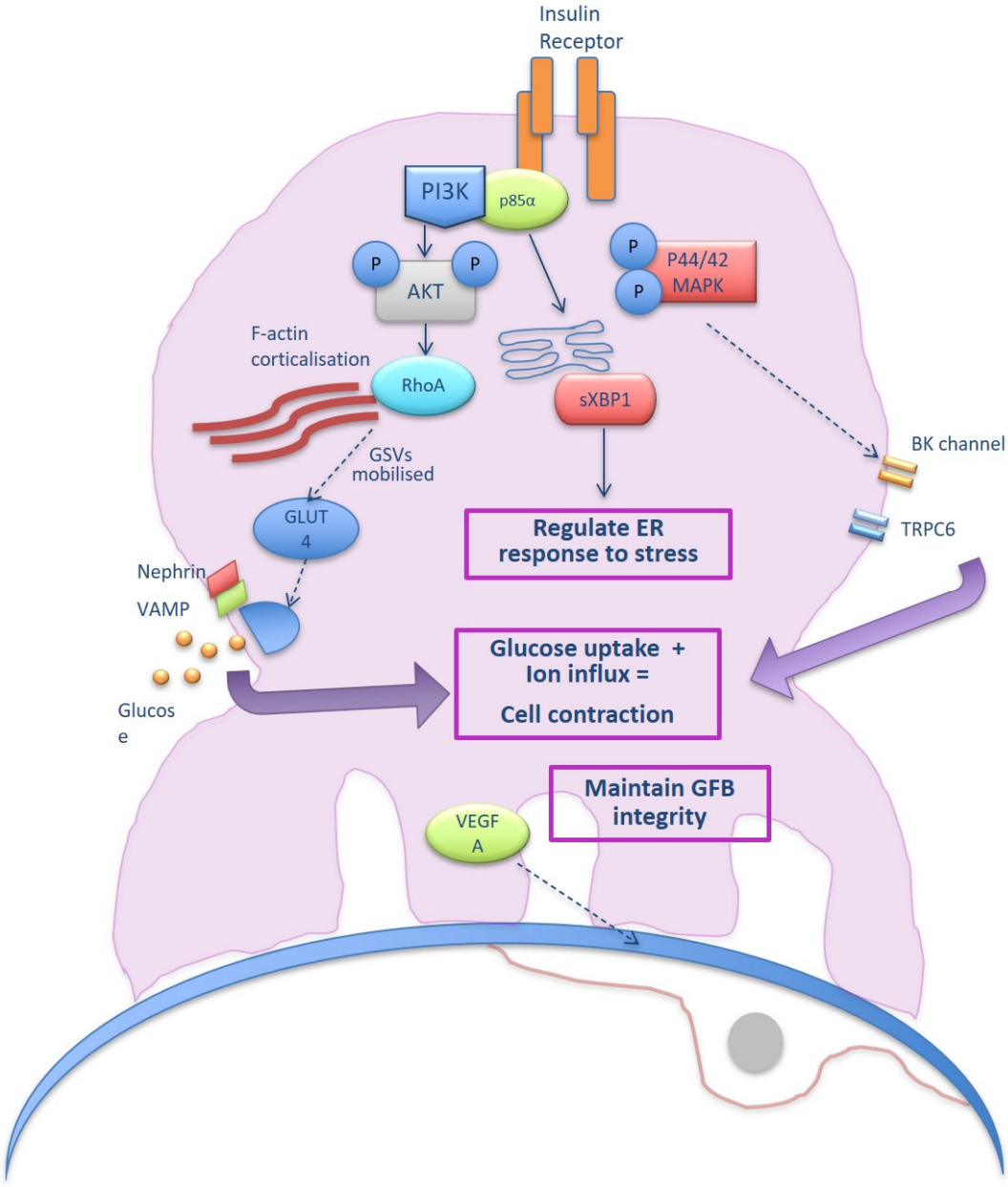

Figure 1.7 Pathways and consequences of podocyte insulin signalling. Insulin signals to the podocyte via the insulin receptor and effects key regulatory aspects of podocyte biology (highlighted in purple boxes) predominantly via the PI3K/Akt and MAPK pathways (148). Insulin-mediated mobilisation of glucose transporters and ionic channels to the plasma membrane enable glucose and ionic influx, which facilitates contraction of the podocyte on the GBM (150, 151). Insulin signalling via PI3K regulatory subunit p85α promotes the nuclear localisation of sXBP1 which regulates the ER stress response in podocytes (157). VEGF-A expression is modulated by insulin and functions to maintain the health of the GFB (155). BK= big potassium, GSV= Glucose transporter (GLUT) storage vesicle, sXBP1= spliced X-box binding protein-1, TRPC6= Transient receptor potential cation subfamily C, member 6, VAMP= vehicle-associated membrane protein, VEGF= vascular endothelial growth factor. Adapted from (161).

1.6.2 Mechanisms of Podocyte Insulin Resistance

Key nodes in the podocyte insulin-signalling cascade have been identified as important targets in the development of podocyte insulin resistance under diabetic conditions. These are summarised in Figure 1.8. From proximal to distal, the insulin receptor (IR) is a target of lysosomal and proteosomal degradation following prolonged exposure to insulin *in vitro* (162) and hyperglycaemia-induced elevation of Src homology-2 domain-containing phosphatase-1 (SHP-1) results in IRβ subunit binding, disabling onward signal transduction (163). (This effect has been shown to persist even in the absence of ongoing hyperglycaemia, owing to epigenetic histone modifications of the SHP-1 promoter, the so called "metabolic memory" effect (164)).

High levels of intracellular lipids, such as cholesterol and sphingolipids have also been shown to affect IR function, reviewed recently by Mitrofanova *et al* (165). Overexpression of sphingomyelin phosphodiesterase acid-like 3b (SMPDL3b) results in disruption of the IR/caveolin-1 interaction, preventing IR expression at the plasma membrane and reducing Akt phosphorylation, leading to increased podocyte injury *in vitro.* Furthermore, *in vivo* models of podocyte-specific SMPDL3b deficiency were protected from the development of DKD, demonstrating reduced albuminuria and preservation of podocyte numbers (166).

Elevated levels of obesity-associated SH2-domain containing inositol polyphosphate 5-phosphatase 2 (SHIP2) have been shown to reduce binding affinity of the IRS proteins, resulting in diminished Akt signalling in podocytes *in vitro* (167). Nucleotide-binding oligomerisation domain containing 2 (NOD2), an activator of the innate immune system, may also inhibit IRS1, resulting in downstream interference with p85α subunit of PI3K, and reduced GLUT4 translocation. The significance of these *in vitro* findings were substantiated by the findings that NOD2 deletion was protective against developing DKD in mice (168).

Podocyte insulin resistance may also manifest as a consequence of interruptions to distal insulin signalling. As previously mentioned, nephrin (in association with VAMP2) is critical in the docking of glucose transporters at the plasma membrane. Nephrin loss is a well established feature of diabetic kidney disease in both human and animal models (169-171) and mechanisms for nephrin loss include hyperglycaemia-induced activation of Notch-1, increased Protein kinase C alpha (PKCα) (negative regulator of WT1/nephrin promoter) and increased histone deacetylase 4 (HDAC4) which causes deacetylation of nephrin, ultimately targeting it for degradation (172-174). Interestingly, nephrin has also been shown to interact with the IRB isoform and PI3K/Akt, the latter independently of insulin signalling, although the relevance of these interactions to the development of podocyte insulin resistance is not clear (175).

Unravelling the interplay between podocyte insulin signalling and other experimentally validated contributors to DKD, such as oxidative stress, mitochondrial dysfunction and mTOR regulation, is proving insightful. For example, insulin enhances Nox4-dependent ROS production, and this has been linked to changes in the activity of protein kinase G type Iα (PKGIα) which regulates the permeability of the podocyte barrier, thereby linking insulin signalling, oxidative stress and albuminuria (176). The role of mTOR signalling in podocyte insulin resistance continues to evolve, with evidence for deleterious effects of too little or too much activity of mTOR complexes (177, 178)(see effects of rapamycin, below). Further work is needed to fully delineate these mechanisms but the evidence suggests that podocyte insulin signalling is pertinent to many critical metabolic pathways.

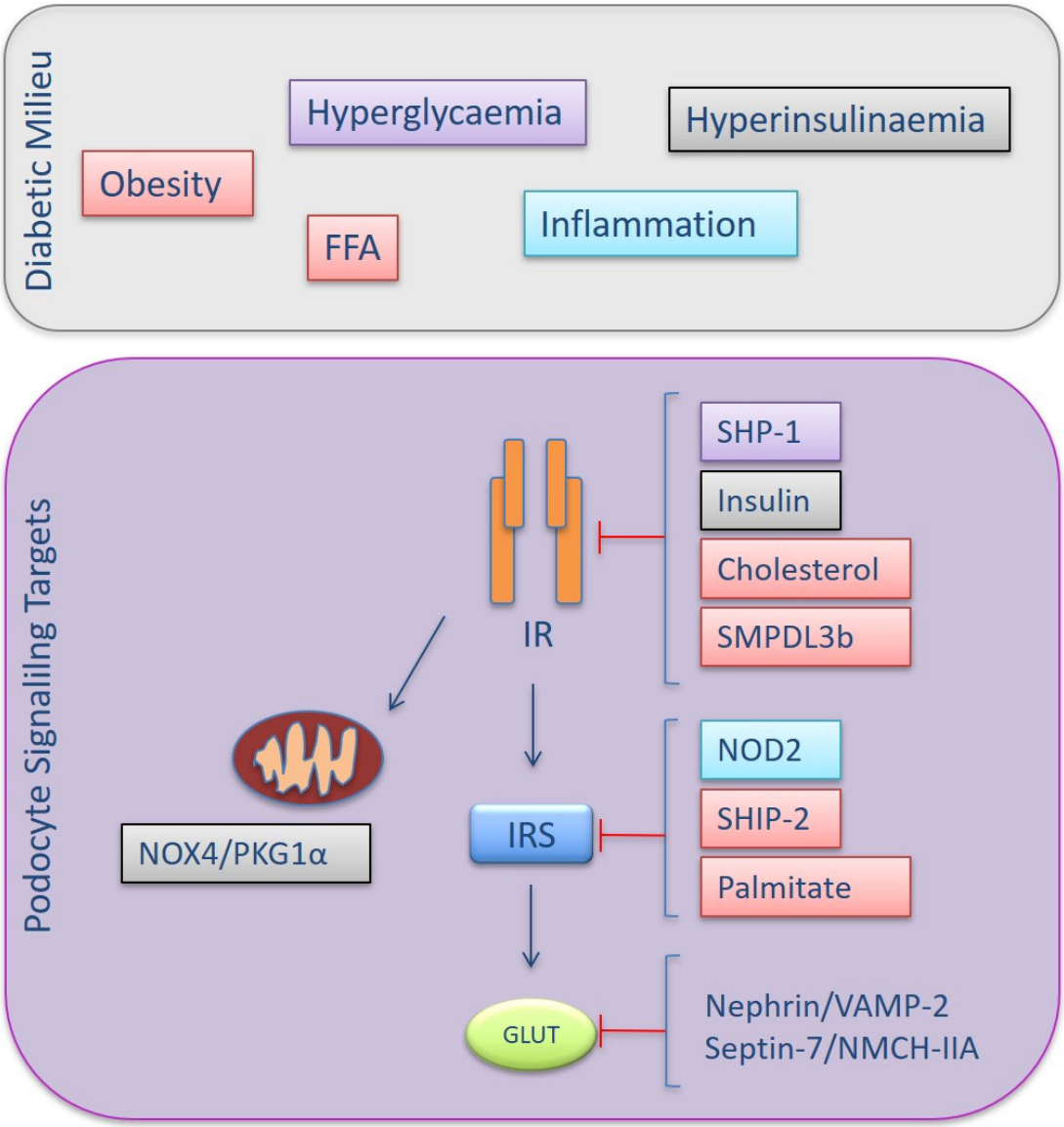

Figure 1.8 Mechanisms of podocyte insulin resistance. Numerous components of the diabetic milieu are implicated in the development of podocyte insulin resistance. Molecules targeting key nodes in insulin signalling pathway are shown, colour coded by the predominant diabetic stimuli with which they are associated. SHP-1 binds to the IRβ subunit and interrupts onward signalling (163). High levels of insulin result in lysosomal degradation of the insulin receptor (162). Overexpression of cholesterol and sphingomyelin phosphodiesterase acid-like 3b (SMPDL3b) leads to loss of IR/caveolin-1 interactions, which results in decreased phosphorylation of Akt and increased podocyte injury (166). Insulin receptor substrate (IRS) signalling is inhibited by phosphoinositide phosphatase SHIP-2 (167) and Nucleotide-binding oligomerisation domain containing 2 (NOD2) (168). IRS1 phosphorylation is disrupted by palmitate (179). The docking and fusion of glucose transporters at the cell membrane is disrupted by loss of nephrin, vehicle-associated membrane protein-2 (VAMP-2), septin-7 and non-muscle myosin heavy chain IIA (NMHC-IIA) (180). Mitochondrial dysfunction via a Nox4/PKG1α mechanism may also contribute to podocyte insulin resistance (176). SHP-1= Src homology-2 domain-containing phosphatase-1, PKG1α = protein kinase G type Iα.

1.6.3 Potential therapeutic implications of podocyte insulin sensitisers

The above evidence is strongly supportive of podocyte insulin resistance playing a significant role in the development of DN. Consequently; there has been consideration to pharmacological agents that may be capable of preserving or restoring podocyte insulin sensitivity. These are summarised in Table 1.5, and examples of those receiving greatest interest discussed below.

The peroxisome proliferator-activated receptor (PPAR)-γ agonist class of systemic insulin-sensitising drugs have been shown to reduce microalbuminuria in human DKD (181, 182), and are additionally protective from glomerulosclerotic changes in animal models of DN (183) and non-DN CKD (184). Lennon *et al* showed that Rosiglitazone directly effects podocytes by augmenting insulin-directed glucose uptake via a GLUT1 dependent mechanism (185). Unfortunately, the potential benefit of these drugs are outweighed by significant off-target effects including increase in cardiovascular deaths that led to the market withdrawal of rosiglitazone in 2010 (186).

The mTOR inhibitor, Rapamycin (Sirolimus), is used in the prevention of rejection in renal transplant patients, owing to its inhibitory effects on T and B cells. Inhibition of mTORC1 results in activation of autophagy and inhibition of podocyte apoptosis, which has been shown to prevent progressive DN in animal models (187, 188). Accordingly, over-activation of mTORC1 inhibits autophagy and accelerates DN in mice (189), leading researchers to speculate that mTOR inhibitors may be useful therapeutic agents in DN. However, in patients, Rapamycin often has a proteinuric effect, now thought to be a result of mTORC2 inhibition (190), and subsequent loss of Akt2 activation in podocytes (159). As mentioned above, Akt2 is the dominant isoform in podocytes and is chiefly involved in insulin-mediated PI3K/Akt signalling with a specific role in regulating cytoskeletal organisation. Canauad *et al* propose that this property is critical to the adaptation of surviving podocytes to nephron loss (159). This work has therefore seen a shift in focus from the utility of rapamycin in DN to the potential for mTOR1-specific inhibitors and/or AKT2 activators, which are intrinsically linked to podocyte insulin signalling.

GIT27 is a selective toll-like receptor (TLR) 2/4/6 inhibitor that has been shown to reduce albuminuria and urinary nephrin in the db/db mouse, suggesting that its renoprotective effects may be via a pro-podocyte survival mechanism (191). This hypothesis was supported by demonstration that GIT27 blocks Nox4 expression in podocytes *in vitro*, the overexpression of which has been implicated as a mechanism of podocyte insulin resistance, as described above (176).

As our understanding of the significance and mechanism of podocyte insulin resistance grows, so new potential therapeutic targets become apparent. Existing drugs, such as glitazones and metformin, may also be repurposed to specifically improve podocyte insulin sensitivity in DN. However the barriers to clinical translation are numerous and therefore the hunt for easily manipulated targets without significant off-target effects remains top priority. One relatively new class of agents, microRNAs, may hold significant promise in this regard, and will be reviewed below.

Drug/Class	Target	Outcome	Ref
Rosiglitazone (Thiazolidinediones)	PPAR-γ agonist	Improves podocyte insulin sensitivity (GLUT1) Reduces proteinuria Reduces TGF-β, restores nephrin, decreases ROS, decreases RAS-induced stretch Increased CV mortality, hepatotoxicity	(185, 192)
GIT27	TLR2/4/6 inhibitor Nox4 inhibitor	Reduce proteinuria/urinary nephrin Inhibits podocyte Nox4/ROS production Attenuates podocyte proinflammatory cytokine synthesis	(191)
Resveratrol (trans-3,5,4-trihydroxystilbene) Natural polyphenol	Antioxidant Anti-inflammatory (miR-383-5p and NFκB suppression)	Improves insulin sensitivity (systemic) Reduces inflammatory cytokines (systemic) Stimulates podocyte autophagy Increases nephrin and podocin expression Reduces proteinuria	(193, 194)
Berberine (Chinese Herb)	Activates PPAR-γ coactivator-1α (PGC-1α) signalling pathway	Protects podocytes against ROS damage and mitochondrial dysfunction Reduced FFA deposition in glomeruli Improves insulin sensitivity (systemic) Reduces proteinuria	(195)
Metformin (Biguanide)	SHIP2 inhibition AMPK activation	Improves insulin sensitivity (systemic) Increases podocyte glucose uptake Reduces podocyte apoptosis/loss Contraindicated eGFR<30ml/1.73m^2/min	(196, 197)

Table 1.5 Pharmaceutical agents proposed to improve podocyte insulin sensitivity. AMPK= adenosine monophosphate-activated protein kinase, FFA= free fatty acid, PPAR γ= peroxisome proliferator activated receptor gamma, RAS= renin-angiotensin system, ROS= reactive oxygen species, SHIP2= SH2-domain containing inositol polyphosphate 5-phosphatase 2, TGF- β= transforming growth factor beta.

1.7 MIcroRNAs: Overview of Function

MicroRNAs (miRNAs) are endogenous, non-coding, single stranded RNA transcripts of 19-25 nucleotides in length. Ambros *et al* identified the first miRNA, lin-4, in the nematode Caenorhabditis elegans (C.elegans) in 1993 (198). This was followed by an explosion of research, which identified miRNAs as critical gene regulators in virtually all biological processes through embryogenesis to apoptosis pathways. Indeed, miRNAs are estimated to regulate up to 60% of protein coding genes in the human genome (199). The latest version of miRbase lists 1917 identified miRNA transcripts in the human genome, but not all of these have been functionally validated (200). MiRNAs have been detected in blood, urine and other body fluids either packaged into microvesicles and/or exosomes, or transported by RNA-binding proteins (Argonaute 2 complexes) and lipoproteins, which protect them from degradation by ribonucleases (201).

Like other related members of the RNA interference (RNAi) pathway, such as short interfering (siRNAs) and Piwi-RNAs (piRNAs), miRNAs inhibit gene expression in a sequence specific manner. Most miRNAs will bind to a specific sequence at the 3′-untranslated region (3′-UTR) of their target mRNAs via classical Watson-Crick base pairing. Perfect sequence complementarity between miRNA and target mRNA 3′-UTR results in mRNA cleavage by argonaute 2 protein (AGO2), and imperfect complementarity results in translational repression and/or target degradation achieved by mRNA deadenylation and decapping (202, 203). MiRNA binding sites are additionally, but less commonly present in mRNA 5′ UTR, as well as within coding sequence and promoter regions (204), the latter being associated with a converse *induction* of transcription, by direct and indirect mechanisms (205, 206).

In 2007, Landgraf *et al* published their miRNA atlas, documenting the miRNA expression and abundance of 340 miRNAs in 26 different tissues (207). Since then, the advances in profiling techniques have permitted the investigation of differential miRNA expression even at a cellular level (208, 209). These studies

demonstrate the cell-specific nature of certain miRNAs, or miRNAs clusters, and their significance in relation to the specific biological function of that cell. Furthermore, it has been recently proposed that miRNAs can exhibit "flexible targeting" of mRNAs dependent on miRNA concentrations, enabling a miRNA to change its target repertoire under specific physiological conditions, thereby expanding the range of possible miRNA-regulated biological outcomes (210). This may explain the finding that miRNAs may act as rheostats in fine tuning of gene expression (previously thought to be dependent on degree of target site binding complementarity, and to miR/mRNA abundance (211)) but are equally capable of "master regulation" where a single miRNA can act as a critical on/off switch. The biological diversity in miRNA expression, mode of action and regulatory outcomes presents numerous challenges to researchers keen to harness their therapeutic potential, as discussed below.

1.7.1 MiRNA biosynthesis

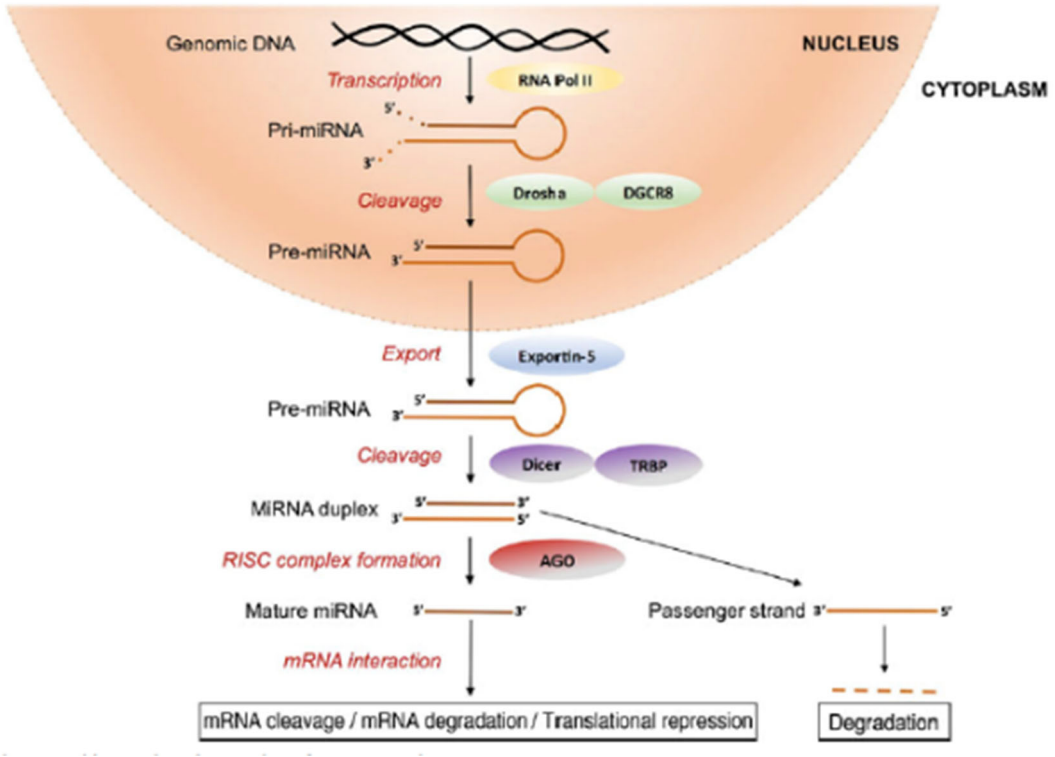

Figure 1.9 Canonical miRNA biogenesis. MiRNAs are transcribed as capped and polyadenylated primary transcripts (pri-miRNAs) containing a hairpin structure that is excised by the endonuclease Drosha, which associates with Di-George Critical Region-8 (DCGR8). The liberated stem-loop (pre-miRNA) is transported to the cytoplasm by exportin 5 and cleaved by Dicer, under the direction of TAR RNA-binding protein (TRBP), into the mature miRNA duplex. The guide strand is loaded onto the RNA-induced silencing complex (RISC), which leads to target mRNA silencing through cleavage or translational repression. The passenger strand is degraded. AGO= argonaute protein. Image extracted from our published review article (212).

Approximately half of all miRNAs are intragenic and processed mostly from introns and relatively few exons of protein coding genes, while the remaining are intergenic, transcribed independently of a host gene and regulated by their own promoters. MiRNA families may additionally be transcribed as one long transcript called a cluster, which may share seed (binding) regions (213).

Canonical miRNA biogenesis (Figure 1.9) begins with nuclear transcription, most frequently by RNA polymerase II, into primary miRNA (pri-miRNA) transcripts that form a distinctive stem loop structure. Pri-miRNAs are cleaved into precursor miRNAs (pre-miRNAs) by a multiprotein complex of a ribonuclease III (RNase III) enzyme called Drosha and its cofactor, Di George syndrome critical region gene 8 (DGCR8). DGCR8 binds to pri-miRNAs at a precise distance from the single stranded (ssRNA) -double-stranded (dsRNA) junction and directs Drosha to cleave the pri-miRNA, resulting in a 70–100 base pair pre-miRNA (214). Pre-miRNAs have a characteristic hairpin structure that is recognised by exportin-5, a dsRNA binding protein that facilitates transport of pre-miRNAs into the cytoplasm. Here, pre-miRNAs are cleaved by RNase III enzyme Dicer, under the direction of TAR RNA-binding protein (TRBP), which guides Dicer to the correct cleavage site. Cleavage results in loss of the terminal loop and formation of the mature miRNA duplex. The mature miRNA duplex is made up of two ss miRNAs; a dominant guide strand (miRNA) and the passenger strand (miRNA*), where the directionality of the miRNA strand determines the name of the mature miRNA form, i.e. 5p strand arises from the 5′ end of the pre-miRNA hairpin and the 3p strand originates from the 3′ end. The mature miRNA guide strand is loaded onto the RNA-induced silencing complex (RISC), which includes the argonaute (AGO) proteins, after which the passenger miRNA is typically degraded. The selection of the 5p or 3p as the dominant guide strand is species/cell specific, and is determined partly by the thermodynamic stability at the 5′ ends of the miRNA duplex, where the strand with lower 5′ stability, or presence of 5′ uracil is deemed the guide strand (215). The active miRNA-containing RISC (miRISC) is then recruited to target mRNAs that express specific, partially complementary binding sites.

1.7.2 MiRNAs in Renal Health and Disease

Conditional deletion of Dicer in various animal models has demonstrated that renal development is critically dependent on normal microRNA function. Loss of Dicer in the early metanephric mesenchyme results in severe renal dysgenesis due to loss of nephron progenitors, whilst Dicer knockout in ureteric buds disrupts ciliogenesis leading to the development of renal cysts (216, 217).

MiRNAs are also vital regulators of normal renal physiology, with studies that demonstrate their involvement in juxtaglomerular renin production, electrolyte transport and maintenance of osmolarity (218-220).

Unsurprisingly, miRNAs have been implicated in the pathogenesis of many renal diseases. Examples of miRNAs and their targets in disease are listed in Table 1.6. Some miRNAs are commonly dysregulated across renal injury models, including those associated with fibrosis, which represents a final common pathway in ESRD. TGF-β-driven miR-21 has been extensively studied in this regard, where it is significantly elevated across patient and animal models of CKD of a variety of aetiologies (220-222). Targets of miR-21 include proliferator-activated receptor alpha (PPARα), a key regulator of lipid metabolism, Mpv171, an inhibitor of mitochondrial ROS production, and Smad7, an inhibitor of TGF-β signalling (220, 223). Loss of let-7c, which targets several members of the TGF-β1 signalling (e.g TGF-β receptor type 1), has also been well described in renal fibrosis, and dysregulation of this miRNA and its targets are recapitulated in human biopsies of renal fibrosis (224). Conversely, differential expression of some miRNAs show relative specificity for renal diseases, such as miR-30 family in FSGS, as discussed below.

Disease	miRNA	Target	Effect	Ref
FSGS	↑miR-193a	WT1	Induces FSGS	(225)
	↓miR-30s	NOTCH1, p53, TRPC6	Podocyte cytoskeletal damage	(226) (227)
PCKD	↑miR-17	PKD1, PKD2	Cyst growth	(228)
	↑miR-92	HNF-1β	Cyst growth	(229)
IgAN	↑miR-148b	C1GALT1	IgA1 aberrant glycosylation	(230)
	↓miR-223	Importin α4/5	GEnC proliferation	(231)
AKI	↑miR-494	ATF3	ER stress	(232)
	↑miR-24	HO-1, H2AX	Oxidative stress	(233)
LN	↑miR-148a	PTEN	Mesangial proliferation	(234)
	↓miR-371	HIF-1α	Mesangial cell proliferation	(235)

Table 1.6 MIcroRNAs implicated in the pathogenesis of renal disease. ATF3= activating transcription factor 3, AKI= acute kidney injury, C1GALT1=Core 1 Synthase, Glycoprotein-N-Acetylgalactosamine 3-Beta-Galactosyltransferase, ER= endoplasmic reticulum, FSGS= focal segmental glomerulosclerosis, GEnC= glomerular endothelial cell, H2AX= H2A histone family member X, HNF-1β= hepatocyte nuclear factor, HO-1= haem-oxygenase 1, LN= lupus nephritis, PCKD= polycystic kidney disease, PKD= polycystin, TRPC6= Transient receptor potential cation channel, subfamily C, member 6, WT1= Wilms tumour-1.

1.7.3 MiRNAs in DN

A wealth of data exists regarding the differential miRNA expression of patients with DKD, with profiling of patient blood, urine and renal biopsy tissue reported, highlighting the possibility that miRNAs may be used as biomarkers to predict disease course, discussed in detail below. Published data by our Cardiff lab have contributed to this and our findings of an increased urinary miR-155, miR-29b and miR-126 in DKD patients are presented in chapter 4 of this thesis (236).

The mechanistic roles of miRNAs in the pathogenesis of DN continue to be elucidated. Prominent miRNAs and their mRNA targets are summarised in Table 1.7. One of the earliest established, and most well characterised miRNA in DN is miR-192. Renal biopsy tissue expression of miR-192 has been correlated with markers of DN progression, such as eGFR decline and histopathological evidence of tubulointerstitial fibrosis (237). As described above for miR-21, miR-192 expression is also influenced by TGF-β1, although the direction of expression change and resultant anti- or pro-fibrotic effects (mediated via ZEB1/ZEB2 targets) is apparently dependent on renal cell type (238). Importantly, inhibition of miR-192 using both miR-192 KO mouse models and exogenous miR-192 antagonists have been shown to protect from development of fibrosis and proteinuria in diabetic rodents (239, 240).

TGF-β1 has also been shown to induce miR-377 under hyperglycaemic conditions in mesangial cells. This results in repression of targets Pak1 and superoxide dismutases (SOD1, SOD2) leading to increases in fibronectin production and oxidative stress, respectively (241).

MiR-29 family members are heavily implicated in DN development, where they exert an anti-fibrotic, renoprotective effect via ECM-related target genes, such as collagens. Wang *et al* demonstrated that miR-29a, miR-29b, and miR-29c were reduced in kidney disease models of both early and late stage renal fibrosis in diabetic and non-diabetic animals (242). MiR-29b has been shown to exert its protective effect via inhibition of TGF-β/SMAD3 signalling pathway and NFκB-driven renal inflammation in db/db mice (243) . Recently, podocyte-specific effects of miR-29 family have been elucidated, as discussed below.

MiRNA	Target	Effect	Ref
↑miR-21	Smad7 PPAR-γ Mpv171 PTEN	Glomerular Fibrosis EMT induction	(223) (220) (244)
↑miR-34a	SIRT1	Tubulointerstitial fibrosis Increased TGF-β1	(245)
↑miR-377	PAK1 SOD1/2	Increased Fibronectin (ECM) Increased oxidative stress	(241)
↑/↓miR-192	SIP1 ZEB1/2	Increased renal fibrosis	(237, 238)
↓let-7/7b	Collagens TGF-βR1	Increased renal fibrosis	(246)
↓miR-29s	Collagens HDAC	Renal fibrosis Podocyte dysfunction	(174)
↓miR-25	Nox4 CDC42	Increased oxidative stress Accelerates fibrosis and proteinuria	(247) (248)

Table 1.7 MicroRNAs implicated in the pathogenesis of Diabetic Nephropathy. CDC42= Cell division control protein 42 homolog, ECM= extracellular matrix, EMT= epithelial -mesenchymal transition, Nox4= Nicotinamide adenine dinucleotide phosphate oxidase 4, PPAR= Peroxisome proliferator-activated receptor, PTEN= Phosphatase and tensin homolog, SIRT= silent mating type information regulation 2 homolog, SOD= superoxide dismutase, SIP1= Smad interacting protein 1, ZEB= Zinc Finger E-Box Binding Homeobox.

1.7.4 Podocyte miRNAs in DN

Podocyte-specific miRNAs are critical for glomerular health and survival, as exemplified by a series of eloquent studies involving targeted deletion of Dicer and Drosha that resulted in deranged cytoskeletal dynamics, tubular dysfunction, proteinuria and glomerulosclerosis in mice (249-252). A subset of miRNAs has been shown to be enriched in the podocyte, and these are, unsurprisingly, associated with cytoskeletal regulation (253), however miRNAs have been additionally implicated in the control of podocyte cell cycle, differentiation and VEGF-A release (254, 255). An overview of miRNA regulation of normal podocyte function is depicted in Figure 1.10. Dysregulation of these miRNAs are chiefly implicated in the pathogenesis of primary podocyte-disordered pathologies, such as FSGS, with miR-30s shown to be significantly downregulated in animal models, possibly via a TGF-β/Smad-2 dependent mechanism. Indeed, the therapeutic effects of glucocorticoids in FSGS have been attributed to the resultant increase in podocyte miR-30 (226, 256).

In DN, miR-29 family members are generally considered to be anti-fibrotic and therefore renoprotective, however overexpression of miR-29c in podocytes represses target Sprouty homolog-1 (Spry-1) leading to podocyte apoptosis *in vitro*, and diabetic mice treated with anti-miR-29c showed attenuated proteinuria and reduced (mesangial) extracellular matrix deposition (257). Low levels of miR-29a in hyperglycaemic conditions promotes histone deacetylation of nephrin leading to podocyte apoptosis, proteinuria and renal dysfunction (174). MiR-155 has also been shown to play a role in the maintenance of nephrin, where knockdown of this miRNA is protective against hyperglycaemia and TGF-β-induced nephrin loss and apoptosis (258, 259).

MiRNAs are also important regulators of podocyte responses to oxidative and ER stress. Xu *et al* recently reported that miR-423-5p expression was reduced in biopsy tissue of patients with DN, and in podocytes treated with high glucose *in vitro*. Enforced overexpression of miR-423-5p was protective against hyperglycaemia-induced podocyte damage by inhibiting ROS generation via

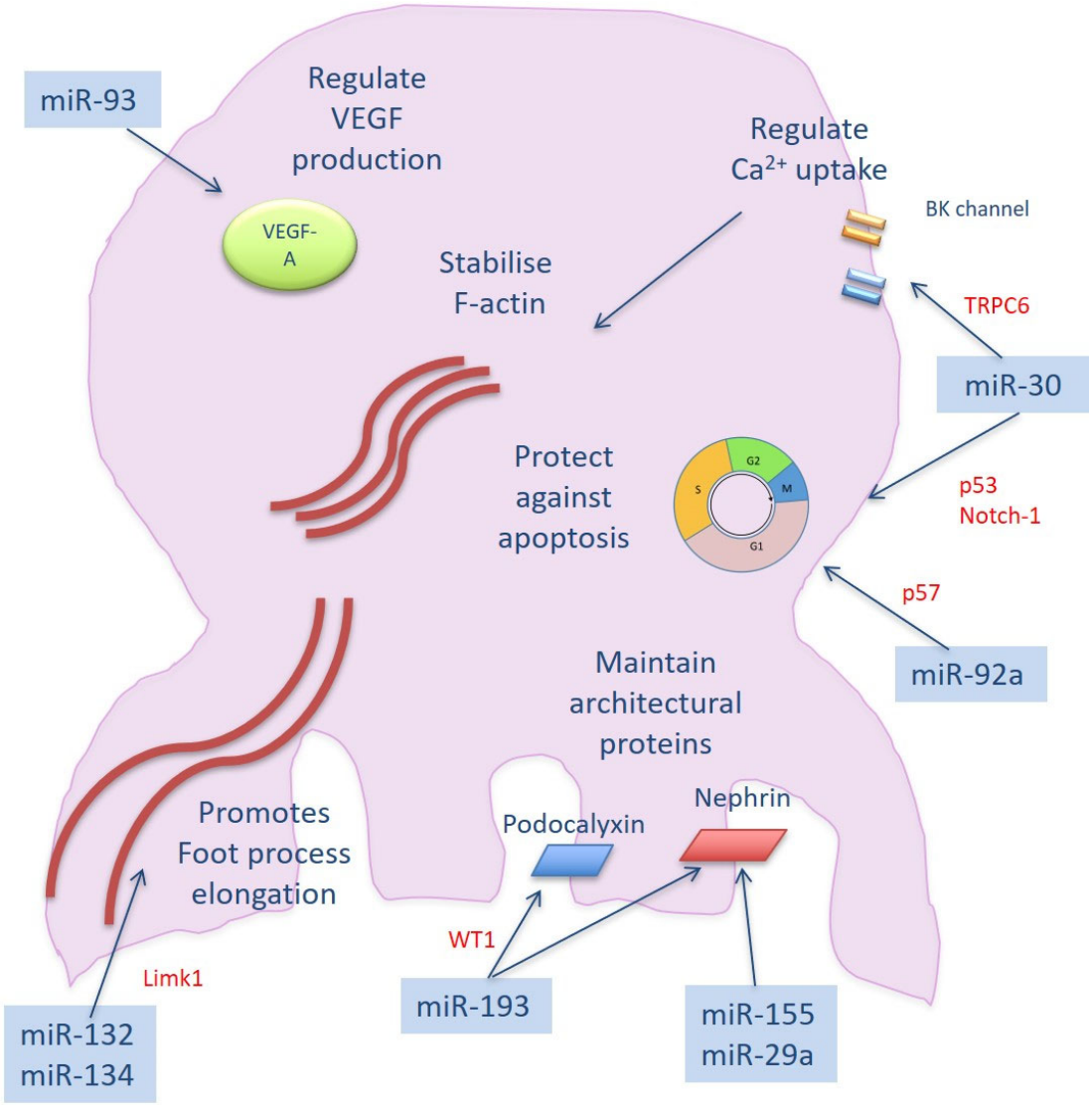

Figure 1.10. MicroRNA regulation of podocyte biology. MiR-93 regulates VEGF-A production *in vitro* and *in vivo*, (255), elevated miR-132 and decreased miR-134 result in reparative actin polymerisation, via target Limk1 (Lim domain kinase 1), which favours foot process elongation (260). MiR-193 stabilises nephrin and podocalyxin via regulating critical transcription factor Wilms tumour 1 (WT1) (225). MiR-155 and miR-29a both promote acetylation of nephrin (174, 259). MiR-92a safeguards the cell cycle quiescence of the differentiated podocyte via its target p57 (254). MiR-30 also plays a role in cell cycle regulation, being protective of apoptosis via actions on targets Notch-1 and p53 (226). MiR-30 also targets TRPC6 (Transient Receptor Potential Cation Channel Subfamily C Member 6), in addition to catalytic subunits of calcineurin (not shown here), thereby regulating calcium (Ca^{2+}) and calcineurin signalling, which promotes the stability of F-actin filaments (227).

direct target Nox4 (261). MiR-27a upregulation has been shown to induce endoplasmic reticulum (ER) stress in podocytes via repression of FOXO1 (262). Interestingly, there is a significant overlap in miR-mediated mechanisms of diabetic podocytopathy described here, and those pathways regulated by podocyte insulin signalling.

1.7.5 MicroRNAs in Insulin Resistance

A growing body of evidence recognises the importance of miRNAs in the development of insulin resistance in classical peripheral target organs. In the livers of diabetic patients and mice, miR-103 and miR-107 are upregulated, corresponding to repression of target caveolin-1, thus preventing the stabilisation of the insulin receptor at the cell membrane, leading to insulin resistance (263).

MiR-29a is overexpressed in muscle biopsy tissue from patients with T2DM, and is additionally induced by palmitate, resulting in repression of IRS1 (264). Further work ascertained that miR-29 is a master modulator of glucose utilisation in skeletal muscle, with additional targets such as hexokinase 2 (HK2), GLUT1, PIK3R3 and Akt2 also implicated (265).

In adipose tissue, miR-181b levels are reduced in models of obese mice, leading to increased expression of PHLPP2 (Pleckstrin Homology domain leucine-rich repeat protein phosphatase-2) and inactivation of Akt and impaired insulin signalling. Furthermore, miR-181b rescue resulted in improved glucose tolerance through enhanced insulin-mediated Akt phosphorylation at Ser473 and induction of endothelial nitric oxide synthase, nitric oxide activity and FOXO1 phosphorylation. These effects were seen specifically in white adipose tissue, and not in liver or in skeletal muscle, highlighting the cell specificity of miR-action in the regulation of insulin responses (266).

MicroRNAs have been postulated to be the link between insulin resistance, obesity and inflammation in diabetes. For example, miR-155, a well-established

proinflammatory miRNA, was upregulated in exosomes extracted from adipose tissue macrophages in obese mice. Transplantation of these exosomes to lean mice resulted in the development of insulin resistance, supporting a hypothesis of paracrine miRNA regulation in obesity-associated inflammation (267).

The role of miRNAs in the regulation of podocyte-specific insulin signalling, and its significance in DN development, has been explored in only a couple of studies to date. In 2015, our Bristol group reported that IRS2 was a critical molecule for sensitising the podocyte to insulin through its ability to modulate PTEN expression (a negative regulator of Akt) (158). A few years later, Sun *et al* demonstrated that miR-217 (which is upregulated in serum from T2DM patients and positively correlated with albuminuria) directly targets PTEN in podocytes (268). Blocking miR-217 restored defective autophagy pathways, inhibited ROS and apoptosis, whilst also increasing nephrin expression and glucose uptake (269), therefore highlighting the potential for multiple downstream signalling effects when miRNAs regulate proximal nodes in insulin signalling.

A small study performed by Ding *et al* showed that the mechanism of fructose-induced podocyte insulin resistance was via loss of miR-206 targeting of protein tyrosine phosphatase 1B (PTP1B), a negative regulator of insulin receptor and IRS signalling. Both curcurmin (a natural diphenolic compound found in turmeric) and pioglitazone restored expression of miR-206 *in vitro* and *in vivo* under fructose stimulated conditions, thereby abolishing the upregulation of PTP1B and restoring expression of pINSR, pIRS1, pAkt and pERK1/2 (270).

Whilst there may be few studies that specifically address miRNA regulation of podocyte insulin signalling, it is clear from the evidence above that there are multiple miR-mediated podocyte networks that may be intrinsically linked to insulin responses.

1.7.6 MiRNAs as biomarkers and therapeutic agents

MicroRNA signatures of disease are increasingly well elucidated following advances in sequencing technology. Importantly, differential miRNA expression has been clearly correlated to clinically relevant disease outcomes. MiRNAs are attractive as biomarkers because they are stable in plasma and urine owing to their association with Argonaute protein complexes, lipoproteins, or packaged into microvesicles/exosomes, as recently reviewed by us (271). Urinary miRNAs are of particular interest in nephrology, as they predominantly originate from cells of the urinary tract (although there are reports of freely filtered miRNAs from the systemic circulation in extreme conditions (272)). Furthermore, we have shown that urinary miRNAs are resistant to extremes of pH, multiple freeze-thaw cycles and following prolonged storage at room temperature (273) and have recently reported our optimised method of urinary miRNA extraction and straightforward PCR-based detection (274). Urinary miRNAs have therefore been described as highly convenient "liquid biopsies" due to the clinical information that can be gleaned in a non-invasive manner that may be amenable to point-of-care testing in the near future (275). Given the fact that urinary podocyte loss is seen in DN (276) and that miRNAs may function as mediators of crosstalk from one cell type to another (277), it is conceivable that a podocyte-specific urinary miRNA signature may be detected in early DN that not only correlates with loss of podocyte insulin sensitivity, but also represents a means of communicating this early diabetic insult to other parts of the nephron.

The use of miRNAs as therapeutic agents is based on two approaches: miRNA inhibition with "antagomiRs" (most commonly, antisense oligonucleotides designed against the mature sequence of miRNAs) or miRNA replacement with "agomiRs" (oligonucleotide mimics). Chemical modifications are required to maximise stability and prevent nuclease degradation, and to permit entry through a negatively charged cell membrane (278). However the major challenges of miRNA therapy are ensuring correct target delivery at appropriate dosage, without significant adverse effects, which have been the cause of high

profile trial terminations (279). Unlike miRNA biomarkers, a number of which are used as part of routine clinical practice (most notably as a diagnostic tool in thyroid cancer (280)), no miRNA-based therapeutics have yet been approved for clinical use, although there are numerous phase I and phase II clinical trials in progress, as reviewed recently (279).

The most well documented miRNA-based therapeutic is Miravirsen, a miR-122 antagonist that completely abolishes Hepatitis C viral replication (281). Unfortunately for Roche pharmaceuticals, market prospects have been considerably quashed by the breakthrough success of Gilead Sciences' ledipasvir plus sofosbuvir, direct acting anti-viral agents that have effectively cured HCV genotype 1 infection. Nevertheless, the full results from phase II clinical trials of Miravirsen are eagerly awaited to provide important proof of concept for anti-miRNA based therapy.

MiR-21 targeting therapies have been an obvious choice for development as therapeutics, as their anti-fibrotic effects may be applicable across a wide range of pathologies, including renal disease. RG-012, an antagomiR of miR-21, has been trialled as a treatment for Alports nephropathy, based upon the anti-fibrotic effects of anti-miR-21 observed in α3-chain type IV collagen KO mice (282). Despite promising results from phase 1 trials of healthy volunteers, phase II trials were suspended mid-2018 due to the reorganisation of the funding pharmaceutical companies. More recently, a miR-29b mimic, Remlarsan, has been developed for the treatment of keloid scars (ClinicalTrials.gov identifier NCT03601052). Given the well-established association between miR-29 family and fibrosis in DN, the results from this phase II clinical trial may have a significant wider impact. Mesenchymal stem cells have also been manipulated to deliver exosome-packaged anti-fibrotic let-7c to areas of renal cell damage, attenuating renal fibrosis in mouse models (283), thereby highlighting novel means of targeted miRNA therapeutic delivery which may be translated into clinical trials in the near future.

1.8 Hypothesis, Aims and Impact

My research hypothesis is that microRNAs regulate podocyte insulin signalling and loss of this miR-regulation is a critical early step in the development of DN.

My research aims are:

1. Investigate the differential expression of miRNAs in insulin-resistant podocytes *in vitro*
2. Investigate the evolution of differential expression of miRNAs in a diabetic mouse model during the development of DN
3. Determine the roles of candidate miRNAs in the regulation of podocyte insulin signalling pathways, *in vitro*

The translational impact of this work lies in the potential for development of candidate miRNAs as biomarkers to identify, and hence risk-stratify those diabetics who may be more likely to develop DN. In addition, novel microRNA targets in podocyte insulin signalling may be manipulated to restore the early loss of podocyte insulin responses, thus preventing a deleterious cascade of pathophysiological events that result in DN.

2 Materials and Methods

2.1 Cell culture

2.1.1 Cell lines

Podocyte cell lines were produced and obtained from Bristol Academic Renal Unit. Mouse podocytes (C2 cell line), conditionally immortalised via transfection of a temperature-sensitive viral oncogene, SV40 (284) were maintained in RPMI-1640 (Sigma, #R0883)) and supplemented with 2 mM L-Glutamine and 10% (v/v) Fetal Calf Serum (SeraLab), at 5% $C0_2$. Cells were grown at the permissive temperature (33°C) until 40% confluent before being thermoswitched (37°C). Growth media was replenished every 2-3 days. Cells were considered fully differentiated at 10 days.

HEK293T used for lentiviral production were maintained in Dulbecco's modified Eagle's medium (DMEM) (Thermo Fisher Scientific #11966025), supplemented with 2mM L-Glutamine, 100 units/ml penicillin, 100 µg/ml streptomycin and 10% (v/v) FCS.

2.1.2 Cell Sub-culture

On attaining confluence, cells were sub-cultured 1:3 and either maintained for further experiments or cryopreserved, as described below. Typically, a 75cm^2 culture flask was treated with 5 ml 0.05% v/v Trypsin EDTA (Sigma, #T3925) and incubated at 33°C for 3 minutes before flasks were agitated to encourage detachment of cells. Equal volume FCS was added to flasks to neutralise protease activity and cell suspension collected and centrifuged at 500 g for 5 minutes, at room temperature. Cells were re-suspended in appropriate volume of media for reseeding requirements. Cell passages P5-P20 were used in this work.

2.1.3 Cryostorage

For cryostorage of podocytes, cells were pelleted as above and re-suspended in 500 µl FCS, 400 µl RPMI medium and 100 µl DMSO (Sigma, #D2650) to total 1 ml volume and stored in passage-labelled cryovials at -80°C for 24 hours before transfer to liquid nitrogen (-150°C) for long term storage. Cryopreserved cells were revived by rapid thawing in a 37°C water bath.

2.2 Cell counting

2.2.1 Beckman Coulter Counter

Cells were counted using a Beckman Coulter Particle Count and Size Analyser. For each cell count, 20 µl of cell suspension was added to 20 ml of Coulter Isoton diluent. An average of three counts was used to calculate cell number in accordance with the following equation:

Average cell count x 1000 = cell/ml

2.2.2 Haemocytometer

Haemocytometry was employed during the pelleting of cells in Cell-to-Ct™ experiments (Chapter 5). 16 µl cell suspension was pipetted into the middle chamber of the haemocytometer. The number of cells counted in each of the 4 quadrants was averaged (excluding cells traversing the bottom and right borders of the counting squares) and used to calculate total number of cells in accordance with:

Mean no. of cells per grid x 10^4 = No. of cells/ml

2.3 In vitro Cell Assays and Stimulations

2.3.1 Normal insulin response *in vitro*

For short-term insulin stimulation, culture medium was replaced with serum- and insulin-free RPMI-1640 for 4-6 hours, and podocytes were challenged with human insulin (Tocris) at 100 nmol/l for 15 mins.

2.3.2 Induction of insulin resistance *in vitro*

To induce insulin resistance, podocytes were cultured in RPMI-1640 containing 25 mM Glucose (Sigma), 100 nM insulin (Tocris) and 1ng/ ml Recombinant human IL-6 and TNF-α (Biotechne #210-TA-005 and 206-IL-010) throughout the differentiation period (10 days). Fresh media was applied to the cells every 2/3 days.

2.3.3 Radiolabelled Glucose Uptake Assay

Podocytes grown in 12-well plates were serum-starved for 4-6 hours and then washed x 3 in filtered PBS before addition of 0.45 ml per well of modified Krebs Ringer Phosphate (KRP) buffer (Table 2.1) for 15 minutes at 37°C. The cells were then transferred to a 37°C water bath, and challenged with 100 nM insulin for 15 minutes. Radiolabelled glucose, purchased from Perkin Elmer (Deoxy-D-Glucose, 2-(1,2-3H(N)) #NET328A250UC) was added drop-wise to a final concentration of 50 µM (0.5 µCi per well) and incubated for 5 minutes. Cells were washed with ice cold PBS x 3 to halt glucose uptake, and solubilised in 0.5 ml 1% (v/v) Triton X-100 in PBS. The solubilised cell suspension was then added to 2ml scintillant fluid and vortexed. β-Emission was measured by Tri Carb liquid Scintillation Analyser (Perkin Elmer).

Component	Concentration	Volume
Calcium-free KREBS salts:	1.36 M NaCl 47 mM KCl 125 mM $MgSO_4$	5 ml
2 x Sodium Phosphate Buffer:	10 mM NaH_2PO_4 10 mM Na_2HPO_4 (pH 7.3)	25 ml
$NaHCO_3$	2 mM	50 µl 2M stock
HEPES	25 mM	1250 µl 1M stock
$CaCl_2$	12.5 mM	5 ml
dH_2O		Up to 50 ml

Table 2.1. Components of modified KRP buffer used in glucose uptake experiments.

2.3.4 Alamar Blue Assay

To assess podocyte viability prior to/during experimental stimulation of cells, medium was removed from each well and replaced with 1 ml of RPMI- medium containing 10% (v/v) Alamar blue reagent (Thermo Fisher Scientific, #DAL1025). Control wells contained medium and 10% alamar blue only. Samples were incubated for 30 minutes at 37°C. 100 µl of medium from each well was then transferred into a black 96-well plate in duplicate and analysed by fluorescent spectroscopy with wavelengths of 544nm excitation and 590nm emission using the Fluostar Optima Spectrometer. Fluorescence reads were calculated relative to non-treated control wells. The assay utilises an oxidation-reduction (REDOX) indicator, resazurin, which undergoes colorimetric change in response to cellular metabolic reduction. The reduced form (resorufin) is pink and highly fluorescent, and the intensity of fluorescence produced is proportional to the number of living cells respiring, thus enabling quantitative measurement of cell viability and cytotoxicity.

2.4 Immunofluorescence Staining and Imaging

Podocytes were transfected and stimulated as indicated in 8-well chamber slides before fixation in 4% (v/v) paraformaldehyde (PFA) in PBS, 100 µl per well, for 15 minutes. Cells were permeabilised with 0.1% (v/v) Triton-X100/PBS and washed x 3. Phalloidin-iFlour 488 (abcam, #ab176753) was prepared in PBS and 1% (w/v) BSA as per manufacturers instruction and 100 µl added to each well and incubated for 60 minutes. Cells were washed with PBS x 3 before application of DAPI stain (Thermo Fisher Scientific #62248), 1 µg/ml prepared in PBS, applied at 1:5000 dilution, for 5 minutes, to achieve nuclear staining. After 3 further PBS washes, Gold Antifade Mountant (Thermo Fisher Scientific #P36930) was applied to the slide and coverslip sealed. Slides were read using the Zeiss LSM880 Airyscan confocal microscope.

2.4.1 Semi-automated immunofluorescence imaging

Semi-automated immunofluorescence imaging and quantification was performed using the IN Cell Analyzer imaging platform and workstation 3.5 analysis software (GE Healthcare, Amersham, UK). Cells were grown in Corning 96-well Black microplates (Sigma, CLS3904) and stimulated as required before 4% (v/v) PFA in PBS fixation (100 µl per well) for 15 minutes. Alexa Flour-488 Phalloidin stain (Thermo Fisher Scientific #A12379) was added at 1:200 dilution in an antibody buffer of 1X PBS, 1% (w/v) BSA and 0.3% (v/v) Triton-X100 and incubated overnight at 4°C. Cells were DAPI stained as previously (1:5000 for 5 minutes) and washed in PBS x 3. 200 µl fresh PBS was applied to wells immediately prior to machine reading. Mean fluorescence intensity of the phalloidin staining in the central (nuclear) region (expressed as arbitrary fluorescence units, AFU) was used for quantification. Cells considered to have undergone insulin-stimulated actin remodelling were defined as those with a loss of defined central F-actin structures, i.e. a movement of F actin from central to cortical cell regions, above a threshold level of 5% (degree of variation that may be expected to occur by chance). 3 technical replicates were performed within each experiment, with 4 fields of view per well; yielding data for approximately 3000 cells per condition, per experiment.

2.5 RNA work

2.5.1 RNA extraction by TRI reagent

Total RNA was extracted from cultured/cell-sorted podocytes using Tri Reagent™ (Thermo Fisher Scientific #AM9738) according to manufacturers protocol. Briefly, cells were lysed using 1ml of Tri Reagent per well of a 6-well tissue culture plate (scaled accordingly for smaller well plates). Samples were subsequently transferred to a 1.5 ml micro-centrifugation tube and incubated at room temperature for 5 minutes to enable nucleoprotein complex dissociation. 200 µl of chloroform was added per 1ml of Tri Reagent used and agitated by inversion for 15 seconds. After incubation at room temperature for 5 minutes, samples were centrifuged at 12,000 g for 15 minutes at 4˚C. This results in sample separation into 3 distinct phases: a lower red phenol phase, a white interphase and a top aqueous phase. The latter was carefully pipetted into a new 1.5 ml eppendorf and 500 µl of isopropyl alcohol added to each sample and vortexed. Following an incubation period of 15 minutes at room temperature, samples were centrifuged at 12,000 g for 10 minutes at 4˚C. The RNA pellet was then washed with 75% ethanol (equivalent volume as Tri-Reagent used) before being vortexed and re- centrifuged at 7500 g at 4˚C for 5 minutes. This process was repeated to a total of 3 washes. Following the final wash, ethanol was carefully pipetted off and the pellet air-dried for 30 minutes. 10-16 µl of RNase-free water was added to solubilise the pellet. Purified RNA samples were quantified (ng/µl), using a Nanodrop 3300 Fluorospectrometer (Thermo Fisher Scientific), (see 2.5.4). The volume required for 1 µg of sample was quantified using the following equation:

$$\mathbf{1000 / (Total\ RNA\ ng/\mu l)}$$

2.5.2 RNA extraction from cells using miRnEasy micro column extraction kit

For low yield samples, such as flow sorted podocyte and glomerular RNA extractions, RNA was extracted in accordance with Qiagen miRnEasy micro kit protocol (Qiagen, #217084). No greater than 1 x 10^6 cells were pelleted by centrifugation, 300 g at 20˚C for 5 minutes. Glomerular preparations transferred

in RNA later (Thermo Fisher Scientific) were placed in a magnetic holder to pull dynabead-containing glomeruli to the eppendorf side whilst RNA later was removed by pipetting. 700 ul Qiazol was added directly to cell pellets/glomeruli and cells were disrupted and homogenised by vortexing for 1 minute. Homogenate was incubated at room temperature for 5 minutes to promote nucleoprotein complex dissociation, before addition of 140 µl of chloroform and inversion of the sample for 15 seconds. After a further incubation at room temperature for 3 minutes, samples were centrifuged at 12,000 g at 4˚C for 15 minutes. Aqueous phase was transferred into a fresh eppendorf as above, and 1.5 x the volume removed in this stage of 100% ethanol was added to each sample and pipette mixed. 700 µl of sample was then added to the miRnEasy MinElute spin column and centrifuged at 10,000 g at 20°C for 15 seconds. Flow-through was discarded and the above repeated with any remaining sample. 700 µl of Buffer RWT (provided in miRneasy kit) was then added to the spin column and centrifuged at 10,000 g at 20°C for 15 seconds and flow-through discarded. This was repeated using 500 µl of Buffer RPE. 500 µl of 80% ethanol was then added to the spin column and centrifuged at 8000 g at 20°C for 2 minutes, and the spin column transferred to a new 2 ml collection tube to enable drying by centrifugation at 10,000 g at 20°C for 5 minutes, with the column lid in the open position. The columns were further air dried for 5 minutes before adding 10 µl of RNase-free water (minimum elution volume used) to solubilise RNA.

2.5.3 RNA extraction from urine using miRnEasy micro column extraction kit

For the extraction of miRNAs from patient urine, 20 ml of (second pass) morning urine was obtained and processed immediately. Samples were centrifuged at 2000 g for 10 min at 4 °C, and supernatants transferred to universal containers. RNA was isolated using the miRNeasy kit as detailed above, with the following protocol amendments: 1 µg Carrier RNA (MS2 RNA; Roche Diagnostics Limited, Burgess Hill, West Sussex, UK) was added to 350 µl of urine sample. 0.5 pM Caenorhabditis elegans miR-39 (Life Technologies, Thermo Fisher Scientific, #MC10956,) spike-in control was subsequently added to permit confirmation of extraction efficiencies across samples. 750 µl Qiazol was added per sample, inverted to mix and incubated at room temperature for 5

minutes before addition of 200 µl chloroform. Samples were incubated at room temperature for 3 minutes, then centrifuged at 12,000 g at 4˚C for 15 minutes. Aqueous phase from each sample was loaded onto a single affinity column and processed further in accordance to manufacturers guidelines, as above.

2.5.4 RNA quantification and quality control

Following extraction, RNA was quantified and assessed for contaminants using the Nanodrop 3300 Fluorospectrometer (Thermo Fisher Scientific). A ratio of the absorbance at 260 nm and 280 nm (A_{260nm}/A_{280nm}) was used to detect presence of (predominantly) protein contaminants; ratios of ~2.0 were deemed to represent "pure" RNA, lesser ratios being indicative of sample contamination. A_{260nm}/A_{230nm} ratio was used as a second indicator of nucleic acid sample purity, with ratios of ~2.0 – 2.2 accepted as "pure" RNA, and lesser values indicative of contaminants strongly absorptive at the lower wavelength of 230 nm, such as phenol, TRI-reagent itself, and EDTA. All RNA samples utilised had ratios of at least 1.5, thus minimising risk of RNA concentration overestimation and/or interference in downstream analysis. Due in part to the inaccuracies of the Nanodrop at the lower end of the RNA detection range (for flow sorted podocyte fractions particularly- usable range of the Nanodrop is between 0.4 - 15,000 ng/µl), but also because of the need to ascertain excellent RNA quality prior to miRNA/RNA sequencing experiments, the Agilent 2100 Bioanalyser was also employed to analyse RNA samples. This was performed by the Central Biotechnology Service (CBS) of Cardiff University, using either a nano-chip or pico-chip, depending on the predicted RNA concentration (RNA 6000 Pico assay detection range being 50 – 5000 pg/µl). The Agilent 2100 Bioanalyser uses a microfluidics-based platform for sizing, quantification and quality control of RNA, which includes a read out of RNA Integrity number (RIN), ranging from 1 (wholly degraded RNA) to 10 (wholly intact RNA). The RIN is calculated using an algorithm that factors in the ratio of fluorescence detection of the 18S:28S ribosomal subunits (which falls with RNA degradation), in addition to other electropherogramatic features as shown in Figure 2.1 below. RNA samples with RIN value >7 were considered of adequate quality for downstream sequencing experiments.

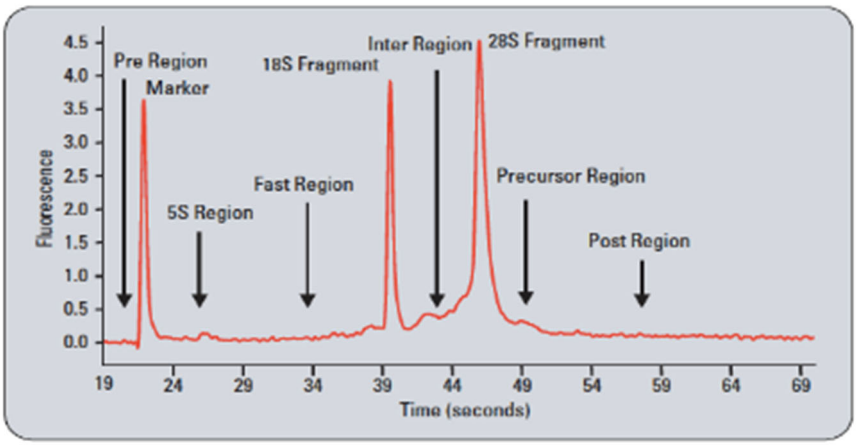

Figure 2.1 Electropherogram detailing indicators of RNA purity. RNA degradation is indicated by loss of signal intensity for ribosomal band 28s, followed by loss of 18s, and increase in baseline signal in the inter region. Signal in the Fast region indicates how fast degradation has occurred. (Adapted from Agilent Technologies, USA (285))

2.6 RNA Detection

MiRNA size (~ 22 nt) and absence of polyA tail preclude the use of RT-qPCR kits designed for the detection and amplification of mRNAs. MiRNA detection necessitates use of a miRNA-specific RT primer that contains nucleotides complementary to the mature miRNA 3' end, and an additional long unrelated sequence. This unrelated component forms a stem-loop structure that cannot interact with non-specific molecules in the RT reaction including pre- and pri-miRNA, hence determining assay specificity. Methods of miRNA and mRNA detection employed in this work are detailed below.

2.6.1 MicroRNA Reverse Transcription

MiRNA reverse transcription (RT) was performed using the High-Capacity cDNA Reverse Transcription Kit (Thermo Fisher Scientific, #4368813). RT master mix contained: 4.16 µl RNAse-free water, 1.5 µl 10x Reverse Transcription Buffer, 0.15 µl 100 mM deoxynucleotide triphosphates (dNTP), 0.19 µl 40 U/µl RNase Inhibitor (New England BioLabs® Inc, #M0307S), 1 µl 50 U/µl MultiScribe Reverse Transcriptase and 3 µl of 5x miRNA RT-primer specific (listed in Table 2.2). 10 µl of RT master mix was added to 5 µl of RNA (10 ng). RT non-template control (RT-NTC) contained 5ul water as RNA substitute. Thermal cycling conditions used were as below (Table 2.3). Generated cDNA was diluted with 30 µl RNAse-free water (1:2 dilution) prior to RT-qPCR.

Gene	Taqman Assay ID (Life Technologies, Thermo Fisher Scientific)
mmu-miR-222-3p	002276
mmu-miR-146a-5p	000468
mmu-miR-155-5p	002571
mmu-miR-204-5p	000508
mmu-miR-497-5p	001346
mmu-miR-338-3p	002252
U6 snRNA	001973
Nephrin (NPHS1) mmu	Mm00497822_g1
Podocin (NPHS2) mmu	Mm01292252_m1
PECAM 1 mmu	Mm01246166_m1
PDGFRβ mmu	Mm00435546_m1
Eukaryotic 18s rRNA	4310893E

Table 2.2. Taqman assays used

Stage	Temp	Time
Annealing stage	16°C	30 min
Extension stage	42.5°C	30 min
Dissociation stage	85°C	5 min
Cooling stage	4°C	Indefinitely

Table 2.3 Thermal Cycling conditions for miR RT

2.6.2 Random Primer Reverse Transcription

For mRNA detection, RT was carried out using the random primer method with the High-Capacity cDNA Reverse Transcription Kit used in 2.6.1 above. 125 ng-1 µg of RNA (made up to a final volume of 10 µl with RNase-free water) was combined with an RT master mix consisting of: 2.0 µl 10X random primers, 0.8 µl 25x 100mM dNTPs, 1 µl RNase inhibitor, 2 µl 10X RT buffer, 1 µl Multiscribe and 3.2 µl RNase-free water; total RT reaction volume of 20 µl. RT-no template control (NTC) contained 10 µl of water as a substitute for RNA. Thermal Cycling conditions used were as below (Table 2.4). Generated cDNA was diluted with 60 µl RNAse-free water (1:3 dilution) prior to RT-qPCR.

Stage	Temp	Time
Annealing stage	25°C	10 min
Extension stage	37°C	120 min
Dissociation stage	85°C	5 min

Table 2.4 Thermal cycling conditions for random primer RT

2.6.3 Real time Quantitative Polymerase Chain Reaction (RT-qPCR)

Both Taqman and Syber Green technologies were employed for the amplification and detection of miRNAs and mRNAs. The Taqman probe contains a fluorescent reporter dye and quencher dye at the 5′ and 3′ ends, respectively. When the probe is intact, the proximity of the reporter dye to the quencher results in repression of reporter fluorescence. During the PCR reaction, the probe is cleaved, thus spatially separating the dyes and relieving the quencher repression to allow reporter dye detection. Advantages of the Taqman method include a greater specificity in primer-probe binding and amplification, and the ability to multiplex (i.e., detect more than one gene in the same sample by using different reporters, such as VIC, JOE, FAM etc.). Syber Green is an intercalating dye that binds directly to dsDNA. As the number of double stranded amplicons in the PCR reaction increases, so the binding of the

dye will increase and hence fluorescence detected is proportional to the gene product. Because Syber Green will bind to any dsDNA, the reaction is far less specific than above, and melt curves must be carefully examined for the presence of non-specific PCR product/ primer-dimer interference.

2.6.3.1 Taqman RT-qPCR

MiRNA/mRNA gene analysis was performed using RT-qPCR, combining 1 µl of miRNA/mRNA specific PCR primers and TaqMan probe, 5 µl of water and 10 µl of Universal PCR Master Mix consisting of an optimised and thermostable solution of DNA polymerase, deoxynucleotides, and passive reference dye ROX (Thermo Fisher Scientific, #444040). 16 µl of miRNA specific master mix and 4 µl of (1:2) diluted cDNA, diluted RT-NTC or water (qPCR-NTC) were added to wells of an Optical 96-Well Fast Plate (Thermo Fisher Scientific, #4346906) and sealed using MicroAmp Optical Adhesive Film (Thermo Fisher Scientific, #4311971). U6 was used as reference gene in all miRNA PCR experiments. For mRNA, 18s rRNA was employed as a reference gene. ViiA7 Real-Time PCR System (Thermo Fisher Scientific #4453534) was configured as per manufacturer's recommendations: 10 min at 95°C, 40 cycles of 15 secs at 95°C and 1 min at 60°C.

2.6.3.2 Power SYBR Green RT-qPCR

Primers were custom designed using Primer-BLAST (286) using search specifications of product length 70-150 base pairs, spanning exon-exon junction, self complementarity score less than 3 (where possible). Power SYBR Green PCR Master Mix (Thermo Fisher Scientific #4367659) was used as follows: 10 µl of Power SYBR Green PCR Master Mix, 0.6 µl of 10 µM custom-designed forward primer and 0.6 µl of 10 µM custom-designed reverse primer, 4.8 µl RNAse-free water plus 4 µl of 1:3 diluted cDNA (total PCR reaction volume 20 µl). qPCR-NTC wells contained water as a substitute for cDNA. Both U6 and/or β-Actin were used as endogenous reference genes. Expression analysis was carried out using the ViiA-7 Real Time PCR System as above. Melt curves for custom-designed primers were examined to rule out the existence of non-specific amplicons in the reaction. A representative melt curve is shown in Figure 2.2

A.

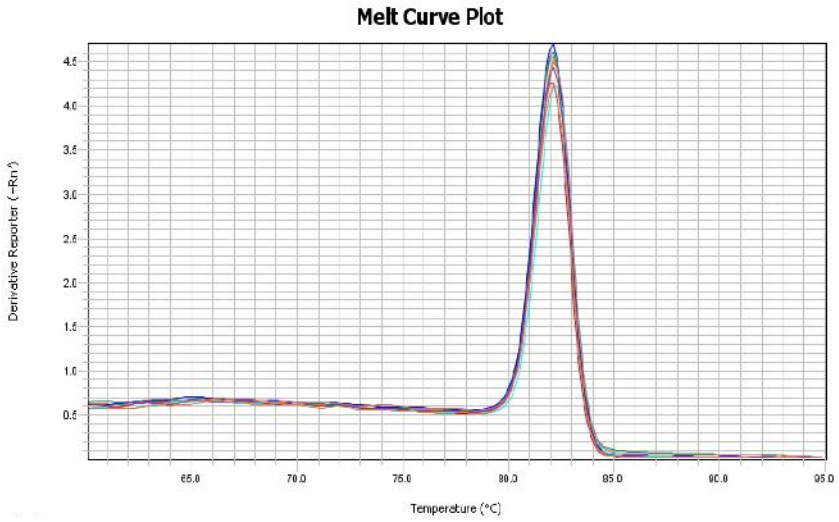

B.

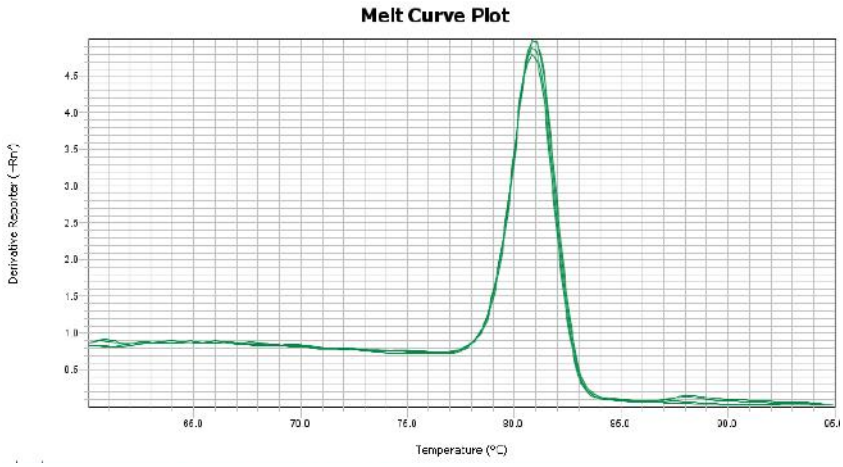

Figure 2.2. Melt curves derived from custom-designed primers A) CSF1R B) PIK3R1. Melt curves identify the temperature at which dsDNA strands separate. Tm (melting temperature) represents the temperature at which 50% of strands are hybridised. Tm is sequence specific, and therefore multiple peaks on the melt curve are indicative of unwanted PCR products, such as primer dimers.

Gene	Direction	Primer sequence
CD2AP	Forward	AGGATCATGGGAAAGAACTGGA
	Reverse	GGTCCACACCACCTCAAGAC
Synaptopodin	Forward	CTGGGATGTAGTGAAGGCCG
	Reverse	GCCCAACGCTGGTTTCTG
Beta Actin	Forward	GACAGGATGCAGAAGGAGATTACT
	Reverse	TGATCCACATCTGCTGGAAGGT
RhoA	Forward	CCGTCGGTTCTCTCCATAGC
	Reverse	TCTCAGATGCAAGGCTCAAGG
SHIP-1/ INPP5D	Forward	AAGAATGGTCCTGGCACTGT
	Reverse	TGGTCTTCAGTGTGGCGTAG
PIK3R1	Forward	ATAGAAATGGATCCACCAGCAC
	Reverse	TTCACTTCTTCCCTTGAGATGT
SOCS1	Forward	GTCCTGCCGCCAGATGAG
	Reverse	GAGACAGAGGCAGTGAGCC
MAP3K10	Forward	GAACAAGCTGACGCTACCCA
	Reverse	CCAGCATTCCTCCAGTAGGC
CSFR1	Forward	GAAGCACCCTGACCACAAGA
	Reverse	GTGGGCCGGATCTTTGACAT
PODN	Forward	GCCCAGTCTTCGGTGTGTAA
	Reverse	CCACAAGCTTATCTGTTAAGAGCAG
PDK4	Forward	AGCCCTGTCAGAGTTTGTAGAC
	Reverse	TGCCTTGAGCCATTGTAGGG
NGEF	Forward	CAGGACCGTGGATGGGAAAG
	Reverse	CTTCATCAGTTTTCAGTGCTGCC
INSR	Forward	GACGGCTGTGCCATTGCTGGT
	Reverse	CCATACCAGGGCACACCTCTCCA

Table 2.5. Custom designed Syber Green RT-qPCR primers used

2.6.3.3 Relative Quantification

Relative quantification was calculated using the comparative CT method. The cycle threshold (CT) value of the reference gene was subtracted from the CT value of the target gene in order to obtain a delta CT (dCT) value. The mean dCT was then calculated for control experiments. The relative quantification (RQ) for the experimental target genes was then calculated as below (287) :

2^- (dCT(Experimental Target) - dCT(Mean Control Group))

2.7 MicroRNA Hybridisation array

Conditionally immortalised podocytes were rendered insulin resistant as described in 2.3 above, and RNA extracted and quantified as described in 2.5. MiRNA profiles of the insulin resistant samples (n=5) were compared to insulin-responsive Wild type (WT) podocytes grown under standard culture conditions (n=5), using Exiqon miRCURY LNA™ Array (7th Gen). 1 µg of RNA was used per sample. The assay was performed by Exiqon services in Denmark, according to manufacturers instruction. Briefly, samples were labelled using the miRCURY LNA™ microRNA Hi-Power Labelling Kit, Hy3™/Hy5™ and hybridised on the miRCURY LNA™ microRNA Array (7th Gen). A normalisation step was performed to account for background signal (non-specific binding, dye and spatial bias), with background threshold calculated for each individual microarray slide as 1.2 times the 25th percentile of the overall signal intensity of the slide. Lowess regression algorithm was utilised to perform supervised and unsupervised data analysis to cluster samples into groups, based on miRNA expression profiles, as detailed further in Chapter 3.

2.8 Urinary microRNA profiling by TaqManArray Human MicroRNA cards

Urine samples from diabetic and control patients were obtained, by myself, from consenting patients in renal and diabetic outpatient clinics. Urinary microRNA profiles were analysed by Dr Kate Simpson of the Wales Kidney Research unit, by use of low-density Taqman Array (TLDA) cards, as previously

described (236). Briefly, samples were reverse transcribed using the Megaplex Primer Pools (Human Pools A version 2.1 and B version 3.0; Thermo Fisher Scientific) and products amplified using Megaplex PreAmp Primers (Primers A version 2.1 and B version 3.0; Thermo Fisher Scientific). Samples were diluted to a final volume of 100 µL, and pooled to control for sex, age and eGFR, accordingly. TaqManArray Human MicroRNA Cards A version 2.1 and B version 3.0 (Thermo Fisher Scientific) were used to quantify 754 human miRNAs. RT-qPCR was performed on an Applied Biosystems 7900HT thermocycler (Thermo Fisher Scientific) as per manufacturer's recommendations.

2.9 Next Generation Sequencing (NGS)

NGS was employed to interrogate the miRNA and mRNA transcriptomes of whole glomeruli from the db/db mouse model. Rationale and optimisation steps for the chosen sequencing platform are provided in Chapter 5.

2.9.1 Small RNA Sequencing (smRNAseq/miRseq)

Two small RNA library preparation kits were employed in this work; the first method using Illumina TruSeq®, performed and optimised in house, the second kit (NEB) was used by the Wales Gene park in the outsourced sequencing experiments, detailed further in Chapter 5.

Illumina TruSeq® small RNA library preparation kit (#RS-200-0012) was used in accordance with manufacturers guidelines. A modified workflow is depicted in Figure 2.3. Firstly, adapters were ligated to the 3' and 5' ends of each sample. 1 µl of 3' adapter was pipette mixed with 200 ng- 1 µg of RNA in 5 µl nuclease-free water and incubated on the thermal cycler for 2 minutes at 70°C. A mix of 2 µl of HML ligation buffer, 1 µl RNAse inhibitor and 1 µl T4 RNA Ligase 2, Deletion mutant (at 200U/ µl) was mixed and centrifuged before addition of 4 µl of the adapted 3' RNA mixture (RA3); total volume 10 µl per sample. This was incubated on the thermal cycler for 60 minutes at 28°C. 1 µl stop solution was added and pipette mixed before continuation of incubation at 28°C for a further 15 minutes. To ligate the 5' adapter, 1 µl of RA5 was preheated to 70°C in a new 200 µl PCR tube on the thermal cycler to for 2 minutes, before addition of 1 µl ATP and 1 µl T4 RNA ligase. 3 µl of this mix was added to the previous RA3

mixture (total volume per sample 14 µl) and pipette mixed before incubating at 28°C for 60 minutes. All samples were placed on ice immediately after retrieval from the thermal cycler.

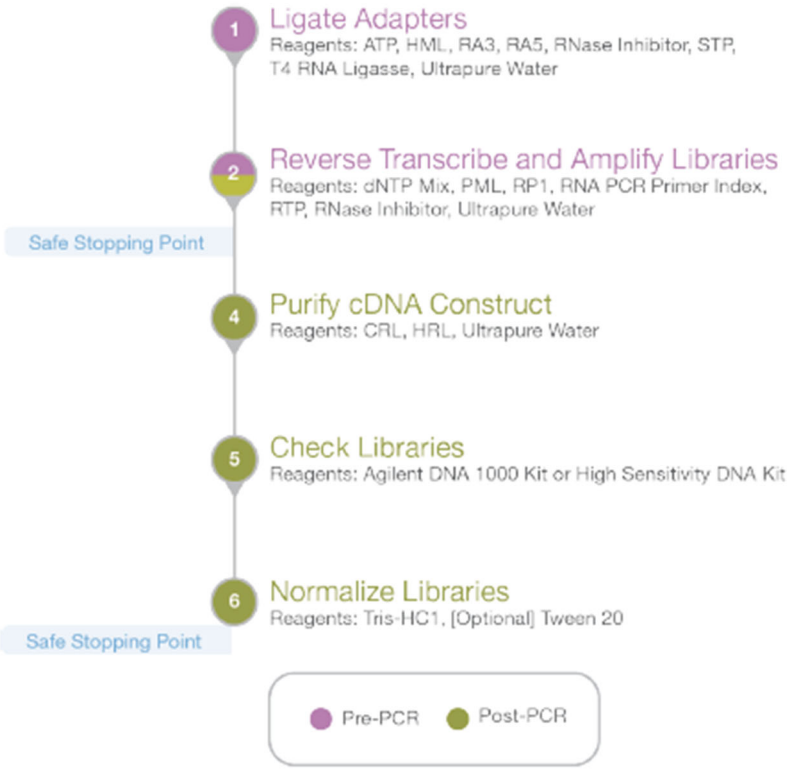

Figure 2.3 Work Flow through Illumina TruSeq® small RNA library preparation kit, adapted from Illumina Small RNA Library Prep Reference guide, 2016 (288).

Reverse Transcription was performed as follows: 6 µl of adapter-ligated RNA was transferred to a new PCR tube strip. 1 µl of RNA RT primer was added, mixed and centrifuged and incubated in the thermal cycler for 2 minutes at 70°C. A mastermix of 2 µl First Strand buffer, 0.5 µl 12.5 mM dNTP mix, 1 µl 100 mM Dithiothreitol (DTT), 1 µl RNAse inhibitor, and 1 µl Superscript II Reverse Transcriptase was pipette mixed and 5.5 µl of this was added to the adapter-ligated RNA/primer mix (total volume 12.5 µl). This was incubated on the thermal cycler for 60 minutes at 50°C, then placed immediately on ice.

PCR mastermix for library amplification was made up as follows: 8.5 µl ultrapure water, 25 µl PML PCR mix, 2 µl RP1 RNA PCR primer and 2 µl of selected labelling index for that sample (total volume per library 37.5 µl). After

pipette mixing and brief centrifuge, 37.5 µl of this mastermix was added to the adapter-ligated RNA and PCR performed in accordance with the below settings (Table 2.6):

Cycle No.	**Temp**	**Time**
1	98°C	30 secs
11	98°C	10 secs
	60°C	30 secs
	72°C	15 secs
1	72°C	10 minutes
HOLD	4°C	

Table 2.6 PCR cycling settings for Illumina TruSeq® Small RNA library preparation

Size selection of cDNA was performed using BluePippin machine (Sage Science), as per manufacturers protocol. Collection mode target was set at 150 base pairs (bp). 30 µl sample was mixed with 10 µl of marker and loaded into the cassette sample wells, and elution buffer removed and replenished as advised in the protocol. 40 µl of eluate was placed into a 96 well plate and mixed with magnetic purification beads (AMPureXP, Beckman Coulter, Fisher Scientific #10136224) in a 1.8:1 (v/v) ratio and incubated at room temperature for 5 minutes before placing in a magnetic holder. Once the DNA-bound beads were clearly visible against the well wall and solution clear, the supernatant was carefully pipetted off, and the beads were washed in 80% ethanol x 2. Beads were air dried for approximately 5 minutes, and DNA was eluted in 10 µl re-suspension buffer. Purified samples were analysed on a high sensitivity DNA chip using the Agilent 2100 Bioanalyser. DNA with final molarity >1500 pmol/L was used for final sequencing.

Sequencing runs were performed by external providers within Cardiff University, using the HiSeq 4000 sequencing system (Illumina). This system permits parallel base-by-base sequencing of millions of DNA fragments ("high through-put") using a reversible terminator-based method that detects individual bases as they are incorporated into growing DNA strands. A

fluorescently labelled terminator is imaged as each dNTP is added and then cleaved to allow incorporation of the next base.

2.9.2 Total RNA Sequencing (RNAseq)

All mRNA sequencing, and glomerular miRNA sequencing was outsourced to the Wales Gene Park, Cardiff University. NEB Next® Small RNA Library Preparation kit (New England Biolabs #E7330) (100 ng RNA input/sample) and NEBNext® Single cell/low input RNA Library Preparation kit (#E6420) (5 ng RNA input/sample) were used for microRNA and whole RNA sequencing, respectively, in accordance with manufacturers' protocols. The technical variations and merits of these library preparation kits are discussed further in Chapter 5.

2.10 Protein Work

2.10.1 Protein extraction

Experiments were carried out in 6-well cell culture plates. 75 µl of ice-cold Radio Immunoprecipitation Assay (RIPA) buffer (Santa Cruz, Biotechnology, USA), containing 10 µl of 100 mM sodium orthovandate, 10 µl of 200 mM phenylmethylsofonyl fluoride (PMSF) and 10 µl of 200 mM protease cocktail inhibitor per 1 ml of RIPA buffer used, was added directly to PBS-washed cells. 2 wells were combined per sample and 150 µl total of protein lysate was collected and stored at -80°C until further analysis.

2.10.2 Protein Quantification

2.10.2.1 Bradford Assay

In early experiments, protein was quantified using the Bradford Assay method (Bio-Rad Laboratories Inc.). Samples were diluted 5µl:125µl with Bradford Assay. Quantification was performed in triplicate using absorbance spectroscopy (Fluostar Optima Spectrometer), with wavelengths of 620nm excitation and 590nm emission. Serial dilutions of bovine serum albumin (BSA) were used as standard reference samples. 2nd Polynomial fit was employed in analysis of data. This method proved unreliable in early experiments, leading to

inconsistent protein loading, possibly due to cross reactivity of the assay and the RIPA buffer.

2.10.2.2 BCA Assay

Pierce ™ BCA Protein assay (Thermo Fisher Scientific #23225) was adopted for protein quantification post 2017. The working range of this assay is 125-2000 µg/ml. Working reagent (WR) volume was calculated as below:

(#standards + #samples) x (#replicates) x 200 µl = total volume WR

BCA reagent A (containing sodium carbonate, sodium bicarbonate, bicinchoninic acid and sodium tartrate in 0.1M sodium hydroxide) was mixed with BCA reagent B (4% cupric sulphate) in a ratio of 50:1. Samples were diluted to a concentration within the working range of the assay (usually in a 1:3 dilution) and 10 µl of each standard/sample was pipetted into a 96-well microplate and pippete-mixed with 200 µl of WR. The plate was covered and incubated at 37°C for 30 minutes, before measurement of absorbance at 562nm on the Fluostar Optima Spectrometer as described above.

2.10.3 SDS-PAGE/Western Blot Analysis

Protein separation and identification was performed by SDS-PAGE/Western blot, using a BioRad Mini Protein II apparatus (Bio-Rad Laboratories). 20-30 µg of sample was heated at 95°C for 5 min with 1/3 reducing buffer (pre-prepared and containing 2.4 ml glycerol, 4.8 ml 10% SDS (w/v), 1 ml 0.5 M Tris (pH 6.8), 1.2 ml β- Mercaptoethanol and 2 drops of 0.05% (w/v) Bromophenol Blue). A total volume of 40 µl sample/reducing buffer was loaded into the wells of a 7.5% polyacrylamide gel, made up as shown (Table 2.7). A Chemiluminescent protein ladder was loaded on each gel (LI-COR Biosciences, USA). To separate the proteins, electrophoresis was carried out at 100 V for 20 min followed by 150 V for 40 min under reducing conditions. Following electrophoresis, samples were transferred at 100 V for 70 minutes onto a nitrocellulose membrane (GE Healthcare, UK). Running and transfer buffers were made up as shown in Table 2.8. To prevent non-specific binding, the nitrocellulose membrane was blocked with 5% (w/v) powdered milk in 0.1% (v/v) Tween/PBS for 1 hour. The

membrane was then washed in 0.1% (v/v) Tween/PBS three times for 5 minutes. The primary antibody of interest was diluted in 0.1% (v/v) Tween/PBS, containing 1% (w/v) BSA and applied to the membrane overnight at 4°C (antibodies and concentrations used shown in Table 2.9). The membrane was then washed before the addition of the secondary antibody, conjugated to horseradish peroxidase (HRP), diluted in 0.1% (v/v) Tween/PBS containing 1% (w/v) BSA. Following a further wash step, Enhanced Chemoluminescence (ECL) detection reagent (GE Healthcare #RPN2232) was applied to the membrane for 1 minute before reading on C-Digit Western blot scanner (LI-COR Biosciences). Normalisation of protein loading was performed using the densitometry analysis function, relative to β Actin/ GAPDH, and/or to total protein levels in the case of phosphorylated proteins. Membranes were stripped by incubation for 10 minutes using a solution containing Glycine 15 g, 10 ml 10% (w/v) SDS, 0.1% (v/v) Tween in 1 L water, at pH 2.2, and re-blocked and re-probed as above.

Component	Volume
dH_20	9.9 ml
Resolving buffer 1.5 M (Tris 18.5g/100ml dH_20, pH 8.8)	4.5 ml
10% SDS	180 µl
40% Acrylamide	3.37 ml
10% Ammonium Persulphate	90 µl
Tetramethylethylenediamine (TEMED)	12 µl

Table 2.7. Constituents of 7.5% polyacrylamide gel used for Western Blot.

Component	Running Buffer	Transfer Buffer
Tris-HCL	30g/L	30g/L
Glycine	144g/L	144g/L
10% SDS	10g/L	n/a
pH	8.3	n/a

Table 2.8 Constituents of Running and Transfer buffers (10X) for Western blotting.

Antibody Target	Type & Host	Supplier & Catalogue No.	Dilution
Synaptopodin (H-140)	Polyclonal-Rabbit	Santa Cruz sc-50459	1:1000
CD2AP (H-290)	Polyclonal-Rabbit	Santa Cruz sc-9137	1:1000
Nephrin	Polyclonal-Sheep	R&D AF4269-SP	1:1000
SV40	Monoclonal-mouse	Gene Tex GTX 16879	1:1000
Phospho-AKT (Ser473)	Monoclonal-Rabbit	Cell Signalling 4060s	1:2000
Total AKT	Monoclonal-Rabbit	Cell Signalling 9272s	1:1000
Phospho-p44/42 MAPK (ERK 1/2) (Thr202. Tyr 204)	Monoclonal-Rabbit	Cell Signalling 4377s	1:1000
Total p44/42 MAPK (ERK1/2)	Monoclonal-Rabbit	Cell Signalling 4695s	1:1000
Beta Actin	Monoclonal-Mouse	Cell Signalling 3700s	1:10,000
GAPDH	Monoclonal-Mouse	Abcam Ab8245	1: 1000
Insulin Receptor β	Monoclonal-Rabbit	New England Biolabs 3025s	1: 1000
Anti-Mouse-IgG HRP	Polyclonal-Goat	Abcam ab205719	1: 5000
Anti-Rabbit-IgG HRP	Polyclonal-Goat	Abcam Ab205718	1: 5000

Table 2.9 Antibodies and dilutions used in Western Blot experiments

2.11 Glomerular Isolation

2.11.1 Glomerular Perfusions

Glomerular isolations were performed by the Coward lab, Bristol Renal Academic unit, as described previously (289). Briefly, terminally anaesthetised mice were injected with 10 ml of 8 x 10^7 dynabeads in Hanks' balanced salt solution (HBSS) directly into the left ventricle via butterfly needle. Kidneys were subsequently removed, minced and digested in 1.5 ml 1mg/ml collagenase A and incubated for 30 minutes at 37°C, before passing through 100 µm cell strainer. Filtrate was further washed with HBSS and re-passed through the cell strainer before pelleting at 200 g for 5 minutes. The pellet was re-suspended in 500 µl HBSS (repeated twice over) and transferred to a 1.5 ml eppendorf which can be racked on a magnetic strip to draw dynabed-embolised glomeruli to the side of the tube. Glomeruli were then washed 3 times with 500 µl HBSS. Glomeruli not destined for podocyte isolation were stored in RNA later (Thermo Fisher Scientific) until the point of RNA extraction. When proceeding to immediate podocyte isolation by FACS, samples were placed on ice.

2.11.2 Glomerular digestion to a single cell suspension

Glomerular preparations were expedited from Bristol to Cardiff on ice. Samples were then centrifuged at 500 g, 4°C for 5 minutes and pellet re-suspended in 2 ml of freshly prepared digestion solution (HBSS containing calcium and magnesium + 0.2 mg/ml Liberase (Sigma #**05401020001)** + 1 mg/ml collagenase IV (Thermo Fisher Scientific #17104019) + 100 µl /ml DNase I). This was transferred to a 15 ml falcon and incubated for 1 hour in a shaking incubator, 80 rpm at 37°C. Following incubation, cell suspension was passed through a 40 µm mesh cell strainer into a 50 ml falcon containing 1 ml FCS to halt the digestion reaction. Cell sieving was gently facilitated with the head of a 5 ml syringe plunger, and washed with HBSS buffer. Filtrate was centrifuged at 500 g, 4 ^{0}C for 5 minutes and re-suspended with 1 ml HBSS. 1 µl Live/Dead Fixable *Near-IR Dead* Cell Stain (Thermo Fisher Scientific #L10119,) was added to cells and incubated in darkness at room temperature for 15 minutes, before

being re-spun at 500 g, for 5 minutes at 4°C. Supernatant was discarded, pellet washed with 1 ml MACS buffer (DPBS 1X + 5 mM EDTA + 0.5% (w/v) BSA) and finally re-suspended in 1 ml MACS buffer in preparation for FACS sort.

2.12 Podocyte Isolation

2.12.1 Fluorescence Activated Cell Sorting (FACS)

All manual steps of flow cytometry were performed by Central Biotechnology Service (CBS) of Cardiff University using an Aria III Cell sorter (BD Biosciences-US). Gating settings were performed by myself during sorts.

2.12.2 Cell-to-Ct™ Taqman Kit

Purity of podocyte sort from initial attempts at isolating podocytes from whole glomeruli was assessed using the Taqman Cell-to-Ct™ one step kit (Thermo Fisher Scientific #A25605). The rationale for choosing this is discussed further in Chapter 5.2.2.

Cells were taken directly from the FACS sort in FACS buffer, transferred to a 15 ml falcon and centrifuged at 350 g for 5 minutes at room temperature. Pelleted cells were re-suspended in 50 µl chilled PBS per 10^5 cells (calculated using flow-counts), re-spun as above and suspended in a final volumes of PBS at 5 µl per 10^3 cells. Samples were transferred to a 96 well plate (in triplicate if volumes allowed) and added to 50 µl of lysis solution, pipette mixed. After incubation at room temperature for 5 minutes, 5 µl STOP solution was added to inactivate the lysis reagents as to not inhibit RT and PCR reactions. Cell lysates were frozen at -20°C overnight.

RT and PCR reactions were performed as a single step, prepared using 5 µl of PCR Mastermix, 1 µl Taqman gene assay, 12 µl RNAse-free water and 2 µl of sample cell lysate (total reaction volume = 20 µl). ViiA7 Real-Time PCR System was configured as shown (Table 2.10):

Stage	Cycle No.	Temp	Time
RT	1	50 °C	5 mins
RT inactivation/ denaturation	1	95°C	20 secs
Amplification	40	95°C	15 secs
		60°C	1 min

Table 2.10 PCR cycling settings for Cell-to-Ct Taqman 1 step kit

2.13 MicroRNA Manipulation *in vitro*

2.13.1 Lentiviral Transfection

MiR-155 and miR-control lentiviral plasmid constructs were designed by Dr Robert Jenkins, Cardiff University, as shown in Figure 2.4. The control virus contained a 22nt, artificial microRNA sequence that, although processed by the cell as a microRNA, exerts no mRNA-targeting effect. Green-fluorescent protein (GFP) was incorporated into both control and miR-viral constructs to enable identification of infected cells. HEK293T cells were trypsinised and counted using a haemocytometer. 6 x 10^6 cells were seeded into a T75 flask and rocked on a horizontal plane to achieve maximal seeding efficiency. Cells were incubated at 37˚C for 24 hours before transfection using the Effectene transfection kit (Qiagen #301425). The miR-155/miR-control (1 µg), pCMVΔ8.91 (750 ng) and pMD2G (500 ng) plasmids (encoding structural virion proteins and viral envelope proteins respectively) were mixed in an eppendorf, made up to 300 µl with condensation buffer EC. Enhancer (18 µl) was then added, briefly vortexed and left at room temperature for 5 minutes to enable DNA condensation. Effectene (60 µl) (non-liposomal lipid transfection reagent) was added and gently vortexed for 10 seconds. The solution was incubated at room temperature for 10 minutes to enable micelle complex formation around condensed DNA, and then transferred to a 15 ml falcon containing 2.622 ml of complete media and mixed gently with a pipette.

A.

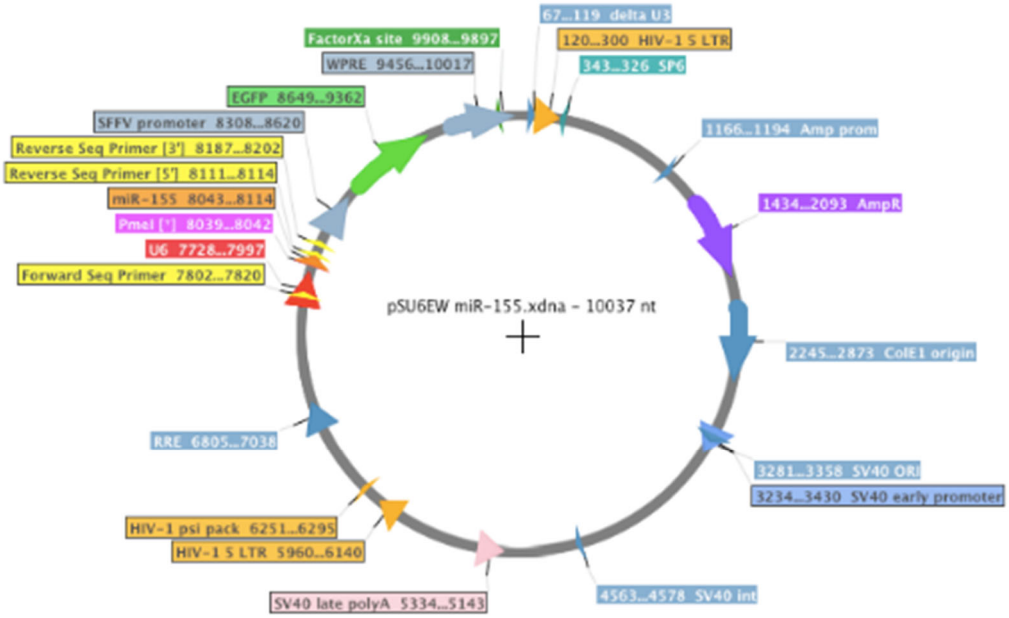

B.

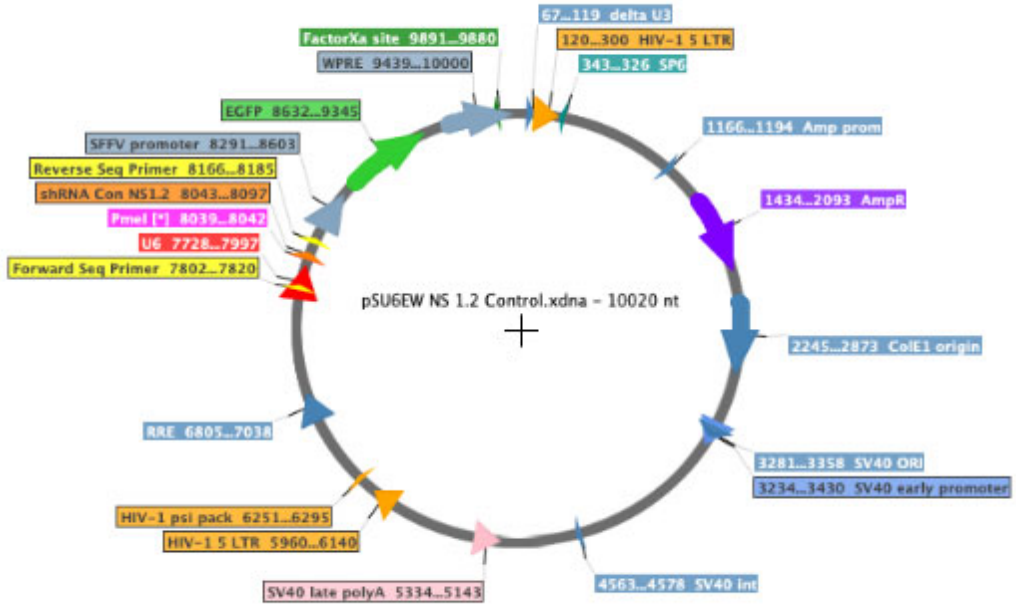

Figure 2.4(A) miR-155 lentiviral plasmid construct (**B)** miR-control lentiviral plasmid construct (named NS1.2).

The viral solution was added in a drop-wise fashion evenly across the cell monolayer (total flask volume 15 ml). Flasks were rocked gently to ensure even coverage before incubation at 37˚C for 48 hours. MicroRNA control lentivirus was taken from existing frozen aliquots as a kind gift from Dr Magdalena Czubala, Cardiff University.

2.13.1.1 Viral particle concentration

At 48 hours, cell supernatant was pipette transferred into a 50 ml falcon, and then passed through a 0.45 µm sterile millex®GP filter (Millipore Ireland Ltd.) 3 ml 20% sucrose gradient was made up in a Beckman ultracentrifuge conical tube, and the supernatant carefully overlaid as to not disrupt the sucrose layer. Ultracentrifuge tubes were topped up to 30 ml using complete media. Samples were ultracentrifuged at 26,000 rpm for 90 min at 4°C, and supernatant discarded. Virus pellets were re-suspended in media, gently pipette mixed and incubated at room temperature for 20 minutes. Virus was aliquoted into cryotubes and stored at -80°C.

2.13.1.2 MicroRNA overexpression by lentiviral transduction in podocytes

Mouse podocytes were seeded into 24 well plates and thermoswitched at 40% confluency and grown for 7 days (two thirds of the way through full differentiation) before viral application. This time point was considered a sensible compromise between maintaining cell viability by transducing (slowly) dividing cells, and inducing the miRNA overexpression at an established enough point in differentiation that it would be unlikely to interrupt a crucial phase of podocyte maturation. Cells were washed with PBS and 250 µl fresh media applied to each well. MiR-155 lentivirus was added to the wells drop-wise. MicroRNA control lentivirus of equivalent volumes was added to miR-control wells. At 1 hour, wells were topped up with a further 250 µl media, and incubated at 37˚C for 72 hours (fresh application at 48 hrs). At 72 hours, cells were examined under fluorescent microscopy to ascertain viral uptake (GFP positivity). Virally infected cells were trypsinised, equal volume of FCS added and samples centrifuged at 350 g for 5 minutes. Cells were re-suspended in 200 µl PBS and gently pipette mixed. 30 µl of each sample was transferred to a flow

tube and fixed with equal volume of 2% paraformaldehyde to enable analysis of percentage infectivity using the Attune NxT flow cytometer (Thermo Fisher Scientific). Remaining sample was re-pelleted (350 g for 5 minutes) and Qiazol Tri Reagent (700 µl) added to each. Non-infected controls were lysed with Qiazol directly from the wells (350 µl per well, 2 wells combined per sample). RNA was extracted as described in 2.5.2 for downstream RT-qPCR.

2.13.2 MicroRNA Manipulation using *Mir*Vana™ mimics and antagomiRs

Commercially available miRNA mimics composed of double stranded oligonucleotides may be transfected into mammalian cells where they mimic the actions of the mature miRNA transcript. Accompanying "control miRNAs" are random sequence miRNA mimic molecules that have been validated to not produce identifiable target effects. To inhibit naturally occurring miRNA, complementary single stranded oligonucleotides may be used to irreversibly bind and inactivate miRNAs.

*Mir*Vana™ miR-155 mimic, miR-155 inhibitor and respective controls were purchased from Thermo Fisher Scientific (Table 2.11) and used in accordance with manufacturers protocol. Briefly, podocytes were seeded to achieve 60-80% confluency at full differentiation. Lipofectamine RNAimax transfection reagent (Invitrogen #13778-075) was diluted with Opti-MEM® media, 50:1 (Thermo Fisher Scientific #31985070). MiR mimic/antagomiR and corresponding negative miR control was prepared in Opti-MEM® media to final concentration 30nM (determined from optimisation experiment detailed further in Chapter 4.2.3). Diluted miR mimic/antagomiR and lipofectamine were mixed together in 1:1 ratio and incubated for 30 mins at room temperature. The miR-lipid complex was added drop-wise to cells and left for 12 hours before replacing with usual podocyte media. Cells were further incubated for 24 hours before RNA or protein extraction using aforementioned Tri Reagent and RIPA buffer methods.

***mir*Vana™ Product**	**Catalogue Number (Thermo Fisher Scientific)**
miRNA mimic mmu-miR-155-5p	4464066
miRNA mimic negative control	4464058
miRNA Inhibitor mmu-miR-155-5p	4464084
miRNA inhibitor negative control	446076

Table 2.11 *miR*vana™ miR-155 mimics and antagomiRs used

2.14 Bioinformatic and Statistical Analysis

All statistics were performed in Prism, v7. All data was assessed for normality using the D'Agostino-Pearson test and, where 2 conditions (unmatched) compared, analysed using students unpaired t-test or Mann Whitney test as appropriate, α=0.05. For multiple experimental conditions, one way ANOVA and Tukeys post hoc testing was performed for unpaired parametric data; Kruskal-Wallis and Dunns multiple comparisons were performed for equivalent non-parametric data. Statistical significance is displayed as indicated in the figures: *, $p<0.05$; **, $p<0.01$; ***, $p<0.001$. Statistical methods pertaining to microarray analysis are discussed in 2.7, above.

2.14.1 DESeq2 Analysis of Sequencing Data

RNAseq and miRseq analysis was performed by bioinformatician Dr Robert Andrews, Cardiff University. Briefly, NGS reads from the Illumina HiSeq 4000 underwent adapter trimming and low quality bases/absence of sequence between adapter primers deleted as an initial quality control measure. Remaining reads were then mapped to the selected reference genome (miRbase 22.1 (200) and Ensembl release 94 (290)) using the splice away aligner STAR algorithm (291). Read counts per gene were calculated using the featureCounts software (292). Raw read counts were analysed in DESeq2 in Bioconductor (293). Read counts were normalised to the total number of reads

per sequencing lane to control for inconsistencies in loading. RNAseq data was further normalised to account for potential over-sequencing of longer gene transcripts (Fragments per kilobase of transcript per million, FPKM), a step not required for ubiquitously small microRNAs. Differential expression analysis was performed within the DESeq2 bioconductor package, which performs an internal normalisation by calculating the geometric mean for each gene across all samples. Individual sample counts for that gene are then divided by this mean value, thereby minimising the library size and RNA composition bias that can arise when only a small number of genes are very highly expressed in one experimental condition. Negative binomial generalised linear models were used to calculate p-value significance using the Wald test. Benjamini-Hochberg test was used to calculate p-value adjusted for multiple testing. Log2FC was calculated using the DEseq2 fitting model that "shrinks" fold change towards zero, which has the effect of "flattening" the high levels of variability exhibited in very lowly expressed genes. Filtering was applied to exclude genes with fewer than 10 read counts across all samples, prior to gene enrichment analysis.

2.14.2 MicroRNA Target Prediction Databases

To investigate predicted miRNA targets, the following databases were interrogated with the stated search threshold settings: DIANA Tools miRPath v.3 (stringency threshold 0.7)(294), TargetScan Mouse release 7.1 (cumulative weighted context score >-0.24)(295) and miRDB (target score >80)(296) . A summary of parameters used by each of the named databases is provided in Table 2.12. A fourth database, miRTarBase (release 7), of experimentally validated miR-mRNA interactions obtained from literature data mining algorithms was also used, with search threshold setting of "strong validated evidence" only (297).

Criteria	Diana	miRDB	TargetScan
Seed match	+	+	+
Conservation	+	+	+
Free Energy	+	+	
Site accessibility	+	+	
Machine Learning	+	+	
Target site abundance	+		
Reference	(294)	(296)	(295)

Table 2.12. Prediction criteria specifications for miRNA target prediction algorithms. 3 prediction databases, available online, were utilised in this work. Seed match= miRNA and mRNA target prediction based on Watson-Crick match between an mRNA sequence and the seed sequence of the miRNA. Conservation = maintenance of the miRNA binding site sequence across species, where a higher level of evolutionary conservation reflects a more reliable prediction. Free energy = measure of stability of the predicted miRNA-mRNA interaction inferred by predicting the energy that would be generated when miRNA and mRNA hybridise. The greater the stability of the interaction, the more likely it is representative of a true target interaction. Site accessibility = a measure of the ease with which a miRNA can locate and bind to an mRNA target. The greater the energy required to 'unfold" an mRNA to reveal the miRNA binding site, the less likely it is to represent a true target site. Target site abundance = used only by DIANA, this refers to the specific prediction of target sites in the mRNA 3'UTR, considered to be the most functionally relevant. Table adapted from (298).

2.14.3 Ingenuity Pathway Analysis (IPA)

NGS and microarray data were analysed for gene enrichment pathways and miR-mRNA target interaction using IPA (QIAGEN Inc., https://www.qiagenbioinformatics.com/products/ingenuity- pathway-analysis). This web-based tool compares uploaded datasets with a literature-derived "knowledge base" and assigns significance of associations based on the ratio of the number of molecules from the data set that map to a pathway, divided by the total number of molecules that map to the Ingenuity Knowledge Base for that pathway. Fisher's exact test is used to determine the probability that the association between the genes in the data set and the pathway of interest is "true" i.e. $p<0.05$. Specific details of individual analyses performed are provided in figure legends (Chapter 6).

3 MicroRNAs are differentially expressed in podocyte insulin resistance *in vitro*

3.1 Introduction

The podocyte is an integral component of the glomerular filtration barrier, and podocyte dysfunction is well recognised as a salient feature of early DN (299). Welsh *et al* demonstrated that the podocyte is an insulin-sensitive cell that responds to insulin via the Akt and MAPK pathways, resulting in rearrangement of the actin cytoskeleton to present GLUT4 to the cell membrane, facilitating glucose uptake (147) . Furthermore, they showed that podocyte-specific insulin receptor deletion elicits glomerular changes mimicking a number of features of early DN, including glomerulosclerosis, podocyte loss and thickened basement membranes (148). These findings imply that insulin signalling is a critical determinant of podocyte phenotype, and that development of podocyte insulin resistance may be a key causal element in DN.

MicroRNAs regulate insulin responses in "classically" insulin-sensitive tissues such as fat, liver and muscle, with elegant data to support differentially expressed miRNA profiles in insulin-resistant states in both mouse and humans. Importantly, the aberrantly expressed miRNAs may also be manipulated to restore an insulin-sensitive phenotype in adipocytes, hepatocytes and myocytes, thus demonstrating the importance of these miRNAs and their potential as new therapeutic targets (263, 300).

The role of miRNAs in regulating important aspects of podocyte biology has been clearly demonstrated. Podocyte-specific deletion of miRNA-maturation machinery, such as the RNAse III enzyme Dicer, leads to podocyte dedifferentiation, proteinuria, glomerulosclerosis and death in mice, highlighting the importance of podocyte miRNAs not simply in maintaining the glomerular filtration barrier, but for the overall survival of the mouse (249-251).

It is noteworthy, however, that the miRNAs responsible for regulating insulin responses in adipocytes, myocytes and hepatocytes, and the precise molecular mechanisms by which they induce insulin resistance, are highly cell specific. Therefore, attempts to extrapolate findings from these cell types to the

podocyte was deemed an inefficient approach to investigating those miRNAs that may be critical for insulin signalling regulation in this unique cell type.

This chapter details the selection of a robust *in vitro* model of podocyte insulin resistance and use of an unbiased microarray profiling approach to investigate differentially expressed microRNAs in this important cell.

3.1.1 Chapter Aims

1. Establish baseline characteristics of the podocyte cell line
2. Develop an *in vitro* model of podocyte insulin resistance
3. Investigate differential expression of microRNAs in insulin-resistant podocytes *in vitro*

3.2 Results

3.2.1 Baseline Characteristics of C2 podocyte cell line

Prior to attempts to develop an *in vitro* model of insulin resistance, baseline characteristics of the selected immortalised cell line were established, as below.

3.2.1.1 Podocyte differentiation by inactivation of SV40

Mouse podocytes were grown at the permissive temperature (33°C) to 40% confluence, at which point they were transferred to 37°C and incubated for 10 days. Figure 3.1 depicts the typical morphology of the cells in the undifferentiated and differentiated states, with a progression to a flatter, arborised cell with elongated, connected cytoplasmic processes.

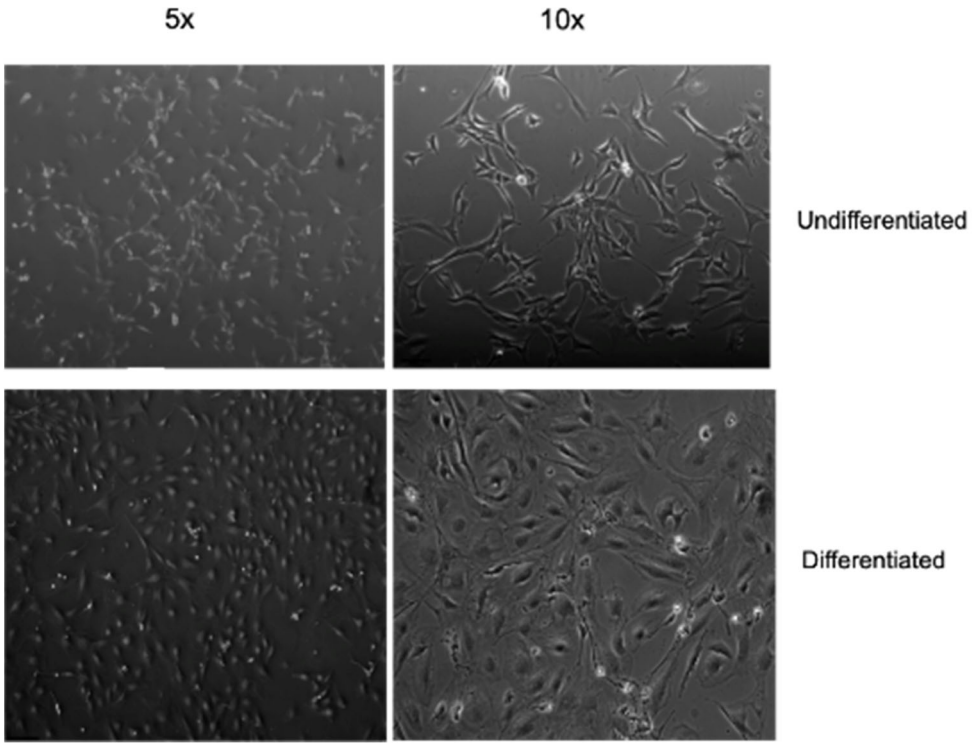

Figure 3.1. Light Microscopy images of mouse podocytes in the undifferentiated and differentiated state, achieved by thermoswitching of cells to inactivate the temperature-sensitive SV40 antigen. (5x lens= 50x magnification, 10x= 100x magnification).

The hallmarks of the mature, differentiated podocyte include expression of the slit diaphragm proteins nephrin, synpatopodin, CD2AP and podocin, and the acquisition of insulin sensitivity, associated with increased expression of the insulin receptor (IR) (162). Markers of podocyte differentiation were investigated at the mRNA level (Figure 3.2 A) and protein level (Fig 3.2 B). MRNA expression of synaptopodin, nephrin and IR were increased three-, eight- and five-fold in differentiated podocytes, respectively. CD2AP expression was unchanged at the mRNA level, however protein expression was clearly increased in the differentiated state in all of the podocyte-specific markers. SV40 was effectively silenced at the non-permissive temperature (Fig 3.2 C).

A

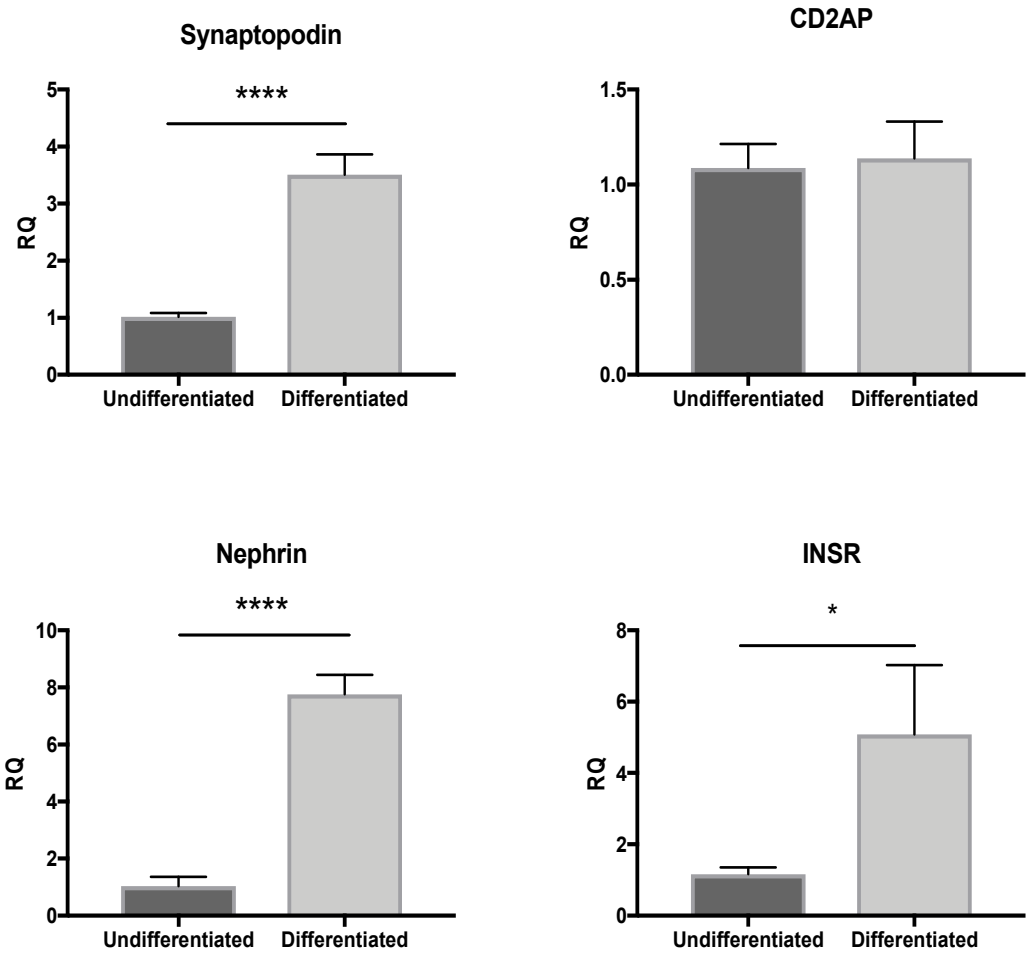

B

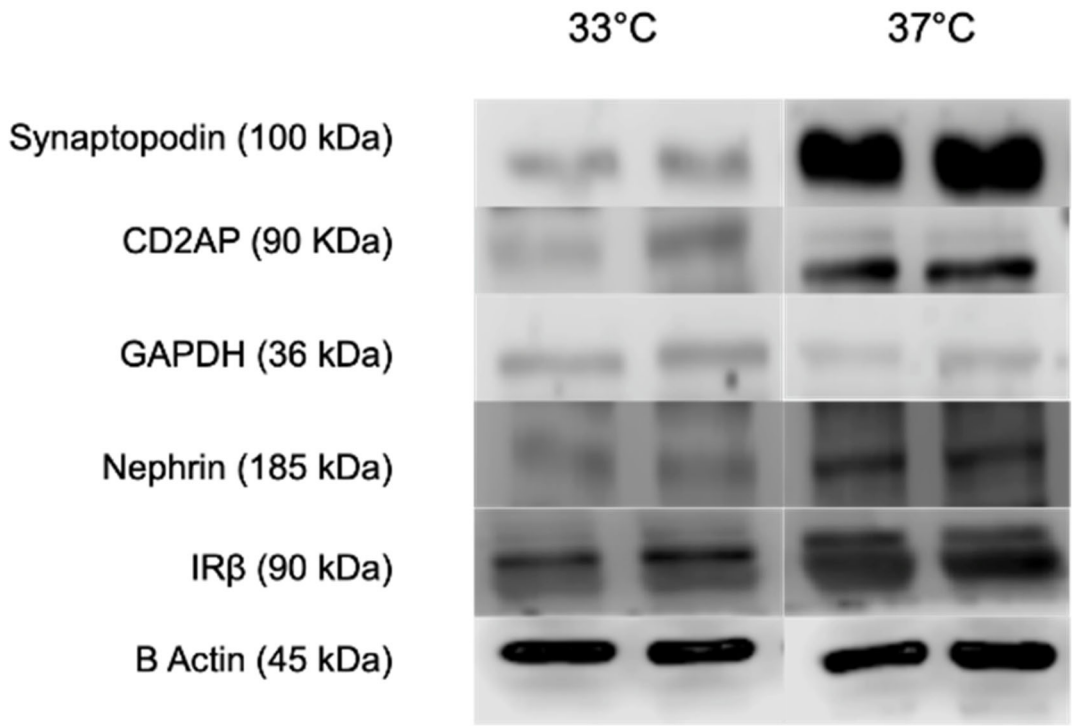

C

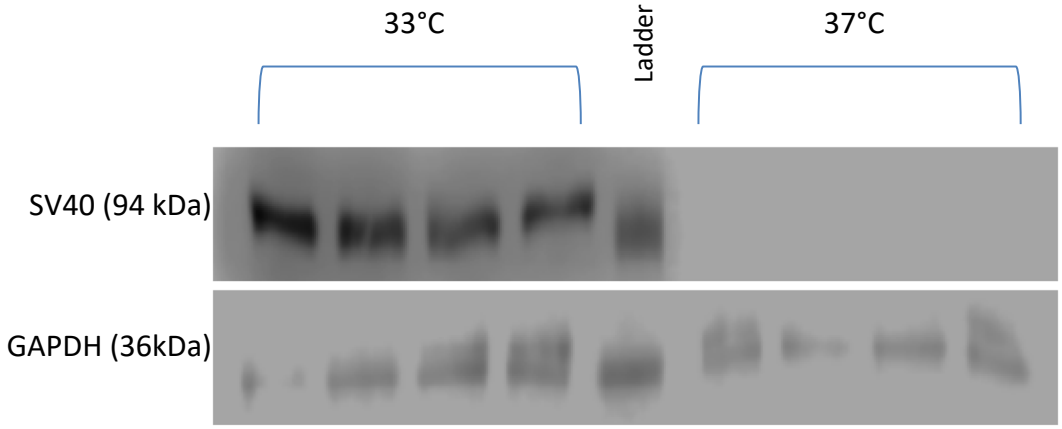

Figure 3.2 Inactivation of SV40 results in podocyte differentiation *in vitro.* **(A)** RT-qPCR mRNA expression in differentiated podocytes. Mean +/- SD of n=3 independent experiments, U6 used as reference gene. Significance calculated by students two-tailed t test *, $p<0.05$; **, $p<0.01$; ***, $p<0.005$; **** $p<0.001$. INSR= insulin receptor. **(B)** Protein expression of podocyte markers by western blot analysis. **(C)** Differentiation of podocytes is achieved by silencing of the temperature-sensitive SV40 at the non-permissive temperature (western blot shown).

3.2.1.2 Confirmation of podocyte response to insulin

Podocytes demonstrate an incremental response to insulin via dose-responsive increase in phosphorylation of Akt and MAPK (148). Figure 3.3 demonstrates confirmation of insulin sensitivity in the selected mouse podocyte cell line, with a relative increase in expression of pAkt and pMAPK of eighteen- and twelve-fold respectively in response to standard experimental insulin dose of 100 nM.

A

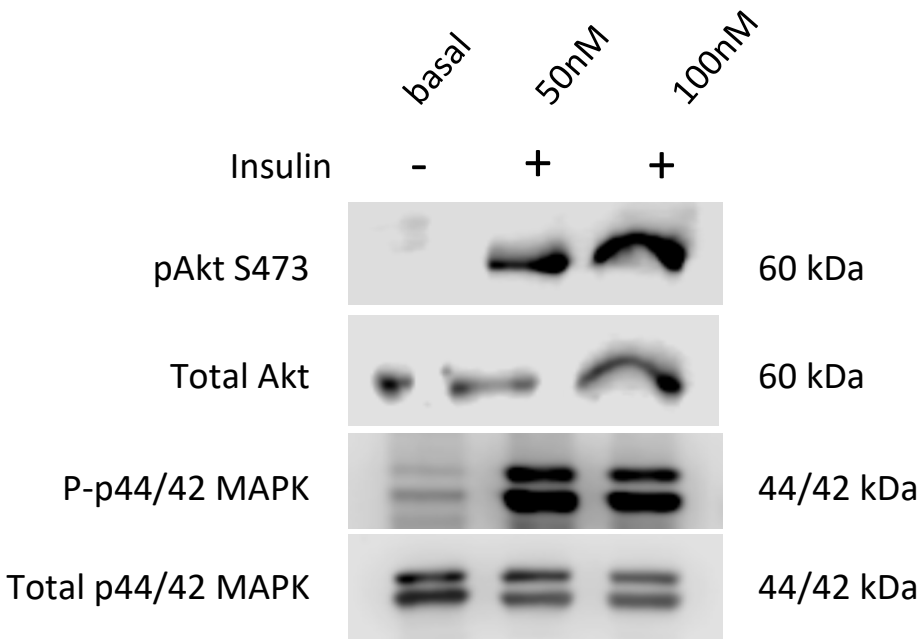

B

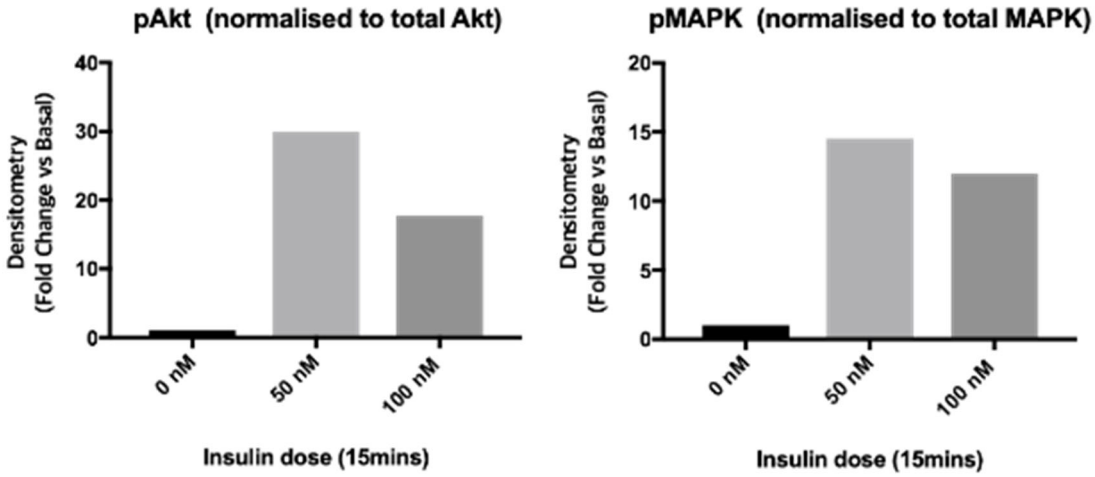

Figure 3.3 Wild Type mouse podocytes are insulin sensitive. **(A)** Western Blot showing protein phosphorylation of pAkt (Serine 473) and pMAPK (p42/44) in response to 50 nM and 100 nM insulin stimulation. **(B)** Densitometry shown, fold change calculated relative to basal phosphorylation reading. N=1 performed without repeat, owing to confirmatory nature of investigation of a known podocyte response.

3.2.2 Podocytes become insulin resistant in diabetogenic medium

Podocytes may be rendered insulin resistant using a variety of monostimuli including high dose insulin, high dose glucose, IL-6 and TNF-α (162). In the *in vivo* setting, animals and patients with T2DM are simultaneously exposed to all of the above stimuli, with diabetes increasingly recognised as a chronic inflammatory condition in which IL-6 and TNF-α are potent mediators (301). To accurately reflect the *in vivo* diabetic milieu for *in vitro* experiments, a multi-stimuli model of podocyte insulin resistance was devised for the purpose of investigating differential microRNA expression. Podocytes were cultured in 25 mM glucose, 100 nM insulin, 1 ng/ml IL-6 and TNF-α throughout the differentiation period. Differentiated podocytes were serum/insulin starved for 6 hours before stimulating with 100 nM insulin. Figure 3.4 demonstrates the reduction of insulin signalling in these cells at a proximal/mid point in the insulin signalling pathway; the phosphorylation of Akt and MAPK (A), and additionally, a 50% reduction in glucose uptake into the cell (B), thus providing an objective downstream marker of insulin resistance in these cells.

A.

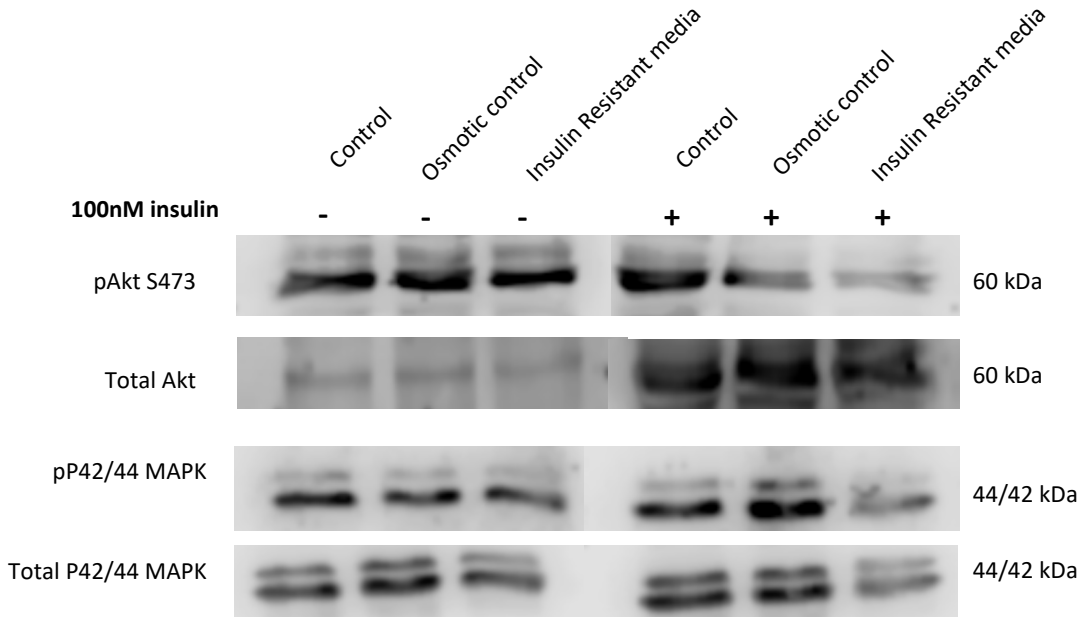
Control
Osmotic control
Insulin Resistant media
Control
Osmotic control
Insulin Resistant media
100nM insulin
- - - + + +
pAkt S473
60 kDa
Total Akt
60 kDa
pP42/44 MAPK
44/42 kDa
Total P42/44 MAPK
44/42 kDa

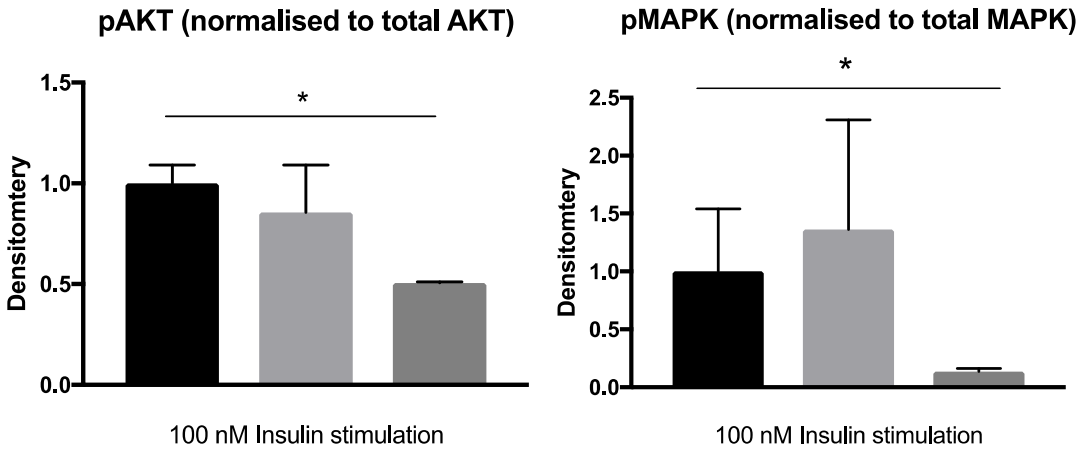
pAKT (normalised to total AKT)
Densitomtery
1.5
1.0
0.5
0.0
*
100 nM Insulin stimulation
pMAPK (normalised to total MAPK)
Densitomtery
2.5
2.0
1.5
1.0
0.5
0.0
*
100 nM Insulin stimulation

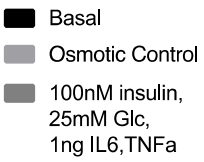
Basal
Osmotic Control
100nM insulin,
25mM Glc,
1ng IL6,TNFa

B.

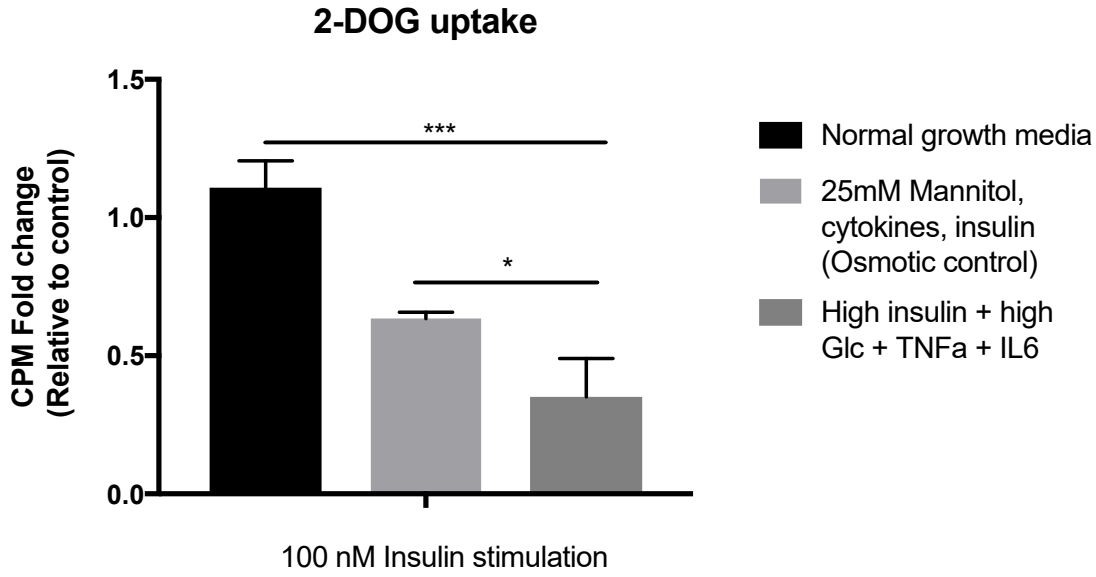

Figure 3.4 Podocytes are rendered insulin resistant in diabetogenic medium. Podocytes were cultured in 25 mM glucose, 100 nM insulin, 1 ng/ml IL-6 and TNF-α. Controls were grown under standard conditions. An additional osmotic control contained cytokines and insulin at the aforementioned doses and 25 mM mannitol as a glucose substitute. Following a period of serum starvation, cells were stimulated with 100 nM insulin for 15 minutes. **(A)** Western blot analysis of phosphorylated Akt and MAPK and corresponding densitometry (representative image from n=3 experiments shown) **(B)** DEOXY-D-GLUCOSE, 2-(1,2-3H (N)) (2-DOG) uptake assay showing glucose uptake in the multi-stimuli treated podocytes as compared to podocytes grown under standard conditions. Mean +/-SD of n=3 independent experiments shown. Significance calculated using One way ANOVA and Tukeys test for multiple comparison *, $p<0.05$; **, $p<0.01$; ***, $p<0.005$. CPM= counts per minute.

3.2.3 MicroRNA hybridisation array profiling

Having ascertained that the multi-stimuli diabetogenic environment resulted in podocyte insulin resistance (IR) *in vitro*, RNA was extracted from mouse podocytes grown throughout differentiation in the presence of 100 nM insulin, 25 nM glucose and 1 ng/ml TNF-α and 1 ng/ml IL-6 (n=5) and compared to wild type (WT) podocytes cultured under standard conditions (n=5) using a hybridisation microarray approach.

442 miRNAs (of 1203 screened) were present in the podocyte, of which, 103 were significantly up- or downregulated in insulin-resistant podocytes. Figure 3.5 A and B demonstrate a clear distinction in miRNA signature between the WT and IR samples, using Principal component analysis (PCA) and two-way hierarchical clustering, respectively. The most significantly up- and downregulated miRNAs are presented as a volcano plot in Figure 3.5 C.

A.

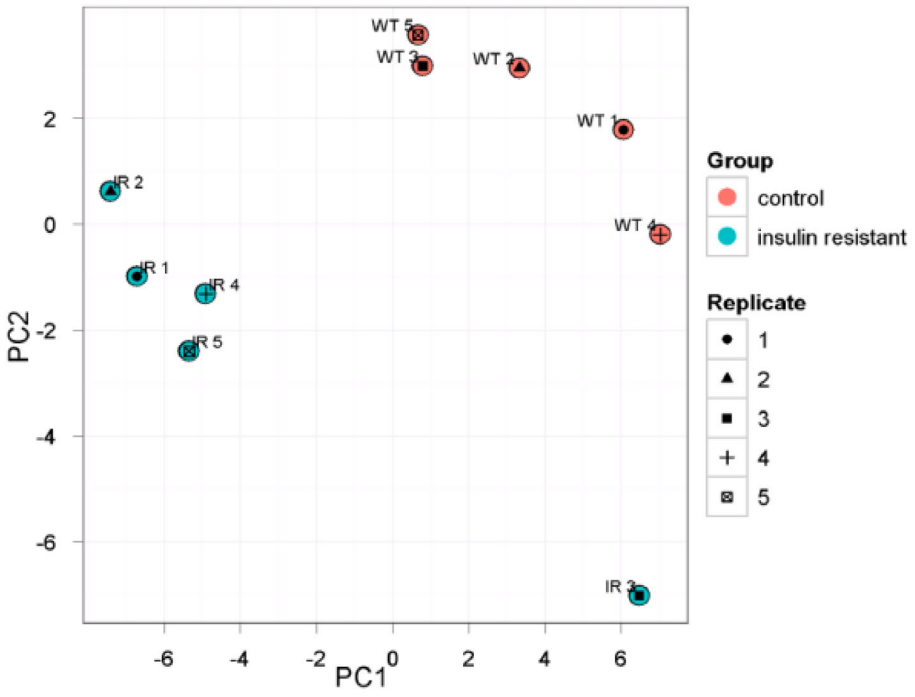

B.

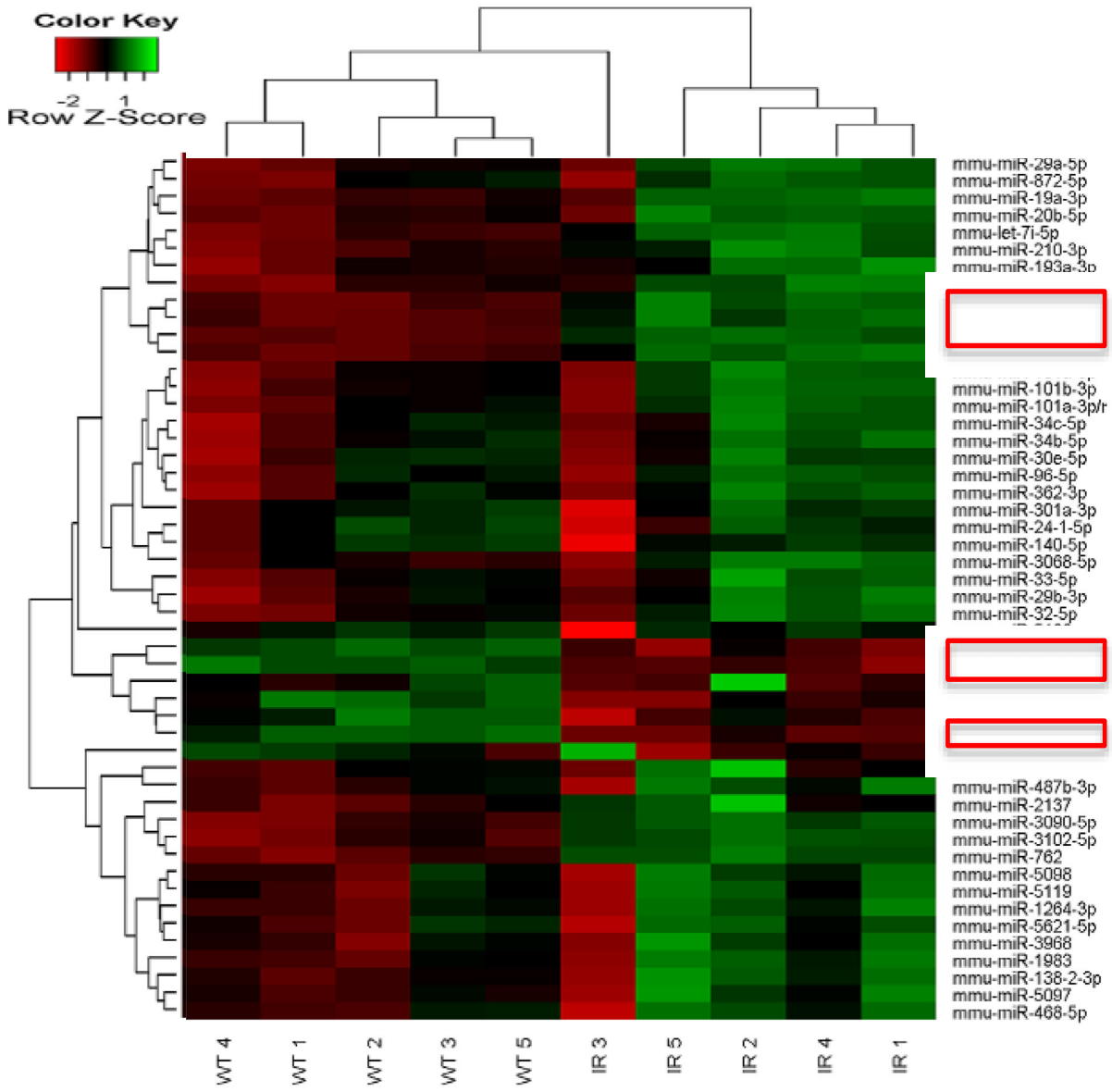
Color Key
-2
1
Row Z-Score
mmu-miR-29a-5p
mmu-miR-872-5p
mmu-miR-19a-3p
mmu-miR-20b-5p
mmu-let-7i-5p
mmu-miR-210-3p
mmu-miR-193a-3p
mmu-miR-101b-3p
mmu-miR-101a-3p/r
mmu-miR-34c-5p
mmu-miR-34b-5p
mmu-miR-30e-5p
mmu-miR-96-5p
mmu-miR-362-3p
mmu-miR-301a-3p
mmu-miR-24-1-5p
mmu-miR-140-5p
mmu-miR-3068-5p
mmu-miR-33-5p
mmu-miR-29b-3p
mmu-miR-32-5p
mmu-miR-487b-3p
mmu-miR-2137
mmu-miR-3090-5p
mmu-miR-3102-5p
mmu-miR-762
mmu-miR-5098
mmu-miR-5119
mmu-miR-1264-3p
mmu-miR-5621-5p
mmu-miR-3968
mmu-miR-1983
mmu-miR-138-2-3p
mmu-miR-5097
mmu-miR-468-5p
WT 4
WT 1
WT 2
WT 3
WT 5
IR 3
IR 5
IR 2
IR 4
IR 1

C.

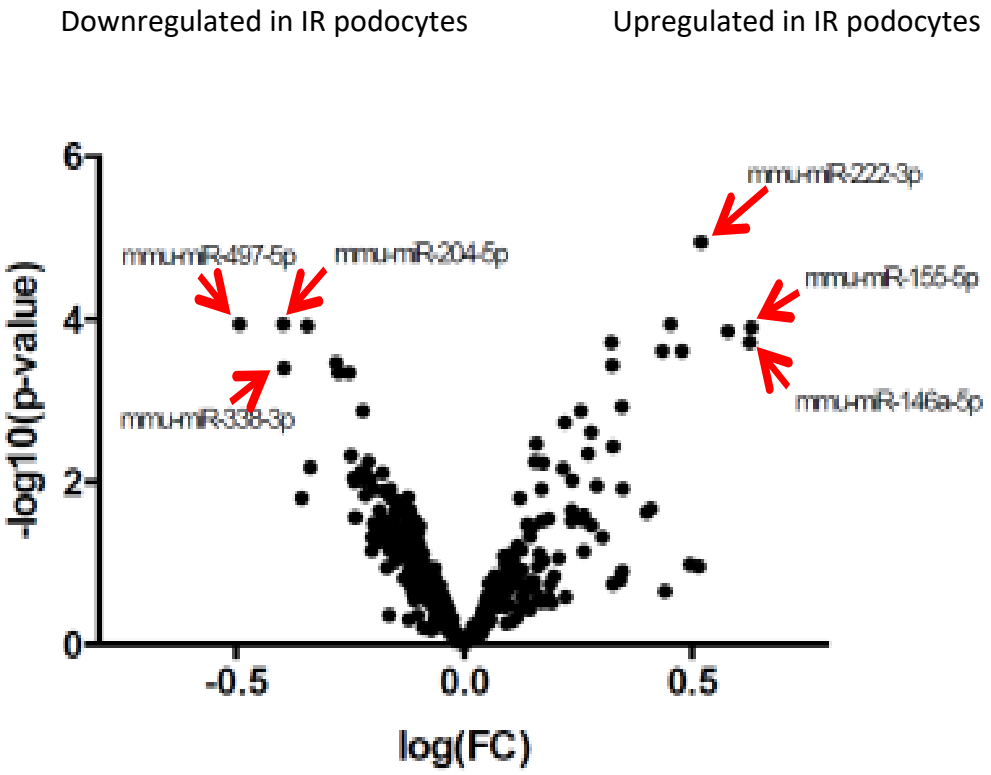

Figure 3.5. **Hybridisation array analysis of differential miRNA expression in insulin-resistant podocytes**. Conditionally immortalised podocytes were incubated with high glucose (25mM), high insulin (100nM) TNF alpha and IL-6 (1ng/ml) to achieve insulin resistance (IR) and their miRNA profile compared to insulin-responsive Wild type (WT) podocytes. 442 miRNAs (out of 1206 analysed) were expressed in the podocyte, of which 103 were significantly differentially expressed between the 2 groups. **(A)** Principal Component Analysis Plot demonstrating clear differences in biological groups between IR and WT podocytes. Sample clustering is based on miRNA variance in each sample. **(B)** Heat Map and unsupervised two-way hierarchical clustering showing clear distinction in miRNA expression between IR and WT podocytes. Red= expression level below the reference. Green = expression higher than the reference, where each row represents a miRNA and each column represents a sample. The clustering was performed on all samples, and on the top 50 miRNAs, and analysed using normalised log ratio values. **(C)** Volcano plot showing the relationship between the logarithm of the p-values and the log fold change (FC) between IR and WT podocytes (p values corrected for multiple testing using the Benjamini Hochberg statistic). MiRNAs at the upper and outer aspects of the "V"-plot are the most significantly up- and downregulated miRNAs in the IR cf. WT podocytes. Arrowed= miRNAs selected for study.

The differentially expressed miRNAs were then ranked based on p-value, magnitude of fold change and baseline expression. A literature review was subsequently performed to identify existing evidence of mRNA targets within, or associated with, insulin signalling pathways. 6 miRNAs, 3 up- and downregulated respectively, were selected for further investigation. A summary of the microarray parameters used to select candidate miRNAs, and their known biological functions, are shown in Table 3.1.

UPREGULATED miRNAs	Principal miRNA functions	Potential targets of interest in Insulin Signalling
miR-222 Hy3 signal: 9.6 Intensity p-value rank: 1 Fold Change: 1.4	**Vascular remodeling roles** • Inhibits eNOS leading to endothelial dysfunction (302) • High miR-221/222 associated with pre-clinical artherosclerosis (303) **Oncogenetic roles** • Glioblastoma, Thyroid, HCC, breast, prostate cancer • Numerous targets: PTEN, p57, p27, Kip1 (304) **Tumour suppressor roles** • In OSCC and erythroleukaemic cells (304) • Inhibits macrophage chemotaxis/ suppresses tumour growth in breast cancer (via target CXCL12) (305)	**ERα/GLUT4**- silencing of miR-222 in adipocytes results in increase in: ERα, GLUT4 expression, insulin-stimulated translocation of GLUT4 (306) **PTEN**- silencing of miR-222 in oral squamous cell carcinoma (OSCC) results in upregulation of PTEN and inhibition of proliferation/invasiveness of OSCC (307) **PPP2R2A**- miR-222 is upregulated in HCC resulting in repression of PPP2R2A (negative regulator of Akt phosphorylation) resulting in increased Akt activity and greater metastatic potential (308) **IRS1**-Overexpression of miR- 222 in mouse hepatocytes attenuates insulin-stimulated Akt phosphorylation via repression of IRS1 (309)
miR-155 Hy3 signal: 9.7 Intensity p-value rank: 6 Fold Change: 1.5	**Immune cell regulation** • Master regulator of immune responses including lymphocyte development (310), antibody-mediated signalling (311), T cell signalling (312) and macrophage cytokine production (310) • Dysregulated in autoimmunity e.g. RA, SLE (313, 314) **Oncogenic roles** • Upregulated in breast, nasopharyngeal, colon, pancreas, HCC (315) and B-cell malignancies (316) **Metabolic regulation** • Regulates cholesterol and FA metabolism in hepatocytes via target LXRa (317) • Regulates glucose metabolism in breast Ca cells (318)	**p85α/PIK3R1-** Roles in oncogenic translocations and tumour suppression via ↓p85α =unregulated PI3K/AKT pathway activation **SHIP-1/INPP5D-** negative modulator of PI3K/AKT pathway. High miR-155 in B-cell neoplasia de-represses AKT to increase B cell signalling (319) **RhoA-**Leads to disruption of tight junctions, promoting cell migration and invasion in murine mammary epithelial cells (320). RhoA also critical to facilitate podocyte response to insulin (147) **SOCS1-**promotes macrophage M1 phenotype via SOCS1 targeting; subsequent dysregulation of JAK/STAT signalling resulting in adipocyte insulin resistance in mice (321). Also regulates T-helper cell production of IL-17, implicated in deacetylation of nephrin (259)

miR-146a Hy3 signal: 7.0 Intensity p-value rank: 9 Fold Change: 1.5	**Immune cell regulation** • "Anti-inflammatory" miR via role in NF-κB pathway activation, antagonises proinflammatory effects of miR-155 (322) **Oncogenic roles** • Upregulated in numerous cancers including breast, colorectal and oral cancer (323-325)	**TRAF6/IRAK-** intravitreal delivery of miR-146 inhibits diabetes-induced NF-κB activation and retinal microvascular defects in a diabetic rat model (326) **Notch-1/ErB4-** TGF-β driven podocyte-specific miR-146a knockout relieves repression of Notch-1 and ErB4; results in accelerated glomerulopathy and albuminuria (327) **INSR-** inhibits TNF-α-induced adipogenesis in porcine adipocytes via targeting INSR (328)

Table 3.1(A). Selected Candidate upregulated MicroRNAs. Principal miRNA functions and specific targets of interest derived from literature search highlighted in bold. Hy3 signal intensity refers to the fluorescence intensity from the miRNA hybridisation probe, which provides a surrogate marker of relative miRNA abundance in the sample. HCC= hepatocellular cancer, PTEN= Phosphatase and tensin homolog, OSCC= oral squamous cell carcinoma, CXCL12=, C-X-X motif chemokine 12, RA= Rheumatoid arthritis, SLE= Systemic Lupus Erythrematosus, LXRa= Liver-X receptor alpha, FA= fatty acid, ERα= Estrogen receptor alpha, GLUT4= Glucose transporter type 4, PP2R2A= regulatory subunit of protein phosphatase 2A , IRS1= insulin receptor substrate-1, PIK3R1= Phosphoinositide-3-Kinase Regulatory Subunit 1, INPP5D= Inositol Polyphosphate-5-Phosphatase D, PPARγ=Peroxisome proliferator-activated receptor gamma, RhoA=Ras homolog family member A, TRAF6= TNF-receptor associated factor 6, IRAK1= interleukin-1 receptor associated kinase, ErB4= Erb-B2 Receptor Tyrosine Kinase 4, INSR= insulin receptor.

DOWN REGULATED miRNAs	Principal miR functions	Potential targets of interest in Insulin Signalling
miR-204 Hy3 signal: 8.3 Intensity p-value rank: 2 Fold Change: 0.8	**Embryological roles** • Master regulator in eye development (329) **Pulmonary Hypertension** • Enhanced proliferation of smooth muscle cells leading to pulmonary artery hypertension (330) **Regulate adipogenesis** • Promotes differentiation of mature adipocytes (331) **Tumour suppressor roles** • Commonly via induction of apoptosis via target BCL-2 in numerous solid tumours e.g. prostate & gastric cancer (332, 333)	**BDNF-** Low miR-204 results in BDNF overexpression and subsequent activation of Rac1 and actin reorganisation through the Akt/mTOR signalling pathway leading to cancer cell migration and invasion (334) **ACAB-** acetyl-CoA carboxylase β enzyme, which catalyses the carboxylation of acetyl-CoA to malonyl-CoA and plays a role in mitochondrial fatty acid oxidation in adipose tissue. Lower levels of ACAB in liver and adipose are associated with improved insulin sensitivity (335) **BDKRB2**- miR-204 prevents high glucose-induced apoptosis through downregulation of Bradykinin receptor B2, the suppression of which is known to induce pro-apoptotic p38 MAPK pathway (336)
miR-497 Hy3 signal: 7.0 Intensity p-value rank: 4 Fold Change: 0.7	**Tumour suppressor roles** • Suppress proliferation and promote apoptosis in pancreatic cancer (337) • Inhibit tumour angiogenesis in HCC (338) and ovarian cancer cells (339) • Suppresses migration & invasion in prostate cancer cells(340) • Increase chemosensitivity in colorectal cells (CRCs) (341)	**IGF-R and IRS1**- Over expression of miR-497 in CRC leads to reduction in insulin- stimulated Akt and ERK phosphorylation, acting via IGF1-R and IRS1 (342, 343) **INSR**- negatively regulates IRS1/PI3K/Akt/GSK-3β/GS pathway and induces hepatic insulin resistance in rats (344) **VEGF-A-** inhibits angiogenesis via the VEGFR2-mediated PI3K/AKT and MAPK/ERK pathways in ovarian cancer cells (339)

miR-338 Hy3 signal: 7.4 Intensity p-value rank: 14 Fold Change: 0.8	**Tumour suppressor roles** • Inhibits EMT in hepatocellular (345) and gastric cancer cells (346) • Inhibits proliferation & migration of gastric cancer (347) and renal cell carcinoma (348) **Anti-Fibrotic roles** • Protects against TGF-β induced lung fibrosis via target LPA1 (349)	**IRS2-** inhibits NSCLC cell proliferation, migration, invasion and induced apoptosis (350) **PREX2** –a negative regulator of PTEN/Akt pathway, found to suppress metastatic proliferation and invasion of neuroblastoma cells (351) **PP4r1** - regulates PP4 expression, a mediator of hepatic insulin signalling. High TNF-α induced insulin resistance results in downregulation of miR-338 and impaired AKT/GSK3β signalling (352)

Table 3.1(B). Selected Candidate downregulated MicroRNAs. Principal miRNA functions and specific targets of interest derived from literature search highlighted. EMT= epithelial-mesenchymal transition, LPA1= Lysophosphatidic acid receptor, BDNF= Brain derived neurotropic factor, VEGF-A= Vascular endothelial growth factor A, IRS= insulin receptor substrate, NSCLC= non-small cell lung carcinoma, PREX2= Phosphatidylinositol-3,4,5-Trisphosphate Dependent Rac Exchange Factor 2, PP4r1= Serine/threonine-protein phosphatase 4 regulatory subunit 1.

3.2.4 RT-qPCR validation of miRNA candidates

RT-qPCR validation of the miRNA expression changes detected by microarray was performed for the 6 selected miRNA candidates (Figure 3.6). Podocytes were rendered insulin resistant by culture in diabetogenic media as previously. Significant upregulation of miRs -155, -146a and -222, and downregulation of miR-204 in insulin-resistant podocytes was confirmed, however the expected downregulation of miRs -338 and -497 was not seen. Additionally, the relative abundance of miR-338 was confirmed to be low in WT podocytes (Mean Ct 34), suggesting any change in detection level may not be as biologically relevant in insulin resistance.

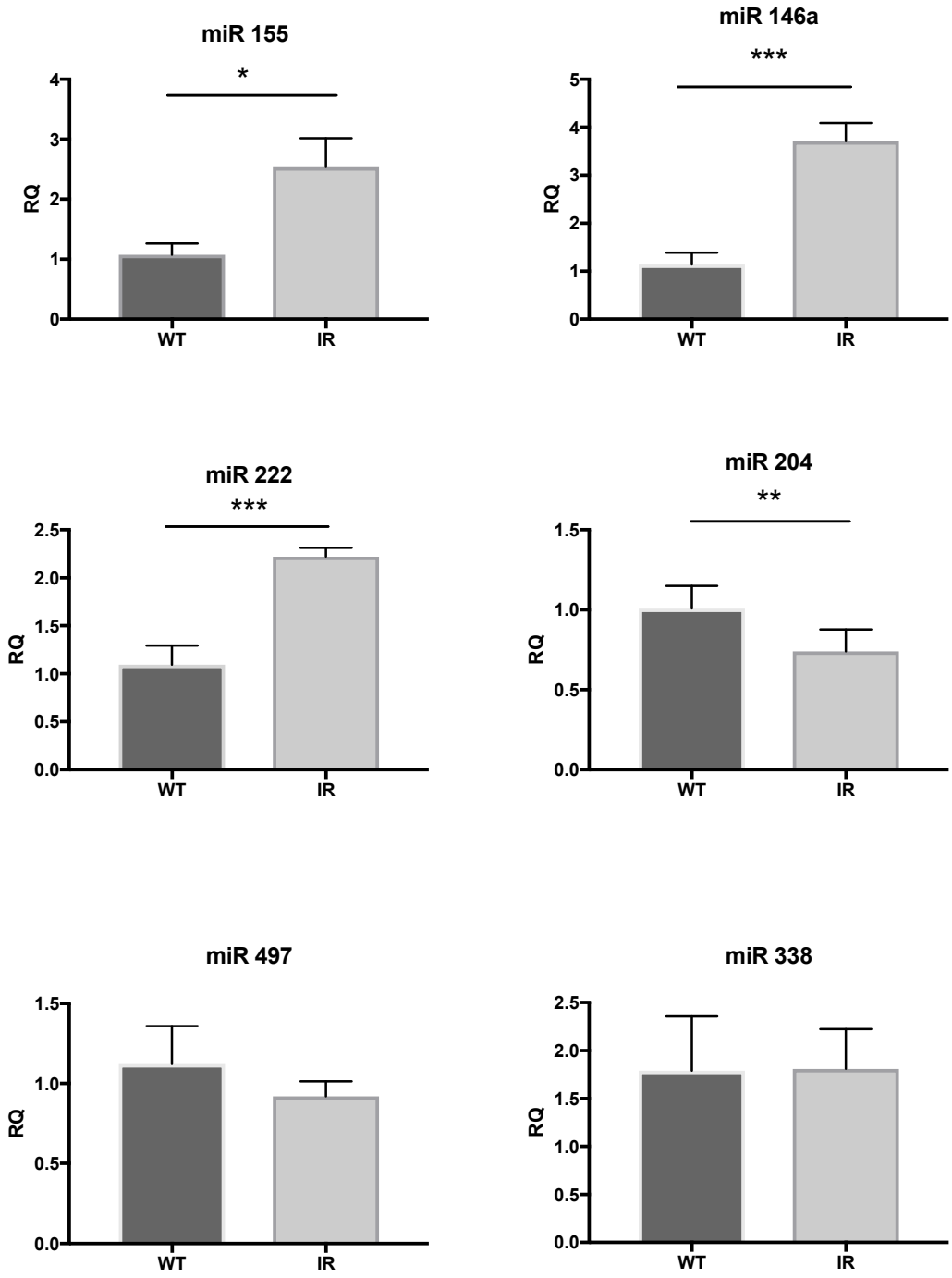

Figure 3.6. RT-qPCR validation of differentially expressed candidate miRNAs detected by microarray. Podocytes were rendered insulin resistant by culture in diabetogenic media containing 25 mM glucose, 100 nM insulin, 1 ng/ml IL-6 and TNF-α, and relative quantification (RQ) of the selected miRNA candidates calculated as compared to expression in Wild Type (WT) podocytes grown under standard conditions. U6 used as reference gene. Mean +/- SD of n=3 independent experiments shown, Significance calculated by students two-tailed t test *, $p<0.05$; **, $p<0.01$; ***, $p<0.005$;****$p<0.001$.

3.3 Discussion

The microarray analysis described in this chapter has demonstrated clear differences in miRNA expression in podocytes rendered insulin resistant using a multi-diabetogenic stimuli approach. Of the most significantly differentially expressed miRNAs, 5 out of the 6 candidates selected have direct or indirect targets in Akt signalling, which has been established as the predominant pathway via which insulin signals to the podocyte to enact the conformational cytoskeletal changes which both enable the cells to take up glucose, via membrane insertion of GLUT4, but are also hypothesised to "brace" the cell for an increased filtration load in the post-prandial state. Welsh *et al* postulate that the insulin-induced corticalisation of F-actin in the podocyte ensures that the cells are able to contract along the basement membrane, which affords greater protection from the sheer stress associated with higher glomerular filtration rates (GFR) (148). Supraphysiologic elevation of GFR is a well-established primary insult in the natural history of diabetic nephropathy, which is, itself, associated with greater risk of development/progression of albuminuria (353). The loss of Akt signalling may, therefore, have dire mechanistic consequences for the podocyte, and is the rationale for the focus on miRNA candidate targets within or associated with this pathway. However, the role of Akt in insulin signalling and glucose metabolism is merely one example of a multi-purpose signal transduction pathway that is additionally involved in regulating cell cycle progression and encompasses, for example, regulation of apoptosis, cellular migration and angiogenesis. Resultantly, the vast majority of research into miRNA involvement in this pathway is biased towards cancer research, as is evident in the "Principal miR Functions" column of Table 3.1 More detailed evidence for the potential relevance of the 6 selected miRNAs in podocyte insulin responses is presented below.

3.3.1 Upregulated MicroRNAs

3.3.1.1 MicroRNA-155 (miR-155-5p)

MiR-155 is a highly plausible candidate for involvement in regulating podocyte insulin sensitivity given its established reputation as an "inflammamiR". Most miR-155 research is focused around its role as a master regulator of immune cell functions, such as macrophage, B cell and T cell responses (310-312, 319). Upregulation of inflammatory pathways is a recognised feature of conditions associated with insulin resistance, such as diabetes, obesity and the overarching 'Metabolic Syndrome" (MetSyn) (301). However, existing evidence for miR-155 is contradictory, with some reporting deleterious effects of miR-155 on insulin sensitivity whilst others suggest it may protect against the development of insulin resistance.

One recent study reports that miR-155 promotes the M1 macrophage phenotype via direct targeting of Suppressor of cytokine signalling-1 (SOCS1) and subsequent dysregulation of JAK/STAT signalling, resulting in local insulin resistance in adipocytes in mice, as shown by reduced Akt phosphorylation and glucose uptake (321). The role of miR-155 in promoting inflammation and influencing adipocyte differentiation led Gaudet *et al* to hypothesise that whole miR-155 knockout would confer protection against development of obesity. Indeed, female miR-155 knockout mice fed a high fat diet were resistant to the development of obesity and this was associated with improved glucose tolerance. Parallel *in vitro* work showed upregulation of direct miR-155 targets involved in brown adiopogenesis and energy release (e.g. mitochondrial uncoupling protein, Ucp1) as well as upregulation of GLUT4 and IRS1, which the authors suggest may provide a synergistic mechanism for this effect (354).

Conversely, Xiaolin Lin *et al* reported that global miR-155 *overexpression* in mice resulted in hypoglycaemia, improved glucose tolerance and enhanced insulin sensitivity of peripheral tissues, explained in part by enhanced glucose uptake through elevated phosphorylation of Akt which the authors conclude was a result of miR-155 target repression of important *negative* regulators of insulin sensitivity: C/EBPβ and HDAC4 (355). The variable direction of miR-155

effect in these studies may partly be explained by the cell-specificity exhibited by many miRNAs. It may also reflect the notion that miRNAs, as post-transcriptional gene regulators, provide "fine tuning" of dynamic and adaptive processes; their expression, therefore, might well be expected to fluctuate in an attempt to modulate cell homeostasis.

Evidence for a podocyte-specific role of miR-155 appears more consistent, albeit in a very limited number of studies. The Yang group showed that miR-155 knockout in hyperglycaemia-induced nephropathy is protective against nephrin and WT1 loss, which correlated with a decrease in urinary protein in these mice. They hypothesise that this is a result of increased expression of miR-155 target SOCS1 which suppresses T-cell release of IL-17 (259). Further work by this group also implicated miR-155 as a mediator of TGF-β1-induced podocyte injury, where *in vitro* knockdown of miR-155 attenuated expression of injury markers desmin and caspase-9, alleviated nephrin loss, and reduced podocyte apoptosis rates (258, 259). This may be highly significant in my model, given that both insulin-stimulated insertion of GLUT4 and the subsequent F-actin cortical rearrangement are both nephrin-dependent mechanisms, and nephrin loss is seen early in many diabetic nephropathy models (149, 169).

3.3.1.2 MicroRNA-146a (miR-146a-5p)

Given its reported anti-inflammatory properties, miR-146a has received attention in elucidating therapeutic targets in insulin resistance, obesity and diabetic nephropathy specifically.

Wu *et al* showed that TNF-α treatment of porcine adipocytes led to elevated levels of miR-146a, which directly targeted and repressed expression of INSR and phosphorylated IRS1, with the outcome of inhibiting adiopogenesis (328).

In a diabetic nephropathy context, miR-146a knockout in streptozotocin (STZ)-induced diabetic mice resulted in accelerated DN, exemplified by exacerbated proteinuria, renal macrophage infiltration, glomerular hypertrophy, and fibrosis. Diabetes-induced upregulation of proinflammatory and profibrotic

genes was significantly increased, suggesting a protective role for miR-146a in DN via the downregulation of target inflammation-related genes such as TRAF6 and IRAK2 (356).

A single study reports a role for miR-146a in podocytes, where miR-146a is decreased in a diabetic milieu characterised by high TGF-β1, resulting in de-repression of Notch-1 and ErbB4, which induces podocyte injury. MiR-146a knockout mice treated with STZ demonstrated accelerated glomerulopathy and albuminuria. Use of ErbB4/EGFR inhibitors to block the deleterious signalling pathway resulted in suppression of podocyte injury *in vitro* and glomerulopathy *in vivo*. MiR-146a levels were also found to be lower in microdissected glomeruli from patients with T2DM; a finding which was inversely correlated with albuminuria and positively correlated with decreased synaptopodin staining, suggestive of podocyte loss (327).

From this evidence, it is possible that miR-146a upregulation seen in my insulin-resistant podocyte model may be an adaptive, anti-inflammatory response to the diabetogenic stimuli (and possibly, in response to co-elevation of proinflammatory miRNAs, as below).

3.3.1.3 MicroRNA-155 and -146a; A signature of inflammation?

MiR-146a is frequently reported to be elevated in concert with miR-155, where it has been shown to antagonise the inflammatory effects of miR-155, thus creating a regulatory feedback loop, as reported by Mann *et al* in the context of NF-κB pathway regulation in macrophage responses (357). Indeed, the co-upregulation of miR-155 and miR-146a in plasma has been reported as a potential biomarker of mortality outcomes in patients with severe sepsis, a condition characterised by rampant systemic inflammatory activation (358).

MiR-155 and miR-146a were simultaneously elevated five-fold in renal biopsy tissue from patients with DN, which additionally correlated to serum creatinine levels (359). The same group investigated the effects of miR-155 and -146a overexpression in human GEnCs *in vitro* and found that high glucose treatment induced upregulation of both TNF-α and TGF-β1, and

activation of NF-κB. The proinflammatory and profibrotic phenotype induced by this miRNA "double-act" has not been reported in podocytes to date, so the congruous elevation of these miRNAs, in a pure podocyte model of insulin resistance, is an interesting finding.

3.3.1.4 MicroRNA-222 (miR-222-3p)

MiR-222 was the most significantly upregulated miRNA in the insulin-resistant podocyte model. Predominantly implicated in oncogenesis (304), renal-specific roles of miR-222 are rarely reported. However, a number of interesting miR-222 targets relating to diabetes and insulin resistance have been experimentally validated, such as IRS1, which is repressed by high circulating levels of miR-222 in mouse models of fatty liver disease. Moreover, overexpression of miR-222 in hepatocytes *in vitro* attenuates phosphorylation of Akt in response to insulin. (309). MiR-222 is also implicated in the mechanism of development of gestational diabetes (GDM). Zhonghua Shi *et al* reported upregulation of miR-222 in omental adipocytes of women with GDM and repression of confirmed targets GLUT4 and Estradiol receptor alpha (ERα). *In vitro* silencing of miR-222 resulted in 40% increase in glucose uptake and restored target expression levels of ERα and GLUT4 (306). If these miR-mRNA target effects are replicated in insulin-resistant podocytes, then miR-222 directed repression of IRS1 and GLUT4 could account for the observed attenuation in Akt signalling and glucose uptake in my experimental model.

3.3.2 Downregulated MicroRNAs

3.3.2.1 MicroRNA -204 (miR-204-5p)

MiR-204 has been reported as a potential modulator of the Metabolic syndrome given its correlation with body mass index, waist-to-hip ratio and HDL cholesterol levels in a large population study of patients with MetSyn (335). Civelek *et al* showed inverse expression of predicted target acetyl coenzyme A carboxylase b (ACACB) in this cohort, and parallel *in vitro* work confirmed repression of this gene, thought to control mitochondrial fatty acid oxidation in miR-204 overexpressing HeLa cells.

The downregulation of miR-204 seen in the insulin-resistant podocyte model has also been reported in adipose tissue of mice that were fed a high-fat diet, further implicating this miRNA in the obese phenotype (360)

At the podocyte level, a single report suggests that miR-204 may prevent high glucose-induced apoptosis through downregulation of Bradykinin B2 receptor Bdkrb2 (336) , the suppression of which is known to induce pro-apoptotic p38 MAPK pathway (361). Therefore, the observed downregulation of miR-204 in my model may represent loss of an important protective mechanism in DN.

3.3.2.2 MicroRNA -497 (miR-497-5p)

MiR-497 targets some very prominent genes in insulin signalling, such as the insulin receptor (IR), insulin-like growth factor 1 receptor (IGF-1R) and insulin receptor substrate-1 (IRS1). Most research to date has focused on tumour-suppressing effects of this targeting in promoting mitogenesis and oncogenesis, often meditated via the Akt and ERK pathways (342, 343).

However, a few studies investigated the role of miR-497 in insulin resistance specifically. Wang *et al* confirmed direct targeting of IR in rat hepatocytes leading to negative regulation of IRS1/PI3K/Akt/GSK-3β/GS pathway (344). MiR-497 has also been shown to stimulate β-cell insulin release via repression of confirmed target UCP2, mitochondrial uncoupling protein (362). In the former study, elevated miR-497 was considered to reduce insulin sensitivity, whilst the latter attributes this to the *loss* of miR-497 (as replicated in my data). This highlights the importance of considering the mechanism of insulin resistance investigated (here comparing a *response* to insulin with the production, and thus *availability* of insulin) and also the cell-specific nature of miRNA action.

3.3.2.3 MIcroRNA -338 (miR-338-3p)

Decreased expression of miR-338 seen in the insulin-resistant podocyte model has also been reported in the livers of db/db and high fat diet (HFD) fed mice (352) . MiR-338 has been shown to mediate TNF-α induced insulin resistance in

hepatocytes via targeting of protein phosphatase 4 regulatory subunit 1 (PP4R1), and its overexpression can rescue hepatic insulin resistance both *in vitro* and *in vivo* (352).

Insulin receptor substrate 2 (IRS2) has been reported as a target of miR-338 in non-small cell lung carcinoma. Zhang *et al* found low expression of miR-338 was associated with advanced tumour staging and presence of metastases, whilst its overexpression *in vitro* suppressed cell proliferation and migration which was rescued on overexpressing the repressed target, IRS2 (350). This is particularly interesting given that IRS2 is the dominant form of IRS in podocytes, known to be critical for activation of Akt, GLUT4-mediated glucose uptake and cytoskeletal remodelling (158).

3.3.3 Caveats with the *in vitro* model of podocyte insulin resistance

The multi-stimuli approach to rendering podocytes insulin resistant *in vitro* was considered to be the most accurate representation of the diabetic milieu in T2DM patients. However, it may be argued that the use of supraphysiological doses of insulin and high physiological doses of cytokines and glucose may be more likened to "extreme" diabetic conditions. Precisely how realistic this model is, is difficult to define. However, ongoing work by the Bristol renal unit has confirmed that each of the stimuli in isolation may induce podocyte insulin resistance, and that this is likely to be via different mechanisms, some of which have been well characterised (e.g. lysosomal degradation of the insulin receptor in response to prolonged hyperinsulinemia (162)). By including multiple diabetogenic stimuli, there is greater chance of replicating the interplay of aberrant mechanisms that effect the development of podocyte insulin resistance. The downside to this is that as pathways become more complex, so the potential network of miRNA regulation increases, making it difficult to tease out miRNAs of critical importance in insulin signalling.

The microarray analysis performed here provides an unbiased readout of differentially expressed miRNAs in this model. All of the top 3 selected upregulated miRNAs were validated by RT-qPCR, but for only 1 of the selected downregulated miRNAs, (miR-204), was this achieved. This finding raises the

possibility that either a false positive (Type 1 error) has occurred in the microarray analysis, or conversely, a Type 2 error has resulted in rejection of miR-338 and -497 during RTqPCR validation. The latter may occur due to the relatively lower baseline abundance of miR-338 and -497 in podocytes, and therefore greater sensitivity may be required to demonstrate an expression change by RT-qPCR. The decision to select 3 up- and 3 downregulated miRNAs from the array results was based on avoidance of a bias in selecting only upregulated miRNAs of interest. However, the lower baseline expression of these miRNAs, coupled with being downregulated in insulin resistance, may ironically have lead to a bias in being unable to detect a change during qPCR validation. This finding effectively ruled out miR-497 and -338 for further investigation.

3.3.4 Conclusion

In conclusion, I have demonstrated a robust *in vitro* model of podocyte insulin resistance that displays a unique microRNA signature, thereby implicating miRNAs as important regulators of the podocyte insulin response. 5 out of 6 of the most significantly up-and downregulated miRNAs have known or predicted targets within insulin signalling pathways; miR-155 in particular is known to regulate insulin sensitivity in other insulin responsive cells. Furthermore, the expression levels of miR-155 have been correlated to important serum and histological parameters in diabetic kidney disease, making this miRNA the most promising of the selected candidates to pursue in further experimental work.

4 The role of microRNA-155 in Podocyte Insulin Resistance

4.1 Introduction

Of the 6 candidate miRNAs identified from the array profiling of the insulin-resistant podocyte model described in the previous chapter, upregulation of miR-155 was of immediate interest given its established roles in inflammatory pathways that are significant in the development of insulin resistance, obesity and the metabolic syndrome. At the level of the kidney, whole tissue expression of miR-155 is elevated in human DN biopsies and correlates with serum creatinine levels (359), and miR-155 knockout in mice promotes nephrin expression and reduces podocyte apoptosis (258, 259). For these reasons, and those described in 4.2 below, miR-155 was selected for focused investigation of mechanistic involvement in podocyte insulin resistance.

In this chapter, I describe the effect of miR-155 manipulation on critical components of podocyte insulin responses. Welsh *et al* have shown that insulin signals to the podocyte predominantly via the PI3K/Akt and MAPK pathways (148), and work presented in the previous chapter confirms loss of this signalling in the devised *in vitro* model of insulin resistance. MiR-155 manipulation effects were, therefore, focused on these pathways, in addition to measurement of downstream glucose uptake. The phenotypic consequences of miR-155 manipulation are focused on conformational changes of the cytoskeleton, where podocytes demonstrate F-actin remodelling in response to insulin (148), hypothesised to be an adaptive mechanism to withstand the transient increase in glomerular filtration rate (GFR) seen in the post-prandial state as a consequence of factors including insulin-mediated nitric oxide release and protein-stimulated hyperfiltration (148, 152, 153). Loss of this cytoskeletal response may be an inciting trigger in the development of diabetic podocytopathy and is, therefore, an important experimental endpoint.

Finally, bioinformatically-predicted targets of miR-155 are explored to establish potential mechanistic action of miR-155 in the development of podocyte insulin resistance, and analysed against RNAseq data from the multi-stimuli *in vitro* model of podocyte insulin resistance described in Chapter 3.

4.1.1 Chapter Aims

1. Test the effect of miR-155 overexpression in podocytes on:
    a. Insulin signalling pathways
    b. Cytoskeletal responses to insulin
2. Perform *in silico* prediction of miR-155 targets, and evaluate target repression using RT-qPCR

4.2 Results

4.2.1 Urinary MicroRNA-155 is elevated in DN

Concurrent work in the Fraser Lab (Cardiff) is focused on the use of urinary miRNAs as biomarkers in diabetic kidney disease (DKD). For this work, 20 patients with DKD and 20 healthy controls were approached and consented by myself and urine samples obtained were registered to the Wales Kidney Research Unit Biobank (clinical characteristics of patient cohort is provided in Table 1 of appendix 1). Taqman Microarray analysis was used to measure the differential expression of urinary miRNAs in this cohort (236). Figure 4.1A shows the volcano plot created from this analysis. MiR-155 was significantly upregulated ≈ 6 fold in this cohort, and this was validated using miR-155 specific RT-qPCR assay (22.9-fold increase, p=0.0024) (Figure 4.1B). A larger validation cohort, composed of patients with clinically or biopsy confirmed DN (n= 89) versus those patients with diabetes with no renal involvement (n= 62) and healthy controls (n= 41), demonstrated the ability of urinary miR-155 to differentiate DN patients from both healthy controls (1.8-fold increase, $p<0.001$) and diabetics without evidence of DKD (1.6-fold increase, p=0.024) as depicted in Figure 4.2. This data therefore strengthened the existing rationale for focus on miR-155, as podocyte injury/cell sloughing represents a plausible source of the detected increase in urinary miR-155 in DKD.

A B

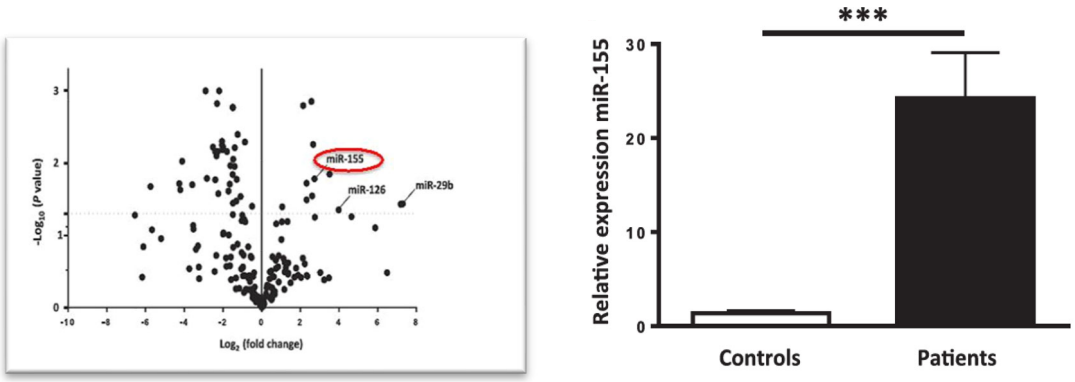

Figure 4.1A Urinary miR-155 upregulation in DKD. Volcano plot depicting differential miR expression in the urine of patients with DKD (n=20) compared to healthy controls (n=20) in an initial discovery cohort, using Taqman Array. MiR-155 highlighted as a significantly upregulated miRNA in DKD. **Figure 4.1B RT-qPCR validation of miR-155 upregulation in DKD patient urine (discovery cohort).** Mean **+/-** SEM of n=20 patient and 20 control urines, unpaired one-tailed t-test with Welch's corrections used, data normalised to endogenous control miR-191. *** p<0.001.

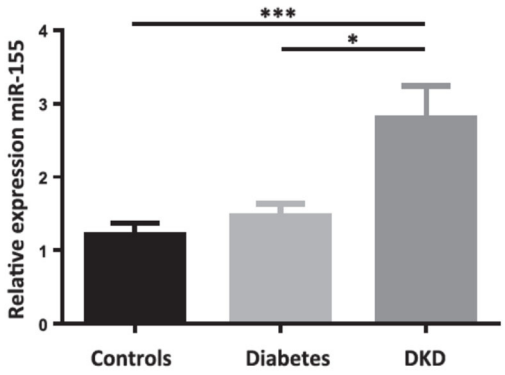

Figure 4.2 Urinary miR-155 can discriminate between DKD patients and those with diabetes without renal disease. Quantitative RT-qPCR measurement of urinary miR-155 in healthy controls (n=41), DKD patients (n= 89) and those with diabetes without evidence of DKD (n=62). Mean +/-SEM shown, unpaired one-tailed t-test with Welch's corrections used, data normalised to endogenous control miR-191. * p<0.05, **p<0.01, *** p<0.001. Figures taken from Beltrami *et al*, *Am J Pathol*, **2018**. (AW Contribution: Research design and planning, patient consenting and urine collection, data analysis of clinical correlative data.)

4.2.2 Lentiviral over-expression of miR-155

Initial attempts to manipulate miR-155 were performed using lentiviral transduction, with the aim of developing a stable podocyte cell line that exhibited enforced expression of miR-155. Incremental doses of GFP-labelled miR-155 and control lentiviruses were added to fully differentiated podocytes (day 13) to establish the dose that would achieve optimum infectivity without compromising cell viability. Figure 4.3B shows the percentage of GFP-positive cells at each viral dose, with highest titrated dose (100 µl) achieving GFP-positivity of 93.2% in the miR-155 transduced cells. The transduction efficiency of the control virus was inferior, with equivalent dose achieving 73.2% GFP-positivity. This was also subjectively evident from the microscopy images, with control wells appearing less fluorescent green than the equivalently dosed miR-155 infected wells (Figure 4.3A).

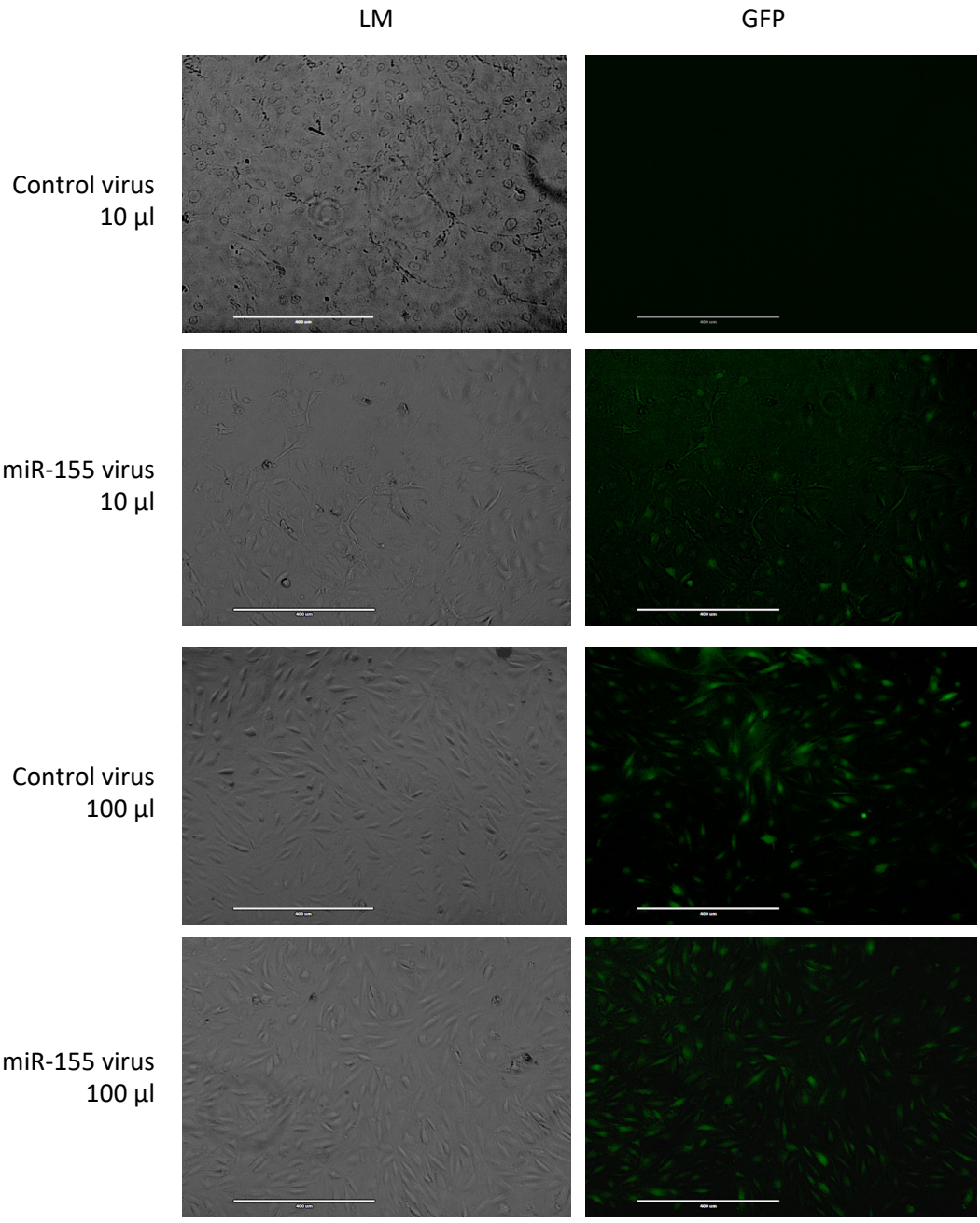

Figure 4.3A Microscopy of GFP-labelled miR-155 overexpressing podocytes. Light microscopy (LM) and Fluorescence microscopy (GFP) of miR-155 overexpressing and control podocytes treated at the lowest (10 µl) and highest (100 µl) viral doses shown. Cells treated with 10 µl control virus appeared morphologically abnormal, indicative of podocyte stress. No fluorescence was detected by microscopy in these wells. Scale bar = 400µM.

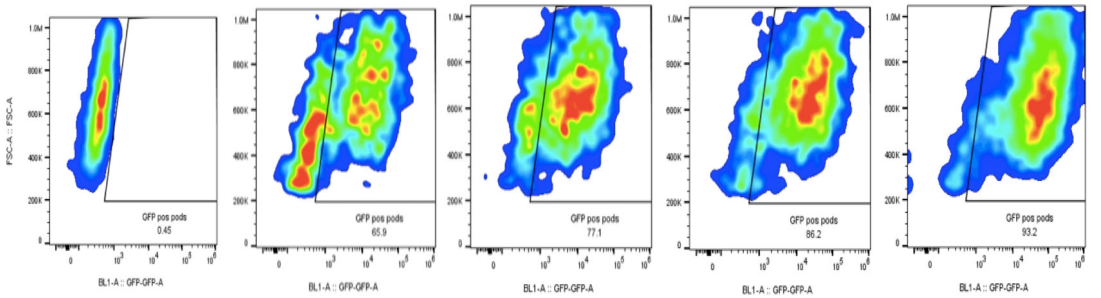

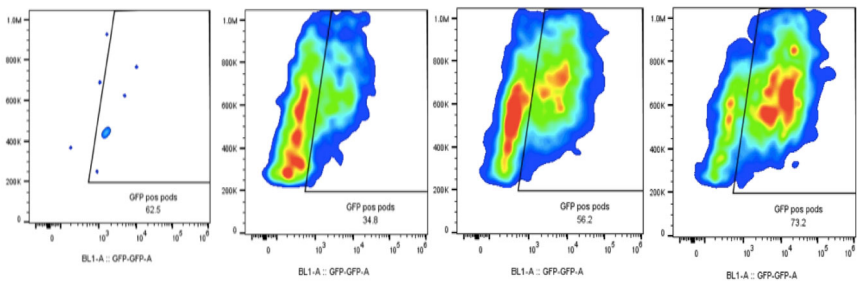

	Dose	NS-1	miR-155	Non-infected
% GFP +ve	10 µl	6.25	65.9	0.45
	20 µl	34.8	77.1	
	50 µl	56.2	86.2	
	100 µl	73.2	93.2	
MFI	10 µl	3651	27552	1836
	20 µl	7046	21244	
	50 µl	10782	41107	
	100 µl	18141	94763	

Figure 4.3B. Flow cytometry assessment of GFP-positive podocytes. Podocytes were transduced with GFP-labelled miR-155 and control viruses (NS-1) at incremental doses as shown. Cells were analysed for GFP-positivity using the Attune NxT flow cytometer. FSC= forward scatter, BL-1= Blue laser detector, GFP= green fluorescent protein, NS-1= control virus batch name, MFI=Mean fluorescence intensity.

RT-qPCR of the transduced cells showed an increase in miR-155 expression at all trialled doses (Figure 4.4), and this did not appear to be dose dependent (5.6-fold increase at 20 µl, 4.1-fold increase at 100 µl). Cells incubated with control virus exhibited altered morphology and reduced cell confluence in some wells, which I inferred to represent decreased survival. Consistent with this, insufficient RNA was extracted for RT-qPCR in two of the samples.

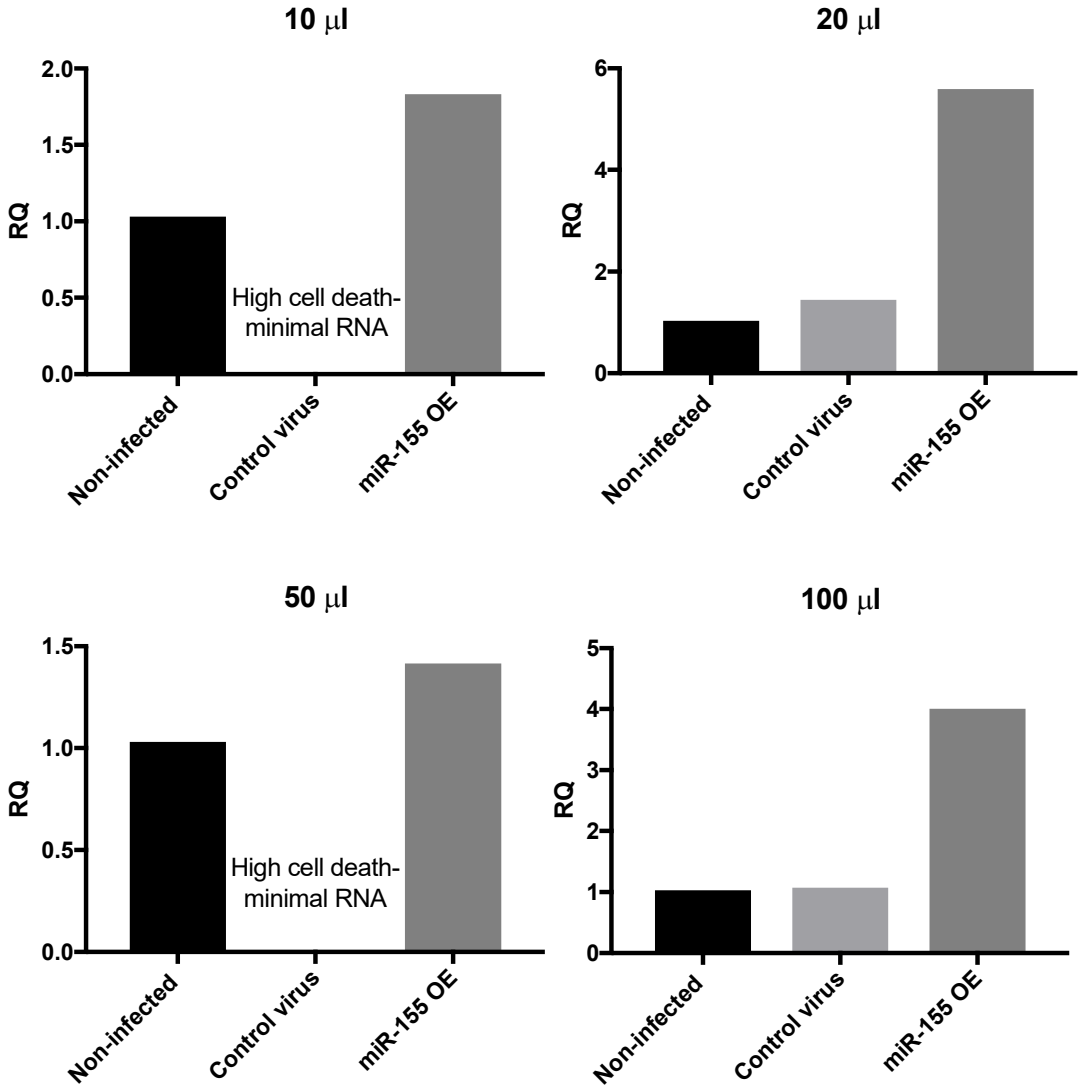

Figure 4.4 MiR-155 overexpression (OE) in lentivirally transduced podocytes. Fully differentiated podocytes (day 13) were transduced with miR-155 and control viruses at the doses shown. RT-qPCR was performed to assess degree of miR-155 overexpression achieved. Results shown relative to non-infected control, owing to insufficient RNA in cells treated with control virus at the 10 and 50 µl doses. U6 used as reference gene, n=1.

The above was repeated using the maximum viral dose (100 µl), applied at an earlier stage of differentiation (day 7), approximately 2/3 of the way through the transition to terminally differentiated cells. This time point was considered a sensible compromise between improving cell viability by transducing (slowly) dividing cells, and inducing the miRNA overexpression at an established enough point in differentiation that it would be unlikely to interrupt a crucial phase of podocyte maturation. Control cell morphology was improved by this method, although wells continued to demonstrate mild reduction in fluorescence on microscopy, compared to equivalently dosed miR-155 infected cells (Figure 4.5A). At the RNA level, miR-155 expression was increased 1.8-fold compared to non-infected controls, yet the same response was observed with the control virus. (Figure 4.5B).

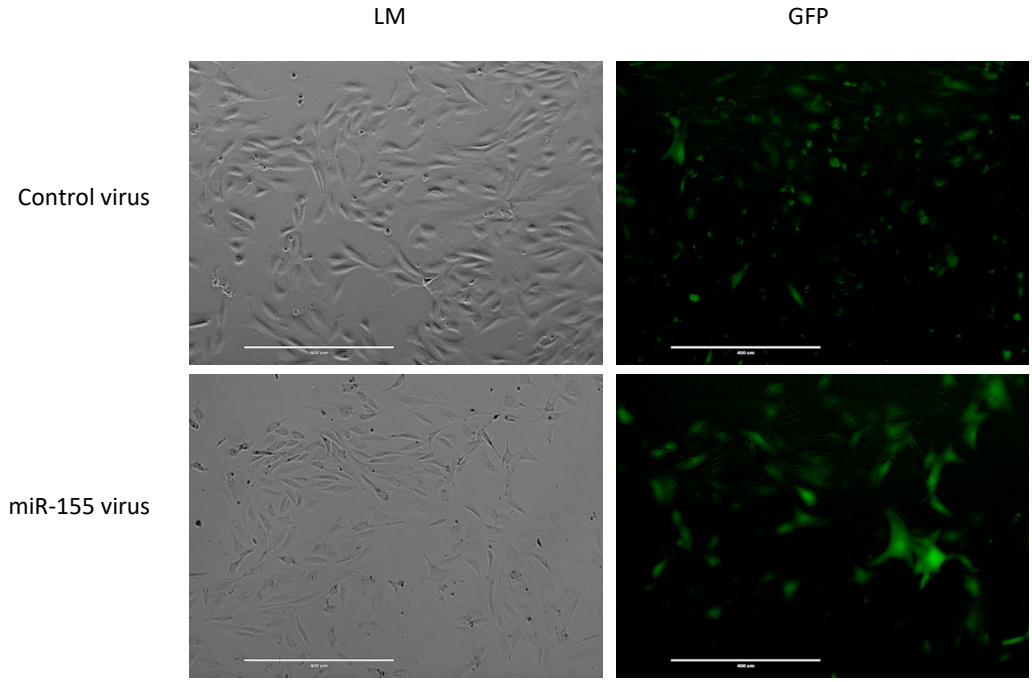

Figure 4.5A Microscopy of GFP-labelled miR-155 overexpressing podocytes: late differentiation model. Podocytes were transduced 2/3 of the way through differentiation (day 7) with 100 µl miR-155 and control virus respectively. Light microscopy (LM) and Fluorescence microscopy (GFP) shown. Scale bar = 400 µm

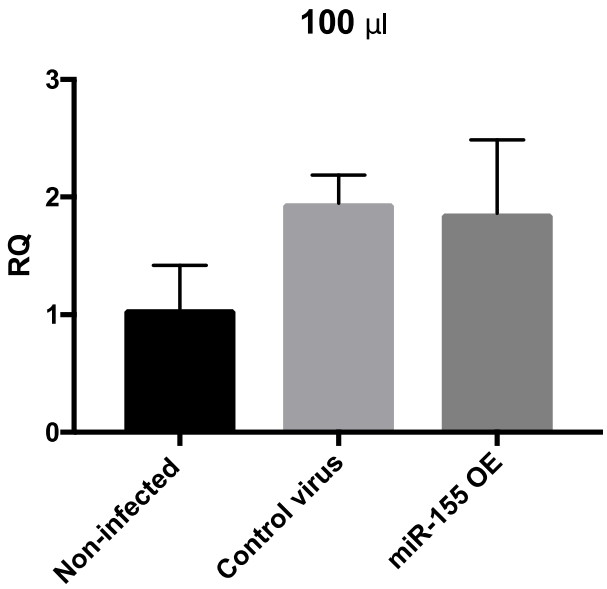

Figure 4.5B miR-155 expression in lentivirally transduced podocytes: late differentiation model. Podocytes were transduced 2/3 of the way through differentiation (day 7) with 100 µl miR-155 and control virus respectively. RT-qPCR was performed to assess degree of miR-155 overexpression achieved. U6 used as reference gene. Mean +/-SD of 3 technical replicates shown.

Whilst the decision to transduce the cells at an earlier stage of differentiation appeared to improve cell viability, the upregulation of miR-155 in control cells was unacceptable, and I therefore opted to evaluate an alternative approach to manipulating miR-155 expression *in vitro*. Commercially available miR-155 mimic and inhibitors were employed for all further work, as below.

4.2.3 MiR-155 manipulation using *mirVana*™ mimics/antagonists

MirVana miR-155 mimic, inhibitor and respective miR-controls were transfected into differentiated podocytes as described in Methods 2.13.2. Initial experiments were conducted to determine the optimum dose of mirVana mimic to achieve overexpression in podocytes, as per manufacturers recommendations. Alamar blue assay was performed to ascertain cell viability after transfection at the stated doses (Figure 4.6). Highest dose (30 nM) of both mimic and control miRNAs had no significant effect on cell viability.

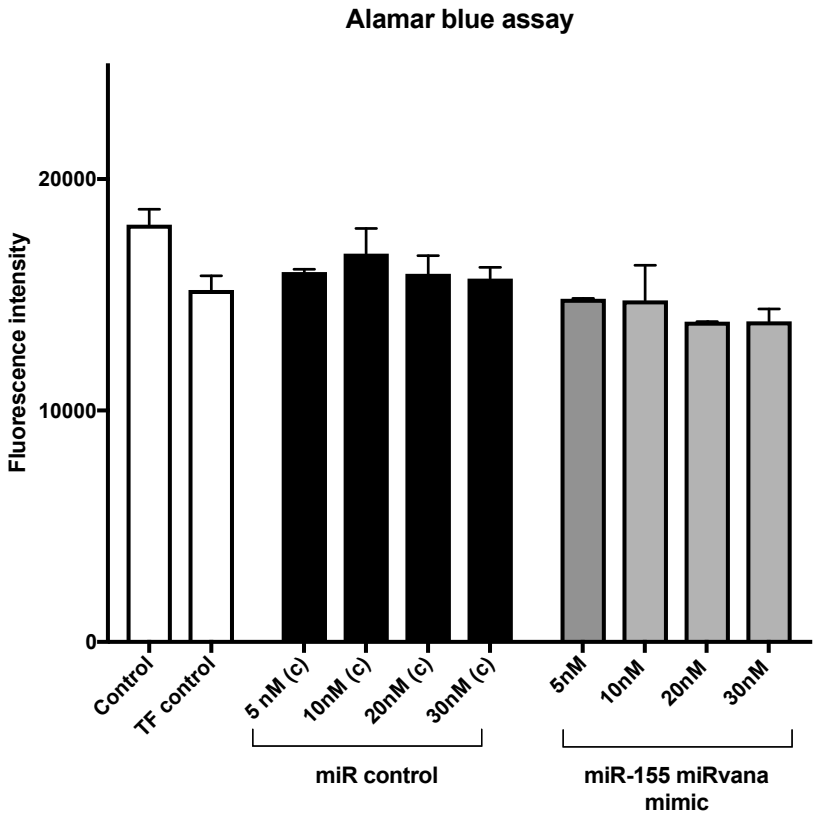

Figure 4.6 Cell viability is unaffected by mirVana mimic transfection. Fully differentiated podocytes (day 11) were transfected with incremental doses of mirVana miR-155 mimic as per manufacturers protocol and incubated for 48 hours. Alamar blue assay was performed immediately prior to RNA extraction and fluorescence intensity recorded by Fluostar Optima Spectrometer. Mean of duplicate reads shown. TF= transfection reagents only control.

The relative quantification of detected miR-155 in the mimic-transfected cells is shown in Figure 4.7. This optimisation experiment was sufficient to establish a working dose of 30 nM, which resulted in greatest miR-155 expression with no evidence of decreased metabolic activity by Alamar blue assay.

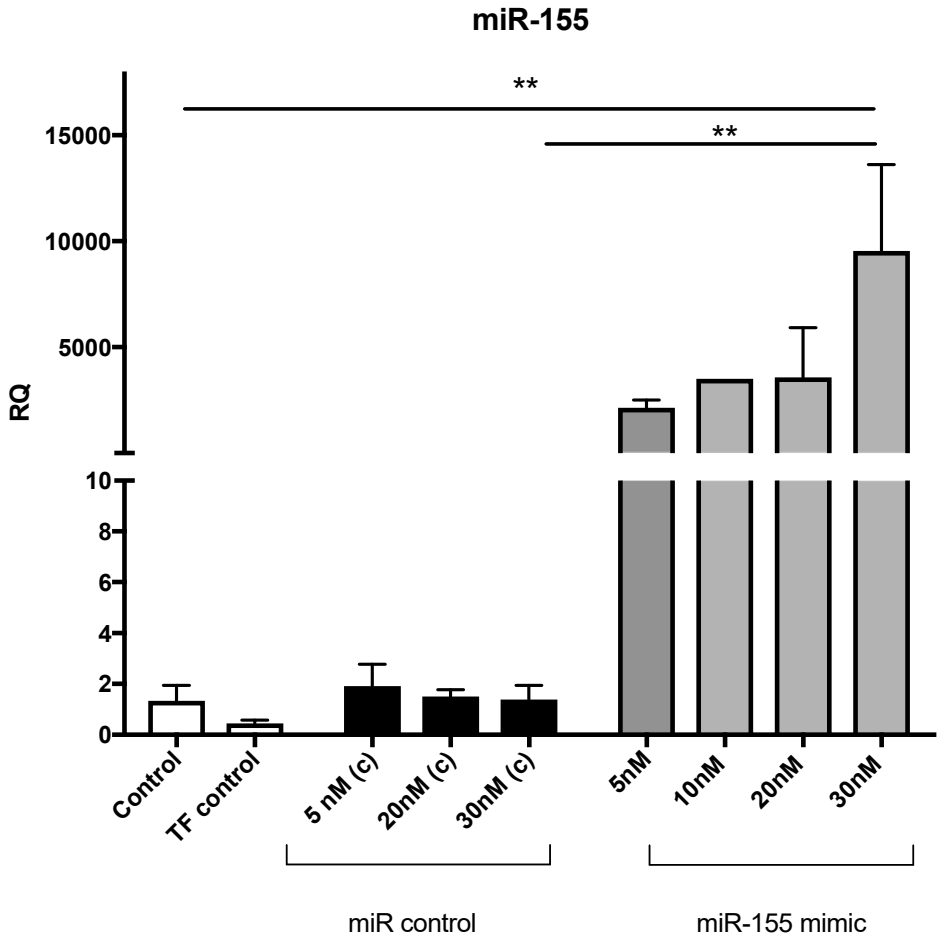

Figure 4.7 miR-155 expression following mirVana mimic transfection. Fully differentiated podocytes (day 11) were transfected as per manufacturers protocol, with incremental doses of mirVana miR-155 mimic and incubated for 48 hours before RNA extraction. RT-qPCR performed using U6 as reference gene, relative quantification (RQ) calculated relative to non-transfected control. Mean +/-SD of n=3 experiments shown. One-way ANOVA and Tukeys multiple comparison testing performed $p<0.05$; **, $p<0.01$; ***, $p<0.005$; **** $p<0.001$.

In order to determine the functional significance of miR-155 mimic transfection, the expression of 4 experimentally validated mRNA targets, selected from previous literature review (see Table 3.1A of previous chapter) were measured by RT-qPCR (Figure 4.8). PIK3R1 was significantly repressed (55% reduction compared to miR-control, p= 0.01), RhoA was repressed compared to expression levels in WT podocytes (69% reduction, p=0.03), but not significantly repressed compared to miR control (p=0.13). MRNA expression of INPP5D (aka SHIP-1) and SOCS1 was not affected by miR-155 overexpression in these experiments.

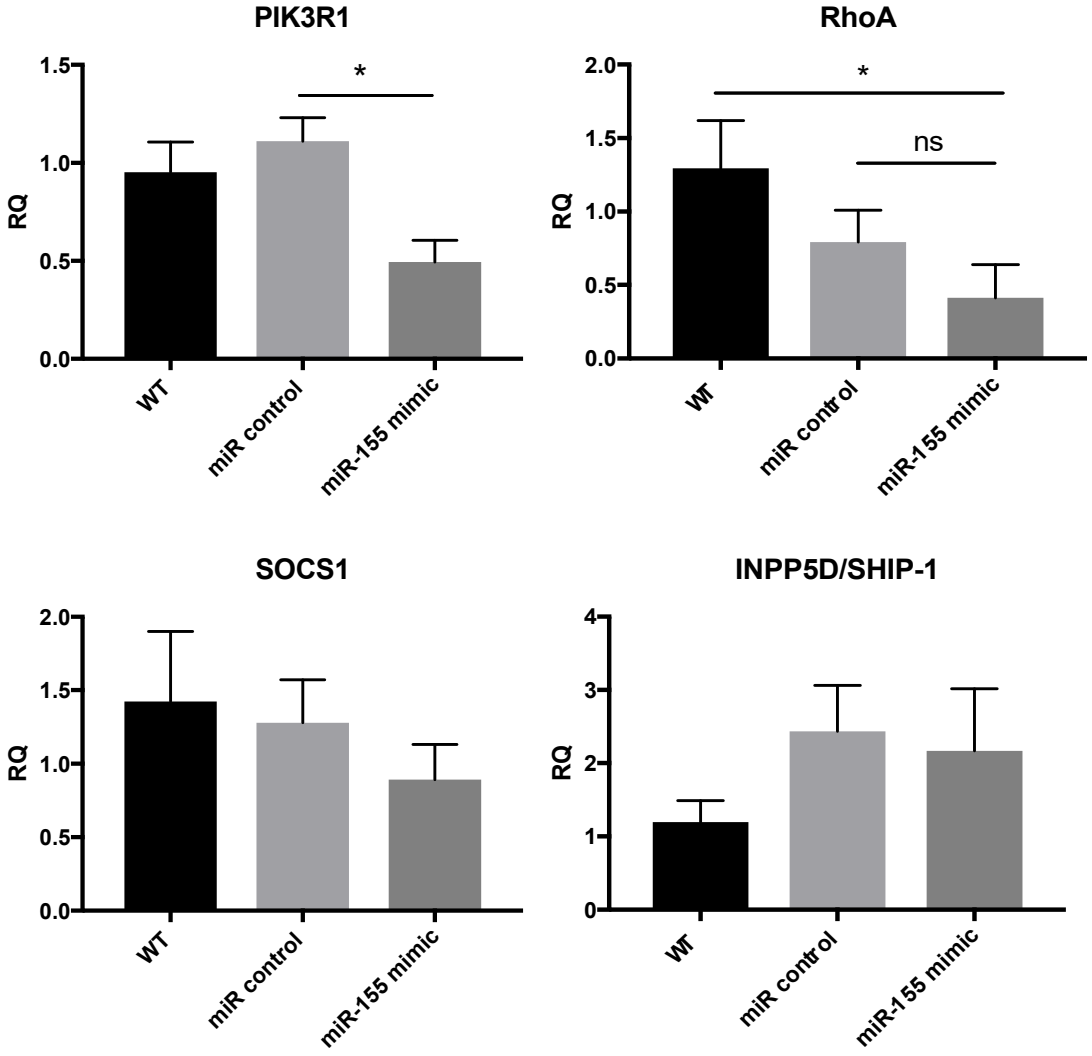

Figure 4.8 Expression of validated miR-155 mRNA targets following miR-155 mimic transfection. Fully differentiated podocytes (day 11) were transfected with 30 nM mirVana miR-155 mimic and respective miR-control, for 48 hours. RT-qPCR was used to determine expression levels of 4 mRNA targets associated with insulin signalling, calculated relative to expression in wild type (WT), non-transfected podocytes. β Actin used as reference gene. Mean +/- SEM of n=3 independent experiments shown. One-way ANOVA and Tukeys multiple comparison testing performed *p<0.05; **p<0.01; *** p<0.005; **** p<0.001

The above was repeated using mirVana miR-155 inhibitor to assess for evidence of target de-repression. None of the mRNA targets investigated were elevated relative to basal expression in unstimulated WT podocytes (Figure 4.9).

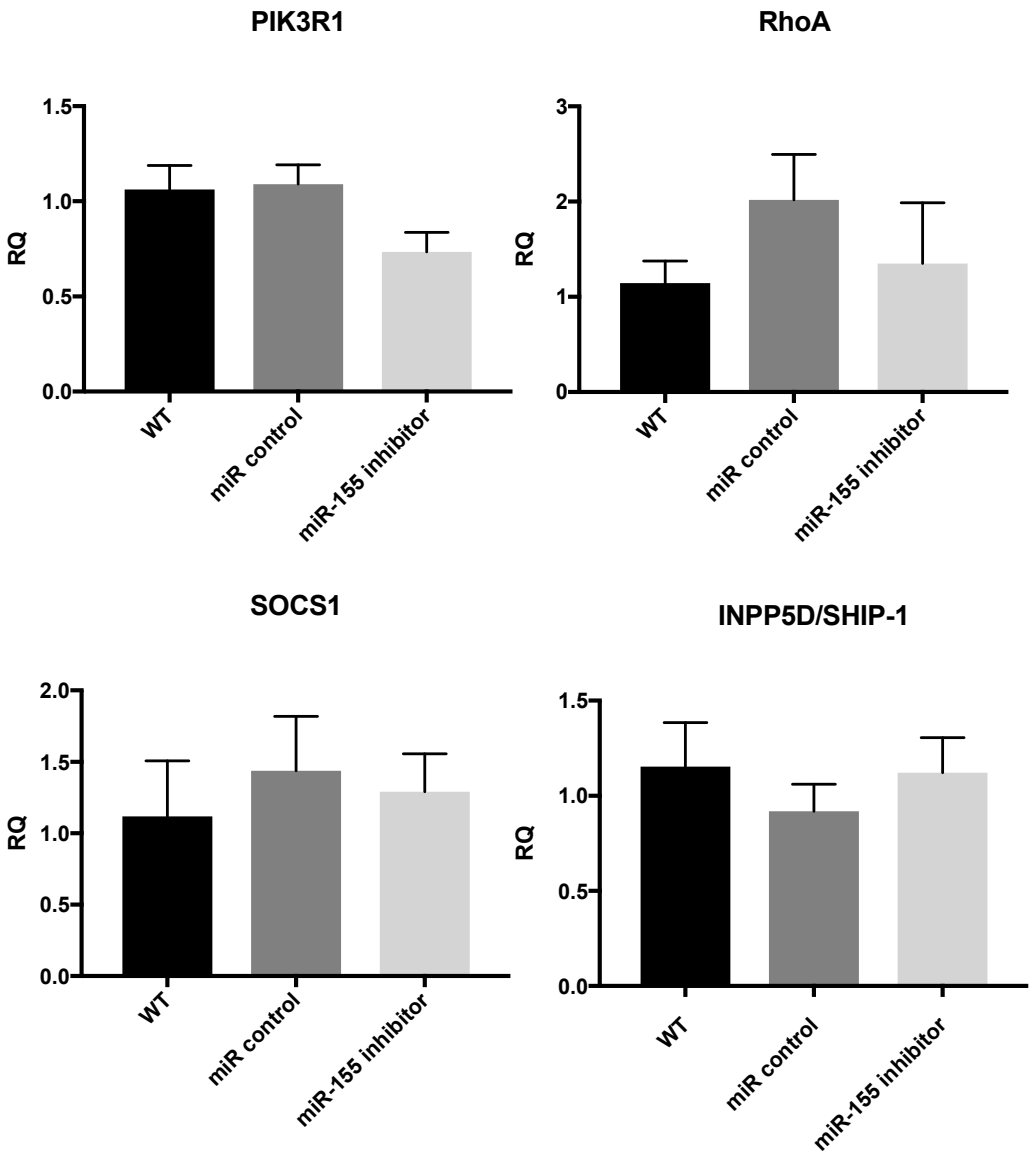

Figure 4.9 Expression of validated miR-155 mRNA targets following miR-155 inhibitor transfection. Fully differentiated podocytes (day 11) were transfected with 30 nM mirVana miR-155 inhibitor and respective miR-control, for 48 hours. RT-qPCR was used to determine expression levels of 4 mRNA targets associated with insulin signalling, calculated relative to expression in wild type (WT), non-transfected podocytes. β Actin used as reference gene. Mean +/- SEM of n=3 independent experiments shown.

4.2.4 Effects of miR-155 manipulation on proximal insulin signalling

Having demonstrated miR-155-induced repression of PIK3R1, an important mediator of PI3K signalling, I proceeded to investigate the effects of miR-155 manipulation on proximal insulin signalling pathways. Podocytes rendered insulin-resistant using diabetogenic media *in vitro* exhibit reduced phosphorylation of Akt and MAPK (Chapter 3). To investigate whether this could be a miR-155 dependent phenomenon, phosphorylation status of Akt (Serine 473) and MAPK (p42/44) was examined in overexpressing miR-155 podocytes in the basal and insulin-stimulated state (Figure 4.10A). Densitometry of n=3 experiments confirmed significant attenuation of insulin-stimulated pAkt (Figure 4.10B), however no change in pMAPK was observed in miR-155 overexpressing cells.

A.

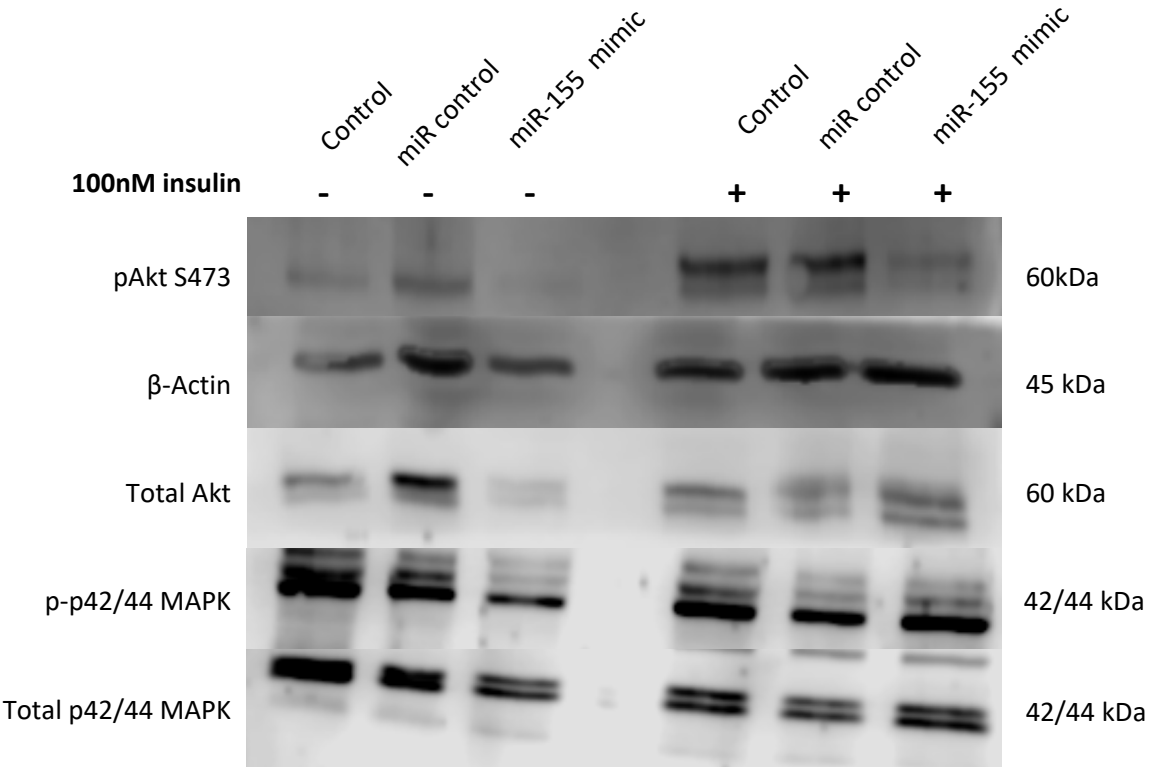

B.

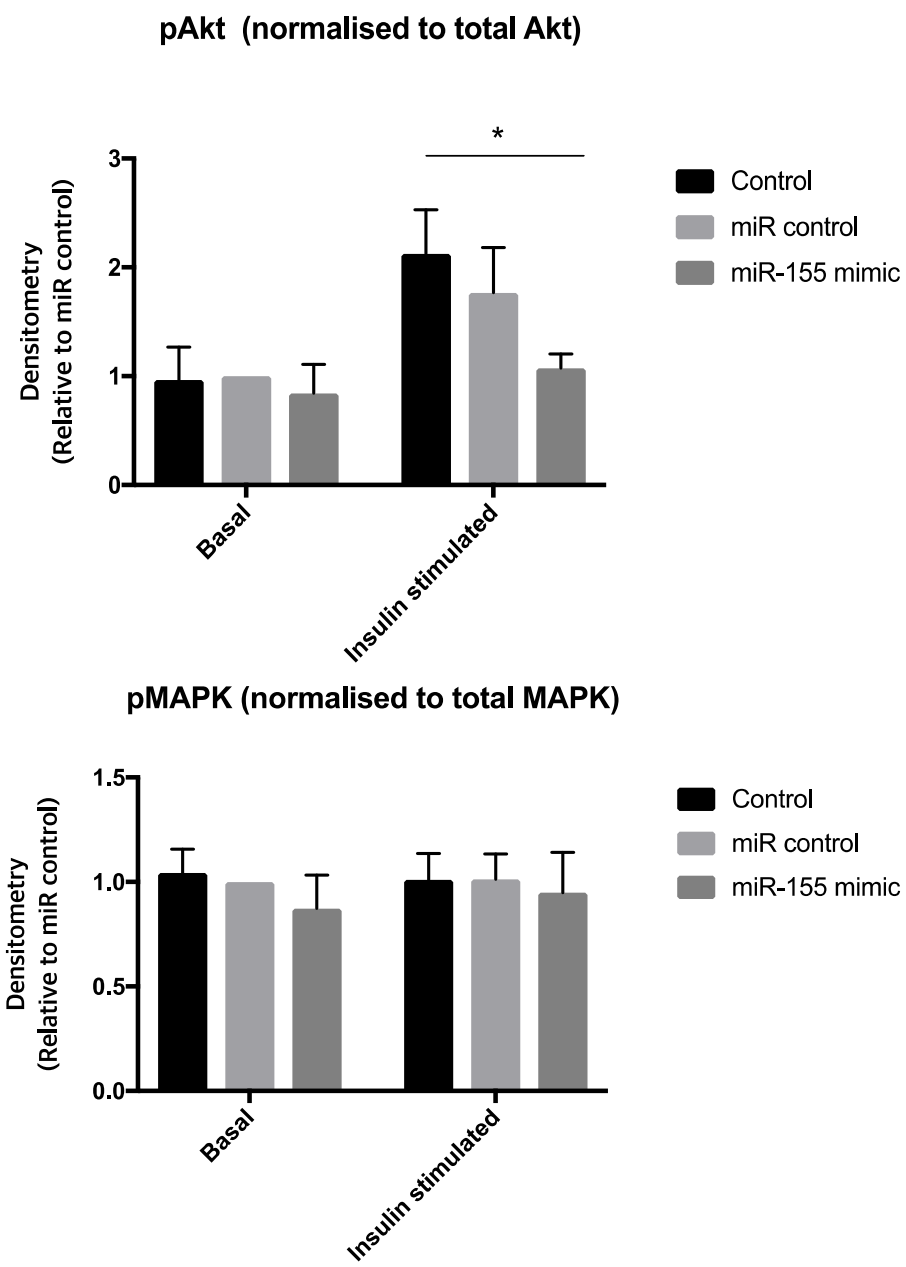

Figure 4.10 Effect of miR-155 overexpression on proximal insulin signalling in podocytes. Podocytes were transfected with 30 nM *mirVana*™ miR-155 mimic and protein-lysed at 48 hours. Insulin-stimulated cells were treated with 100 nM insulin for 15 mins, immediately prior to lysis. **A.** Representative western blot of n=3 independent experiments shown **B**. Corresponding densitometry n=3, calculated relative to basal expression in miR-control samples and normalised to total Akt/MAPK, respectively. Mean +/-SEM of n=3 experiments shown, one-way ANOVA and Tukeys multiple comparison testing performed, *p<0.05.

Subsequently, effects of miR-155 antagonism were evaluated in podocytes transfected and stimulated as above with mirVana miR-155 inhibitor. Insulin-stimulated phosphorylation of Akt (Figure 4.11A) and MAPK (Figure 4.11B) appeared enhanced in miR-155 inhibited podocytes, although this was likely a result of unequal protein loading, as shown by densitometry. As in mimic transfections, control cells responded less avidly to insulin via the MAPK signalling pathway.

A.

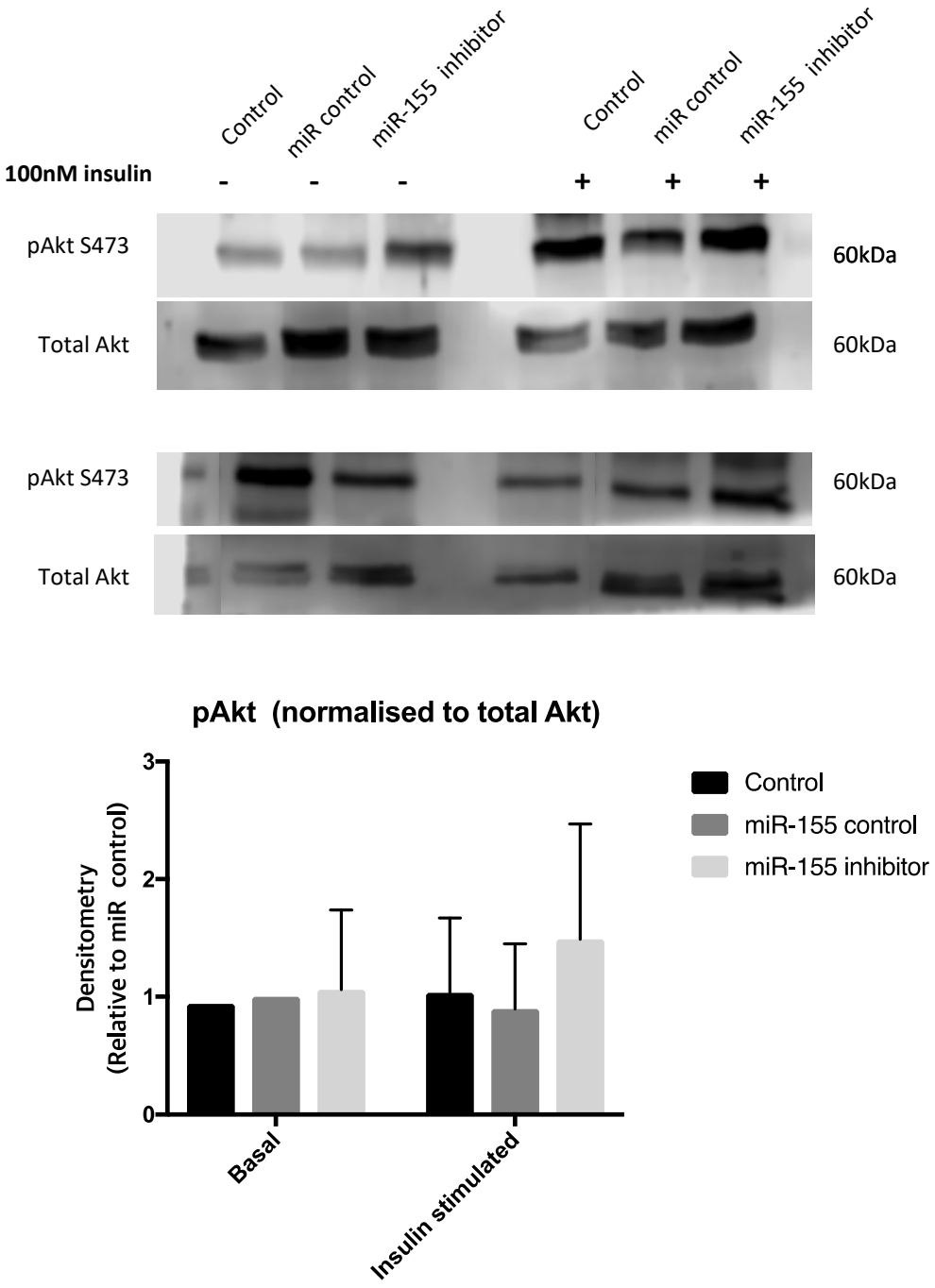

B.

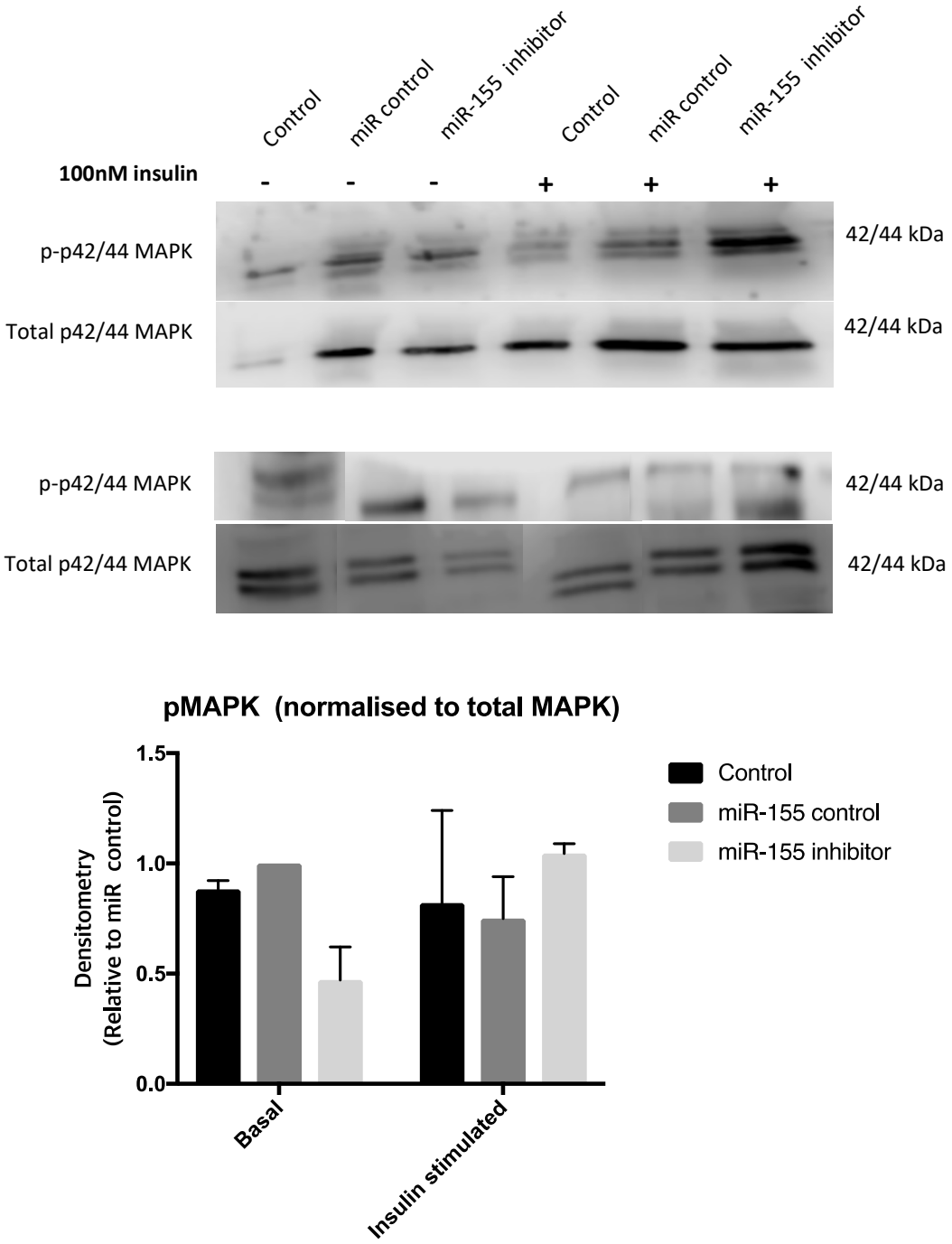

Figure 4.11 Effect of miR-155 inhibition on proximal insulin signalling in podocytes.
Podocytes were transfected with 30 nM *mirVana*™ miR-155 inhibitor and protein-lysed at 48 hours. Insulin-stimulated cells were treated with 100 nM insulin for 15 mins, immediately prior to lysis. **A** Western blot showing n=2 independent experiments of insulin-stimulated pAkt in miR-155 silenced cells, plus corresponding densitometry (mean +/-SEM of n=2 only therefore no statistical test applicable). **B** Western blot showing n=2 independent experiments of insulin-stimulated pMAPK in miR-155 silenced cells, and corresponding densitometry.

4.2.5 Effect of miR-155 manipulation on distal insulin signalling

Whilst Akt and MAPK are known to play key roles in podocyte insulin signalling, it is possible that miR-155 may (directly or indirectly) repress additional targets up-and/or- downstream of phosphorylation of these kinases. Subsequently, radiolabelled glucose uptake in miR-155 manipulated cells was investigated as an objective, common distal marker of podocyte insulin resistance. WT non-transfected controls and miR-control cells showed a significant increase in glucose uptake in response to insulin (1.6-fold, p=0.02 and 1.3-fold, p=0.02, respectively). No response to insulin was observed in miR-155 overexpressing podocytes (Figure 4.12).

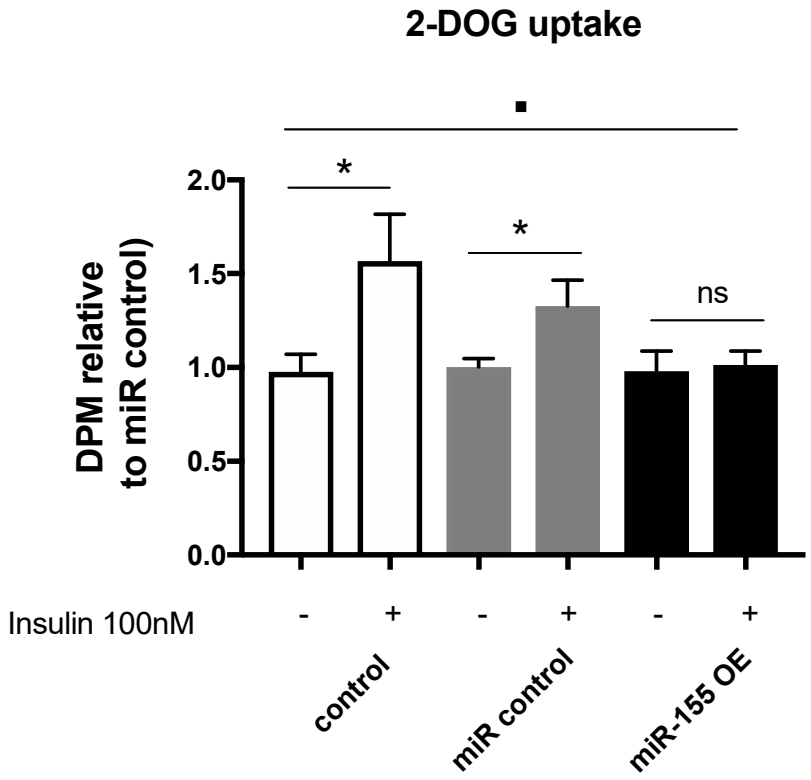

Figure 4.12 MiR-155 overexpression abrogates insulin-stimulated glucose uptake in podocytes. Podocytes were transfected with 30 nM *mirVana*™ miR-155 mimic and control. Cells were challenged with 100 nM insulin for 15 minutes and 50 μM (3H)2-deoxy-D-glucose (2-DOG) for 5 minutes. Cellular uptake of radiolabelled glucose shown as DPM counts relative to miR control. Mean +/- SEM shown for n= 4 independent experiments. One-way ANOVA performed, p= 0.01 (indicated by black square symbol). Unpaired one-tailed t-test performed (indicated by black asterix), *p<0.05. DPM= disintegrations per minute.

4.2.6 Effect of miR-155 overexpression on cytoskeletal conformation

Having established that miR-155 overexpression abrogates insulin-induced uptake of glucose, which is hypothesised to provide the carbohydrate energy source to permit post-prandial cytoskeletal remodelling, I sought to determine the effect of miR-155 overexpression on peripheralisation of F-actin. Podocytes were stimulated with 100 nM insulin for 15 mins, and F-actin distribution compared using immunofluorescence microscopy. Representative images are shown in Figure 4.13. The expected insulin-induced cortical rearrangement of F-actin was not clearly seen in any of the cells (including controls) by this experimental method.

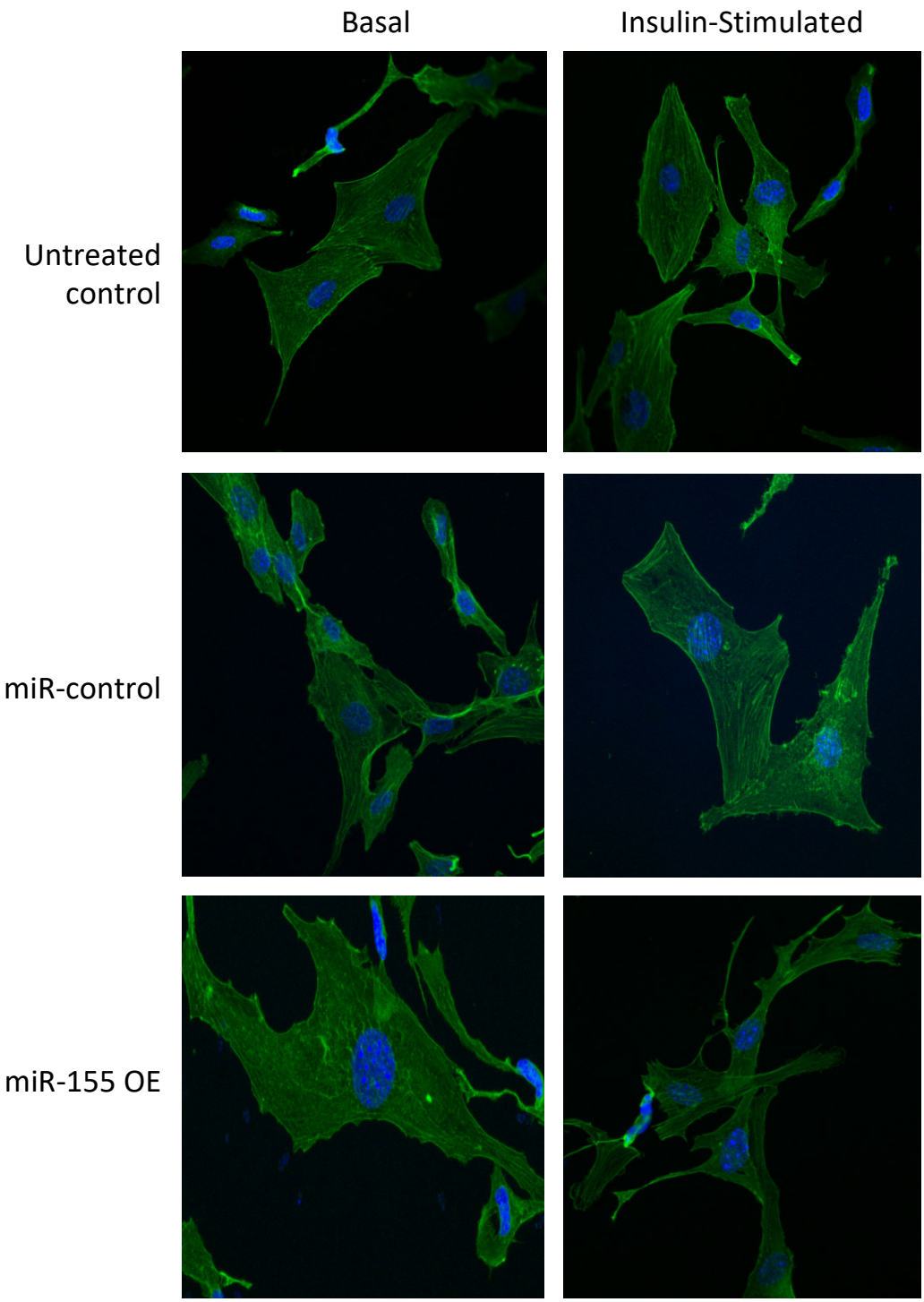

Figure 4.13. Effect of miR-155 on insulin-directed podocyte cytoskeletal rearrangement
Immunofluorescence labelling and confocal imaging of miR-155 over-expressing (OE) podocytes (*mirVana*) compared to wild type insulin-sensitive controls and miR-control transfected cells, before and following 100 nM insulin stimulation. DAPI staining shown in blue, FITC-labelled Phalloidin staining shown in green. F-actin filaments can be seen traversing cells with no discernable peripheralisation in response to insulin in any of the experimental groups shown. Representative images from n=3 independent experiments shown. Magnification = x 630.

A second approach to investigating the above was taken, using an automated imaging and analysis platform: the IN CELL analyser. Figure 4.14 shows representative images of F-actin staining following 10 nM and 100 nM insulin stimulation. As previously, the cells did not appear to respond uniformly to the stimulus, and a varying degree of peripheral staining was seen infrequently across all groups. IN CELL analysis software was used to objectively quantify the degree of insulin-stimulated F-actin movement away from a defined 3 μm nuclear collar. Percentage of cells positive for rearrangement by this measure is shown in Figure 4.15. No significant difference in cytoskeletal reorganisation was detected between conditions.

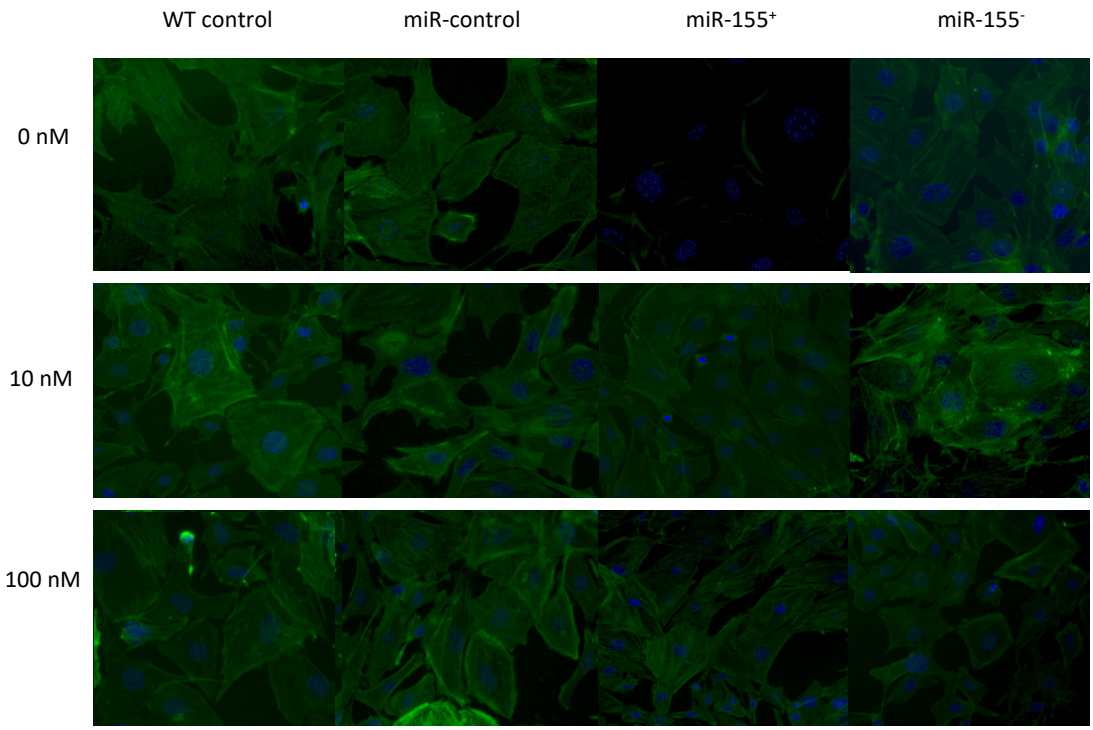

Figure 4.14. Semi-automated immunofluorescence imaging of insulin-directed podocyte cytoskeletal rearrangement. Podocytes were transfected with *mirVana* miR-155 mimic, inhibitor and controls and stimulated with incremental doses of insulin as shown. Cells were fixed, permeabilised and stained with phalloidin and DAPI to visualise F-actin and nuclear regions, respectively. IN CELL analyser high content imaging platform was used to capture images, with a 10x objective. 4 fields captured per well, 3 technical replicates per condition, per 96 well plate. Representative images of n=3 independent experiments shown.

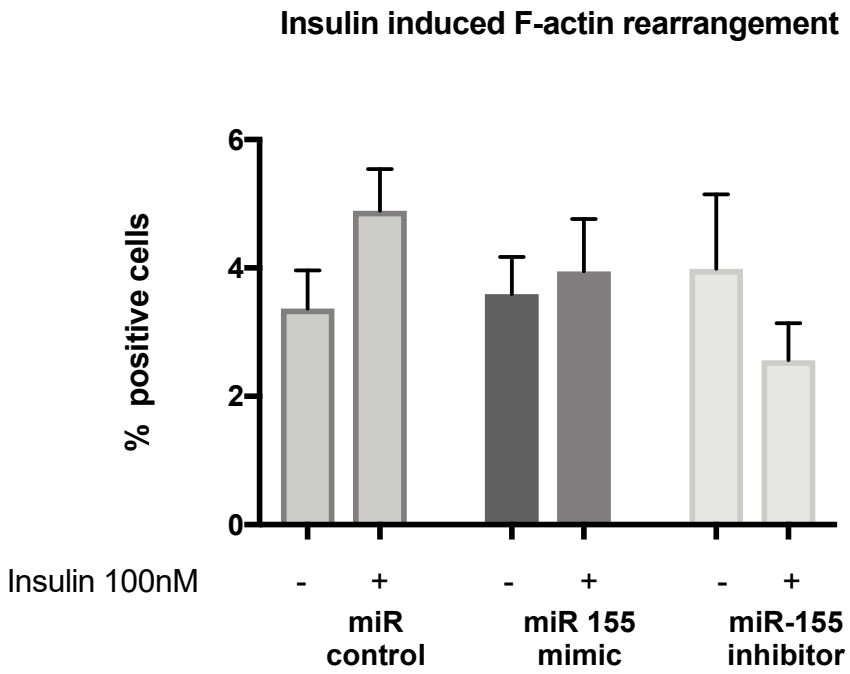

Figure 4.15 IN CELL analysis of insulin-stimulated F-actin peripheralisation in miR-155 manipulated podocytes. Podocytes were transfected with *mirVana* miR-155 mimic, inhibitor and controls and stimulated with incremental doses of insulin (100 nM dose shown only). Cells were fixed, permeabilised and stained with phalloidin and DAPI to visualise F-actin and nuclear regions respectively. Mean fluorescence intensity (in arbitrary fluorescent units, AFU) of a 3 μm diameter nuclear collar was calculated for each cell. A reduction in AFU above a calculated 5% threshold (calculated from WT controls) was considered positive for F-actin reorganisation. Mean +/- SEM of n=3 independent experiments shown.

4.2.7 Mechanistic relevance of miR-155 targets in podocyte insulin signalling

The above results demonstrate that the miR-155 upregulation seen in the *in vitro* insulin-resistant podocyte model may induce insulin resistance via attenuation of insulin-stimulated pAkt and glucose uptake. The potential mechanisms for the observed podocyte phenotype were explored further using a combination of bioinformatics approaches, as outlined below.

4.2.7.1 Target Prediction algorithms

Four established web-based miR-target prediction algorithms, that collectively utilise a variety of targeting prediction techniques (further detailed in Methods 2.14.2), were used to formulate lists of predicted mRNA targets of miR-155. These lists were compared using a Venn diagram as shown in Figure 4.16A. 15 mRNA targets were predicted by all 4 algorithms, a further 35 targets were predicted by 3 algorithms and 127 targets were concordant across at least 2 algorithms. Of the original mRNA targets selected to demonstrate mirVana miR-155 mimic transfection, INPP5D (SHIP-1) was predicted by all algorithms; PIK3R1, RhoA and SOCS1 were predicted by 2 algorithms (highlighted in bold in Figures 4.16B and D, respectively).

A

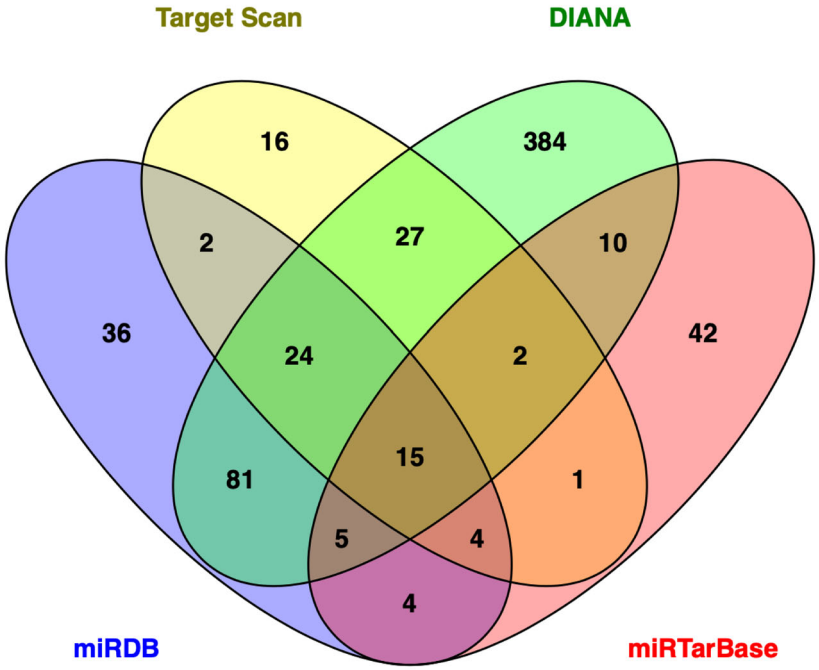

B

Predicted by 4 *in silico* databases							
aicda	csnk1g2	etv3	**inpp5d**	mef2a	myb	tab2	wbp1l
bach1	ets1	fgf7	jarid2	mier3	spi1	tspan14	

C

Predicted by 3 *in silico* databases								
acta1	atxn1l	dhx40	hivep2	kras	olfml3	s1pr1	tbr1	tshz3
actl7a	cebpb	dync1i1	hnrnpa3	mbtd1	rab11fip2	sdcbp	tcf4	vezf1
arid2	csf1r	e2f2	ikbke	myo1d	rps6ka3	sgk3	tcf7l2	zic3
arntl	det1	hbp1	kdm7a	nfe2l2	rreb1	stxbp5l	tle4	

D.

Predicted by 2 *in silico* databases								
aak1	cd274	fgf13	isoc1	mctp1	pea15a	rela	sfpq	tp53inp1
akap10	ckap5	fsd1l	itk	meis1	picalm	rell1	smarca4	traf3
arhgap18	cops3	gdap2	jade1	mgp	pigm	rgp1	smim13	trim32
ash1l	csnk1a1	gdf6	jpt2	mybl1	**pik3r1**	rheb	smim26	trim44
boc	cyb561d1	gpd1l	kansl1	ndn	pkia	**rhoa**	smr3a	trim75
brwd3	cyp7b1	gpm6b	kpna1	ndst4	pkn2	rictor	smug1	trp53inp1
bsdc1	dcun1d3	grhpr	lcorl	nkx3_1	pkn3	rnf123	**socs1**	usp9x
c3orf18	egfr	gria2	lgalsl	nr1h3	pld5	rora	sox1	ust
cab39	emp2	grip1	lrrc59	nrg3	pmaip1	rps6ka5	spef2	washc4
cacna2d1	fam135a	gsk3b	lrrcc1	osr1	rab34	rps6kb1	syvn1	wsb1
cacnb4	fam168a	gzf1	lrrk2	p2ry10b	rab6a	rufy2	tenm3	wwc1
cacul1	fbxl2	il15ra	mafb	pald1	rapgef2	sall1	tmem267	zfp652
card11	fbxo11	il21	map3k10	patj	raver2	scg2	tnip3	znf407
carhsp1	fbxo33	irf2bp2	map3k14	pea15	rcn2	sema5a	tomm20	znf652
								zswim6

Figure 4.16 *In silico* mmu-miR-155 target prediction. Four Web-based miR-target prediction algorithms were used to formulate target lists for mmu-miR-155-5p: Diana miRpath v3.0 (294), miRDB (296), TargetScan v7 (295) and miRTarBase (297). **A.** Venn diagram showing concordance of miR-target prediction algorithms, created using Venny 2.0, accessible via (www.bioinfogp.cnb.csic.es/tools/venny/index.html). Tables represent mRNA targets predicted by all 4 algorithms **(B),** 3 algorithms **(C)** and 2 algorithms **(D).** Previously investigated miR-155 target candidates shown in bold.

4.2.7.2 Ingenuity Pathway Analysis: miR-mRNA interaction analysis

MiRNA-mRNA target effects can be dependent on the specific consequences of that interaction in a particular system, or network. Contemporaneous with my attempts to derive targets of interest using the aforementioned prediction tools, a fellow PhD student in Bristol Renal Academic unit, Dr Mark Graham, performed RNA sequencing analysis of the insulin-resistant podocyte *in vitro* model described in Chapter 3. Using the same experimental conditions, Dr Graham rendered podocytes insulin resistant in diabetogenic media and compared their transcriptome with that of wild type, insulin-sensitive controls using RNAseq. This therefore provided an opportunity to perform a focused analysis of predicted miR-targets that are dysregulated specifically in insulin-resistant podocytes.

Ingenuity Pathway was employed to perform miR-mRNA target analysis of the miRNA array and RNAseq data sets. A flowchart of this analysis is presented in Figure 4.17. 103 differentially expressed miRNAs from the miRNA array analysis ($p<0.05$) were analysed against 8633 differentially expressed genes in the RNAseq data ($p<0.05$). Data for miR-155 was extracted, and 261 mRNA targets divided into up- and downregulated genes. Further stringency criteria were applied (Log2FC>1 or <-1) which resulted in identification of 18 significantly downregulated miR-155 targets, and 26 upregulated targets.

Of note, miR-155 host gene was one of 5 miR host genes mapped to ENSEMBL in the RNAseq data. MiR-155 host gene was significantly upregulated approximately 4-fold in insulin-resistant podocytes (adjusted p value = 9.08E-18, Log2FC 1.93). Although the transcriptional regulation of pri-miRNA transcripts is not fully understood (363), co-expression of pri-miR-155 with its host gene is likely, resulting in an increase in mature miR-155-5p gene product, consistent with findings of my miRNA array data. Consequently, I focused on the downregulated targets in the RNAseq data, assuming a greater potential in the likelihood of demonstrating "direct" target repression in future work. From 18 downregulated miR-155 targets, 4 new targets were selected for further investigation, as listed in Figure 4.17.

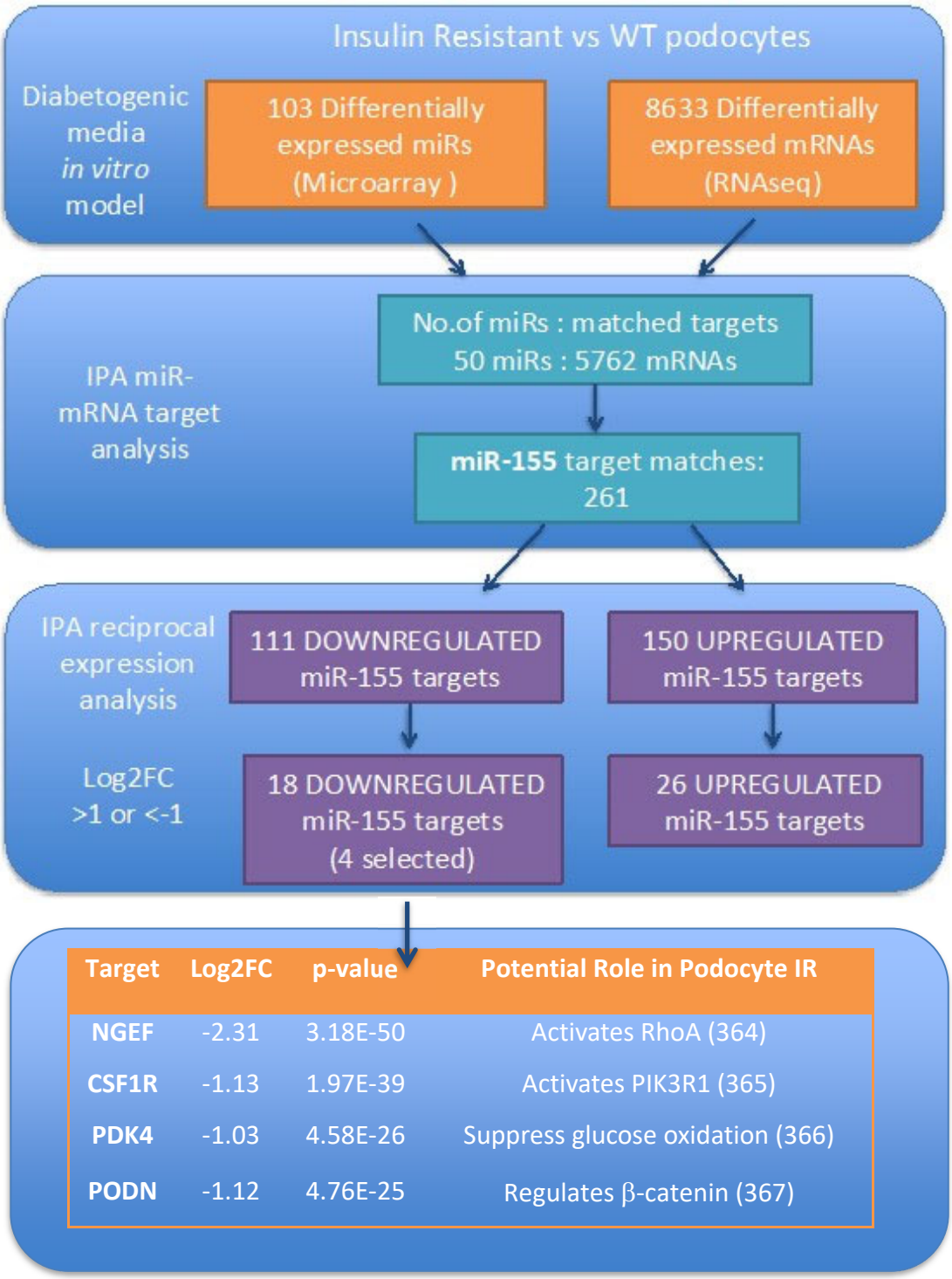

Target	Log2FC	p-value	Potential Role in Podocyte IR
NGEF	-2.31	3.18E-50	Activates RhoA (364)
CSF1R	-1.13	1.97E-39	Activates PIK3R1 (365)
PDK4	-1.03	4.58E-26	Suppress glucose oxidation (366)
PODN	-1.12	4.76E-25	Regulates β-catenin (367)

Figure 4.17 MiR-mRNA target prediction analysis flowchart. MicroRNA array and RNAseq datasets comparing wild type (WT) podocytes and those rendered insulin-resistant in diabetogenic media *in vitro* were uploaded into Ingenuity Pathway Analysis software (QIAGEN Inc., https://www.qiagenbioinformatics.com/products/ingenuity- pathway-analysis). MiR-mRNA target prediction analysis with reciprocal expression pairing was performed on significantly differentially expressed miRNAs/mRNAs (adjusted $p<0.05$). A further stringency setting was applied (Log2FC>1 or <-1) and 4 downregulated targets were selected for further investigation. NGEF= Neuronal guanine nucleotide exchange factor, CSF1R= colony stimulating factor 1 receptor, PDK4= pyruvate dehydrogenase kinase 4, PODN= podocan.

4.2.7.3 RT-qPCR validation of miR-155-induced target repression

The analysis outlined in Figure 4.17 identified 4 new downregulated miR-155 targets in the experimental podocyte model of interest. In order to validate that the downregulation seen could be the specific result of miR-155 target repression, custom PCR primers were designed for the 4 new targets. Figure 4.18 shows 50% reduction in CSF1R expression in miR-155 mimic transfected cells compared to miR controls ($p=0.03$). PDK4 and PODN expression levels showed trend to reduction by 40% and 30% respectively in miR-155 overexpressing cells, relative to miR-control. NGEF was not repressed by miR-155 overexpression, suggesting the downregulation seen in RNAseq data is not a result of miR-155 targeting.

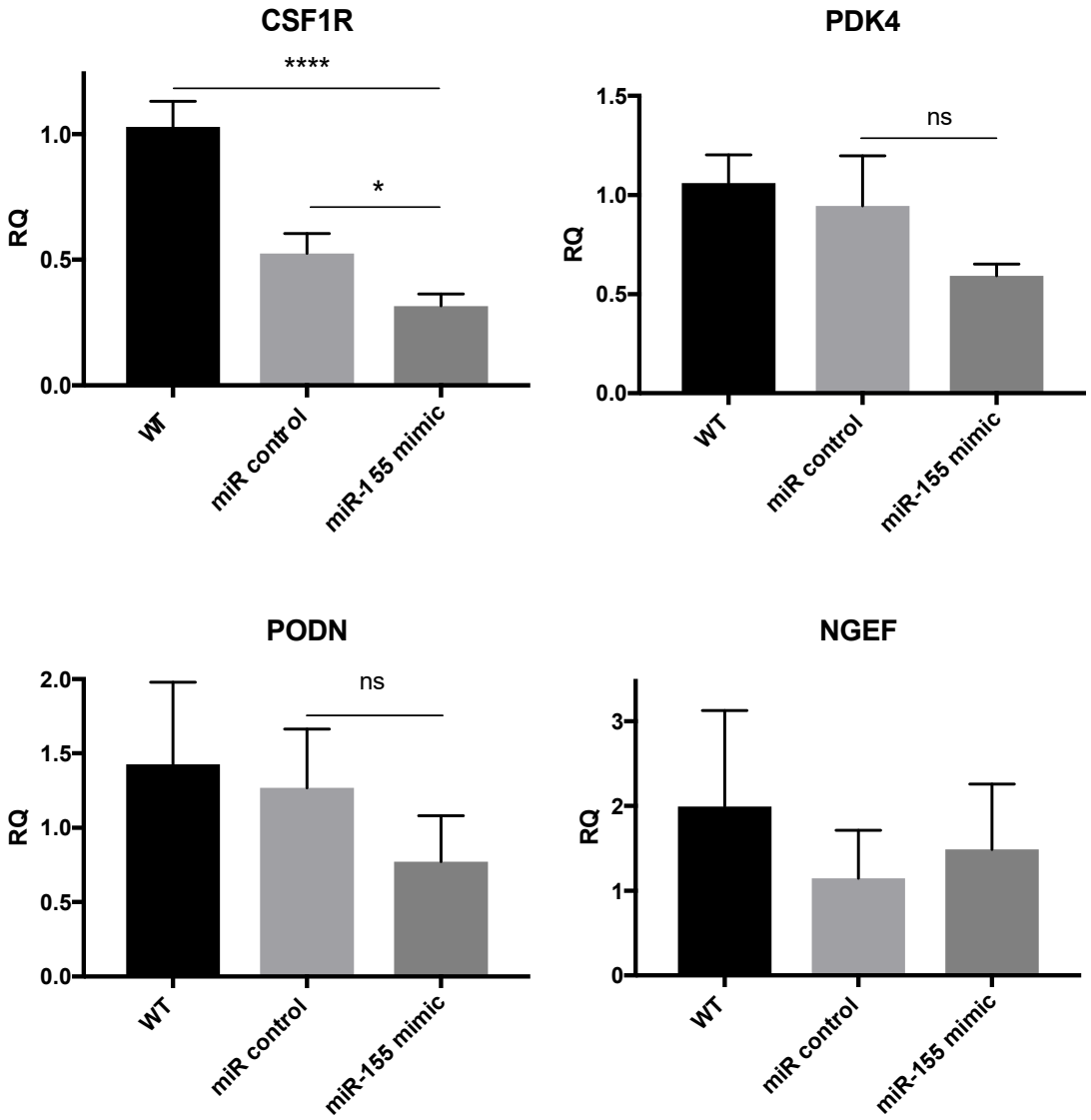

Figure 4.18 Expression of miR-155 mRNA targets identified as downregulated in podocyte insulin resistance, following miR-155 mimic transfection. Fully differentiated podocytes (day 11) were transfected with 30 nM mirVana miR-155 mimic and respective miR-control, for 48 hours. RT-qPCR was used to determine expression levels of 4 mRNA targets of miR-155, shown to be downregulated by RNAseq analysis in an *in vitro* model of podocyte insulin resistance. Relative quantification of expression calculated relative to wild type (WT), non-transfected podocytes. β Actin used as reference gene. Mean +/- SEM of n=3 independent experiments shown. One-way ANOVA and Tukeys multiple comparison testing performed $p<0.05$; **, $p<0.01$; ***, $p<0.005$; **** $p<0.001$

4.3 Discussion

In this chapter, I have shown that urinary miR-155 can differentiate DKD patients from diabetic and healthy controls, and that *in vitro* overexpression of miR-155 results in attenuation of Akt signaling and loss of glucose uptake in podocytes. The selection of miR-155 from the overexpressed miRNA candidates detected in the insulin-resistant podocyte model was based on evidence of its roles in the development of insulin resistance in other cell types (267, 354, 355), as well as being a master regulator of immunity and inflammation (312, 357). Eight miR-155 targets of potential mechanistic relevance in the attainment of the described insulin-resistant phenotype were identified, summarised in Figure 4.19.

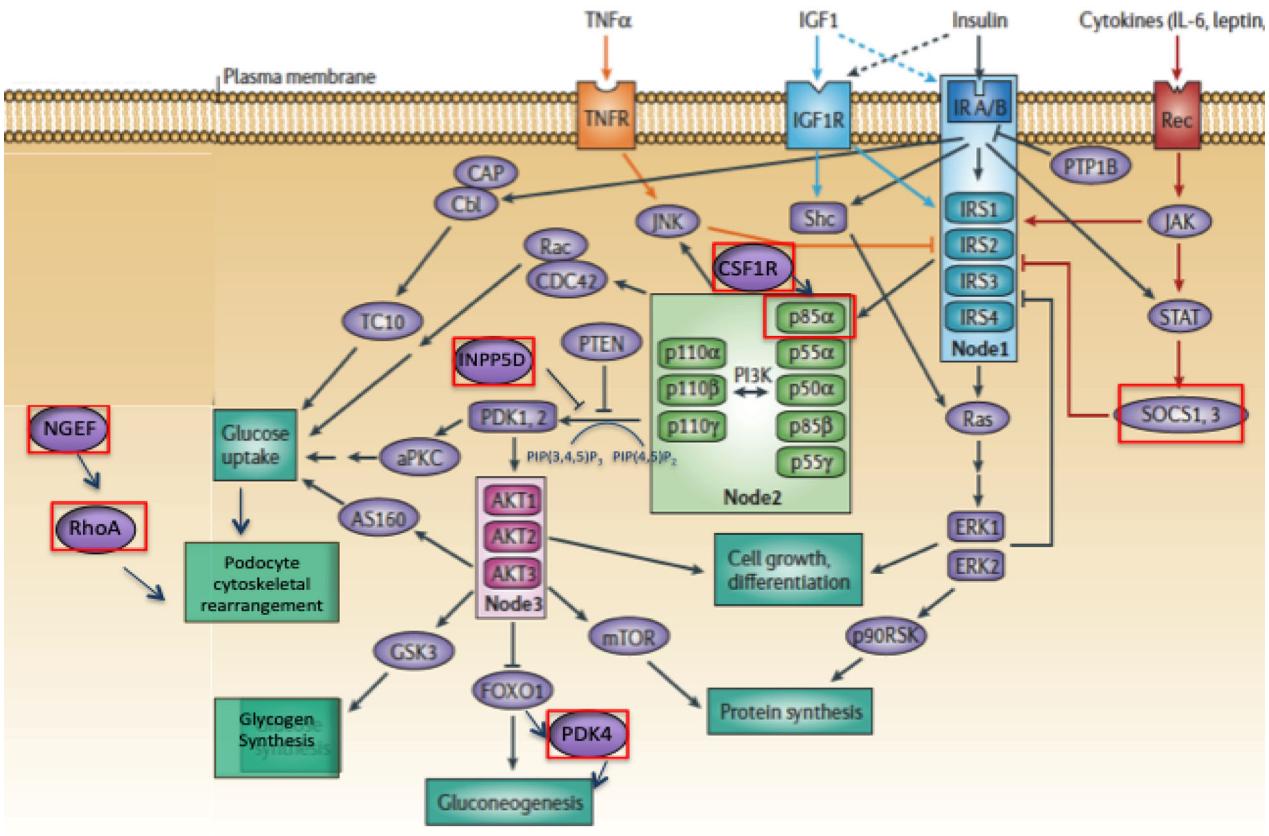

Figure 4.19 miR-155 targets of potential significance in podocyte insulin signalling. Investigated targets of miR-155 are highlighted with a red box. From proximal to distal involvement: SOCS1 inhibits IRS2 (368), p85α is the chief regulatory subunit of PI3K, CSF1R activates PI3K signalling via direct binding to p85α (365), INPP5D (aka SHIP-1) negatively regulates the signalling product of PI3K, PIP (3,4,5)P_3 (369) , PDK4 is upregulated by FOX01 and influences the balance of glucose metabolism via Pyruvate dehydrogenase complex (366), NGEF activates RhoA (364), which is critical for the cytoskeletal rearrangement necessary for podocyte insulin response. PODN (not shown) maintains the GFB and is negatively correlated to development of ACR/DN (370) and regulates Wnt-β-Catenin pathway (367).

aPKC= atypical protein kinase C, AS160= Akt substrate of 160 kDa, , CAP= Cbl-associated protein, CDC42= cell-division cycle 42, CSF1R= colony stimulating factor-1 receptor, ERK= extracellular signal-regulated kinase, FOXO1= forkhead box O1, GSK3= glycogen synthase kinase 3, IRS= insulin receptor substrate, INPP5D= Inositol Polyphosphate-5-Phosphatase D, JAK= Janus kinase, JNK= c-Jun-N-terminal kinase, mTOR= mammalian target of rapamycin, NGEF= Neuronal Guanine Nucleotide Exchange Factor, p90RSK= p90 ribosomal protein S6 kinase, PDK= Pyruvate Dehydrogenase Kinase , PI3K= phosphoinositide 3-kinase, PIP_2 =Phosphatidylinositol-4,5-triphosphate, PIP_3 = Phosphatidylinositol-3,4,5-triphosphate,, PTEN= phosphatase and tensin homologue, PTP1B= protein tyrosine phosphatase-1B, Shc= Src-homology-2-containing protein, RhoA= Ras Homolog family member A SOCS= suppressor of cytokine signalling, STAT= signal transducer and activator of transcription, TBC1D1= TBC1 domain family member 1, TC10= .Ras homologue gene family, member Q. Figure adapted from Taniguchi *et al, Nature Comms*, 2006 (82).

4.3.1 Achieving miR-155 overexpression/inhibition

Initial attempts at miR-155 overexpression were performed using GFP-labelled lentiviral transduction. This technique was chosen over transient methods of transfection with the intention of establishing a stable, miR-155 overexpressing SV40 podocyte cell line, thereby streamlining the workflow for future experiments. However, transfection of the control virus in these experiments also increased miR-155 expression, for reasons that were unclear. This therefore prompted the switch to the use of commercially available miR-mimics. These synthetic oligomiRs, whilst well validated for use (including experience in the host lab), have some disadvantages over the lentiviral technique: for example, RT-qPCR does not accurately reflect the level of functional miRNA, as much of the transfected miRNA remains vesicular bound and hence inaccessible to Argonaute protein binding/loading onto RISC machinery (371). In this work, miR-155 mimic transfection led to a 10,000-fold increase in expression levels by RT-qPCR, compared to the ≈2-fold increase using the lentiviral technique, the latter being concordant with the fold change increase seen by microarray analysis of the insulin-resistant *in vitro* podocyte model. In appreciation of this discrepancy, miR-155 target repression was instead used as a marker of *functional* miRNA expression, but with the caveat that the findings depend wholly on correct selection of well-matched miR-155 mRNA targets (none of which have been experimentally validated in podocytes, to date). Given the cell-specific nature of some miR-mRNA interactions, this may result in an inability to demonstrate chosen target repression, despite successful transfection of the miRNA mimic. The pitfalls of reliance on *in silico* miR-target prediction are further discussed, below.

However, one advantage of using the mirVana technology is that miRNA inhibition may also be achieved using the same experimental workflow. In this instance, it is widely appreciated that abundant vesicular-bound antisense strands, released after cell lysis, can directly inhibit the PCR reaction (371) , and the manufacturers advise against using this as a tool to demonstrate miRNA inhibition. In this work, miR-155 inhibition did not result in the expected

upregulation of resultantly "de-repressed" mRNA targets. This has been well described in the literature with several high throughput analyses reporting increases in mRNA levels of only 33 to 35% (372, 373), and less than 2-fold increases seen at the protein level (374). Demonstrating "de-repression" of mRNA targets in podocytes in the basal, unstimulated state may have diminished the chances of detecting significant expression change in this work. Transfecting miR-155 inhibitor into podocytes grown in my "diabetogenic medium", where endogenous miR-155 is upregulated (and hence targets reciprocally repressed), may have resulted in greater likelihood of demonstrating true "de-repression" of targets. Nevertheless, the significant up-regulation of miR-155 in podocyte insulin resistance remains the driving focus of the research presented in this chapter, and therefore efforts were concentrated on recapitulating this by use of miR mimics, in order to elucidate potential mechanisms of insulin signalling disruption.

4.3.2 Demonstrating the miR-155 overexpressing podocyte phenotype

The work presented in this chapter demonstrates the knockdown of insulin-stimulated pAkt in miR-155 overexpressing cells, therefore indicating loss of PI3K signaling, a critical component of podocyte response to insulin (148). Moreover, miR-155 overexpression resulted in abrogation of insulin-stimulated glucose uptake. This finding has two potential implications: firstly, that miR-155 overexpression has disabled the recruitment and/or function of glucose transporters and secondly, that this would compromise the energy source required for post-prandial podocyte effacement, hypothesised to be protective against increased filtration load. For this reason, I anticipated a loss in insulin-induced F-actin translocation to the cell membrane of the contractile podocyte foot processes in miR-155 overexpressing cells. However, attempts to demonstrate this were hampered by a failure of cells to respond to the insulin stimulus across all experimental groups, using the methods described. The reasons for this are unclear, but recent experience of the Bristol academic unit may be relevant; they have noted that human podocyte cell lines appear to "naturally" lose insulin sensitivity over time. In a recent publication, Lay *et al* (162) describe efforts to overcome this by re-transfecting both the insulin receptor and nephrin into cells, thereby restoring nephrin-mediated GLUT4

membrane docking, required for glucose uptake (149). Using these reconstituted human podocytes, they were able to show both objective evidence of F-actin corticalisation (also using the IN CELL analyser) and glucose uptake that was not obvious from the WT podocytes, nor those transfected with only the insulin receptor or nephrin alone (162). Whilst the mouse podocytes used in this work were considered more robust than the human cell line in maintaining insulin sensitivity under culture conditions, the final experiments reported in this chapter were performed on a later passage of cells and it is possible that the natural insulin sensitivity of these cells had begun to wane, therefore masking any significant miR-155 effect on cytoskeletal phenotype. However, the fact that I was previously able to demonstrate glucose uptake in WT cells, but not in miR-155 OE cells, suggests that insulin-directed GLUT4 translocation was intact, which itself would necessitate F-actin-mediated, cortical propagation of GLUT4 containing vesicles to the cell membrane. A possible explanation for the abrogation of glucose uptake in miR-155 OE cells may well be the disablement of cytoskeletal remodeling, but further work is required to definitively conclude this.

4.3.3 Candidate miR-155 targets in podocyte insulin signalling

Multiple web-based bioinformatic tools were used to formulate a list of putative miR-155 targets. However, there are limitations with these tools, such as the bias towards existing validated targets, reliance on regular updating, lack of cell-specificity and, most notably, the potential for false positive target predictions, with reported rates of up to 65% (375). In this work, 8 mRNA targets were selected for investigation, of which, three were demonstrably repressed by miR-155 mimic transfection in podocytes. Evidence for their potential role in effecting podocyte insulin resistance via the mechanisms herein reported is depicted in Figure 4.20 and discussed in further detail, below.

4.3.3.1 Phosphoinositide-3-Kinase Regulatory Subunit 1 (PIK3R1 aka p85α)

PIK3R1 gene encodes 3 regulatory isoforms of PI3K: p85α, p50 and p55. In response to insulin stimulus, p85α relieves the inhibitory effect of catalytic subunit p110 and PI3K signalling is propagated (376). Existing data are conflicting in deciphering the consequences of PIK3R1 loss, with some reporting an increase in Akt signalling (particularly in the deleterious context of tumour

cell proliferation (318, 377)) and others reporting a reduction in PI3K/Akt signaling. The latter mechanism is proposed as a genetic cause of SHORT syndrome; a syndromic cause of insulin resistance associated with mutations in PIK3R1 inter-Src homology 2 (iSH2) domain, a major interacting domain with p110 catalytic subunits (378). Interestingly, a 50% knockdown of PIK3R1 in mice led to increased insulin-stimulated Akt activity and improved insulin sensitivity (379), yet a more severe PIK3R1 pan-isoform knockout results in glucose intolerance and hyperinsulinemia akin to the physiological state observed in early diabetes (380). It is hypothesised that insulin sensitivity is dictated by the delicate balance between the regulatory p85α and catalytic p110 subunits, and their subsequent ability to interact with IRS proteins. MiRNAs are frequently quoted as "fine tuners" of" dynamic processes (381, 382), making miR-155 involvement credible in this context.

Significantly, p85α has been shown to be critical in regulating podocyte homeostasis, where deletion results in impaired nuclear translocation of down-stream transcription factor Spliced X-box factor-1 (sXBP1), resulting in a maladaptive response to hyperglycaemia-induced endoplasmic reticulum (ER) stress and exacerbation of DN in mice (157). Nuclear localisation of sXBP1 (glomerular) was also reduced in renal biopsy samples from patients with DN. (157) Furthermore, enhancing podocyte insulin signalling by forced overexpression of the insulin receptor and/or knockdown of negative regulator PTP1B has since been shown to be protective against ER stress, suggesting that insulin sensitivity may be mechanistically linked to the well-established findings of ER stress in DKD (383).

MiR-155 directed repression of PIK3R1 might therefore be hypothesised to reduce PI3K signalling in podocytes, which would result in the experimental findings of reduced Akt signal and loss of glucose uptake (Figure 4.20). The resultant insulin resistance, in combination with the ER stress response reported by Madhushudhan *et al*, above, may be a pivotal mechanism in DN progression.

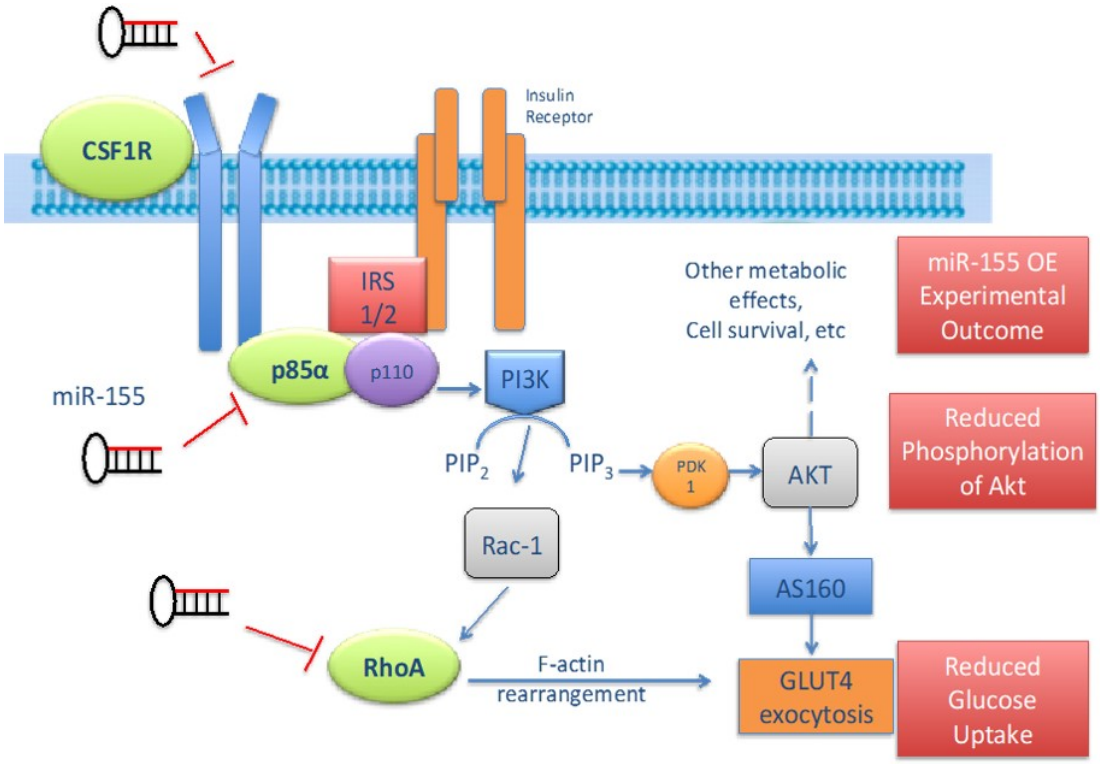

Figure 4.20. Hypothesised role of top mRNA targets in miR-155 directed disruptions to podocyte insulin signalling. 3 out of 8 selected mRNA targets demonstrated the predicted repression following miR-155 overexpression (depicted in green). Experimental outcomes of *in vitro* miR-155 overexpression reported in this work are shown in red. p85α subunit of PI3KRI is targeted directly by miR-155, and indirectly via miR-155 repression of CSF1R, resulting in reduced PI3K/Akt signalling, which in turn reduces glucose uptake. A compound effect may be achieved via miR-155 repression of RhoA, which results in diminished F-actin rearrangement to disable GLUT4 exocytosis. AS160= Akt substrate of 160 kDa, CSF1R= colony stimulating factor-1 receptor, GLUT4= Glucose transporter 4, IRS= insulin receptor substrate, PDK1= Pyruvate Dehydrogenase Kinase 1, PI3K= phosphoinositide 3-kinase, PIP_2 =Phosphatidylinositol-4,5-triphosphate, PIP_3 = Phosphatidylinositol-3,4,5-triphosphate, Rac-1= Ras-related C3 botulinum toxin substrate 1, RhoA= Ras Homolog family member A.

4.3.3.2 Ras Homolog family member A (RhoA)

Kong *et al* were the first to demonstrate that RhoA was a direct target of miR-155, where miR-155 overexpression resulted in disruption of cell polarity and tight junction formation in mammary gland epithelial cells (320). The Coward lab have previously demonstrated the importance of RhoA in effecting insulin-directed changes in podocyte architecture, with *in vitro* inactivation of RhoA GTPase resulting in loss of F-actin corticalisation that is required to present GLUT4 to the membrane, and to effect the responses to insulin (148). MiR-155 directed repression of RhoA could therefore represent a potential mechanism for the reduction in insulin-directed glucose uptake observed in miR-155 overexpressing cells, however this did not translate to objective reduction in F-actin corticalisation, as previously discussed. It is therefore unclear to what extent miR-155/RhoA targeting may be involved in podocyte insulin resistance from these results.

4.3.3.3 Colony Stimulating Factor Receptor-1 (CSF1R)

CSF1R is a tyrosine kinase receptor that mediates the effects of CSF-1 (also known as M-CSF); a cytokine predominantly involved in promoting the differentiation and activation of macrophages. This CSF-1 response is a well established pathogenic insult in renal conditions characterised by inflammation, such as lupus nephritis (384), but has more recently been associated with obesity and insulin resistance, with obese mice (and humans) demonstrating increased expression of CSF1R in circulating natural killer (NK) cells, the conditional knock out of which confers protection against HFD-induced insulin resistance and obesity, effected via an IL-6/Stat3 dependent pathway (385).

Mechanistically, CSF1R has been shown to activate PI3K signalling via direct binding to p85α (PIK3R1), resulting in Akt activation (365) , hence miR-155 overexpression may be postulated to induce podocyte-specific insulin resistance via both indirect (via CSF1R) and direct repression of p85α, resulting in the phenotype demonstrated in this chapter.

4.3.4 Conclusion

In conclusion, the work presented here demonstrates evidence of miR-155-induced disruption in PI3K-Akt signalling and glucose uptake, both critically important in effecting the podocyte response to insulin, the loss of which has catastrophic implications for renal health.

In silico target prediction and paired expression analysis of microRNA array and RNAseq data highlight CSF1R and PIK3R1 as important mRNA targets of miR-155 in podocyte insulin signalling. A compound effect of miR-155 targeting is hypothesised to occur, where repression of CSF1R also attenuates proximal insulin signalling via PIK3R1, thereby presenting a mechanism for the observed downregulation of Akt signalling and subsequent abrogation of glucose uptake.

This work therefore provides clear rationale for evaluating miR-155 as a therapeutic target in DN, and the urinary patient data presented additionally demonstrates its potential as a biomarker in this condition.

5 Optimisation of Podocyte isolation from NPHS2 mCHerry/EGFP$^{+/-}$ reporter mouse

5.1 Introduction

The previous chapters describe the use of an *in vitro* model of podocyte insulin resistance to investigate miRNAs that may play crucial roles in dictating podocyte behaviour in DN. The remaining experimental work in this thesis will focus on recapitulating these changes *in vivo,* by investigating miRNA changes at a podocyte and whole glomerular level. The use of an *in vivo* model is fundamental in appreciating the complexity of miRNA regulation in a physiologically intact, perfused glomerulus, as DN ensues. Animal models also permit the wider study of both renal (e.g. albuminuria) and non-renal parameters (e.g. systemic insulin resistance), thus enabling the correlation of podocyte/glomerular microRNA changes with the development of significant phenotypic traits in diabetic animals.

There are numerous existing mouse models of T2DM that either spontaneously develop the disease as a consequence of a genetic mutation (usually leading to obesity) and/or have superimposing genetic stressors that increase susceptibility to DN. The most commonly available mouse models of T2DM are presented in Table 5.1. Despite extensive experimental development, it has proved difficult to recapitulate all of the pathophysiological features of human DN in a single mouse model. In a bid to standardise the development of new experimental models, the Animal Models of Diabetic Complications Consortium (AMDCC) published a set of validation criteria (386) that cover the fundamental histopathological and biochemical features of human DN, summarised in Table 5.2. To date, a mouse model that fulfills all the specified criteria remains elusive. Consequently, the choice of diabetic mouse model often depends on the desired metabolic derangement (e.g. hyperglycaemia, insulinopenia) in an animal engineered to be susceptible to a specific condition of interest, such as the use of the endothelial nitric oxide synthase deficient mice (eNOS−/−) in investigating endothelial dysfunction in DN (387). Further genetic complexity may be introduced when there is a requirement to "label" a specific cell of interest.

T2DM Model	Typical Strain(s)	Description
ob/ob	BTBR	Leptin deficient obese mouse Phenotype: IR, severe hyperglycaemia, high cholesterol and TGs, albuminuria Histology: Glomerular hypertrophy, mesangial matrix expansion, GBM thickening, podocyte loss, IF (mild), mesangiolysis (388)
db/db	C57BLKS C57bL/6 FVB, DBA	Leptin-receptor deficient obese mouse Phenotype: IR, hyperglycaemia, albuminuria Histology: Glomerular hypertrophy, mesangial matrix expansion, GBM thickening (389)
MKR	FVB	Defective skeletal muscle IGF-1R receptor, non-obese mouse. Phenotype unmasked post uninephrectomy. Phenotype: IR, hyperglycaemia, dyslipidaemia, albuminuria Histology: Mesangial matrix expansion, GBM thickening, podocyte effacement (390)
Agouti (Ay)	KK C57BL FVB	Mutation in Agouti yellow gene affecting hypothalamic melanocortin receptors implicated in weight regulation Phenotype: Obese, IR, yellow fur, albuminuria, hyperglycaemia, high TGs Histology: Glomerular hypertrophy, mesangial matrix expansion (mild), segmental proliferative nephritis (391)
NZO	NZO	Obese, inflammatory model with low level IgM directed against the insulin receptor Phenotype: IR, hyperglycaemia, albuminuria, susceptible to lupus nephritis Histology: Glomerulosclerosis, GBM thickening (mild), arteriolar inflammation, eosinophillic nodules (392)

Table 5.1. Commonly used mouse models of T2DM. Despite the development of multiple mouse models enriched on susceptible genetic strains, no available mouse model fulfils all of the AMDCC validation criteria. IR= insulin resistant, TGs= triglycerides, GBM= glomerular basement membrane, IF= interstitial fibrosis, FVB= Friend Virus B, NKO= New Zealand obese mice.

Criteria	
Biochemical	>50% decline in GFR over the lifetime of the animal
	>10-Fold increase in albuminuria compared to age and sex matched controls of same strain
Histological	Advanced mesangial matrix expansion +/- nodular sclerosis and mesangiolysis
	Arteriolar hyalinosis (any degree)
	GBM thickening by >50% over baseline
	Tubulointerstitial Fibrosis
OMICs	Activation of transcriptomic, proteomic and metabolomic pathways characteristic of human DN

Table 5.2. Proposed criteria for validating progressive mouse models of DN. Adapted from Mouse Models of Diabetic Nephropathy. Brosius et al 2009 JASN (386)

5.1.1 Selection of db/db DBA/2J mouse

Insulin signalling to the podocyte results in a conformational change that involves the rapid corticalisation of F-actin filaments, presumed to be an adaptive mechanism to allow the cell to withstand increased sheer stress arising from greater blood flow in the post prandial period (148). In the insulin resistant state, this peripheralisation of F-actin is not seen (162), which may be a significant, primary podocyte insult in DN. One of the earliest manifestations of podocyte loss/injury is the development of albuminuria (393). It was therefore considered prudent to ensure that the mouse model selected for this work would develop robustly demonstrable insulin resistance and albuminuria, the latter being a particularly variable and strain-dependent trait in commonly utilised diabetic rodents (389) .

The db/db mouse is a firmly established model that fulfills these criteria. The db/db has a genetic mutation in the allele coding for the leptin receptor, a

hormone commonly referred to as the "satiety hormone" which plays an important role in regulating energy balance at the level of the hypothalamus. A G-to-T transversion in this allele creates a donor splice site that causes abnormal splicing and a 106-nucleotide insertion in the transcript, ultimately resulting in signal transduction failure. Without the ability to signal satiety, the db/db mouse over-eats, leading to the development of obesity-induced, insulin-resistant diabetes. The development of insulin resistance in these mice closely mimics that of human T2DM, with a period of hyperinsulinemia and pancreatic hypertrophy followed by eventual pancreatic exhaustion, beta cell depletion and insulinopenia (389). The db/db mouse is infertile in its homozygous form, and heterozygotes are therefore used as breeding pairs, resulting in the genotype frequencies as shown in Figure 5.1. Heterozygotes (db/wt) have no phenotype, and may therefore be used as littermate controls, thereby maximising use of the mice per litter in accordance with the "3R's" principle of reduction, set out by the Animals Scientific Procedures Act 1986.

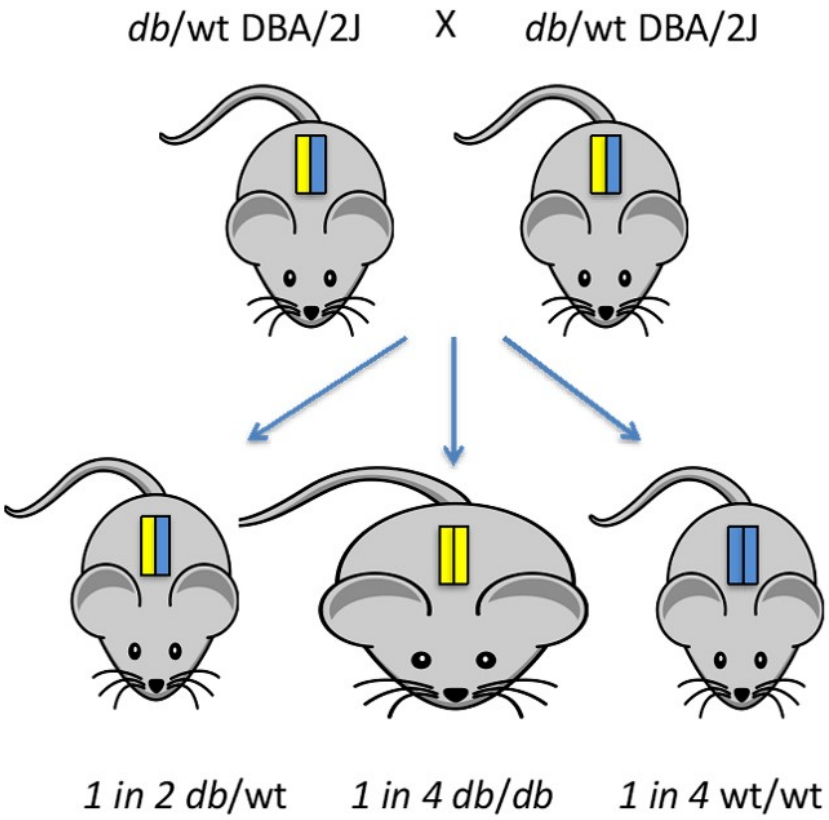

Figure 5.1. Breeding outcome of db/wt mice. Mice are bred as heterozygotes because they are infertile in their homozygous form. Db/wt and wt/wt both display no phenotype and may be used as littermate controls.

As aforementioned, enrichment of a specific genetic background in animal models may be employed to enhance susceptibility to developing phenotypic traits of interest. In 2017, collaborators from our Bristol lab published a comparison of the commonly used db/db BLKS/J model with the db/db DBA/2J model. Whilst both strains exhibited similar degrees of hyperglycaemia and systemic insulin resistance, the DBA/2J background conferred significantly greater albuminuric tendencies (394). An adapted summary of the full phenotype is presented in Table 5.3. Notably, the development of insulin resistance in this model is closely correlated to the development of albuminuria, which supports the use of this mouse in investigating transcriptomic changes in the podocyte in early DN.

		8 week		10 week		12 week	
		wt	**db/db**	**wt**	**db/db**	**wt**	**db/db**
Body weight (g)		24 ± 1.5	33.1 ± 0.7	25.5 ± 1.6	34.9 ± 0.7	27.3 ± 1.5	33.0 ± 1.1
Non-fasted Blood Glucose (mM)		7.88 ± 0.39	16.94 ± 2.09	7.75 ± 0.45	27.31 ± 1.19	7.77 ± 0.32	31.01 ± 0.86
Systemic insulin resistance (AUC)		450.9 ± 64.2	1007.3 ± 87.4	ND	ND	402.3 ± 42.8	1836.8 ± 326.1
Mean Glomerulosclerosis score		ND	ND	ND	ND	0.21 ± 0.10	1.35 ± 0.13
ACR (µg/mg)	**M**	≈100	≈1500	≈110	≈5000	≈98	≈4800
	F	≈80	≈1000	≈70	≈2000	≈70	≈4000

Table 5.3. Phenotypic characteristics of the db/db DBA/2J mouse during the development of DN. Means +/- SE shown. Adapted from: db/db mice are susceptible to early albuminuria and glomerulosclerosis that correlate with systemic insulin resistance, Ostergaard 2017 AJP (394) AUC= area under curve, ACR = albumin:creatinine ratio, ND= not done.

The following chapter documents the optimisation of isolation of a pure population of fluorescent-labelled mouse podocytes for the intended purpose of miRNA and mRNA sequencing at 3 time-points corresponding to validated phenotypic changes in the db/db DBA/2J mouse model.

5.1.2 Chapter Aims

1. Optimise isolation of podocytes from whole glomeruli of a podocyte-specific, GFP-labelled reporter mouse model.

5.2 Results

5.2.1 Crossing of the db/db DBA/2J with a reporter mouse

The proposed method of podocyte extraction is depicted in Figure 5.2A. Terminally anaesthetised mice are perfused with a solution containing magnetic dynabeads, designed to become impacted in the small glomerular capillaries, as shown in Figure 5.2B. Kidneys are then removed and subjected to sieving and digestion steps, which permits the magnetic extraction of the glomeruli for further digestion into a single cell suspension consisting of the 3 predominant glomerular cells; mesangial, glomerular endothelial (GEnC) and podocytes. As the least abundant cell type (< 20%) (395), consideration must be given to methods of maximising the isolation of a pure podocyte population. To achieve this, a fluorescent label is introduced to the podocytes of the db/db DBA/2J mouse (hereafter referred to as "db/db"). This is achieved by crossing the db/db with a Podocin-Cre driven mCherry/EGFP reporter mouse of mixed genetic background with contributions from 129/SV, FVB, DBA2J and C57BL/6. This mouse (hereafter referred to as "reporter") has been genetically modified such that podocytes fluoresce green and all other cells of the mouse fluoresce red, thus enabling identification of mice of the desired genotype via simple application of UV lamp. The appearance of the mice and the breeding schedule is shown in Figure 5.3.

A.

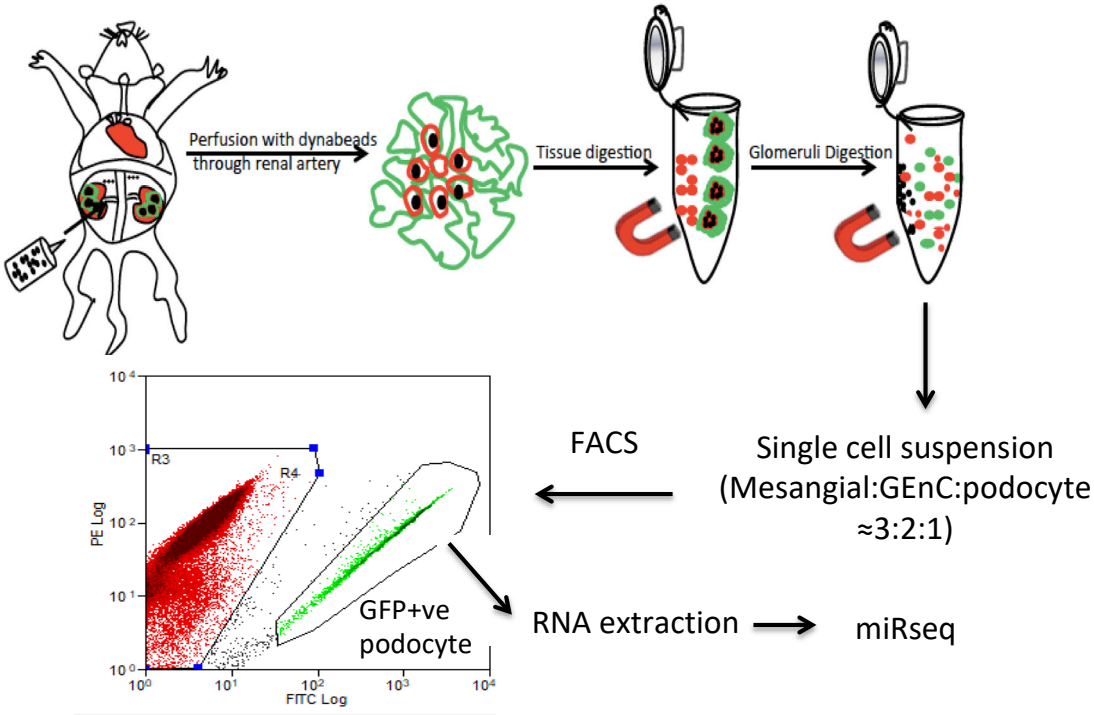

Figure 5.2A. Flow through of experimental procedure for podocyte isolation and sequencing. N=3 mice per group (EGFP$^{+/-}$ db/db and EGFP$^{+/-}$ db/wt) per time point (4, 8 and 12 weeks). Mice were perfused with magnetic dynabeads to enable glomeruli to be extracted from digested kidney tissue. Further digestion resulted in a single cell suspension of the 3 main glomerular cell types. FACS was used to isolate a pure podocyte population based on the expression of GFP in these cells. Podocyte RNA was extracted for microRNA sequencing (miRseq). Glomerular perfusions of anaesthetised mice performed by 2 experienced operators in Bristol Renal Unit; glomerular preparation into single cells performed in Wales Kidney Research unit, Cardiff. GEnC= Glomerular endothelial cell, FACS= Fluorescence activated cell sorting. Adapted from Comparison of Glomerular and Podocyte mRNA profiles in Streptozotocin-induced diabetes (supplementary data) Fu et al, JASN 2016 (396)

B

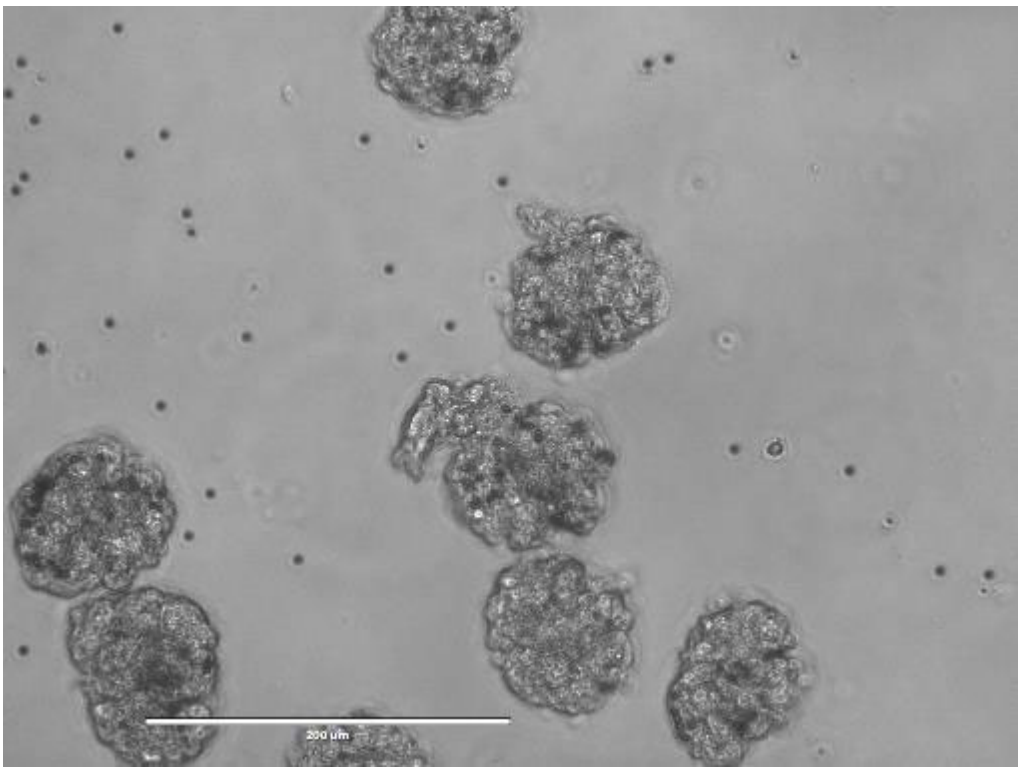

Figure 5.2B. Light microscopy of isolated glomeruli containing magnetic dynabeads. Some extra-glomerular beads can also be clearly seen. Scale bar= 200 µm.

A

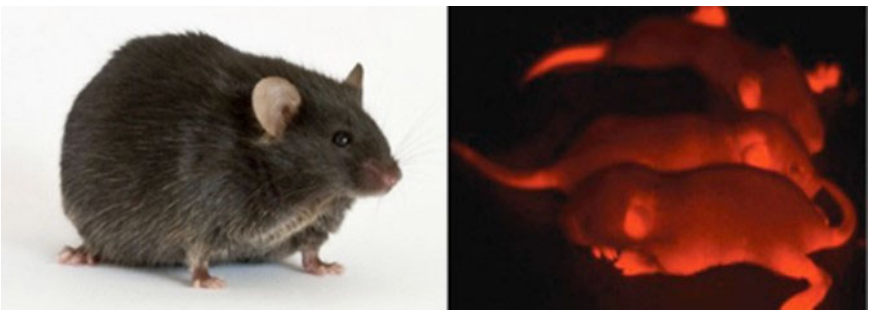

B

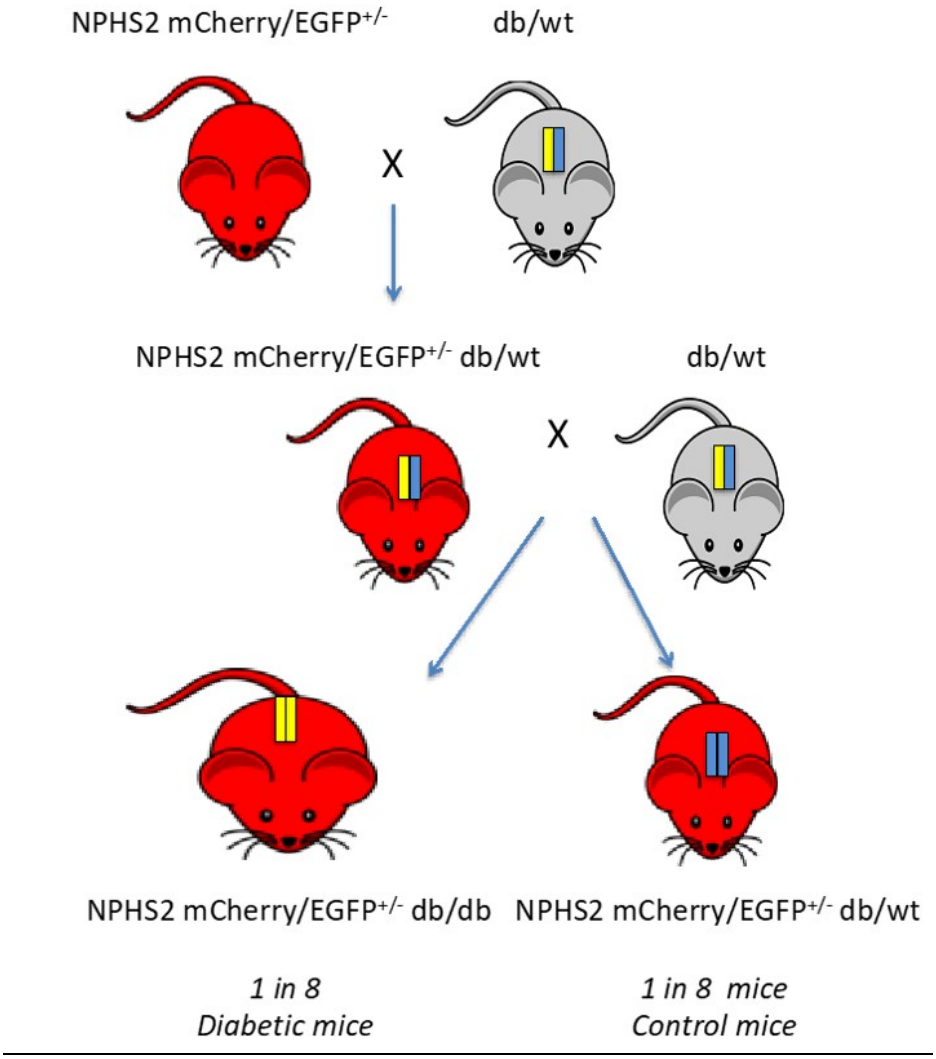

Figure 5.3A. Appearance of the db/db mouse (left) and NPHS2 mCherry/EGFP$^{+/-}$ mice (right). The reporter mouse is genetically engineered to have green fluorescent podocytes (driven by podocin-Cre) and all other cells labelled cherry red to enable ease of identification**.**

Figure 5.3B. Breeding outcome of the db/db and reporter mouse. Db mice must be bred as heterozygotes. Due to the complexity of achieving db homozygotes, maintaining DBA/2J susceptible background and introducing fluorescent tag, only 1 in 8 of the litter are the required genotypes for diabetic and control animals respectively.

5.2.2 Fluorescence activated cell sorting of GFP-labelled podocytes

Initial optimisation experiments were performed using the uncrossed reporter mouse. Glomerular extracts of 3 mice were pooled and digested to obtain a single cell suspension, as described above. Initial FACS isolation proved challenging owing to unexpected detection of fluorescing cells across a wide range of fluorescence intensity. Figure 5.4A shows the gating of a presumed GFP-labelled podocyte population with fluorescein isothiocyanate (FITC) intensity ranging from 10^3-10^5. Using this gating strategy, 25,373 GFP+ve cells were identified, and 33,550 cells designated as GFP-ve. Using these cell numbers alone, it was possible to conclude that the GFP+ve population must contain a high proportion of non-podocyte cells, given that this represented a podocyte count of 43% of the total sorted cells, which is at least twice the expected value. RNA was extracted from the pelleted GFP+ve and –ve cell fractions using direct application of TRI reagent™. Disappointingly low yields of RNA were extracted using this technique (175 ng and 177 ng for the GFP+ve and –ve fractions respectively). Purity of sort was assessed by RT-qPCR for podocyte- specific mRNA marker nephrin and GEnC marker, PECAM-1 (CD31). Whilst the GFP+ve fraction was enriched in nephrin, with an 11-fold increase in mRNA expression in this fraction compared to GFP-ve cells, PECAM-1 expression was also 9.5-fold greater in the GFP+ve fraction (Figure 5.4B) This confirmed initial suspicions that the GFP+ve cells contained a large fraction of contaminating GEnCs that, although not labelled with the exogenous GFP fluorophore, exhibit a natural fluorescence that is sufficient to be detected by FACS. (This property, known as autofluorescence, is intrinsic to all cells to some degree, owing to the presence of light-omitting molecules such as flavins, Nicotinamide-adenine dinucleotide (NAD) and collagen (397)). Post-hoc analysis of the GFP+ve gating suggested the presence of two discrete populations of cells (circled in Figure 5.4A) with those cells fluorescing at the higher FITC intensity presumed to be the “true” podocyte population. Based on this conclusion, it was appreciated that actual numbers of podocytes would be significantly less, which would result in less RNA extracted.

A B

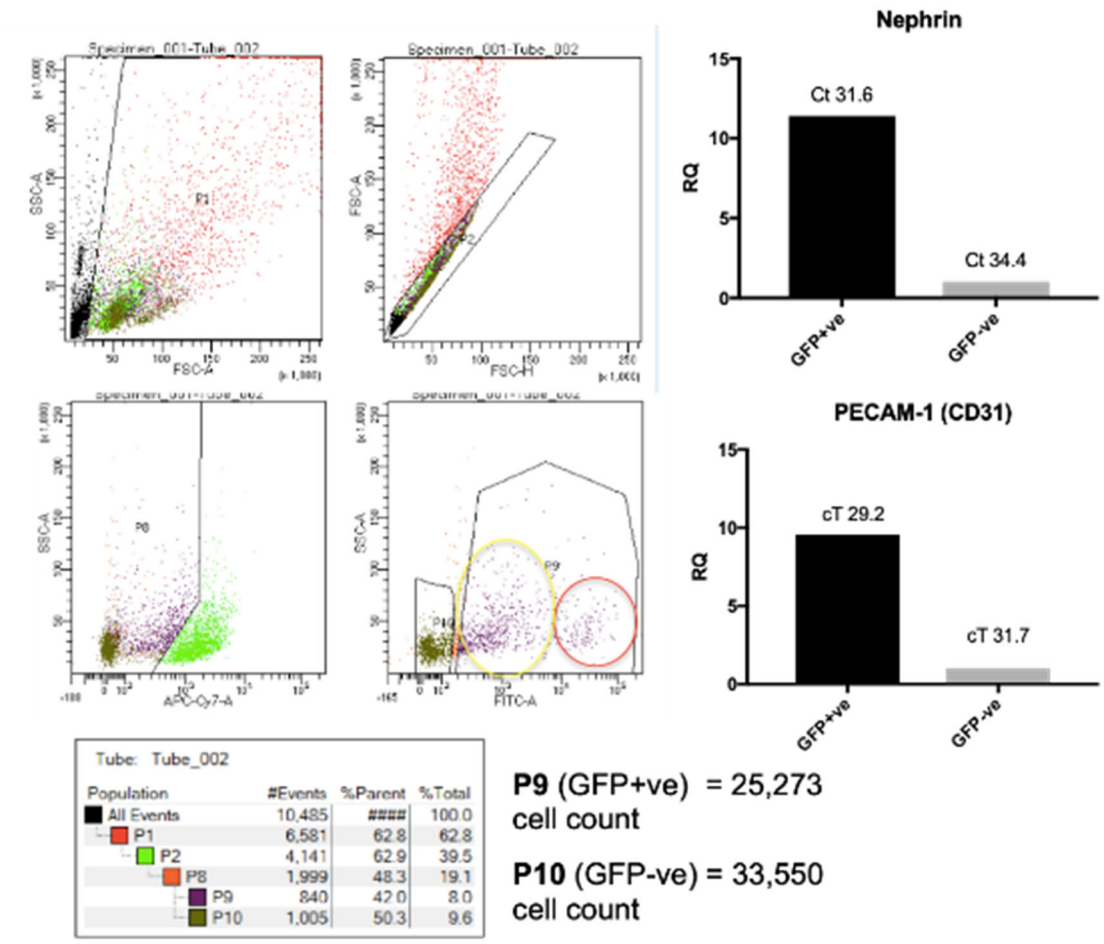

Figure 5.4A. Fluorescence activated cell sorting (FACS) of a GFP+ve podocyte population from NPHS2 mCherry/EGFP$^{+/-}$ reporter mouse. P1 represents cell population after exclusion of cellular debris (top left). P2 represents cell population after exclusion of cell doublets, identified by an increase in forward scatter of light (FSC) (top right). P8 represents cell population after exclusion of dead cells with permeable membranes that have permitted the uptake of LIVE/DEAD viability stain using APC-Cy7 fluorophore (bottom left). P9 and P10 represent the initial gating of GFP+ve and –ve respectively. Ad-hoc analysis concluded that P9 may be a composite of two discrete population of autofluorescing GEnCs (circled in yellow) and highly fluorescing 'true" podocytes (circled in red). **Figure 5.4B. Determination of sort purity by RT-qPCR.** mRNA expression of both podocyte marker nephrin and GEnC marker PECAM-1 were approx. 10-fold greater in the GFP+ve fraction, relative to GFP-ve fraction. Cycle threshold (cT) detection was higher than expected in the reaction owing to low RNA input in RT reaction. 18s rRNA used as endogenous control gene. N=3 mice glomeruli pooled. SSC= side scatter, FITC= Fluorescein isothiocyanate, RQ= relative quantification.

Given that 175 ng represented <20% of the gold standard recommended 1 μg input for RT reaction, and had the knock-on effect of increasing the cycle threshold (cT) detection for nephrin and PECAM-1 by approximately 2 cTs compared to previous performance of these assays with standard cDNA input, there was concern that the RNA yielded from a more stringently gated GFP+ve cell population would be insufficient to demonstrate any improvement in sort purity by RT-qPCR.

To overcome this, the Cell-to-Ct™ 1-step kit was used (see Methods 2.12.2). Cell lysis, RT and RT-qPCR were performed directly from flow sorted cells, negating the need for multiple wash steps associated with the TRI reagent RNA extraction protocol, thereby minimising potential for RNA loss. Figure 5.5 depicts the amended gating strategy to separate the strong and intermediately GFP-+ve cells, resulting in glomerular cell proportions of 3.7% podocytes, equating to 3327 sorted cells, 36.9% GEnCs (33,270 cells) and 56.4% presumed mesangial/other cells (54,430 cells). RT-qPCR using the Cell-to-Ct™ technique confirmed podocyte mRNA marker nephrin was enriched approx. 60-fold in the highly fluorescent population (GFP+++) compared to GFP-ve cells, whilst GEnC marker PECAM-1 was 45-times higher in the intermediate fluorescent cells (GFP+), therefore affirming the prior observation that GEnCs exhibit intrinsic autofluorescence detectable by FACS.

.

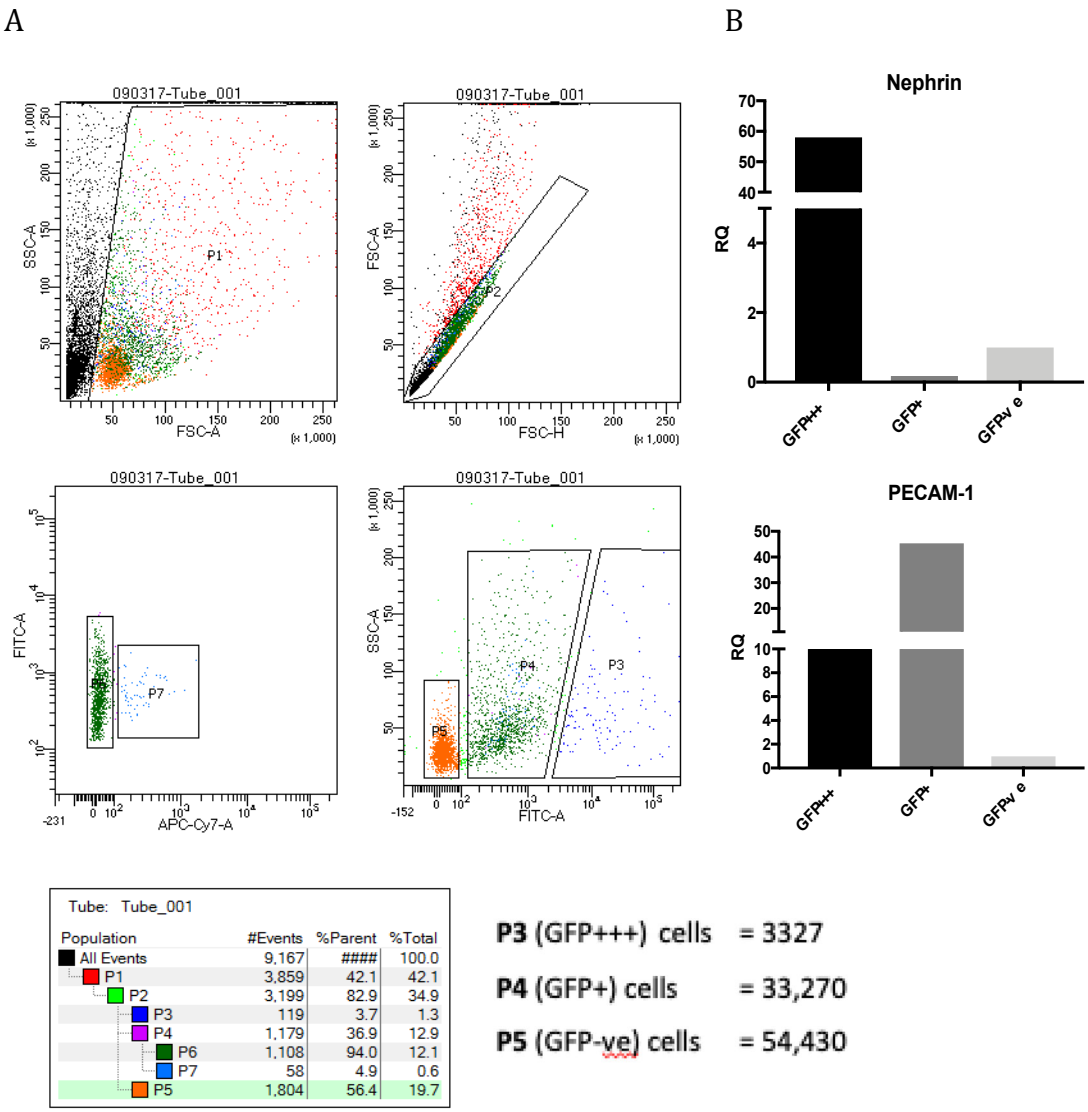

Figure 5.5A. Revised gating strategy for Fluorescence activated cell sorting (FACS) of a GFP+ve podocyte population from NPHS2 mCherry/EGFP$^{+/-}$ reporter mouse. P1 and P2 labelled as per Figure 4.4A. P6 represents cell population after exclusion of dead cells (P7) with permeable membranes that have permitted the uptake of LIVE/DEAD viability stain using APC-Cy7 fluorophore (bottom left). P3 represents the gating of high intensity FITC fluorescence (GFP+++) presumed to be "true" podocytes. P4 represents the population of intermediate FITC fluorescence, postulated to be autofluorescing GEnCs (GFP+). P5 denotes non-fluorescing (GFP-ve) cells. **Figure 5.5B. Determination of sort purity by RT-qPCR.** mRNA expression of nephrin was 58 times greater in the GFP+++ fraction, relative to the GFP-ve fraction. PECAM-1 expression was 45 times greater in the GFP+ fraction, thus affirming the existence of autofluorescent GEnC cells. 18s rRNA used as endogenous control gene. N=4 mice glomeruli pooled.

Having established an appropriate gating strategy, two further sorting experiments were performed, as summarised in Table 5.4. The percentage of cells identified as podocytes ranged from 2.1-4.6%. Mean podocyte count, calculated per mouse, was 4892. The pattern of mRNA sort purity was maintained throughout (Figure 5.6), with enrichment of podocyte and GEnC mRNA markers in GFP+++ and GFP+ populations respectively, although the calculated relative expression was variable in each sort. Mesangial mRNA marker PDGFRβ was enriched 24-fold in the GFP-ve fraction (relative to GFP+++).

FACS Attempt	1	2	3
No. of mice pooled	4	3	5
% live cells*	94	100	92
% GFP Strong (+++)	3.7	4.6	2.1
% GFP intermediate (+)	36.9	51.3	35.3
% GFP-ve	56.4	39.3	56.4
Presumed podocyte cell count	3327	34,722	10,869

Table 5.4. Summary of Fluorescence activated cell sorting (FACS) attempts from NPHS2 mCherry/EGFP$^{+/-}$ reporter mice. 3-5 mice glomeruli were pooled per experiment. Podocyte cell count per experiment was highly variable and not determined by number of mice pooled. *Percentage Live cells following exclusion of gated cellular debris and cell doublets.

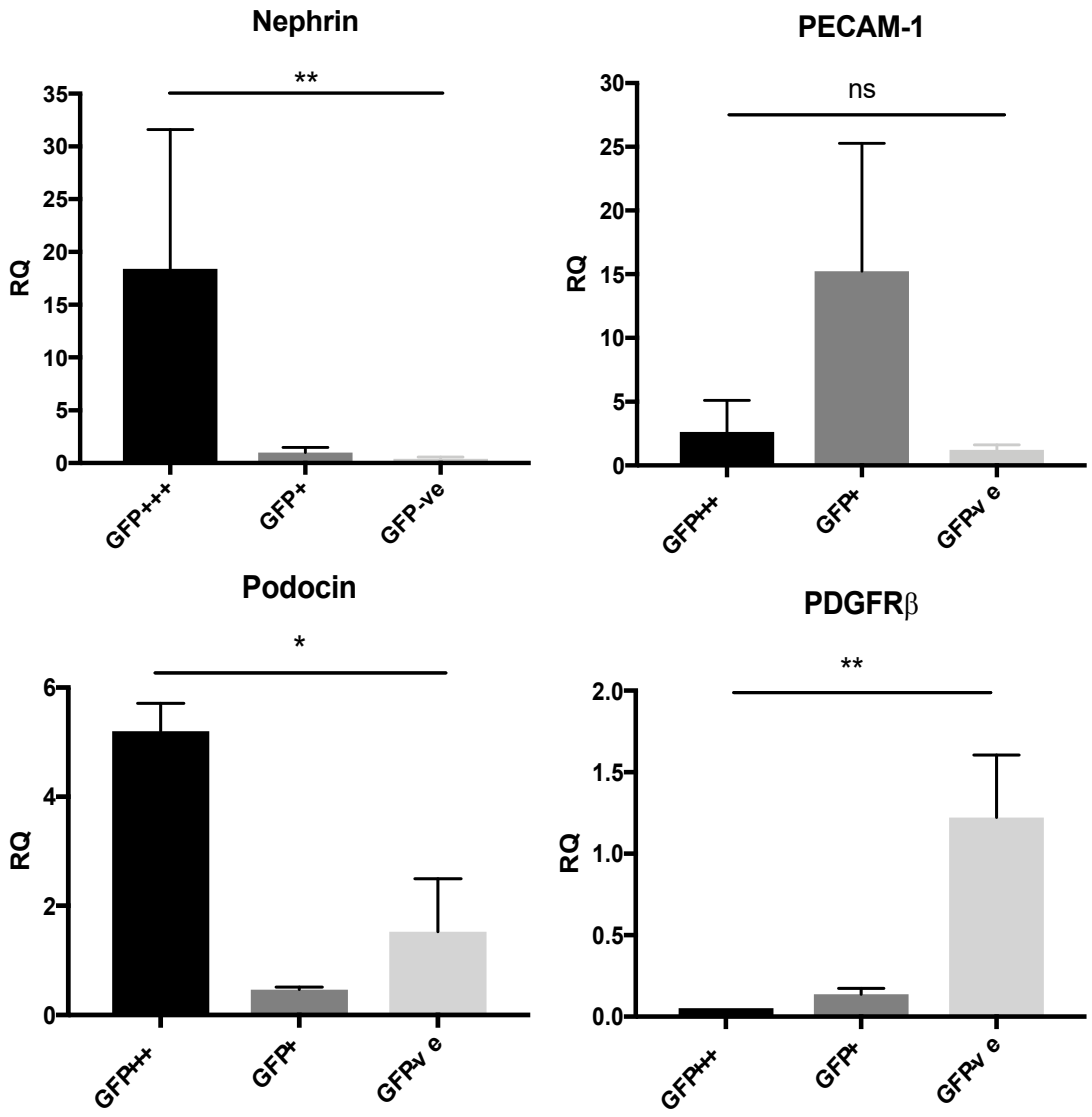

Figure 5.6. Cell marker expression in Fluorescence activated cell sorted (FACS) glomerular cells from NPHS2 mCherry/EGFP$^{+/-}$ reporter mice. Podocyte markers nephrin and podocin are enriched in the highly fluorescent cell fraction (GFP+++), GEnC marker PECAM-1 is abundant in the intermediate fluorescent cell fraction (GFP+) owing to an inherent autofluorescent cell characteristic. Mesangial marker PDGFRβ is enriched in the GFP-ve cell fraction. N=3 independent experiments, 3-5 mice pooled per experiment. Mean and SEM shown. 18s rRNA used as endogenous control. P value assessed using Kruskal-Wallis test, where * $p<0.05$, ** $p<0.01$. RQ calculated relative to GFP-ve fraction.

5.2.3 Calculations of mouse requirements for NGS

The Cell-to-Ct kit permitted RT-qPCR detection of mRNA cell markers for confirmation of FACS sort purity, directly from low numbers of sorted cells. However, the cell lysate product from this one-step reaction is unsuitable for downstream sequencing experiments, which require an input of quantifiable, high quality RNA. The TruSeq small RNA sequencing (smRNAseq) library kit recommended RNA input is 1 μg, although anecdotal evidence from our unit suggested that lower RNA inputs could be successfully amplified. This was a particularly important consideration at this time, as it was appreciated that the pooling of glomeruli from multiple mice, as performed above in preliminary FACS sorts of reporter mice, would not be possible given breeding and cost restraints in the labelled diabetic mouse model (see discussion).

In order to calculate the number of podocytes, and therefore mice required to obtain sufficient RNA for miRseq using the TruSeq kit, two approaches were taken: Firstly, serially diluted fractions of cultured *in vitro* podocytes were counted and then RNA extracted using the miRnEasy micro kit; a column-based extraction kit that is optimised for use with small amounts of cultured/sorted cells. Figure 5.7 shows the RNA concentrations yielded, as measured by the Nanodrop. Based on a calculated mean podocyte count of ≈5000 per mouse (Table 5.4 above), approximated RNA yield using miRnEasy micro extraction kit equated to ≈50 ng/μl (highlighted in red box in Figure 5.7). As the maximum RNA volume permitted in the TruSeq library prep protocol is 5 μl, this represented a total RNA input of ≈250 ng; 25% of the recommended 1 μg.

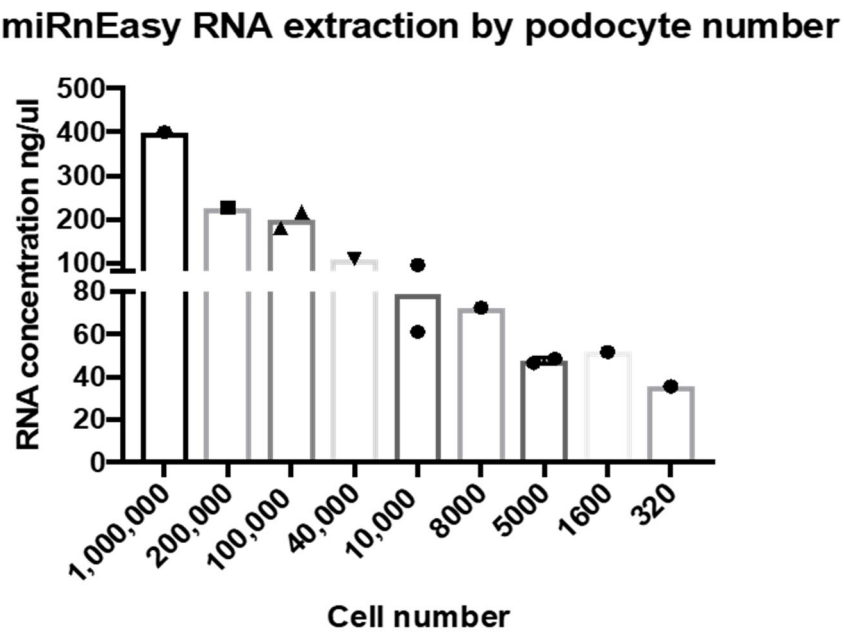

Cell No.	RNA ng/ µl	Total RNA in 5 µl	% of recommended 1 µg input
1000000	399.8	1999	>100
200000	228	1140	>100
100000	199	995	99.5
40000	109.7	548.5	54.9
10000	78.65	393..4	39.3
8000	72.3	361.5	36.2
5000	48.6	243	24.3
1600	51.6	258	25.8
320	35.6	178	17.8

Figure 5.7. RNA yields by podocyte number using miRnEasy micro extraction kit. Cultured podocytes were counted using the Beckman Coulter Particle Counter and RNA extracted and purified using the miRnEasy micro column-based kit. Red highlighted box denotes expected numbers of podocytes, and therefore anticipated RNA yield, from a FACS sort of glomeruli from a single mouse. The TruSeq library preparation kit intended for downstream use recommends an RNA input of 1 µg in maximum reaction volume of 5 µl. Mean of n=2 independent experiments shown.

Secondly, the TruSeq library preparation protocol required modification for the anticipated lower RNA input. Contemporaneously, Baker et al (398) reported success in processing low concentration samples by increasing the number of PCR cycles in the reaction by 73% (11 to 19 cycles), however there were concerns that a PCR bias may have the effect of over-exaggerating miRNAs of highest abundance. I therefore opted to perform a preliminary miRseq experiment comparing the miRseq readouts from a single stock RNA sample at varying RNA concentrations: 1 μg (recommended), 500 ng and 200 ng. To achieve this amount of stock RNA from podocyte extractions alone would require pooling of multiple mice, and therefore whole glomerular RNA from reporter mice was used in this optimisation experiment.

TruSeq library preparation steps are outlined in Methods 2.9.1. Following size selection (Blue Pippin) and bead-purification steps, the cDNA was assessed for quantity and quality using the Agilent bioanalyser. A minimum cDNA molarity of 1500 pmol/l is required for downstream sequencing; lesser-concentrated cDNA may result in an increase in duplicate reads and the occurrence of adapter dimers, produced by intramolecular circularisation reactions. These side products contaminate miRNA sequencing libraries and decrease the sequencing depth achieved by reducing the number of usable reads (399). Figure 5.8 shows the electropherogram readouts and final molarity of the cDNA libraries. The 200 ng sample was insufficient to achieve desired final molarity on first attempt (C), however the TruSeq library preparation protocol uses only 60% of the total indexed PCR product at the size selection stage (owing to volume limitation on the Blue pippin lanes) and therefore it was possible to size-select the remaining PCR product and combine the total cDNA at the bead concentration stage. This protocol amendment resulted in final cDNA molarity of 2027pmol/l (D) without introducing additional PCR bias.

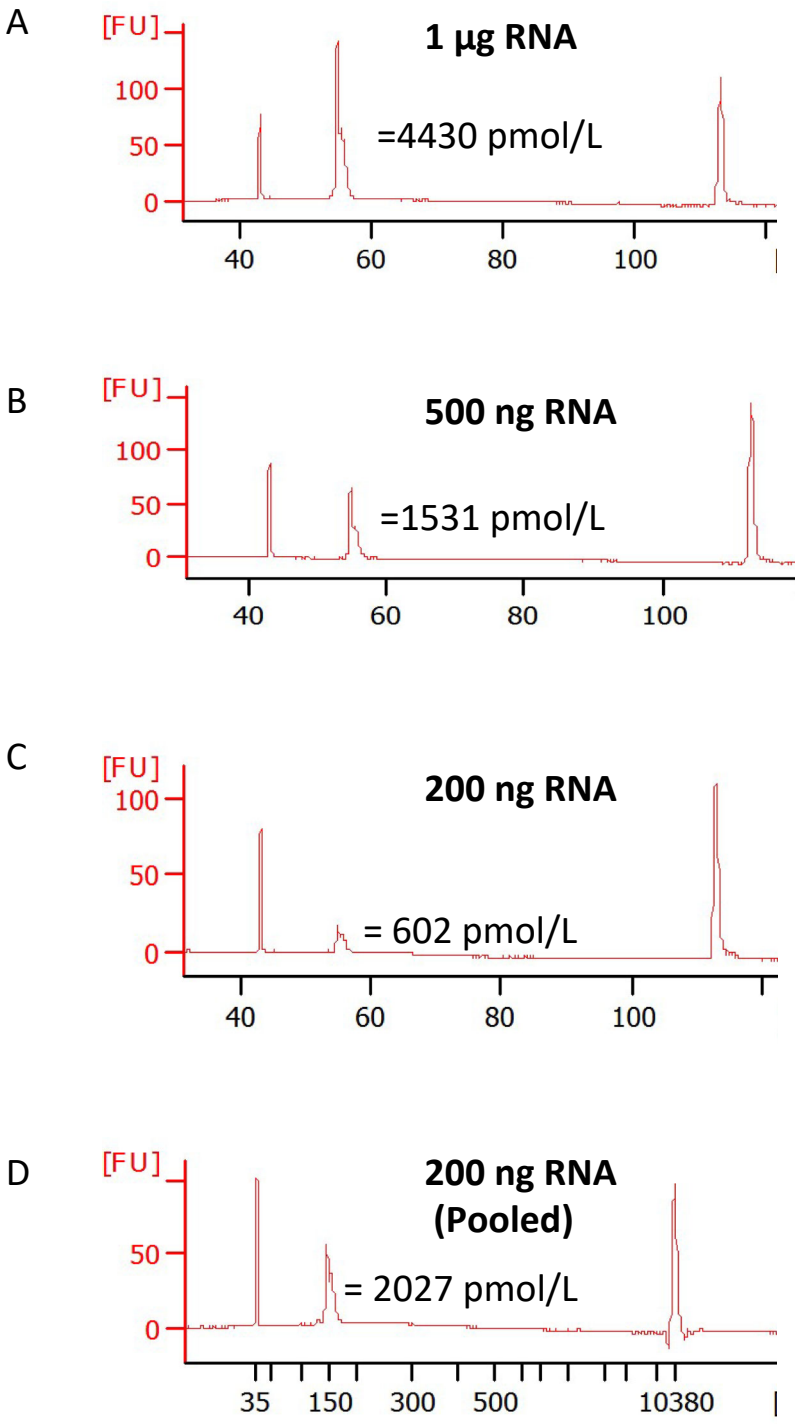

Figure 5.8. Pre-sequencing cDNA library molarity assessment. Agilent bioanalyser was used to measure final cDNA molarity of the sequencing libraries prepared from a single stock sample of whole glomerular RNA, divided into 1 µg **(A)**, 500 ng **(B)** and 200 ng **(C)**. Pooling of cDNA from initial PCR reaction was required in the 200 ng sample in order to reach the 1500pml/l minimum sequencing requirement **(D)**.

Following sequencing, readouts from the 3 samples were compared to assess for loss of total miRNA detection and potential distortion in miRNA expression frequency as a result of the lower input RNA. Of the 377 miRNAs mapped in the 1 ug sample, 266 miRNAs (71%) were mapped in the 500 ng sample and 245 miRNAs (65%) mapped in the 200 ng sample. Despite an apparent loss of detection of 35% of miRNAs in the lowest input sample, the expression of the mapped miRNAs were highly correlated, suggesting no significant distortion of miRNA expression had resulted in the commonly detected miRNAs (Figure 5.9).

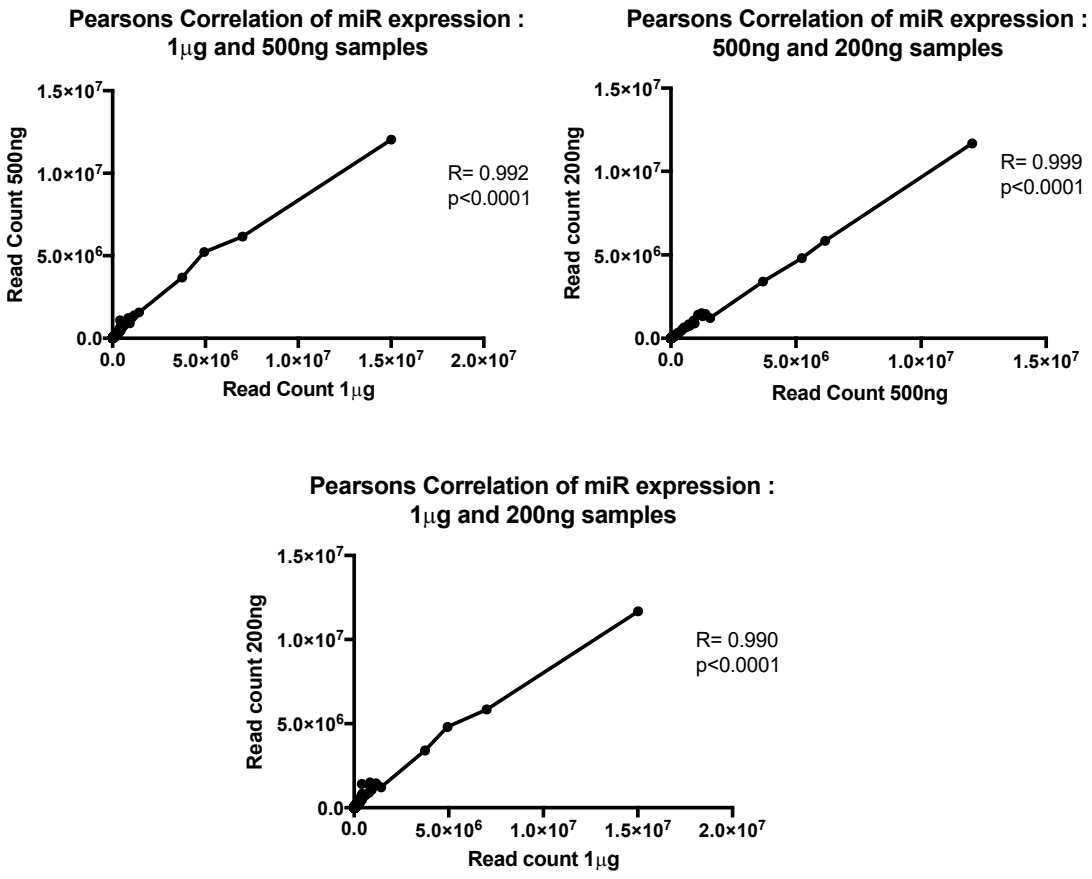

Figure 5.9 Correlation of microRNA expression in varying RNA input TruSeq small RNA sequencing. Whole glomerular mouse RNA was divided into 1 μg, 500 ng and 200 ng samples for construction of cDNA libraries and sequenced using the TruSeq Illumina HiSeq 4000. Expression frequency (read count) for each miRNA was analysed across the sample pairs using Pearsons correlation coefficient (R). No distortion in miRNA expression was observed in the lowest input sample (200 ng) compared to the protocol recommended 1 μg input.

5.2.4 Trial of podocyte sequencing from NPHS2 mCHerry/EGFP+/- reporter mouse

Contemporaneous with attempts to optimise the TruSeq kit for lower input samples, the Wales Gene Park (WGP), a departmental in-house facility at Cardiff University, were trialing a new kit that could enable microRNA sequencing from 100 ng-1 μg of total RNA (NEBNext® Small RNA Library Prep Set), and whole transcriptome sequencing from 2 pg-200 ng of total RNA (NEBNext® low input RNA Library Prep Set). Whilst the 200 ng input optimisation steps described above had resulted in satisfactorily retained expression of abundant miRNAs, the 35% loss of lowly expressed miRNAs would potentially result in a failure to detect miRNAs which become downregulated in the mouse as DN ensues. This, coupled with the lower standard RNA requirement for the newer NEBNext kits, was justification enough to outsource further sequencing attempts to the WGP.

Based on previous FACS sort counts and extrapolation of RNA yielded from column-based extraction of cultured podocytes, a single mouse was expected to achieve sufficient RNA to perform both miRNA and whole transcriptome sequencing (1 mouse ≈ 5000 podocytes ≈ 250 ng RNA, total RNA requirement for miRNA and RNAseq using NEB = 100 ng + 2 pg).

Podocytes were sorted into GFP+++ and GFP-ve fractions using the previously optimised gating strategy, which resulted in lower than expected counts of 1659 and 57,191 cells respectively (Figure 4.10A). RNA was extracted according to miRnEasy protocol and analysed using the Agilent bioanalyser (Figure 5.10B). The low GFP+ve cell count equated to low yield RNA (200 pg/μl) of marginally sub-optimal quality (RIN 6.8) (RIN>7 recommended for downstream sequencing). The larger GFP-ve cellular fraction yielded favorable quality and quantity of RNA (RIN 8.8, 1368 pg/μl,), however the intended combined miRseq and RNAseq of the samples was ultimately limited by the low RNA yield of the GFP+ve fraction. It was therefore decided to perform RNAseq only (2 pg RNA input versus 100 ng for miRseq) with the rationale that mRNA readouts would verify FACS sort purity of the GFP+ve fraction.

A

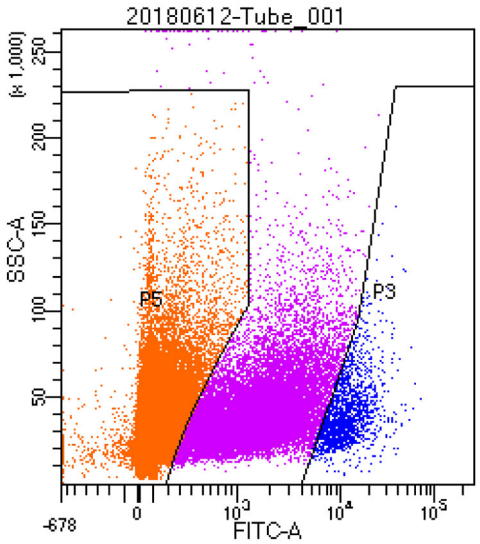

P3 (GFP+ve) = 1659 cell count

P5 (GFP-ve) = 57,151 cell count

B

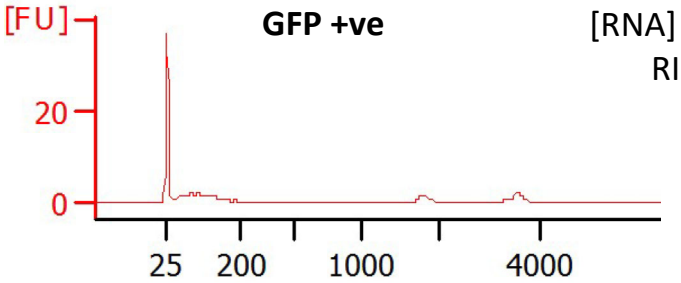

[RNA] = 200 pg/µl
RIN = 6.7

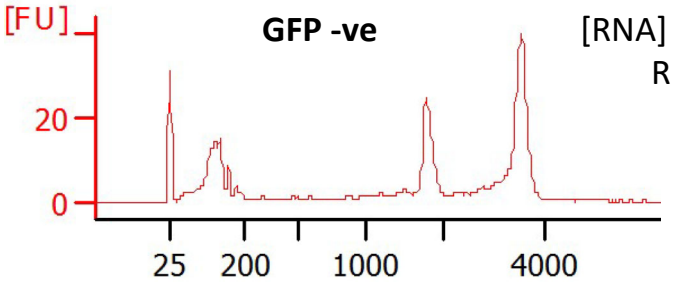

[RNA] = 1368 pg/µl
RIN = 8.8

Figure 5.10A. (Abbreviated) FACS sort of GFP-labelled podocytes from NPHS2 mCherry/EGFP$^{+/-}$ reporter mouse. Glomeruli from n=1 mouse sorted. P3 represents the gating of high intensity FITC fluorescence (blue) presumed to be "true" podocytes. P5 denotes non-fluorescing (GFP-ve) cells (orange). Purple cells of intermediate fluorescence intensity represent Glomerular endothelial cells which exhibit intrinsic autofluorescence (not collected). **5.10B. RNA quality bioanalyser assessment.** RNA extracted from the sorted GFP+ve and –ve fractions was assessed for quality and quantity using the Agilent Bioanalyser. RIN= RNA integrity number.

Figure 5.11A demonstrates the enrichment of podocyte specific markers nephrin (25-fold), podocin (121-fold) and CD2AP (101-fold) in the GFP+ve fraction relative to the GFP-ve fraction, therefore supporting the podocyte purity observed previously using RT-qPCR of Cell-2-Ct lysates. GEnC markers were not significantly enriched in the GFP-ve fractions (Figure 5.11B) which was an expected consequence of gating out the intermediate GFP+ve cells and electing only to collect the 'true" positive and negative fractions (Figure 5.10A). The mesangial cell population was clearly captured in the GFP-ve fractions however, with enrichment of PDGFRβ (38-fold), α-SMA (20-fold) and fibronectin (16-fold) seen (5.11C).

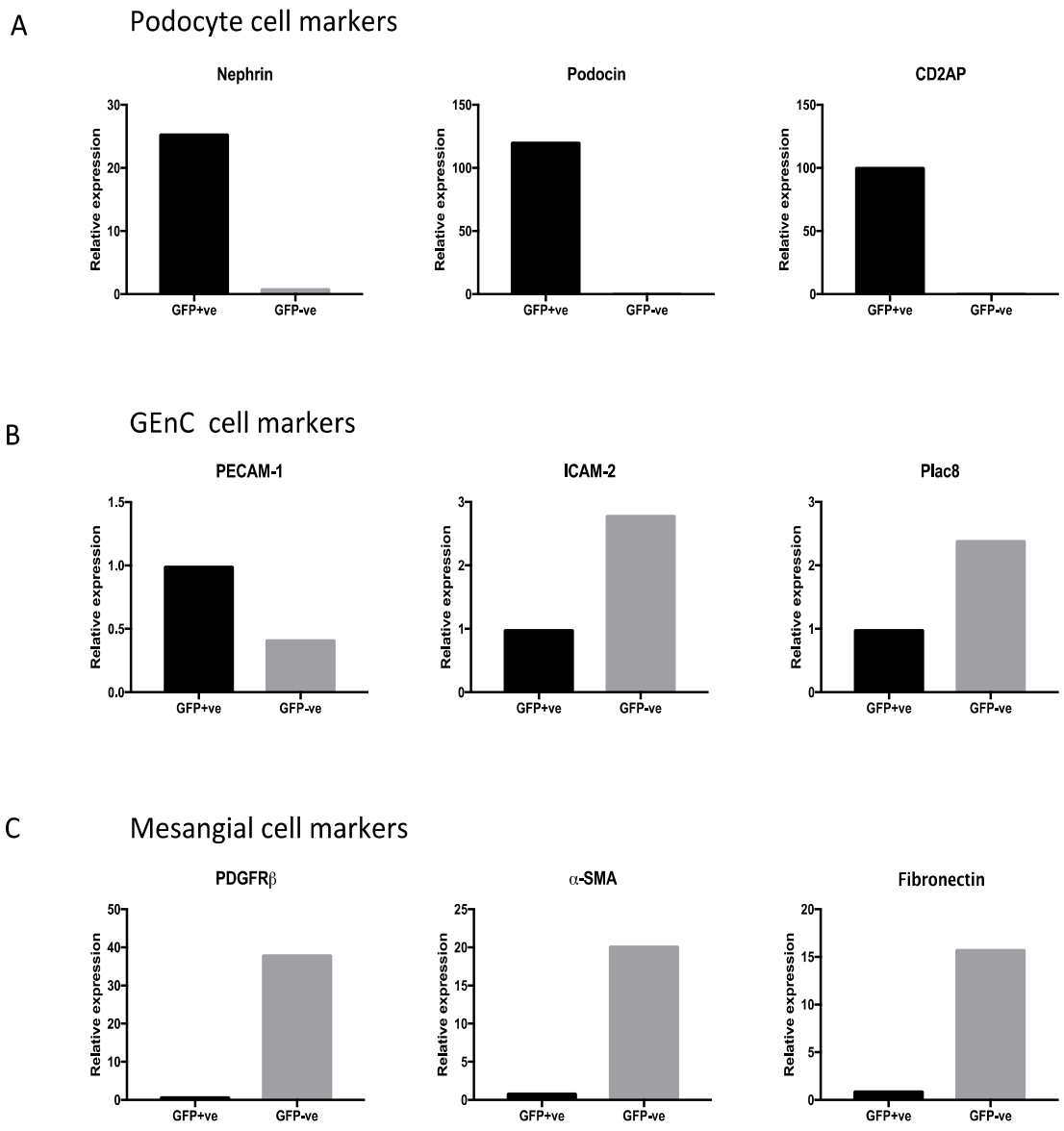

Figure 5.11. Glomerular Cell marker expression by RNAseq in flow-sorted GFP-labelled podocytes from NPHS2 mCherry/EGFP$^{+/-}$ reporter mouse. RNA extracts from GFP+ve and GFP-ve cell sorted fractions were prepared using NEBNext® Small RNA sequencing kit and sequenced using Illumina HiSeq 4000. Podocyte **(A),** GEnC **(B)** and mesangial **(C)** cell specific markers shown. Normalised read counts used to calculate fold change relative to GFP-ve fraction (A) or GFP+ve fraction (B&C). N=1 mouse used. CD2AP= CD2 associated protein, ICAM-2= intracellular adhesion molecule 2, Plac8= Placenta associated-8, α-SMA= smooth muscle actin.

5.3 Discussion

The results reported in this section represent sequential approaches taken to optimise the isolation of a pure podocyte population for the intended purpose of downstream miRNA and whole transcriptome sequencing at progressive stages of DN development in a mouse.

As the least abundant glomerular cell type, gaining sufficient podocyte numbers for analysis has traditionally necessitated the pooling of multiple mice (396, 400). This was not possible due to the unpredictably protracted breeding program of the reporter and db/db mice. To date, there have been few successful breeding pairs that have produced notably small litters. The planned n of 3 samples at 3 separate time points, coupled with the expected mendelian frequency of only 1 in 8 mice of the required genotype ($EGFP^{+/-}$ db/db) was reliant on establishing a robustly productive breeding colony within the time constraints of this PhD. Nevertheless, this did not preclude efforts to optimise the isolation of podocytes using reporter mice only; with the intention of confirming purity of GFP-labelled podocyte sorts for future work in fulfilling this aim.

5.3.1 Podocyte count variability

The podocyte yield per FACS sort attempt was markedly variable and did not correlate with the number of mice pooled per sort. Consequently, attempts to calculate mean podocyte number and predict RNA yields by extrapolation of *in vitro* data proved inaccurate in assuming that a single reporter mouse would provide sufficient material for a trial of podocyte miRseq and RNAseq. A number of possible explanations for the observed heterogeneity exist. Firstly, variable penetrance of the GFP gene and/or variable Cre activity in the reporter mice could impact FACS sort performance, which may, in turn, explain the wide range of expression fold changes seen in the podocyte cell markers over 3 individual experiments (4-60 fold difference in nephrin expression between GFP+ve and –ve fractions). The ongoing backcrossing of the db/db and reporter mice to a minimum number of ten generations would be expected to achieve

>99% penetrance of the phenotype and should therefore eliminate this potential source of FACS bias (401).

Secondly, the technical complexity and duration of each experiment, which included an hour-long transport hiatus between Bristol and Cardiff sites at the glomerular isolation stage, may have led to variable degrees of podocyte loss. Whilst the proportions of live cells recorded by FACS appeared fairly consistent across sorts, because this was measured after exclusion of debris and doublets, it is likely that a varying number of dead podocytes contributed to these excluded cells/debris per experiment. The one-step Cell-to-Ct method employed to process cells directly from sort was an appropriately useful means of minimising late-stage cell/RNA loss and permitting RT-qPCR determination of sort purity from scanty cell numbers, but with the caveat of producing lysates incompatible with downstream sequencing application.

Finally, the most objectively evident variable was the quality of the glomerular isolations. Dynabead perfusion is a technically challenging procedure, requiring 2 experienced operators. Suboptimal perfusion of the renal circulation results in fewer glomeruli "seeded" with dynabeads, hence fewer glomeruli are magnetically separated out for processing. This was occasionally evident at a macroscopic level, with visibly less tissue aligning to the Eppendorf wall on application of the magnet. Size or sex of the mouse was not a determinant of ease of perfusion in these experiments (all reporter mice used were age 8-10 weeks), however it is reasonable to anticipate that obese db/db mice with advanced diabetes may present a more technical challenge in future work (see below).

5.3.2 Sequencing platform options

At the time of investigating, the TruSeq smRNA library kit (Illumina) was the most established kit in use in our centre. During optimisation of the protocol to achieve comparable miRseq results using low input RNA, a newer NEB kit was released which permitted 1/10th of the recommended 1 μg input of the Illumina kit, as standard. The rapid development in new sequencing technology has occurred in parallel with this PhD, and there are now a number of low input

miRseq kits available for use, summarised in Table 5.5. Single cell sequencing (scSeq) of the glomeruli has also been recently reported as a means of analysing distinct glomerular cell populations (402-404), with the added dimension of investigating cellular transcriptomic heterogeneity within cells of the same lineage. Furthermore, many scSeq methods do not rely on the prior sorting of genetically/antibody-labelled cells by flow cytometry; instead, a single cell suspension of a heterogeneous tissue of interest (e. g glomerular cells) can be fed into a chip where individual cells are "captured' and "barcoded" by uniquely labelled oligonucleotides which allow each cell to be identified and sequenced. Alas, currently available scSeq are incompatible with miRNA sequencing as the oligonucleotide "capture" is achieved via recognition of a polyA tail, which mature miR transcripts do not possess (405). Additionally, scRNAseq data analysis uses validated mRNA markers of specific cell types (e.g. nephrin, PECAM-1) to determine cell populations. Whilst it is recognised that certain miRNAs are more abundant in specific tissue types, there is not yet the equivalent specificity to confidently delineate a podocyte from a mesangial cell based entirely on miRNA expression signature.

miRseq Kit	RNA input	Pros	Cons
TruSeq smRNA (Illumina)	1µg in 5µl	• Most established kit • Lowering input to 10 ng did not affect number of reads classified as "too short"(406)	• Strong sequence bias* (407) • Phusion Polymerase used for PCR is bias-prone (408) • Adapter dimers** common (407)
SMARTer smRNA-Seq kit (Clontech)	1ng-2µg in <6µl	• Ligation-free "tailing approach"- 3' adapter added by polyadenylation, 5' adapter added through reverse transcriptase template-switching • Least sequence bias versus other kits (407) • Fastest work-flow (up to gel stage) (409)	• Adapter dimers common • Not exclude mRNA degradation (other kits require intact 5' phosphate and 3' OH groups for adapter ligation) = more reads discarded (409) • Requires gel separation step
NextFlex smRNA-seq kit (Bioo Scientific)	1ng-2µg in 10.5 µl	• Uses degenerated, randomised adapters and PEG to reduce sequence bias • Few adapter dimers (Includes purification step to remove excess 3' adapter) • Best miRNA detection rates (at highest RNA input) (406) • Gel-free size selection • Option to complete entire workflow on one robotic platform	• Lowest RNA range results in increased reads categorised as "too short" (406)
NEBNext multiplex smRNA (NEB)	100ng-1ug in	• Uses Polyethylene glycol (PEG) to increase ligation efficiency and reduce sequence bias • Minimal adapter dimers (407)	• Lowest RNA range results in increased reads categorised as "too short" (406) • Requires gel separation step

Table 5.5. Comparison of commercially available small RNA sequencing Library Preparations kits.

Table 5.5. Comparison of commercially available small RNA sequencing Library Preparation kits. *Sequence bias refers to the phenomena of certain RNA sequence/structure resulting in the preferential ligation of smRNAs with a given adapter sequence**.** Also known as "ligation bias", many kits employ modifications to address this as shown, such as addition of polyethylene glycol (PEG) to improve ligation efficiency, addition of degenerated primers where the last four nucleotides at the ligation junction are randomised, or the avoidance of ligation at all. The SMARTER kit achieves this using a tailing approach, where 3' end is polyadenylated followed by a reverse transcription (RT) reaction primed by an oligo dT primer that incorporates the 3' adapter. The reverse transcriptase enzyme switches template upon reaching the end of each RNA template and utilises this SMARTer oligo as a secondary template to attach the 5' adapter. **Adapter dimers may impede enrichment for miRNAs over other RNA species, thus decreasing the sequencing depth by reducing the number of usable reads.

5.3.3 Future Developments

Despite the limitation in availability of the desired labelled db/db model, much has been learnt from the technical optimisation steps here reported. Whilst podocyte count was variable, purity of sort was consistent, and hence the foundations for future experiments using the latest extremely low RNA input sequencing kits have been well established. However, all experiments were performed using GFP-labelled wild type mice of otherwise normal phenotype and health, at approximately 8-10 weeks of age. Once crossed with the db/db model and sacrificed at the intended time points of 4, 8 and 12 weeks, additional technical hurdles may be anticipated, such as difficult glomerular perfusions in very young or overweight mice and reduced podocyte number in the 12 week diabetic animals. Nevertheless, with latest sequencing library kits optimised for use with very limited numbers of cells and RNA, such hurdles should not be insurmountable.

Future developments of a scSeq technique capable of simultaneously capturing miRNA and (cell-population discriminating) mRNA expression data may circumvent the need for a GFP-podocyte labelled mouse model, thus eliminating the dependence on what has proved to be a challenging breeding program. Comparatively, the db/db mice are reliable breeders and gaining sufficient mouse numbers to conduct scSeq should not present any logistical difficulty.

Further attempts at performing miRNA and mRNAseq of podocytes from the diabetic mouse may, therefore, depend on which becomes available first: an established podocyte-labelled db/db mouse colony, or a scSeq kit capable of small RNA capture.

5.3.4 Conclusion

This chapter reports the optimisation of FACS sorting of enzymatically digested glomerular cells, and specifically, the appreciation of the existence of a discrete population of autofluorescing glomerular endothelial cells that must be excluded in order to isolate a pure podocyte fraction using this method. The

disparity between podocyte yield and high RNA requirement of the Illumina TruSeq smRNA sequencing kit was successfully overcome using a hitherto undescribed protocol amendment which permitted a 80% decrease in RNA input without introduction of additional PCR bias (accepting a consequential loss in detection of very low abundance miRNAs).

Ultimately, the breeding delays of the labelled db/db mouse, combined with sequencing efforts at a time that pre-dated the availability of ultra low RNA input sequencing kits, were limiting factors in achieving the intended aim of investigating podocyte-specific miRNA expression throughout DN development. The following chapter will focus on establishing the evolution of miRNA changes in DN at a whole glomerular level.

6 Whole Glomerular miR/RNA sequencing of db/db mouse

6.1 Introduction

The glomerulus is a highly specialised bundle of capillaries supported by podocytes, mesangial and glomerular endothelial cells. The dynamic responses required to maintain constant rates of filtration necessitate intact cell-cell communication and feedback pathways. Recently, it has been suggested that miRNAs are key coordinators of this glomerular crosstalk (410) . My research hypothesis is focused on the significance of podocyte insulin resistance as a primary insult in DN, which initiates pathophysiological changes in podocytes, as well as other glomerular cells. MicroRNAs are well documented as signal transducers in cell-cell communication, with elegant data describing their intercellular transport via exosomes, microvesicles and lipoproteins in numerous different organs (411-414).

In appreciation of this complex network of miRNA-mediated glomerular crosstalk, it was my intention to investigate and compare the whole glomerular miRNA profile of the db/db mouse in parallel with podocyte-specific sequencing from the same mouse model. Whilst it was not possible to perform podocyte sequencing as originally intended, whole glomerular isolations from db/db mice proved to be of excellent quality. The comparative availability of the (unlabelled) db/db model, and the superior RNA yield extracted from bulk glomerular tissue, permitted investigation of both miRNA and mRNA changes during the development of DN. The following chapter details the analysis of these results, and how they correlate both to mouse phenotype and to the miRNA signature of insulin-resistant podocytes *in vitro*, as reported in Chapter 3.

6.1.1 Chapter Aims

1. Determine:
    a. glomerular microRNA changes and
    b. glomerular mRNA changes in the db/db DBA/2J model during the development of DN
2. Investigate evidence of miR-directed target mRNA changes in the glomeruli of the db/db DBA/2J model
3. Determine extent of crossover between insulin-resistant podocyte and db/db glomerular miRNA profiles.

4.

6.2 Results

6.2.1 Whole Glomerular MicroRNA Sequencing Results

6.2.1.1 Quality Control

Glomeruli were isolated as previously described, and RNA extracted directly using the miRnEasy kit. RNA quality and quantity assessment is shown in Figure 6.1. Suggested thresholds of sample quality for downstream sequencing experiments are RIN >7 for mRNAseq, although values >6 have been reported as acceptable for miRseq (415, 416). As discussed previously, ease of dynabead perfusion was the biggest determinant of successful glomerular extraction, and hence RNA yield. This is reflected in the lower yields in the smallest animals at 4 weeks of age (Table 6.1). One animal (sample b) was particularly small with few glomeruli obtained, leading to low RNA yield (18ng/ul) and suboptimal RIN value (6.5). The sample was processed as planned, with a view to potentially excluding this result if it proved to be a significant outlier post analysis (which it was not). Despite the variation of total RNA extracted from the animals, the combined requirement of 105 ng input (100 ng for miRseq + 5 ng for RNAseq) was achieved for all samples, where 1 sample is representative of glomerular material from a single mouse.

Db and WT littermate pairs were sex-matched where possible, and this was achieved for 7/9 mice pairs (Table 6.1). However, a sex discrepancy exists between experimental time points, with the 4-week pairs being exclusively male, 8-week pairs predominantly female (5/6 mice) and the 12-week pairs predominantly male (5/6). Animals were collected in db and WT littermate pairs, in no particular age order, over a period of 8 months.

Table 6.1 summarises the raw data from the miRseq analysis. A read depth of 1-2 million reads is recognised as gold standard for differential expression profiling of miRNAs (5-8M reads is recommended for discovery profiling (416)) This was achieved in all samples, and >80% of all reads were successfully mapped to the genome, further validating the quality of the sequencing run.

A

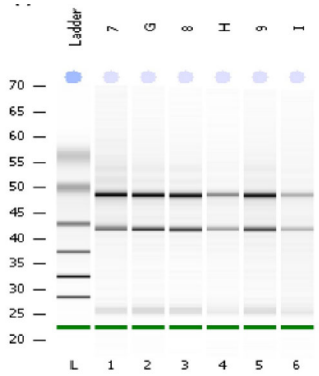
Ladder
7
G
8
H
9
I
70
65
60
55
50
45
40
35
30
25
20
L
1
2
3
4
5
6

B

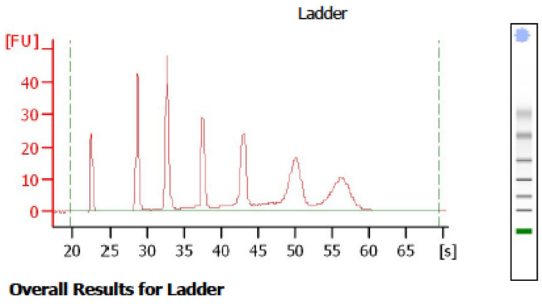
Ladder
[FU]
40
30
20
10
0
20 25 30 35 40 45 50 55 60 65 [s]
Overall Results for Ladder

C

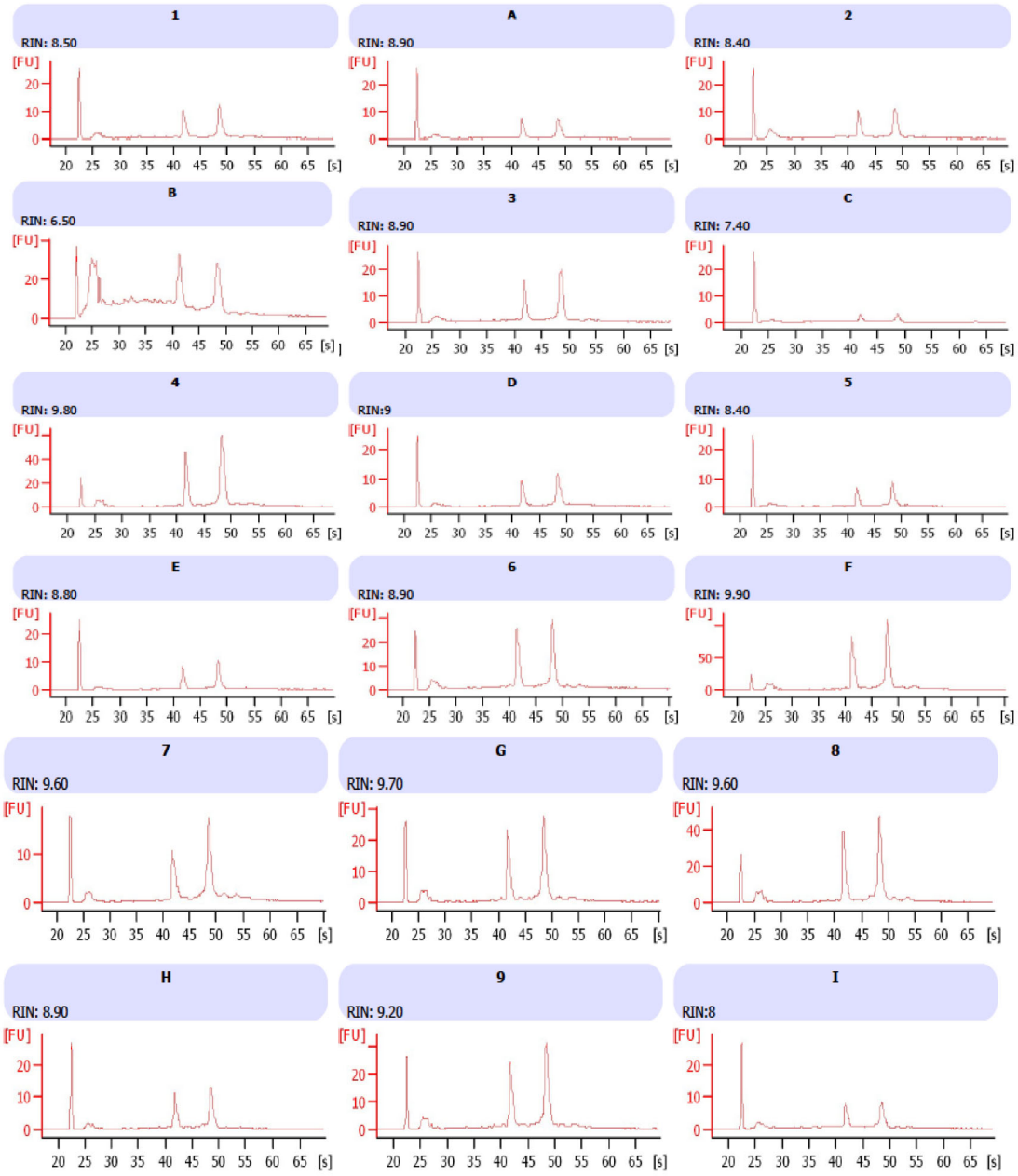
1
RIN: 8.50
A
RIN: 8.90
2
RIN: 8.40
B
RIN: 6.50
3
RIN: 8.90
C
RIN: 7.40
4
RIN: 9.80
D
RIN:9
5
RIN: 8.40
E
RIN: 8.80
6
RIN: 8.90
F
RIN: 9.90
7
RIN: 9.60
G
RIN: 9.70
8
RIN: 9.60
H
RIN: 8.90
9
RIN: 9.20
I
RIN:8
[FU]
20 25 30 35 40 45 50 55 60 65 [s]

Figure 6.1 Assessment of RNA sample quality prior to miR- and mRNAseq. Agilent 2100 Bioanalyser was used to assess RNA integrity of all samples prior to sequencing. **(A)** Capillary electrophoresis of 6 samples (7 to I shown for brevity). **(B)** Ladder. **(C)** Independent electrograms of each sample, where samples were paired as db/db and WT littermate control with diabetic animals represented by numbers 1-9 and paired WT control represented as corresponding letters A-I. Samples 1A-3C are 4-week old mice, 4D-6F are 8-week old mice and 7G-9I are 12-week old mice.

ID	Sample Description	Sex	miRNA ng/ul	RIN	No. reads	No.reads post trim (%)	Mapped reads (%)
s1	**db 4 week**	M	74	8.5	11750681	99.44	86.93
sa	**WT 4 week**	M	50	8.9	6580264	99.79	87.72
s2	**db 4 week**	M	66	8.4	5066171	99.55	87.26
sb	**WT 4 week**	M	18	6.5	5293512	99.45	80.67
s3	**db 4 week**	M	90	8.9	3409617	99.46	87.72
sc	**WT 4 week**	M	30	7.4	10485760	99.55	87.15
s4	**db 8 week**	F	212	9.8	3402426	99.72	94.06
sd	**WT 8 week**	M	64	9	7518254	99.75	93.43
s5	**db 8 week**	F	48	8.4	7460579	99.65	92.35
se	**WT 8 week**	F	50	8.8	10705925	99.63	93.40
s6	**db 8 week**	F	134	8.9	11746635	99.46	90.67
sf	**WT 8 week**	F	404	9.9	8418869	99.64	95.28
s7	**db 12 week**	M	74	9.6	10787367	99.77	95.39
sg	**WT 12 week**	F	122	9.7	10840337	99.66	91.27
s8	**db 12 week**	M	206	9.6	12075417	99.77	92.30
sh	**WT 12 week**	M	62	8.9	11259814	99.65	88.85
s9	**db 12 week**	M	142	9.2	11875151	99.71	90.51
si	**WT 12 week**	M	68	8	9479719	99.75	86.59

Table 6.1 Summary of raw miRseq data from whole glomeruli in db/db and WT mice. Samples were paired as db/db and WT littermate control with diabetic animals represented by IDs s1-9 and paired WT control labelled as corresponding letters sA-I, n=3 pairs per time point. Sequencing read depth of >2 million reads was achieved for all samples, with minimal loss following trimming of adapter primers (identified as an absence of sequence between adapter primers), denoted above as "No. reads post trim (%)". Mapped reads refer to those sequences that were matched to known miRNAs in the miRbase and ENSEMBL database, and should approximate 80-90% as standard.

6.2.1.2 MiRNAs are differentially expressed in whole glomerular tissue from db/db mouse model

A Principal Component Analysis of the miRseq data is presented in Figure 6.2. From this plot, it can be appreciated that age of the mice is an important determinant of miRNA expression, and this effect is most pronounced in the 4- and 8-week time points where the db and WT samples cluster closely together. Sample separation between db and WT groups is, however, observed by 12 weeks, by which time the db mice have been exposed to hyperglycaemia for at least 4 weeks duration (394).

More detailed analysis of miRNA expression per time point revealed that, interestingly, whilst miRNAs were differentially expressed at 4- and 12-weeks, no significant miRNA changes were detected between db and WT in the 8-week old (predominantly female) animals. Figure 6.3 shows the volcano plots derived from this data, and the numbers of miRNAs differentially expressed by unadjusted and adjusted p value (where adjusted p-value refers to statistical correction for multiple testing, which may result in over-stringent rejection of significant results in large datasets, see discussion). The volcano plots are also skewed towards upregulation of miRNAs, with an absence of significantly downregulated miRNAs at weeks 4 and 12.

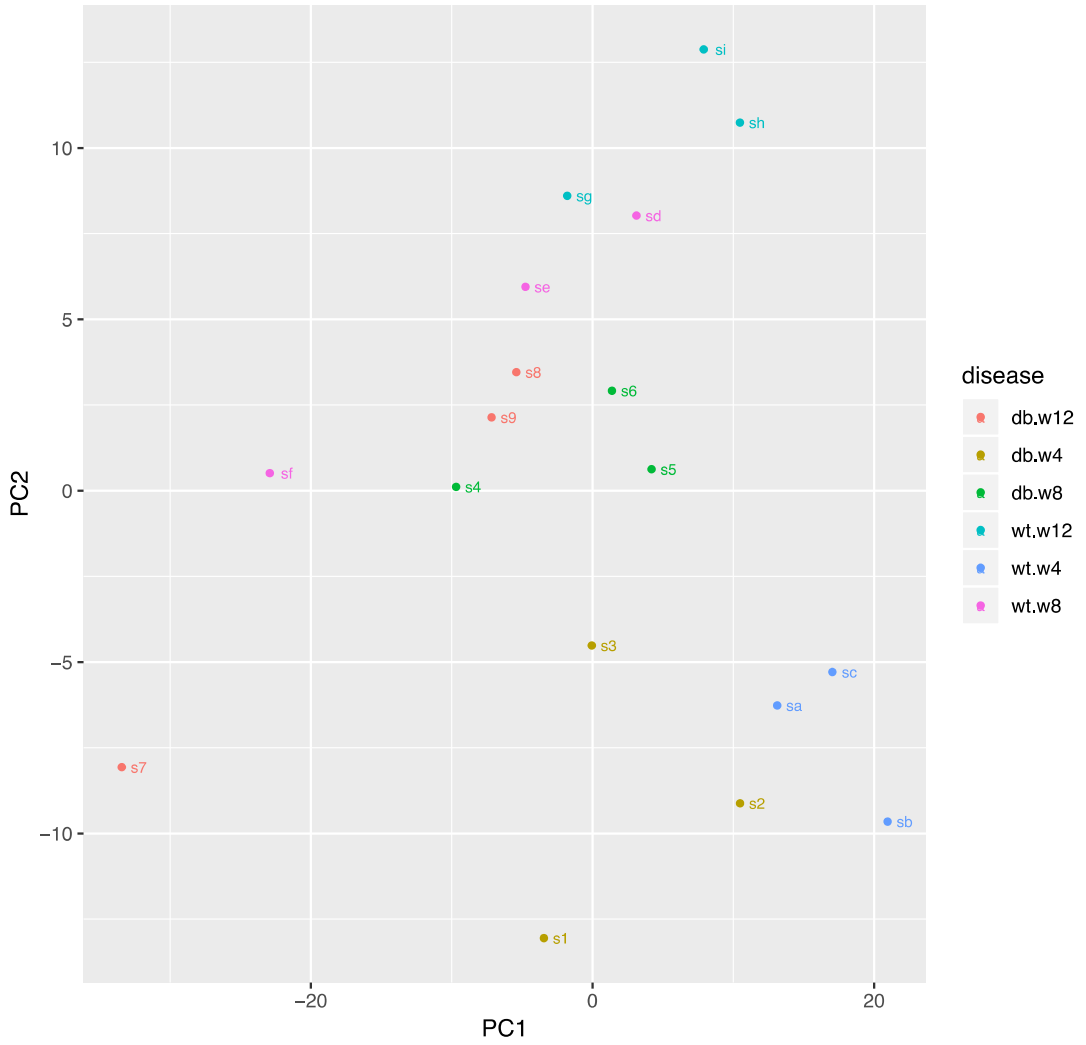

Figure 6.2 Principal Component analysis of microRNA expression in whole glomeruli from db/db and WT mice. Samples were paired as db/db and WT littermate control with diabetic animals labelled numerically and paired WT controls labelled as corresponding letters, n=3 pairs per time point, where s1-3 and a-c represent 4-week old animals, s4-6 and d-f represent 8-week old animals and s7-9 and g-I represent 12-week old animals. PCA plot derived using all significantly differentially expressed miRNAs across all time points.

A.

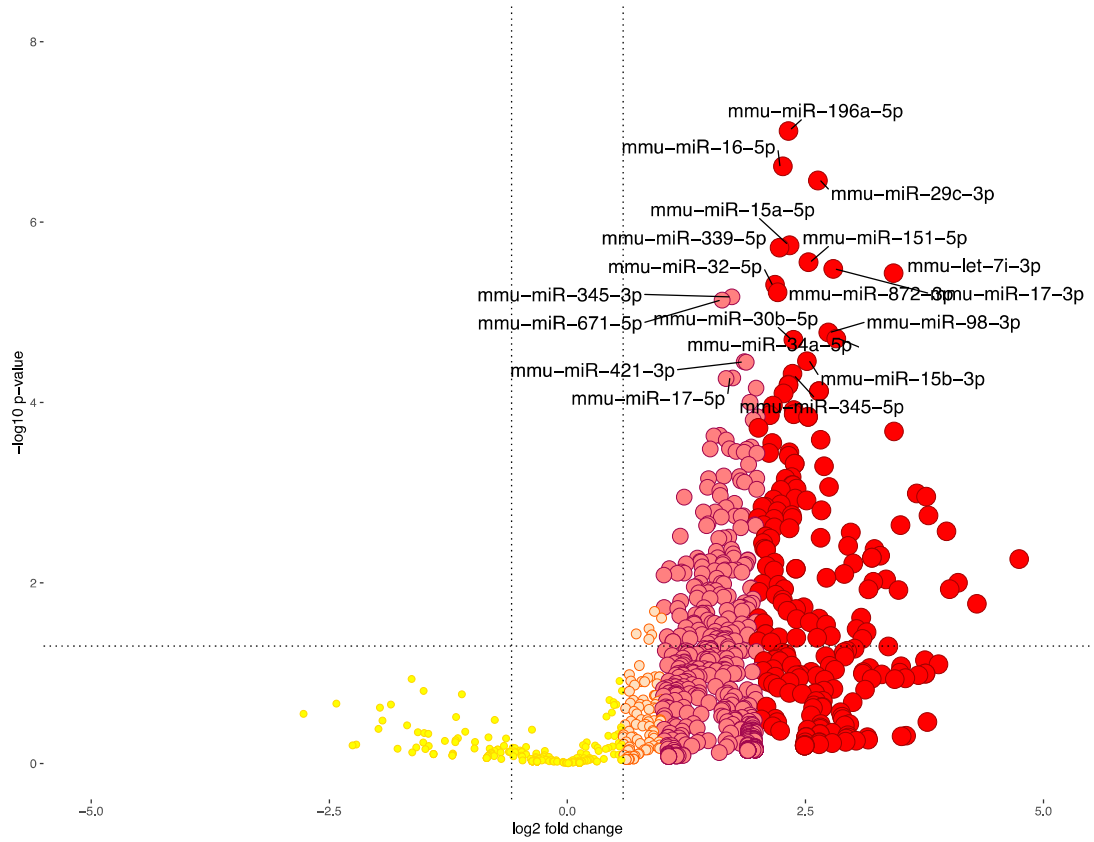

Significant genes	
p-value	Adjusted p-value
291	68

Downregulated in db/db mice Upregulated in db/db mice

B.

Significant genes	
p-value	Adjusted p-value
4	0

C.

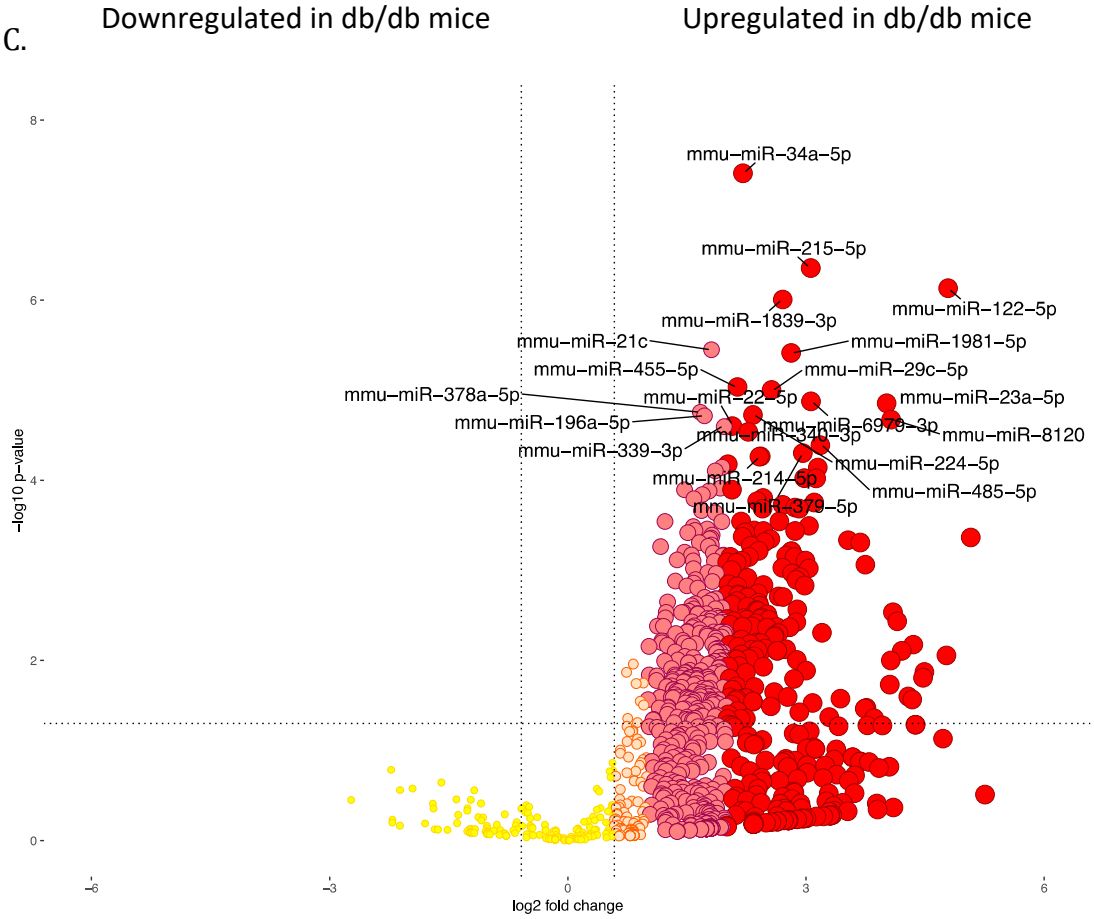

Significant genes	
p-value	Adjusted p-value
407	110

Figure 6.3 Volcano Plot analysis of microRNA expression in db/db whole glomeruli. Plots depict the relationship between the $-\log_{10}$ of the p-values and the log2 fold change in miRNA expression between db/db and WT samples (miRNAs at the upper and outer aspects of the "V"-plot are the most significantly up-and downregulated miRNAs in the diabetic animals, compared to WT controls). Horizontal dissecting line of significance set at p=0.05 (unadjusted). Size and colour intensity of dot indicative of log2 fold change range (e.g pink= 1.5-2 fold increase, deep red = 2-4 fold increase). Numbers of differentially expressed miRNAs by adjusted and unadjusted p-value as shown. **(A)** 4 weeks **(B)** 8 weeks **(C)** 12 weeks.

Figure 6.4 displays the heat maps of the top 50 differentially expressed miRNAs at 4 and 12 weeks, clustered by miRNAs (rows) and samples (columns). At each time point, a single sample appears to be the main determinant of differential expression; db1 at 4 weeks and db7 at 12 weeks. Hierarchical clustering analysis was unable to group samples exactly by diabetes and WT, with a consistent degree of overlap at both time points.

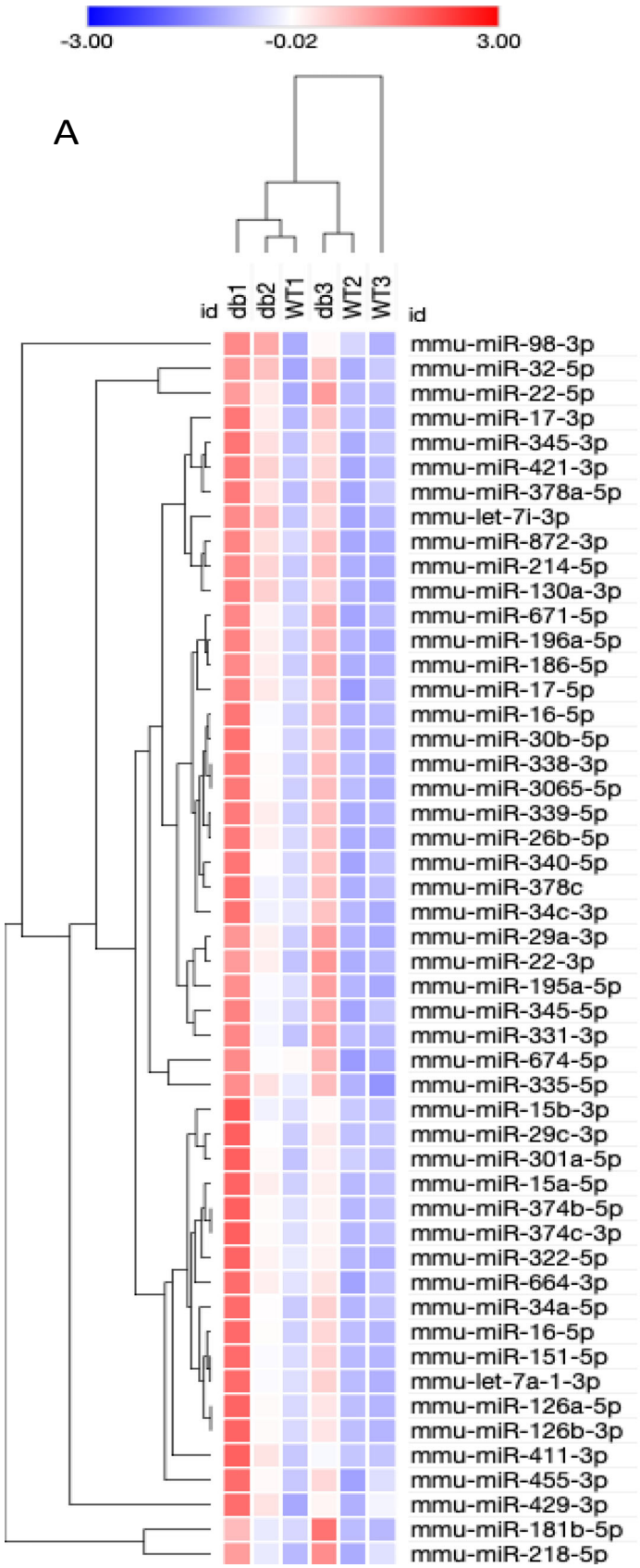
-3.00
-0.02
3.00
A
id
db1
db2
WT1
db3
WT2
WT3
id
mmu-miR-98-3p
mmu-miR-32-5p
mmu-miR-22-5p
mmu-miR-17-3p
mmu-miR-345-3p
mmu-miR-421-3p
mmu-miR-378a-5p
mmu-let-7i-3p
mmu-miR-872-3p
mmu-miR-214-5p
mmu-miR-130a-3p
mmu-miR-671-5p
mmu-miR-196a-5p
mmu-miR-186-5p
mmu-miR-17-5p
mmu-miR-16-5p
mmu-miR-30b-5p
mmu-miR-338-3p
mmu-miR-3065-5p
mmu-miR-339-5p
mmu-miR-26b-5p
mmu-miR-340-5p
mmu-miR-378c
mmu-miR-34c-3p
mmu-miR-29a-3p
mmu-miR-22-3p
mmu-miR-195a-5p
mmu-miR-345-5p
mmu-miR-331-3p
mmu-miR-674-5p
mmu-miR-335-5p
mmu-miR-15b-3p
mmu-miR-29c-3p
mmu-miR-301a-5p
mmu-miR-15a-5p
mmu-miR-374b-5p
mmu-miR-374c-3p
mmu-miR-322-5p
mmu-miR-664-3p
mmu-miR-34a-5p
mmu-miR-16-5p
mmu-miR-151-5p
mmu-let-7a-1-3p
mmu-miR-126a-5p
mmu-miR-126b-3p
mmu-miR-411-3p
mmu-miR-455-3p
mmu-miR-429-3p
mmu-miR-181b-5p
mmu-miR-218-5p

B

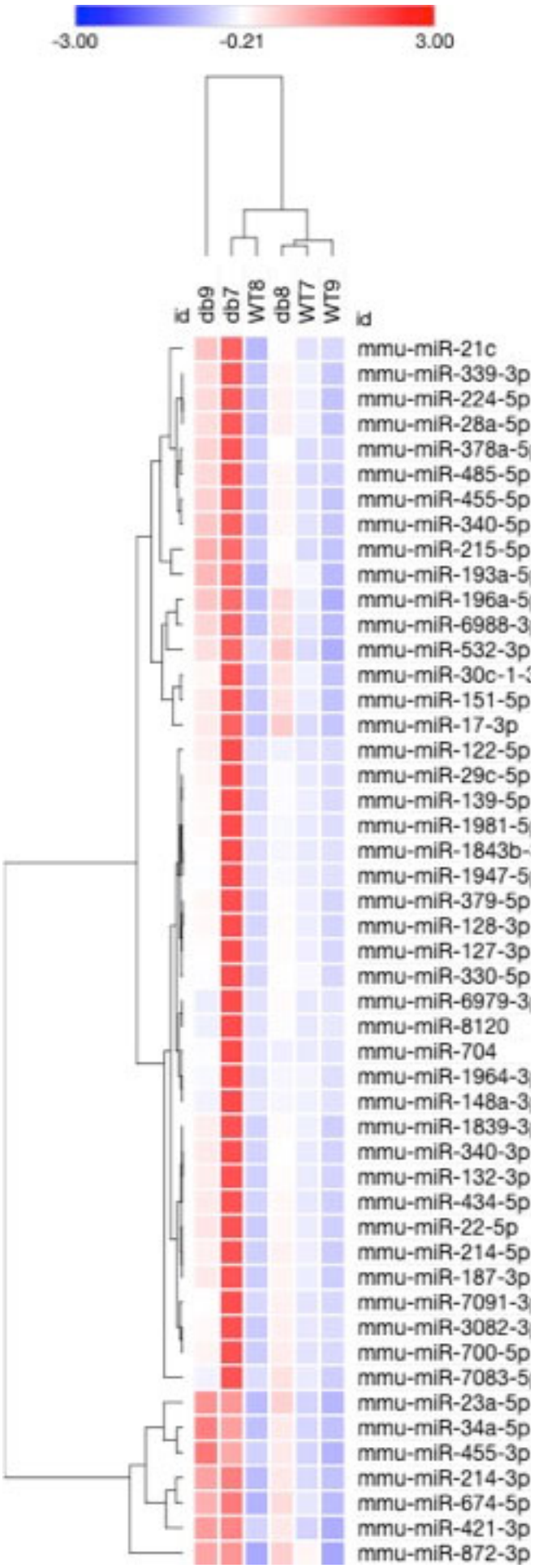

Figure 6.4 Heat map visualisation differentially expressed glomerular miRNAs in db/db mouse. Unsupervised Hierarchical Clustering of samples (columns) and miRNAs (rows) performed on top 50 differentially expressed miRNAs at each time point (sorted by unadjusted p-value). Z-score transformation of normalised read counts performed (subtract mean row count and divide by row standard deviation) and score set as -3 to 3, where red= high miRNA expression and blue =low miRNA expression, relative to expression across all samples in that row. **(A**) 4 weeks **(B)** 12 weeks.

6.2.1.3 *Pathway enrichment: miRNA expression changes are established early in DN development*

Pathway Enrichment analysis was performed using Ingenuity Pathway Analysis (IPA). Only the 4- and 12-week data were compared in the analysis, owing to the absence of differentially expressed miRNAs at the 8-week time point. Figure 6.5 depicts a comparison analysis of "toxic functions" predicted to be influenced at 4 and 12 weeks. MiRNAs associated with class II lupus nephritis were chiefly enriched in both datasets. Other toxic functions of relevance included inflammatory pathologies (hepatitis) and fibrosis (cirrhosis, heart fibrosis). Toxic enrichment profiles were generally very similar at both time points.

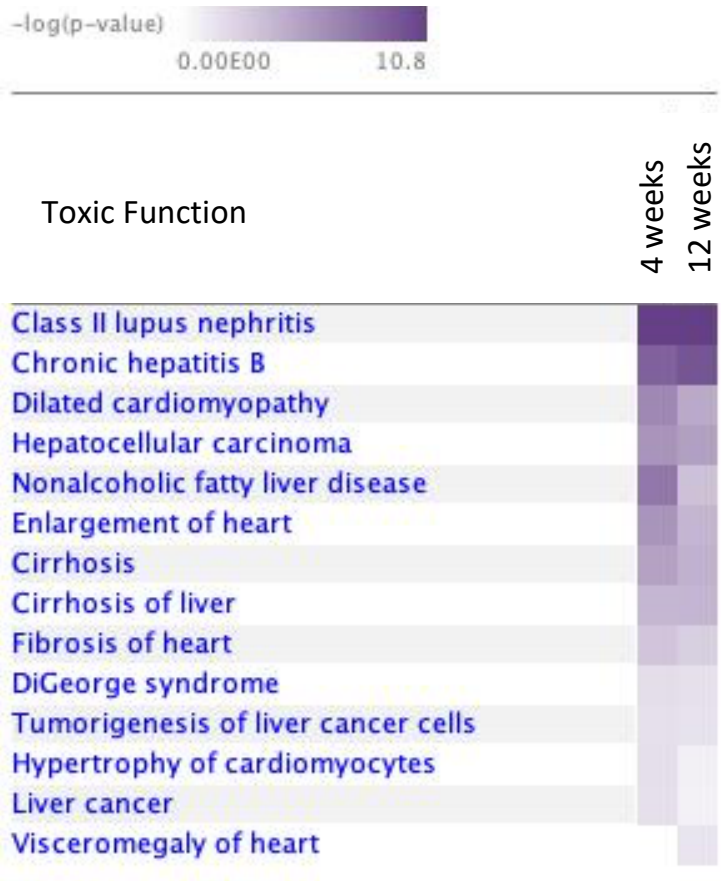

Figure 6.5. Comparison analysis of miRNA enrichment in toxic biological functions. Analysis performed on all differentially expressed miRNAs at 4- and 12-week time points in whole glomeruli from db and WT mice, n=3 per group, per time point. Log of the (unadjusted) p-value used in analysis, performed using Ingenuity Pathway Analysis software.

Biological pathways were refined to those with direct relevance in the mouse model, with an attempt to correlate miRNA changes to known phenotypic traits (Figure 6.6). At 4 weeks, the miRNA signature could already be clearly mapped to pathways of inflammation, nephritis, diabetes and fibrosis despite being phenotypically indistinguishable from the WT mice at this time point. At 12 weeks, a few additional miRNAs were implicated in each of the listed pathological pathways, except fibrosis (27 miRNAs at 4 weeks, 24 miRNAs at 12 weeks).

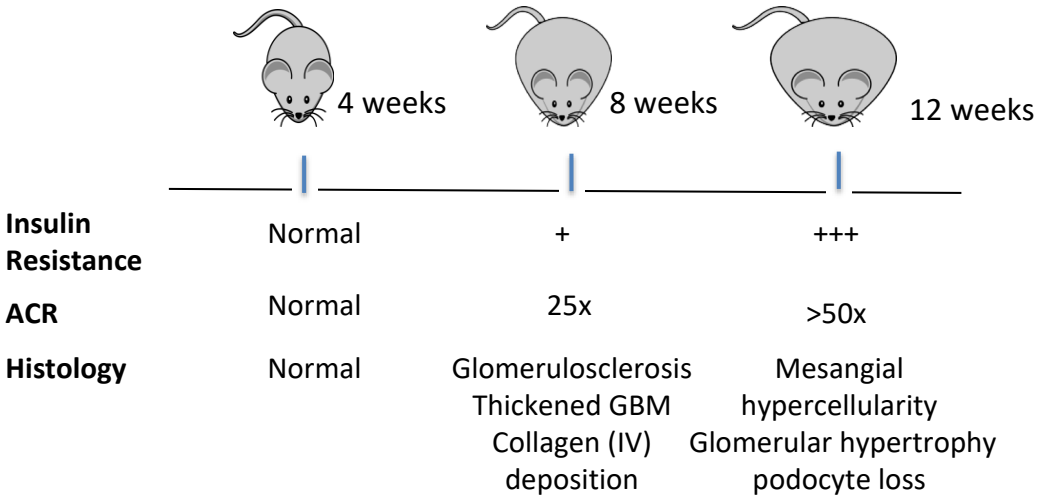

Biological Process	Age (wk)	p value	No . of miRNAs
Inflammation	4	3.87E-19	46
	12	2.6E-19	52
Nephritis	4	1.91E-19	17
	12	1.02E-20	19
Diabetes	4	2.78E-12	38
	12	5.98E-11	41
Fibrosis	4	5.82E-13	27
	12	1.47E-08	24

Figure 6.6. Biological pathway enrichment analysis of miRseq from db/db whole glomeruli. Analysis performed on all differentially expressed miRNAs at 4- and 12-week time points in whole glomeruli from db and WT mice, n=3 per group, per time point. Pathways filtered for relevant correlation with the phenotypic characteristics of the mouse, as shown. P value (Fisher's exact test) represents likelihood of miRNA involvement in named pathway. Number of differentially expressed miRNAs per pathway as shown. All analyses performed using Ingenuity Pathway Analysis.

The miRNA expression findings at 4 weeks were explored further using a network analysis. The top dysregulated network, "organismal injury and abnormality" is displayed in Figure 6.7, and demonstrates prediction of early miR-interactions with key insulin-signalling molecules such as p38 MAPK, Akt, and insulin itself. The inflammatory signal identified at the 4-week time point is predominantly driven by the NFκB and Jnk pathways, whilst the detected enrichment in fibrosis pathways may be dominated by the indirect targeting of Smad2/3 by miR-181a and miR-17. The bi-directional interplay between differentially expressed miRNAs and VEGF is particularly noteworthy in glomerular tissue, given the importance of podocyte-secreted VEGF in maintenance the glomerular filtration barrier (see discussion).

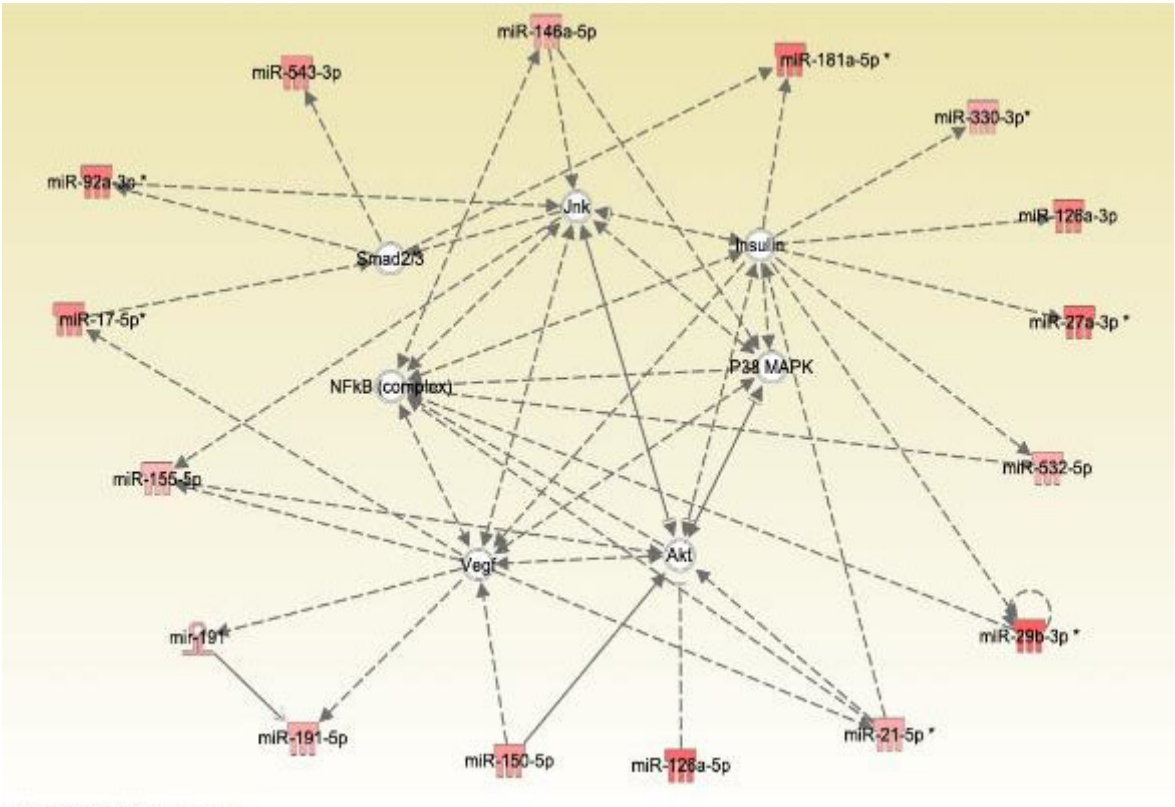

Figure 6.7. Top miRNA- directed gene networks: 4 weeks. Ingenuity Pathway Analysis was used to predict gene networks dysregulated by the differentially expressed miRNAs in db/db glomerular tissue at 4 weeks. Solid line indicates direct interaction, dotted line represents indirect interaction. Intensity of miRNA colour representative of degree of upregulation in the dataset. Jnk= c-Jun N-terminal kinase, Vegf= vascular endothelial growth factor, NFκB= Nuclear factor kappa light-chain-enhancer of activated B cells.

6.2.1.4 Comparison of whole glomerular miRseq and insulin-resistant podocyte microarray

Significantly differentially expressed miRNAs from the *in vitro* model of podocyte insulin resistance (Chapter 3) were overlaid with differentially expressed glomerular miRNAs at the 4- and 12-week time points (Figure 6.8). The largest degree of miRNA signature overlap was seen between glomerular miRNAs at 4 and 12 weeks (44.6%). 232 out of 291 (80%) of all glomerular miRNAs upregulated at 4 weeks were also significantly upregulated at 12 weeks. 38 miRNAs (7.3%) were commonly dysregulated in the insulin-resistant podocytes and in diabetic glomeruli at 4 weeks, rising to 44 miRNAs (8.5%) at 12 weeks. 30 miRNAs (5.8%) were differentially expressed compared to wild type in all 3 models.

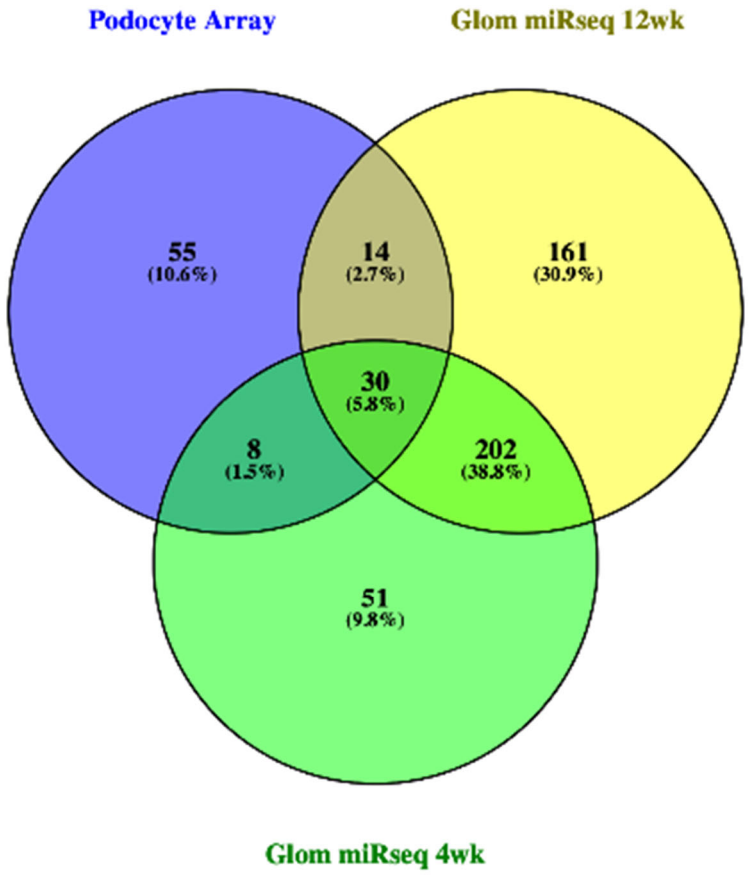

Figure 6.8 Commonly differentially expressed microRNAs in insulin-resistant podocytes *in vitro* and db/db glomeruli *in vivo.* Venn diagram of 107 significantly differentially expressed miRNAs from microarray profiling of an *in vitro* model of podocyte insulin resistance, overlaid with 291 significantly differentially expressed miRNAs in db/db whole glomeruli *in vivo* at 4 weeks and 407 miRNAs at 12 weeks (unadjusted p-value).

The 30 miRNAs commonly differentially expressed at 4 and 12 weeks in the glomerular tissue and in insulin-resistant podocytes were further analysed for gene enrichment in biological pathways. Figure 6.9 demonstrates a clear pattern of renal injury and inflammation, with cirrhotic/fibrotic pathways in other organs also significantly associated with this miRNA signature. These 30 commonly dysregulated miRNAs are listed in Figure 6.10, shown subdivided by existing literature base knowledge for their involvement in DN, fibrosis and renal cell carcinoma (RCC).

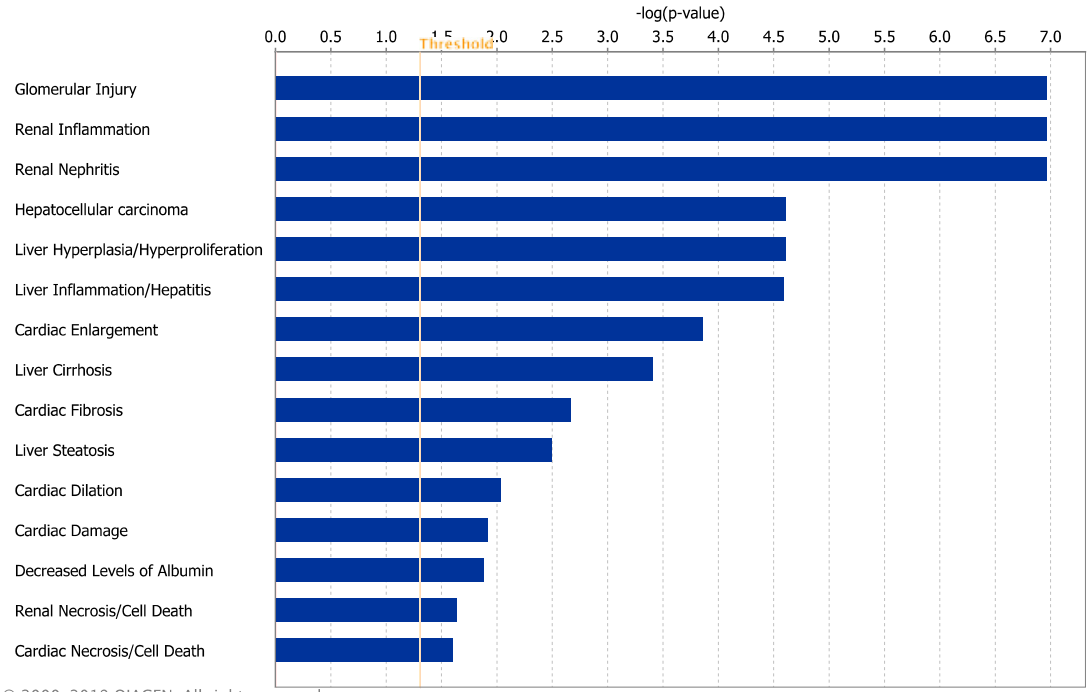

Figure 6.9 Biological Pathway enrichment analysis of miRNAs commonly differentially expressed in glomerular and podocyte models of insulin resistance. MicroRNAs commonly identified as differentially expressed at 4 and 12 weeks in the db/db mouse glomeruli and in the *in vitro* insulin-resistant podocyte model were analysed for pathway enrichment using Ingenuity Pathway analysis software. p=0.05 threshold annotated as vertical orange line.

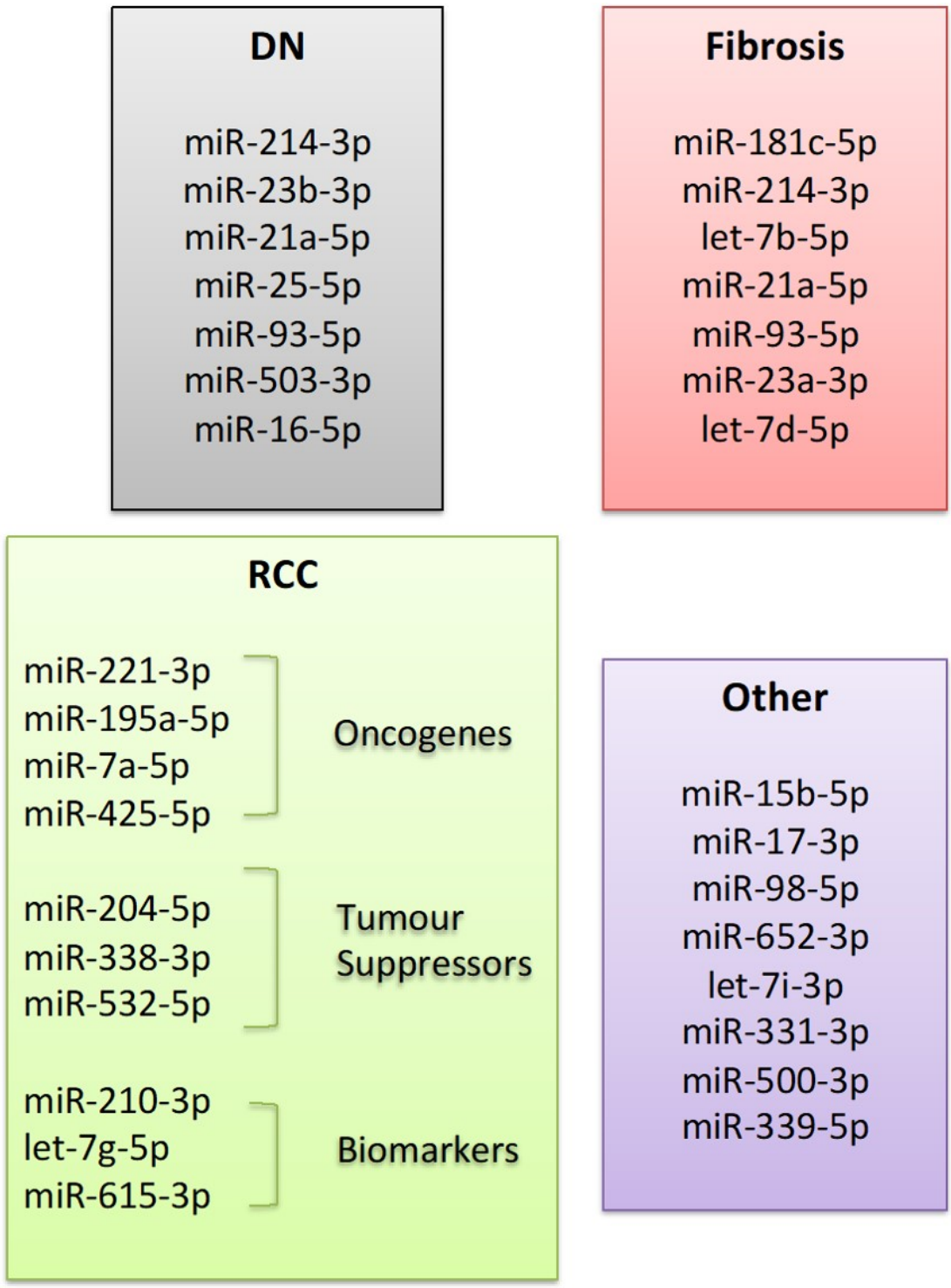

Figure 6.10. Commonly differentially expressed microRNAs in db/db glomeruli and insulin-resistant podocytes. 30 miRNAs were identified as being commonly dysregulated in whole glomerular tissue extracted from db/db mouse at 4 and 12 weeks (determined by miRseq), and in podocytes rendered insulin resistant *in vitro* (determined by microarray). These are shown subdivided into: miRNAs implicated in diabetic nephropathy (DN) pathogenesis (248, 417-422), miRNAs implicated in fibrosis (246, 423-428) and miRNAs implicated in Renal Cell Carcinoma (RCC) as oncogenes (429-432), tumour suppressors (348, 433, 434) and as biomarkers (435-437).

Data for the 6 candidate miRNAs identified from the insulin-resistant podocyte microarray analysis were extracted from the miRseq results to examine trends in their expression levels in whole glomeruli (Figure 6.11). Of the three upregulated miRNA candidates identified in the podocyte model, miR-155 and miR-146a were upregulated at the 4 week time point in whole glomeruli relative to WT controls, (2.29-fold, p=0.008 and 2.96-fold, p=0.004, respectively) and miR-222 was upregulated at 12 weeks (2.27-fold, p=0.006). Notably, as seen in the microarray data, miR-155 and miR-146a showed a congruent pattern of upregulation at both time points, however, the total read counts for these miRNA were not comparable: mean read count of miR-146a at 4-weeks being 11,639 and mean read count for miR-155 at equivalent time point only 39. Due to the aforementioned bias towards upregulation of differentially expressed miRNAs in the glomerular data, it could not be possible to recapitulate the downregulation of the 3 miRNA candidates seen in the insulin-resistant podocyte model. Interestingly, all 3 miRNAs were, in fact, significantly upregulated at both time points (12 weeks > than 4 weeks).

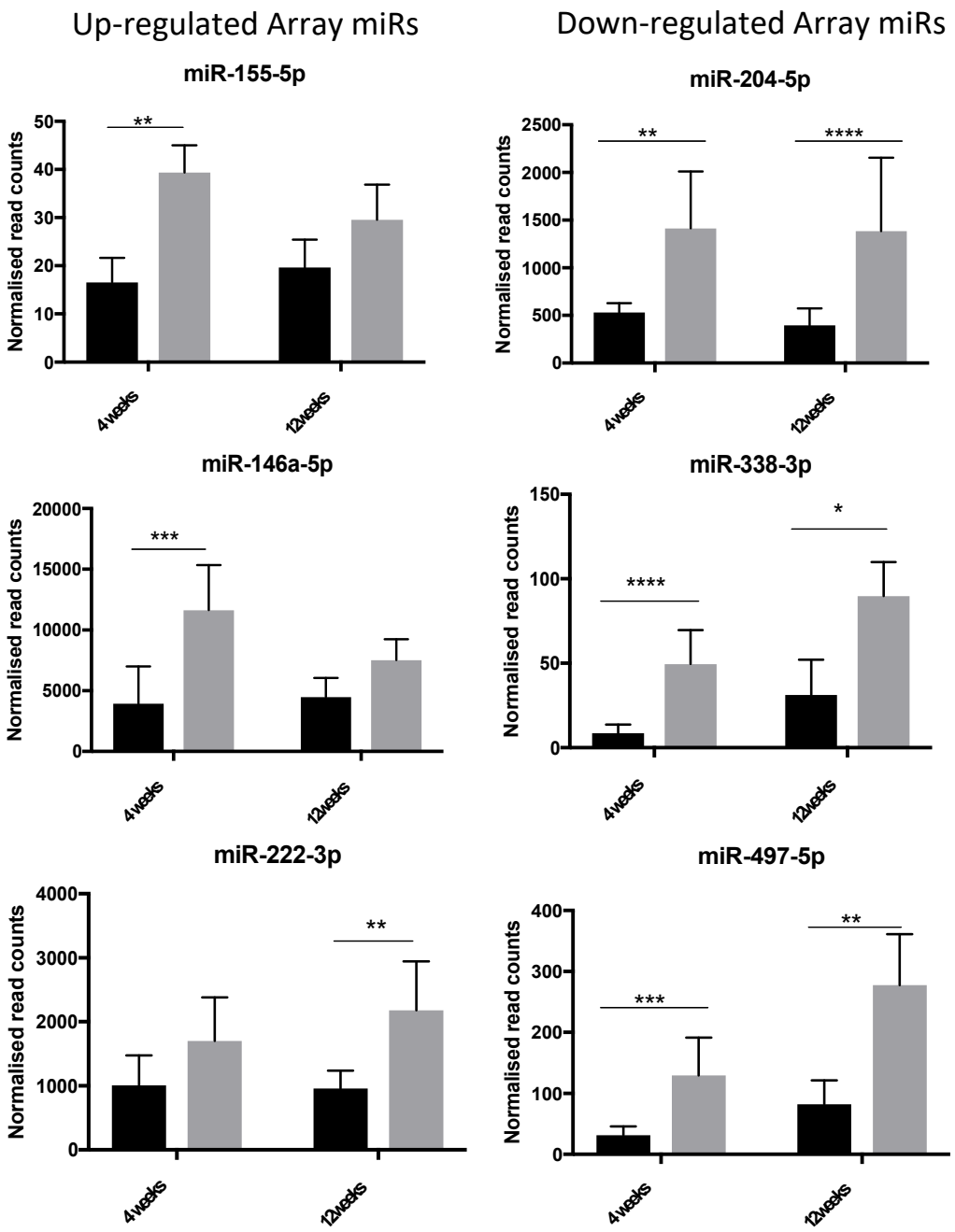

Figure 6.11. Glomerular expression (db/db) of selected miRNAs shown to be dysregulated in podocyte insulin resistance. Normalised read counts for the 3 up- and downregulated miRNA candidates identified from previous microarray profiling of insulin resistant podocytes *in vitro* were extracted from bulk sequencing data from whole glomeruli in db/db mouse and WT controls. 4- and 12-week time points represented only (few significant differences in miRNAs at 8 week time point). Mean +/- SD of normalised read counts across n=3 samples per group, per time point. P value (unadjusted) extracted from DEseq results. * $p<0.05$; **, $p<0.01$; ***, $p<0.005$; ****$p<0.001$.

6.2.2 Whole Glomerular RNA sequencing results

6.2.2.1 Quality control

Parallel RNAseq was performed for all samples. Table 6.2 outlines the technical specifications of the sequencing run. Minimum recommended sequencing depth for detection of differential gene expression of 10-25 million reads was achieved in all but one sample (sample i). Other quality control parameters in RNAseq data include percentage mapping to the Forward or Reverse strand, which is expected to approximate 50:50 under normal conditions but may be biased towards the forward strand if there is heavy mitochondrial or ribosomal RNA representation in the sample. A couple of samples showed skewing towards forward strand mapping (65% in sc and s4) but this was considered to be within acceptable limits.

ID	Sample Description	Sex	RNA ng/ul	RIN	No. reads	No.reads post trim (%)	Mapped reads (%)	F strand mapping(%)	R strand mapping (%)
s1	**db 4 week**	M	74	8.5	32088153	96.38	85.80	55.49	44.51
sa	**WT 4 week**	M	50	8.9	27263816	96.02	86.20	55.12	44.89
s2	**db 4 week**	M	66	8.4	28253672	94.90	87.63	53.83	46.17
sb	**WT 4 week**	M	18	6.5	29953215	95.91	86.58	54.86	45.14
s3	**db 4 week**	M	90	8.9	12627956	94.32	79.27	57.98	42.02
sc	**WT 4 week**	M	30	7.4	27132419	97.00	67.10	65.41	34.59
s4	**db 8 week**	F	212	9.8	16708942	96.97	67.69	65.10	34.90
sd	**WT 8 week**	M	64	9	31527841	96.97	79.88	58.81	41.19
s5	**db 8 week**	F	48	8.4	27656970	96.21	71.29	56.34	43.66
se	**WT 8 week**	F	50	8.8	27117891	96.58	74.26	61.55	38.45
s6	**db 8 week**	F	134	8.9	22344540	96.38	82.90	56.99	43.01
sf	**WT 8 week**	F	404	9.9	21603021	96.02	85.58	55.43	44.57
s7	**db 12 week**	M	74	9.6	13083460	93.36	83.46	55.31	44.69
sg	**WT 12 week**	F	122	9.7	19052527	94.14	81.04	56.96	43.04
s8	**db 12 week**	M	206	9.6	27793914	95.01	83.81	55.89	44.11
sh	**WT 12 week**	M	62	8.9	13150250	93.84	82.34	56.13	43.87
s9	**db 12 week**	M	142	9.2	12798980	95.59	80.29	58.00	42.00
si	**WT 12 week**	M	68	8	6732195	94.20	85.68	54.52	45.48

Table 6.2 Summary of raw RNAseq data from whole glomeruli in db/db and WT mice. Samples were paired as db/db and WT littermate control with diabetic animals represented by IDs s1-9 and paired WT control labelled as corresponding letters sA-I, n=3 pairs per time point. Sequencing read depth of minimum 10 Million was achieved in all samples except sample (i). Minimal loss seen following trimming of adapter primers (identified as an absence of sequence between adapter primers), denoted above as "no. reads post trim (%)". Mapped reads refer to those sequences that were matched to known genes in the ENSEMBL database. F =forward, R=reverse strand.

6.2.2.2 MRNAs are differentially expressed in whole glomerular tissue from db/db mouse model

Principal component analysis (Figure 6.12) shows clustering of all 6 samples at the 4-week time point, which dissipates by 8 weeks. By 12 weeks, samples are clearly separated into diabetic and WT groups, with tight clustering observed within each group, suggesting less intra-group heterogeneity than was seen in the equivalent miRseq analysis.

The volcano plots generated from the RNAseq data (Figure 6.13) demonstrate a more even distribution of differentially expressed genes with no evidence of the upregulation bias observed in the miRseq data. As could be predicted from the PCA plot, no significant differences in gene expression between the db and WT animals were detected at 4 weeks, and only 13 and 16 genes were differentially expressed at 8 and 12 weeks respectively (calculated using adjusted-value). The magnitude of the fold change in differentially expressed genes was notably greater at 12 weeks, as demonstrated by the x-axis scale in Figure 6.13C.

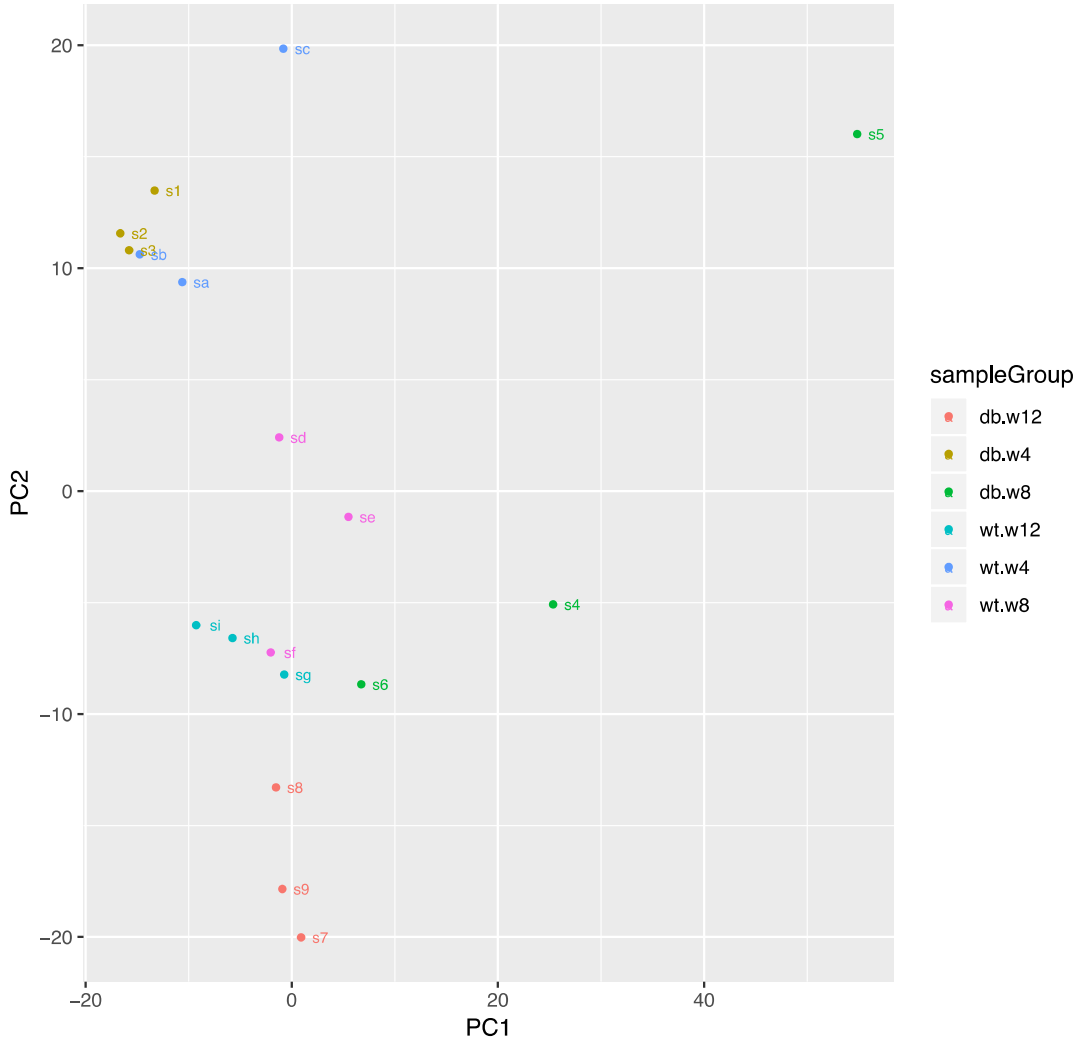

Figure 6.12 Principal Component analysis of mRNA expression in whole glomeruli from db/db and WT mice. Samples were paired as db/db and WT littermate control with diabetic animals labelled numerically and paired WT controls labelled as corresponding letters, n=3 pairs per time point, where s1-3 and a-c represent 4-week old animals, s4-6 and d-f represent 8-week old animals and s7-9 and g-I represent 12-week old animals. PCA plot derived using all significantly differentially expressed mRNAs across all time points.

A.

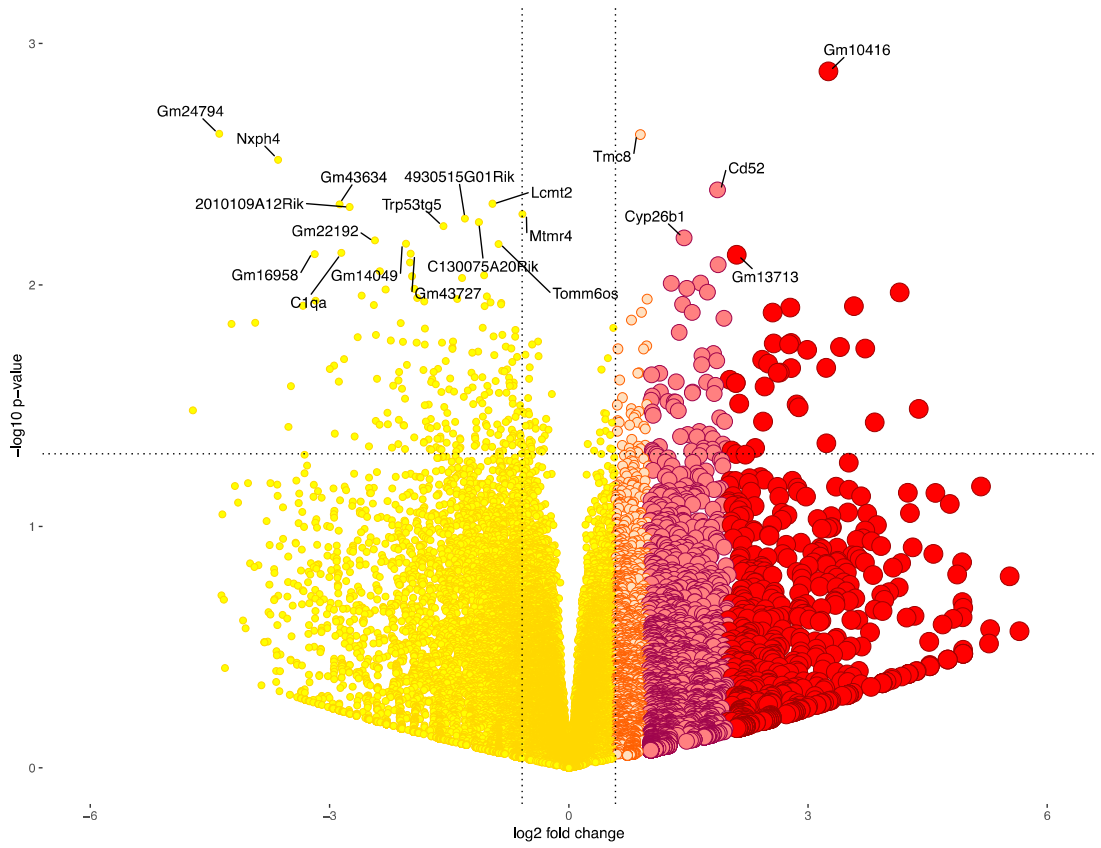

Significant genes	
p-value	Adjusted p-value
471	0

B. Downregulated in db/db mice Upregulated in db/db mice

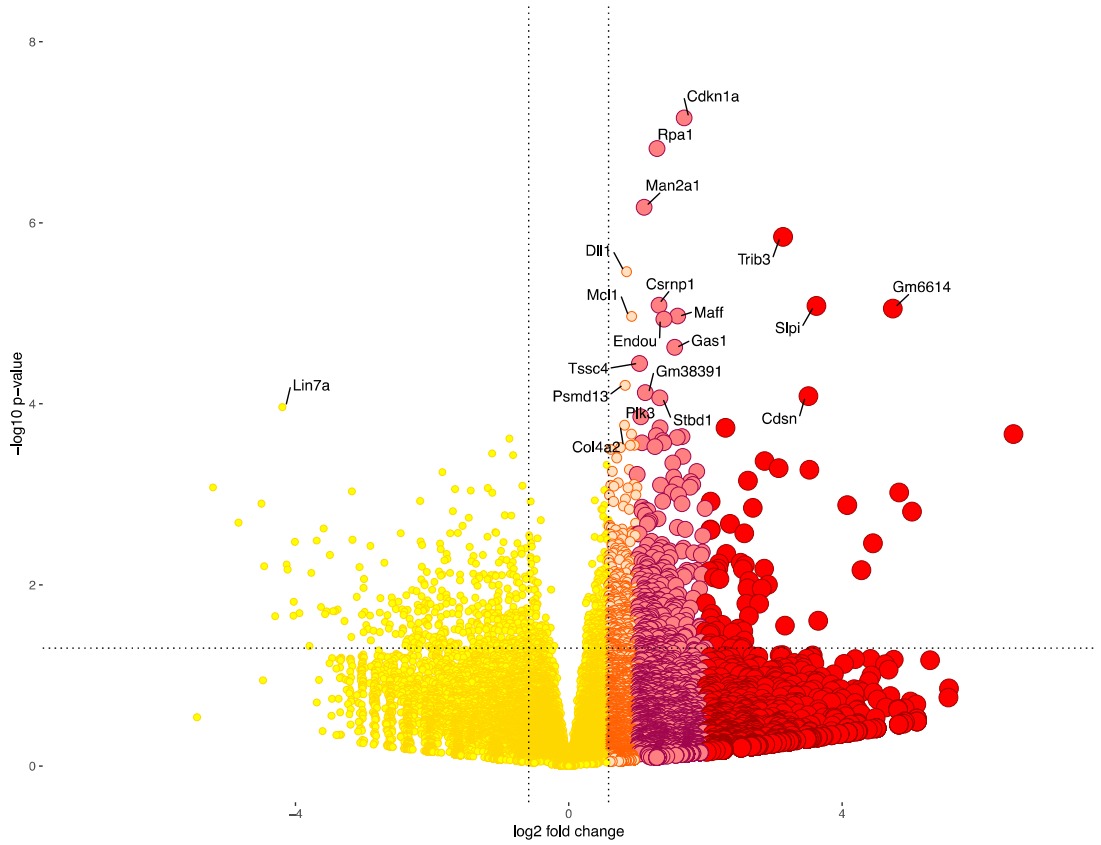

Significant genes	
p-value	Adjusted p-value
1527	13

C.

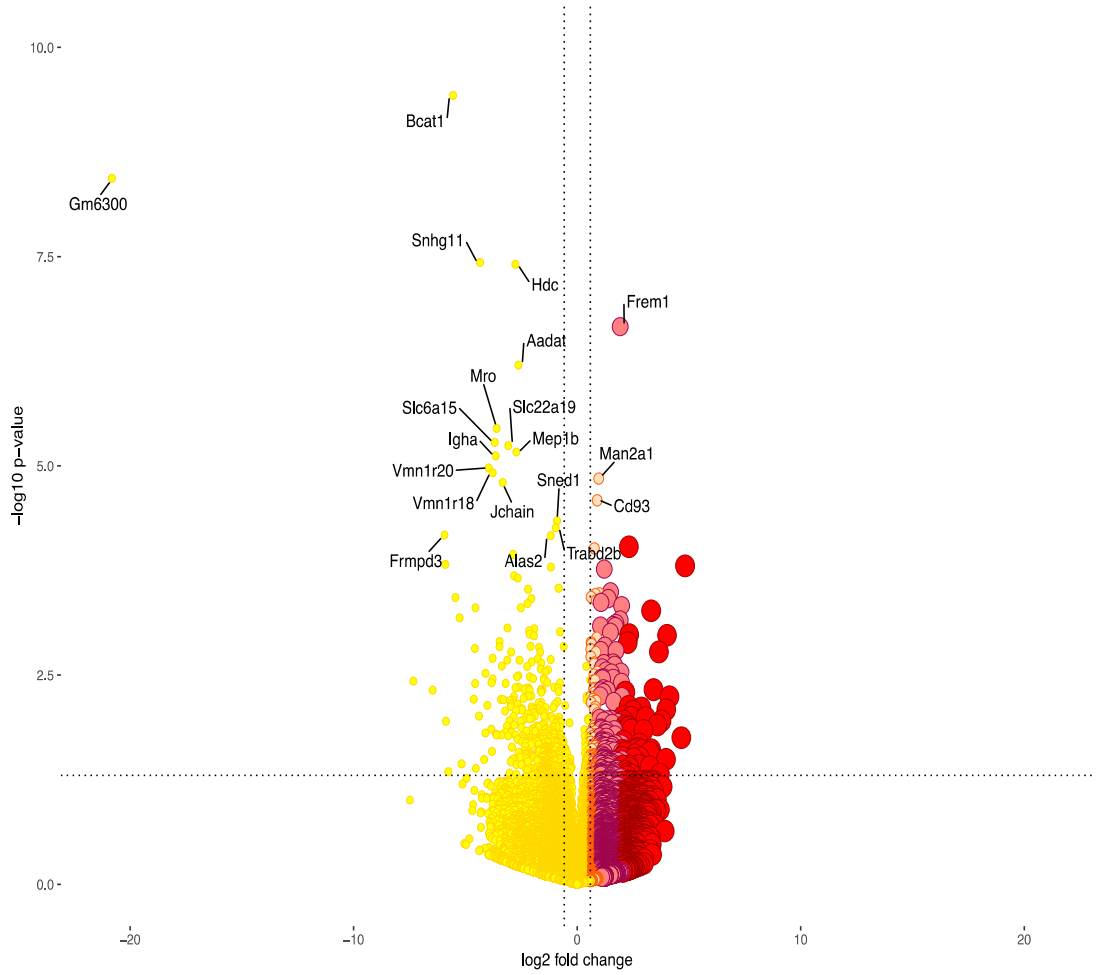

Significant genes	
p-value	Adjusted p-value
890	16

Figure 6.13 Volcano Plot analysis of mRNA expression in db/db whole glomeruli. Plots depict the relationship between the $-\log_{10}$ of the p-values and the log2 fold change in mRNA expression between db/db and WT samples (genes at the upper and outer aspects of the "V"-plot are the most significantly up-and downregulated genes in the diabetic animals, compared to WT controls). Horizontal dissecting line of significance set at p=0.05 (unadjusted). Numbers of differentially expressed mRNAs by adjusted and unadjusted p-value as shown. **(A)** 4 weeks **(B)** 8 weeks **(C)** 12 weeks.

Heat maps of the RNAseq data is shown in Figure 6.14. Compared to miRNA expression in these samples, hierarchical clustering more reliably distinguishes the db/db samples from the WT controls, with far less heterogeneity seen in the 3 animals per group, consistent with the findings from the PCA plot.

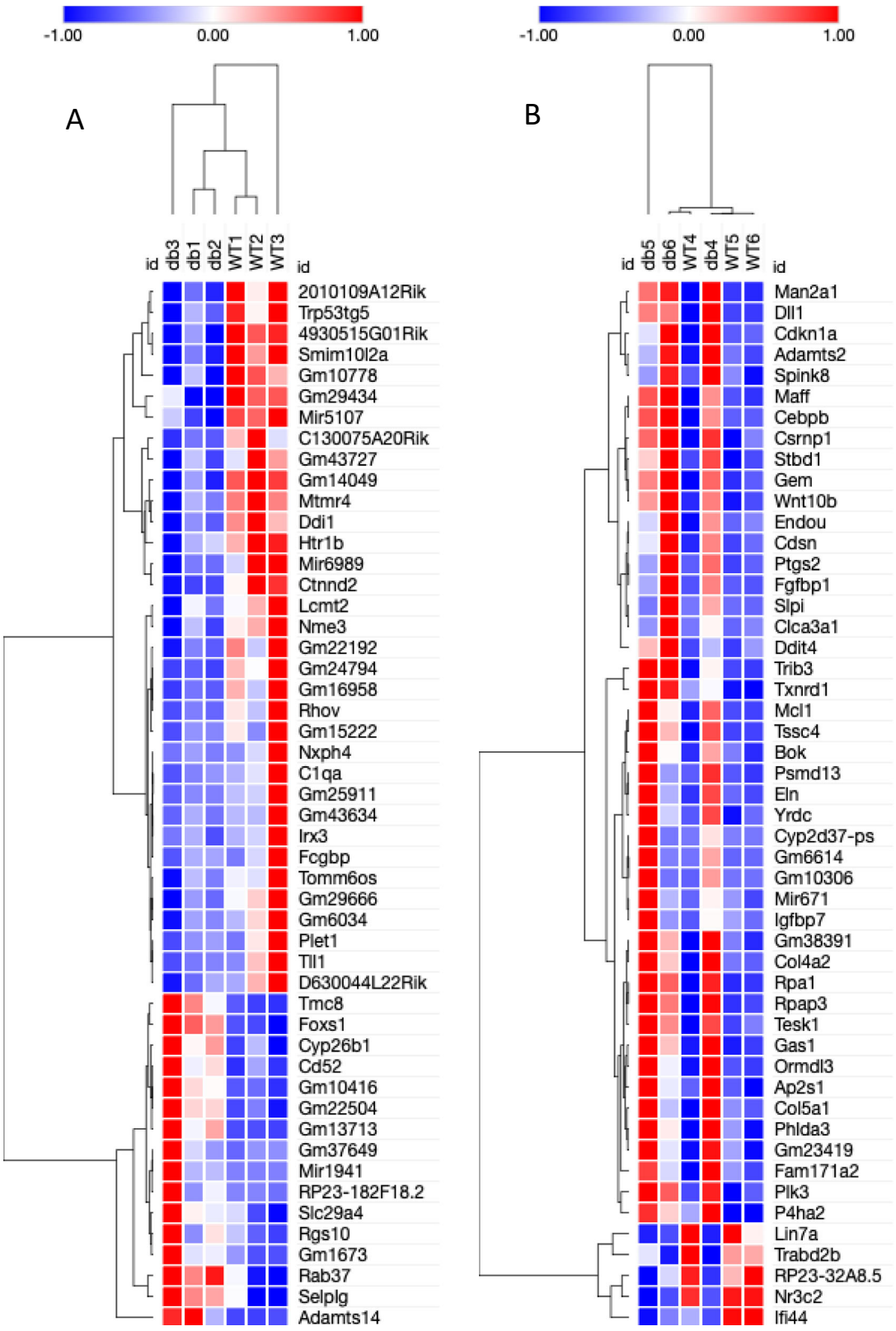

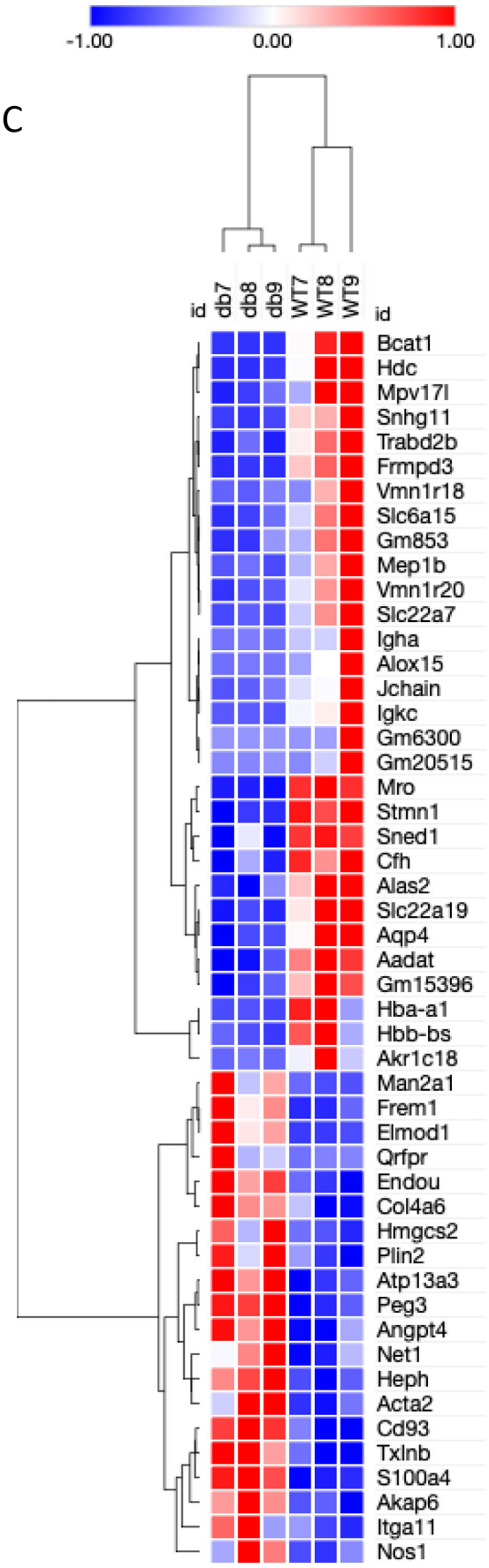

Figure 6.14 Heat map visualisation differentially expressed genes in glomerular tissue from db/db mouse. Unsupervised Hierarchical Clustering of samples (columns) and genes (rows) performed on top 50 differentially expressed genes at each time point (sorted by unadjusted p-value). Z-score transformation of normalised read counts performed (subtract mean row count and divide by row standard deviation) and score set as -1 to 1, where red = high expression and blue = low expression, relative to expression across all samples. **(A)** 4 weeks **(B)** 8 weeks **(C)** 12 weeks.

6.2.2.3 Pathway enrichment: RNAseq results

IPA was used to interrogate RNAseq data as for miRseq data, above. Figure 6.15 shows the comparison analysis of canonical pathways implicated at each time-point. At 8-weeks of age, activated pathways include those associated with oxidative stress, cell cycle regulation and inflammation. By 12 weeks, the predominant picture is de-activation in a number of important pathways within the insulin-signalling cascade, such as insulin receptor, IGF-1 and mTOR signalling. In comparison to the miRseq findings, there is a more notable increase in the number of differentially expressed genes involved in diabetic pathways as diabetes duration increases (Figure 6.16), with the exception of renal fibrosis genes which are more numerous at the 8-week time point at the mRNA level.

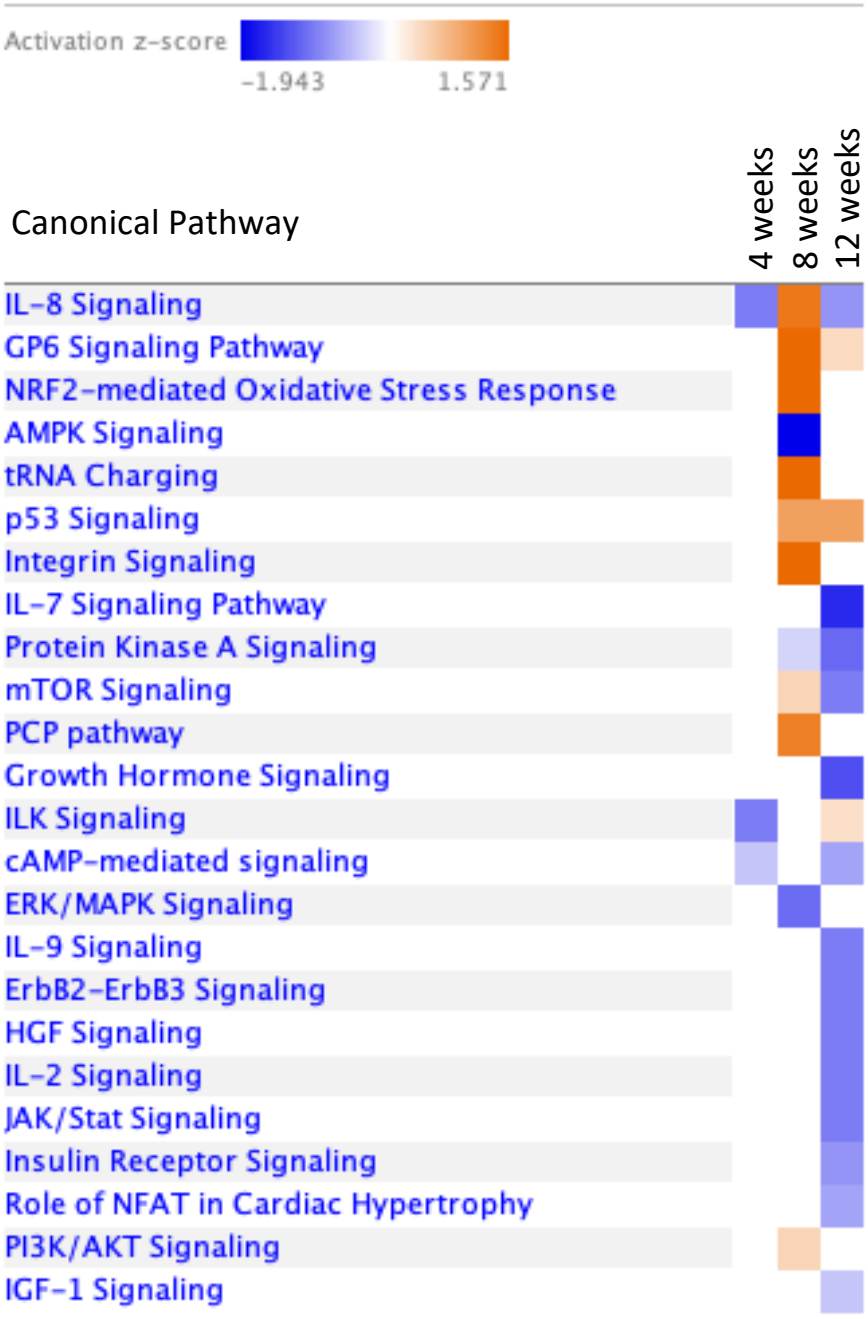

Figure 6.15. Comparison analysis of canonical pathways regulated by mRNAs differentially expressed in db/db mouse. Analysis generated using Ingenuity pathway analysis, on all significant mRNAs (unadjusted p<0.05) at 4, 8 and 12 weeks of age. Z-score shown, where blue represents pathway inactivation and orange represents pathway activation. N=3 samples per group (db and WT) per time point.

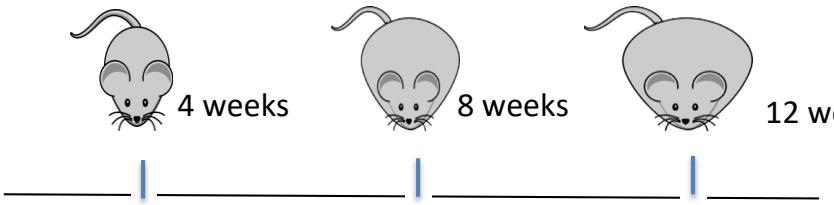

Insulin Resistance	Normal	+	+++
ACR	Normal	25x	>50x
Histology	Normal	Glomerulosclerosis Thickened GBM Collagen (IV) deposition	Mesangial hypercellularity Glomerular hypertrophy podocyte loss

Age (wk)	Biological function/Toxicity Function	P value	No . of genes
4	Metabolic Disease	1.31E-03	14
	Inflammatory Response	3.78E-03	13
	Renal Damage	1.19E-02	7
8	Metabolic Disease	6.59E-11	150
	Inflammatory Response	1.24E-07	166
	Renal Damage	2.59E-02	25
	Renal Fibrosis	7.13E-04	13
12	Metabolic Disease	4.63E-22	166
	Inflammatory Response	1.37E-09	221
	Renal Damage	3.75E-13	37
	Renal Fibrosis	2.63E-03	9

Figure 6.16. Biological pathway enrichment analysis of RNAseq from db/db whole glomeruli. Analysis performed on all differentially expressed mRNAs at 4-, 8- and 12-week time points in whole glomeruli from db and WT mice, n=3 per group, per time point. Pathways filtered for relevant correlation with the phenotypic characteristics of the mouse, as shown. P value (Fisher's exact test) represents likelihood of involvement in named pathway; number of genes refers to number of mRNAs in the dataset present in that pathway. All analyses performed using Ingenuity Pathway Analysis.

6.2.3 Whole glomerular miR-mRNA target prediction analysis

Parallel miRseq and RNAseq of glomerular samples enabled the analysis of possible miR-mRNA relationships during DN progression.

Firstly, I tested the hypothesis that the upregulation bias observed in the miRseq data at 4 and 12 weeks was a result of differential expression of common upstream miRNA-regulatory genes, which would therefore exert a global effect on miRNA transcription. To investigate this, genes associated with miR processing were extracted from the RNAseq data, as shown in Table 6.3. No significant expression differences were, however, observed at any time point.

Gene	Age (wk)	Mean fpkm Wt	db	p value (adj)	log2FC
Drosha	4	11.470	11.564	1.000	0.013
	8	11.420	10.268	0.885	-0.149
	12	12.816	11.637	1.000	-0.142
Dicer1	4	11.651	11.896	1.000	0.026
	8	11.791	10.075	0.903	-0.220
	12	11.733	12.664	1.000	0.111
Dgcr8	4	9.768	10.705	1.000	0.126
	8	9.778	9.621	0.995	-0.013
	12	9.429	9.400	1.000	0.006
Xpo5	4	12.644	13.230	1.000	0.060
	8	11.886	10.848	0.973	-0.118
	12	11.993	12.650	1.000	0.086
Ago1	4	8.739	9.164	1.000	0.066
	8	8.471	7.587	0.927	-0.153
	12	9.995	9.909	1.000	-0.026
Ago2	4	11.440	11.254	1.000	-0.025
	8	9.993	9.141	0.971	-0.123
	12	11.323	12.412	1.000	0.132

Table 6.3 Expression of miRNA-processing genes in RNAseq of db/db glomeruli. Genes implicated in global miRNA maturation were extracted from the glomerular RNAseq dataset (n=3 db/db and WT mice at 4, 8 and 12 weeks) to investigate potential impact on miRNA transcription. Fpkm= fragments per kilobase million, DgCr8= diGeorge syndrome critical region 8, Xpo5= exportin 5, Ago1/2= Argonaute protein.

Secondly, based on the finding of significant upregulation of miR-155 in the glomerular tissue at 4 weeks, I extracted the expression data for the previously highlighted miR-155 targets: CSF1R, RhoA and PIK3R1. Although downregulated in the insulin-resistant podocyte model (Bristol RNAseq data) and/or following miR-155 overexpression (miRVana mimic), these targets were not differentially expressed in the glomerular samples (Table 6.4).

Gene	Age	Log2FC	p-value
CSF1R	4 weeks	-0.18	0.55
	12 weeks	-0.45	0.15
PIK3R1	4 weeks	0.33	0.31
	12 weeks	0.65	0.15
RhoA	4 weeks	0.38	0.20
	12 weeks	0.45	0.16

Table 6.4. Expression of previously investigated miR-155 mRNA targets in RNAseq of db/db glomeruli. CSF1R= colony stimulating factor 1 receptor, PIK3R1= Phosphoinositide-3-Kinase Regulatory Subunit 1, RhoA = Ras Homolog family member A.

Finally, parallel miR-mRNA target prediction analysis of the 4 and 12-week glomerular data was performed. Figure 6.17 shows the flow chart of analysis filters employed to determine the direct miR-mRNA interactions with greatest potential significance in the mouse model. 5 miRNAs, targeting 7 mRNAs, were identified at the 4-week time point, with roles in oxidative stress pathways and transduction of intracellular cell signalling pathways mediated by cAMP and ILK (Figure 6.17A). Notably, the upregulated miR-155-5p was paired with 3 downregulated mRNA targets in the glomerular dataset, including periplakin (PPL), coding for a structural cytoskeletal protein that interacts with Akt1.

At 12-weeks, a greater number of miR-mRNA target interactions were predicted (22 miRNAs targeting 20 mRNAs), as depicted in Figure 6.17B. Canonical pathways of significance were overlaid with this dataset, as shown. The dominance of oxidative stress signals continues at 12 weeks, with involvement in mitochondrial dysfunction and eNOS signalling pathways highlighted. Cytoskeletal regulation is also a common theme, with Rho-family GTPase signalling implicated in this gene set. With respect to 12-week old mouse phenotype, the involvement of IGF-1 signalling and pro-fibrotic hepatocyte growth factor (HGF) signalling is of potential relevance in this insulin-resistant, glomerulosclerotic animal.

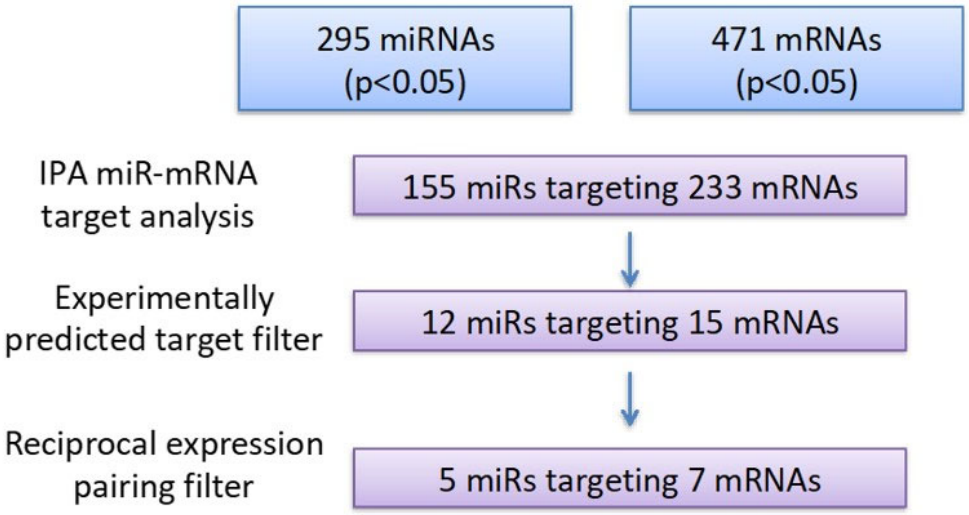

miRNA	mRNA target(s)	Pathways
let-7a-5p	DSP	ILK signalling
miR-141-3p	PITX2	TGF-β/BMP signalling, oxidative stress response
miR-155-5p	ARL10, PPL, TACSTD2	Localisation signal in PKB/AKT-mediated signalling
miR-16-5p	GSTM4	Metabolism signalling, NRF2-mediated oxidative stress
miR-96-5p	HTR1B	cAMP-mediated signalling

Figure 6.17A. miR-mRNA target interaction analysis: 4 weeks. Differentially expressed miRNAs and mRNAs in db/db mice glomeruli at 4 weeks (unadjusted p<0.05) were compared using Ingenuity Pathway Analysis (IPA) for evidence of target pair interaction. Target pairs were refined using filters for experimentally validated targets only, followed by reciprocal expression in miRNA and mRNA pairs (to reflect miRNA induced target repression). Final miRNA and mRNA pairs, and implicated pathways, shown in the table. ARL10= ADP Ribosylation Factor Like GTPase 10, BMP= bone morphogenetic protein, DSP=desmoplakin, GSTM4= glutathione S-transferase M4, HTR1B= 5-Hydroxytrptamine receptor 1B, ILK= integrin-linked kinase, NRF2= Nuclear factor erythroid-2 related factor 2, PITX2= paired like homeodomain 2, PPL= periplakin, TACSTD2= Tumor Associated Calcium Signal Transducer 2.

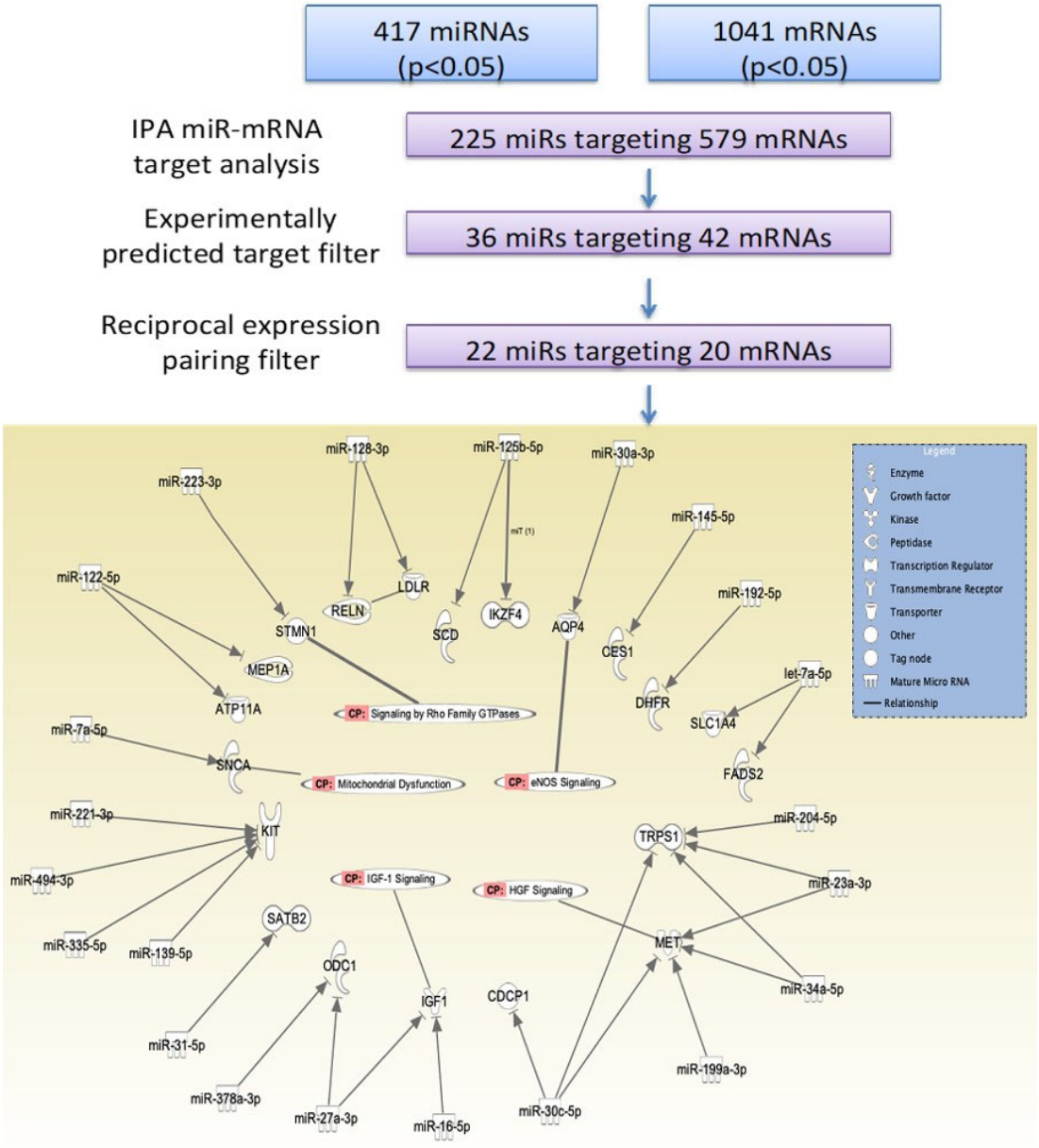

Figure 6.17B. miR-mRNA target interaction analysis: 12 weeks. Differentially expressed miRNAs and mRNAs in db/db mice glomeruli at 12 weeks were compared using Ingenuity pathway analysis for evidence of target pair interaction. Target pairs were refined using filters for experimentally validated targets only, followed by reciprocal expression in miRNA and mRNA pairs. Final miRNA and mRNA pairs, and implicated canonical pathways displayed. AQP4= aquaporin 4, ATP11A= ATPase phospholipid transporting 11A, CDCP1= CUB domain containing protein 1, Ces1= carboxylesterase 1, DHFR= dihydrofolate reductase, FADS2= fatty acid desaturase 2, IKZF4= Ikaros Family Zinc Finger 4, KIT= KIT proto-oncogene, LDLR= low density lipoprotein receptor, IGF-1= Insulin-like growth factor-1, MEP1A= Meprin A, MET= MET proto-oncogene, ODC1= ornithine decarboxylase 1, RELN= Reelin, SLC1A4= solute carrier family 1 member 4, SNCA= synuclein alpha, STMN1= Stathmin1, SCD= Stearoyl-coA Desaturase, TRPS1= transcriptional repressor GATA binding 1, HGF= hepatocyte growth factor, eNOS= endothelial nitric oxide synthetase..

6.3 Discussion

6.3.1 Considerations of the db/db model for whole glomerular sequencing

The db/db DBA/2J mouse was selected based on the robust development of albuminuria that was positively correlated with the development of systemic insulin resistance and glomerulosclerosis score (394). The albuminuric tendency of the db/db mouse was inferred to be indicative of podocyte pathology, and hence an ideal model for the intended investigation of podocyte-specific miRNA evolution during DN development. Time points of 4-, 8- and 12-weeks were selected to address the hypothesis that aberrant miRNA expression disrupts podocyte insulin signalling, and that resultant podocyte insulin resistance in early diabetic kidney disease initiates pathophysiological mechanisms that drive the DN phenotype. The clinical implications of detecting such a premature critical insult include the potential for miRNA therapeutic targeting and new miRNA biomarker development in DN.

However, at the whole glomerular level, there were surprisingly few miRNA and mRNA changes at the selected time points, with no discernable differences at 8 weeks in the miRNA data and no differences at 4 weeks in the RNA data, by adjusted p-value. Whilst this may reflect immaturity of the diabetic model, it may also be an artifact of multiple testing over a large number of genes (>34,000 in RNAseq), thereby resulting in over-stringent rejection of differentially expressed genes above α=0.05. Using only the small number of differentially expressed genes generated by "adjusted" analyses greatly limited the potential of bioinformatically-generated predictions (particularly for miRNAs, where there is already a relative paucity of literacy information available). Unadjusted p-values were therefore used in all IPA analyses, accepting that this may increase the potential for false positive predictions and statistical "noise" which is inherent in most exploratory profiling experiments, such as this.

Statistical limitations notwithstanding, the similarity of RNAseq results from the 4-week old db/db and WT mice could be anticipated; the mice are just weaned at 4 weeks and may not have had sufficient stimulus to acquire the

transcriptional changes associated with diabetes/insulin resistance. Yet, there was clear evidence of miRNA expression change at 4 weeks, with enrichment in pathways that might be associated with a much later stage of disease, such as fibrosis. It is possible, therefore, that miRNA regulatory changes are a primary event in initiating DN, activated long before the mouse displays phenotypic characteristics of diabetes. This finding supports the hypothesis that early miRNA changes at a podocyte level may be dictating insulin responses.

Despite the 4-week findings, intriguingly, minimal miRNA changes were observed at the 8-week time point. This could be attributed to the sex-discrepancy of the mice pairs, where all 8-week old mice were female in contrast to the male predominance at 4 and 12 weeks. Female db/db mice, although more obese, exhibit an overall milder diabetic phenotype than males (438), who are less tolerant of hyperglycaemia and rapidly develop insulinopenia and weight loss by 10 weeks of age (394). However, whole transcriptomic changes in these female mice were evident by RNAseq at the 8-week time point. Given the regulatory nature of miRNA action, it seems unlikely that sex of the mouse could explain absence of changes in miRNAs, but not mRNAs, at the same time point. It is possible that the miRNA changes seen are representative of homeostatic fluctuation around a set point, and that by chance, the miRNA profiles captured at 8 weeks reflects a point of oscillation in miRNA expression from one state to another, resulting in miRNA profiles indistinguishable from the WT controls. However, by 12 weeks, the (predominantly male) mice demonstrated the greatest degree of differential gene expression, with 80% of upregulated miRNAs identified at the 4-week time point also significantly elevated in this data. The ≈50% overlap in differential miRNA signature at 4 and 12 weeks explains the similarity in IPA comparison analysis of toxic functions and the surprisingly small number of additional miRNAs recruited to pathways of inflammation and diabetes at 12, compared to 4 weeks, diabetes duration.

RNAseq data demonstrated greater homogeneity in the WT and db/db sample groups, as shown by clearer heat map clustering of groups at all time points, compared to the miRseq data. RNAseq also showed the expected correlation

between duration of diabetes and number of differentially expressed genes. Furthermore, the dysregulated genes showed increasing recruitment to IPA pathways of direct relevance in the model, such as inflammatory response and renal damage. Interestingly, fibrosis pathways were most prominent at 8 weeks, suggesting, as seen for miRNA data, that these pathways are transcriptionally activated at a very premature stage in DN development, but the consequences of this at the protein level are not evident by histological examination until 12-16 weeks of age.

The activation of oxidative stress response and mitochondrial dysfunction pathways in both RNAseq results and in miR-mRNA target interaction analyses is particularly interesting. Other groups who have performed RNAseq on glomeruli of diabetic mice also report enrichment in these pathways, but at a single time point in mice of greater diabetic vintage (minimum 16 weeks of age) (396, 439). The impact of hyperglycaemia-induced mitochondrial oxidative stress has been proposed as a "unifying hypothesis" in the pathogenesis of microvascular complications of diabetes, including DN (440) although the lack of significant benefits in anti-oxidant based trials has prompted alternative theories that a "physiological level' of mitochondrial superoxide production is renoprotective (441). It is therefore possible that the early activation of such pathways in my model is representative of a "first defence" to newly developed hyperglycaemia.

6.3.2 Conclusions of comparisons of whole glomerular db/db miRseq and (insulin resistant) podocyte array

Comparison of the differentially expressed miRNAs identified in the insulin-resistant podocyte model and those identified at 4 and 12 weeks in the db/db glomeruli were poorly concordant (7.3% and 8.5%, respectively). However, two of the upregulated miRNA candidates from the podocyte array, miR-155 and miR-146a, exhibited the same congruent elevation in the 4-week glomeruli (although repression of previously highlighted miR-155 targets CSF1R, PIK3R1 and RhoA was not observed). It is possible that the elevated miR-155 detected in the glomerular samples may be of podocyte origin; especially given the

generally low read counts (mean normalised read count 39), which might be expected if only being expressed in a lowly abundant glomerular cell type. On the contrary, the high number of reads detected for miR-146a (mean normalised read count 11,639) suggests a more abundant, or collective cellular source for this miRNA, making it impossible to tease out the contribution of podocyte-specific expression. Fu *et al* reported their comparison of whole glomeruli and isolated podocyte mRNA profiles from the streptozotocin-induced diabetic mouse at 18 weeks of age. Using podocyte-specific mRNA markers, they compared the podocyte representation in bulk glomerular tissue to the profile obtained from sorted podocytes and found that podocyte-specific alterations in actin-cytoskeletal genes were effectively masked in whole glomerular data (396). It is likely, therefore, that the same is true for the miRseq/array results reported here, therefore explaining the low degree of overlap in differentially expressed miRNAs in my podocyte and glomerular models. The small subgroup of 30 genes that *were* commonly dysregulated across the models did, however, map unequivocally to glomerular injury, driven by the IPA knowledge bias towards well-established profibrotic miRNAs, such as the miR-21 family, and those involved in renal cell carcinoma.

There were, however, a few findings that could be attributed to podocyte signal within the bulk data: in addition to the aforementioned miR-155 overexpression at low total read counts, the 4 week miRNA network analysis highlighted VEGF as a focus molecule. VEGF-A is released by the podocyte in response to insulin (155) and exerts tight regulatory control of the glomerular endothelium in a paracrine fashion, where too much or too little may be deleterious in causing endotheliosis (swelling) or apoptosis, respectively (442). In insulin resistance, VEGF-A production is suppressed, and has therefore been hypothesised to contribute to the mechanism of glomerulosclerosis observed in podocyte-specific insulin receptor KO mouse models (155). In the 4-week glomerular data, upregulation of miR-150-5p was predicted to target VEGF (which was indeed downregulated in the mRNA data, but did not meet fold change cut-off in the paired miR-mRNA analysis). Chen *et al* report that miR-150-5p inactivates VEGFA/VEGFR2 and the downstream Akt/mTOR signalling pathway in colorectal cancer cells, acting as a tumour suppressor in this context (443). In

my model, it is possible that the insulin-mediated release of VEGF is regulated by miRNAs, which would be compatible with a molecule known to require homeostatic regulation to maintain a narrow therapeutic window of beneficial effect.

MiR-mRNA paired interaction analysis also identified a number of cytoskeletal-associated targets suggestive of podocyte origin, such as cytolinker proteins desmoplakin (DPL) and periplakin (PPL), and microtubule regulator protein stathmin (STMN1). Furthermore, in the 4-week dataset, original podocyte array candidate miR-155 was predicted to directly repress periplakin, an Akt-binding protein shown to provide a localisation signal for Akt, and enhance Akt phosphorylation in endometrial cells (444, 445). PPL has been identified as an intermediate filament binder in rat glomerular tissue, although disease-related roles have not been described in renal cells, specifically (446). MiR-155 mediated loss of PPL may be significant in causing disruption to podocyte cytoskeletal structure and/or signal transduction function, by disabling the shuttle of Akt to its target substrate within cells. This mechanism has not been explored in the context of insulin signalling, to date.

The most likely interpretation is that the miRNA signal detected in whole glomerular tissue represents a composite of the diabetic signature from many different cell types, all of which are contributing to variable degrees that cannot be tangibly extracted from this sequencing approach. As discussed in the previous chapter, single cell sequencing may provide an answer, but the technology is not yet advanced enough to capture small RNAs. An alterative, interim approach might be to culture a panel of different glomerular cells in the diabetogenic medium *in vitro* and assess expression levels of the interesting miR and mRNA targets to determine whether the signal is consistent with, for example, a mesangial cell response to diabetes.

6.3.3 Conclusion

In conclusion, whilst the proportion of differentially expressed genes detected in glomeruli from this young db/db mouse model are relatively small, I have

demonstrated that transcriptional miRNA changes associated with the diabetic phenotype are detectable from as early as 4 weeks of age; 2-4 weeks prior to the onset of demonstrable hyperglycaemia and insulin resistance. Reciprocally expressed miR-mRNA target pairs associated with oxidative stress and mitochondrial dysfunction are also evident at stages earlier than previously reported. Whilst there was a low overlap in miRNA expression signature of insulin resistant podocytes and bulk glomerular tissue, detectable cytoskeletal gene dysregulation highlights the possibility that podocyte signal may not be completely overwhelmed in glomerular data at this early time point. The findings therefore support the hypothesis that miRNAs, and specifically miR-155, are dysregulated early in DN, and that the subsequent disruption of homeostatic regulation may be most immediately observed in the dynamic podocyte, the deleterious effects of which may be transmitted to other cells via the mechanisms of glomerular cross-talk.

7 General Discussion

The research hypothesis addressed in this thesis was devised based on the knowledge that both podocyte insulin sensitivity and intact miRNA function are critical to normal kidney health, but little is known about the relationship between them. MiRNAs regulate insulin responses in other tissues, and manipulation of aberrantly expressed miRNAs has been demonstrated to restore insulin sensitivity in animal models (447). Podocyte dysfunction and loss is one of the earliest pathophysiological events in the development of DN, and is predictive of disease progression (134). It was therefore prudent to explore the role that miRNAs play in the development of podocyte insulin resistance, as this may be an initiating trigger in the development of DN. Given the ongoing development of miRNAs as therapeutic agents, a miR-based podocyte insulin-sensitiser may have significant translational potential in the clinical field.

The work presented in the first part of this thesis clearly demonstrates the unique microRNA signature of an *in vitro* insulin-resistant podocyte model. The multi-stimuli approach used to render podocytes insulin resistant recapitulates the *in vivo* diabetic milieu more truthfully than many other *in vitro* diabetic models that have used hyperglycaemia alone to incite miRNA changes. The microarray profile reported herein reflects an appreciation that miRNAs frequently operate in complex regulatory networks in health and disease. The consequences of dysregulation of numerous miRNAs, simultaneously induced by different environmental stresses, may be key to understanding the diverse and heterogeneous pathophysiological processes that lead to DN.

However, it is also known that a single miRNA may represent a critical switch in a pathway, such as the miR-122 dependent replication of the hepatitis C virus, which has become the flagship miRNA for therapeutic translation in the (ongoing) clinical trials of anti-miR-122 agent, Miravirsen. In this work, I chose to focus on miR-155-5p, which I found to be significantly elevated in insulin-resistant podocytes and in the urine of patients with diabetic kidney disease. Furthermore, urinary miR-155 was able to discriminate between diabetic patients with and without DKD. Podocyturia is frequently reported in DN where

urinary podocyte-associated mRNA correlates with podocyte damage and reduced eGFR (144) and can additionally predate albuminuria in preeclampsia (448). The precise origin of the urinary miR-155 cannot be deciphered from the work reported in this thesis, but release from injured podocytes is a plausible explanation. This finding highlighted the potential significance of miR-155 as a biomarker in DN, and strengthened the rationale for a more detailed mechanistic focus on this miRNA

By manipulating miR-155 *in vitro*, I have shown that overexpression (OE) leads to a reduction in phosphorylation of Akt, a key node in proximal insulin signalling. Downstream uptake of glucose was subsequently abrogated in miR-155 OE podocytes. This work therefore provides clear evidence of a miR-155-directed mechanism of podocyte insulin resistance.

I further investigated the putative targets of miR-155, and confirmed that enforced OE of miR-155 resulted in repression of two important targets: PIK3R1 and CSF1R. As the chief regulatory subunit of PI3K, PIK3R1 (p85α) can exert both positive and negative regulatory effects on PI3K signalling (378-380). This may be dependent on the interaction of its constituent subunits, or may even be cell specific, as exemplified by the podocyte-specific importance of the Akt2 isoform in actioning crucial cytoskeletal responses to PI3K signalling (159). In addition to PI3K/Akt-mediated glucose effects, PIK3R1 plays a critical role in protecting podocytes from hyperglycaemia-induced ER stress. This is achieved via activation of the unfolded protein response (UPR) to mop up misfolded proteins that would otherwise trigger podocyte apoptosis (157). ER stress evidently contributes to DN pathogenesis and progression, and it is notable that several factors associated with podocyte insulin resistance can induce ER stress, including hyperglycaemia and free fatty acids (449). CSF1R, a tyrosine kinase receptor previously linked to inflammation-mediated insulin resistance in obesity, (385) can activate PI3K signalling via its specific interaction with PIK3R1 (365). Based on these findings, and the miR-155 induced mechanism of insulin resistance I have uncovered, I hypothesise a compound effect of miR-155 targeting where proximal insulin signalling is attenuated via direct targeting of PIK3R1, and indirect targeting via CSF1R, resulting in diminished PI3K/Akt signalling and subsequent abrogation of

glucose uptake in response to insulin. As a proximal target in a multi-transduction signalling cascade, miR-155 regulation may additionally contribute to other key phenotypic developments in the diabetic podocyte, such as the aforementioned response to ER stress (see future work).

The second half of this research thesis aimed to investigate the microRNA expression of podocytes and whole glomeruli under diabetic conditions *in vivo.* I hypothesised that podocyte miRNA dysregulation occurs early in the development of DN, and drives podocyte insulin resistance, resulting in the early podocyte damage that is the harbinger of further glomerular injury in DN. To address this hypothesis, I intended to chart the evolution of miRNA change in podocytes extracted from the perfused glomeruli of a live mouse model as it develops DN in "real time". An unforeseen inability to breed sufficient numbers of podocyte-specific, GFP-labelled db/db mice to meet the RNA requirements of currently available miRseq kits has been a major limitation in addressing this research aim. The advances in sequencing technology that have been made during the time course of this PhD has brought us right to the cusp of being able to perform miRseq on small numbers of cells separated from bulk heterogeneous tissue (such as glomerular tissue), using single cell sequencing techniques. Given the unambiguously distinct miRNA profiles of insulin-resistant podocytes that I have demonstrated, pursuing the completion of this work using a novel sequencing technique is highly justifiable (see future work below).

However, bulk glomerular sequencing did confirm that miRNAs become dysregulated as early as 4 weeks in the db/db mouse, with differentially expressed miRNAs associated with pathways of established diabetes, such as inflammation and fibrosis. This is highly supportive of miRNA dysregulation being an initiating trigger in DN pathogenesis. To my knowledge, glomerular miRseq profiles have not previously been obtained from diabetic mice this young, nor have repeated measures been compared over a 12-week period, as was performed in this work, therefore these findings are both novel and noteworthy. Parallel miR- and mRNA-seq of glomerular tissue highlighted miRNA target interactions of relevance in oxidative stress and mitochondrial

dysfunction, which may be consistent with the theory of "mitochondrial hormeosis" i.e. may be an early adaptive response in DN that later becomes detrimental (441). Given the growing association between podocyte insulin resistance and disruptions in mitochondrial function, the miR-mRNA interactions unveiled in this work may hold significance as biomarkers of an early pathophysiological adaptation in DN that could be predictive of disease progression.

MiR-155 was significantly elevated in the db/db whole glomeruli at 4 weeks of age, although repression of targets PIK3R1 or CSF1R could not be detected in bulk RNAseq. Paired miR-mRNA analysis did, however, identify an interesting interaction between miR-155 and validated target periplakin (PPL), a cytoskeletal linker protein known to bind to, and provide a localisation signal for Akt (444). A glomerular role for PPL has not previously been reported, but its known involvement in cytoskeletal regulation and signal transduction (450) may be of significant relevance in podocyte insulin signalling in early DN. Indeed, RNAseq data from the *in vitro* podocyte model (kindly provided by Dr Mark Graham, Bristol PhD student) demonstrated both significant upregulation of miR-155 host gene and corresponding down-regulation of PPL in insulin-resistant podocytes.

In summary, using a combination of microarray and next generation sequencing approaches in representative *in vitro* and in *vivo models* of DN, I have demonstrated that miRNA expression is significantly altered very early in disease, and that miR-155 may effect podocyte insulin resistance via a number of prominent mRNA targets involved in modulating the PI3K/Akt pathway and/or influencing the cytoskeletal response to insulin. The most promising direct targets of miR-155 identified in this thesis are summarised in Figure 7.1 Further work is indicated to fully characterise the mechanistic roles of these miR-mRNA interactions in podocyte insulin signalling, as detailed below.

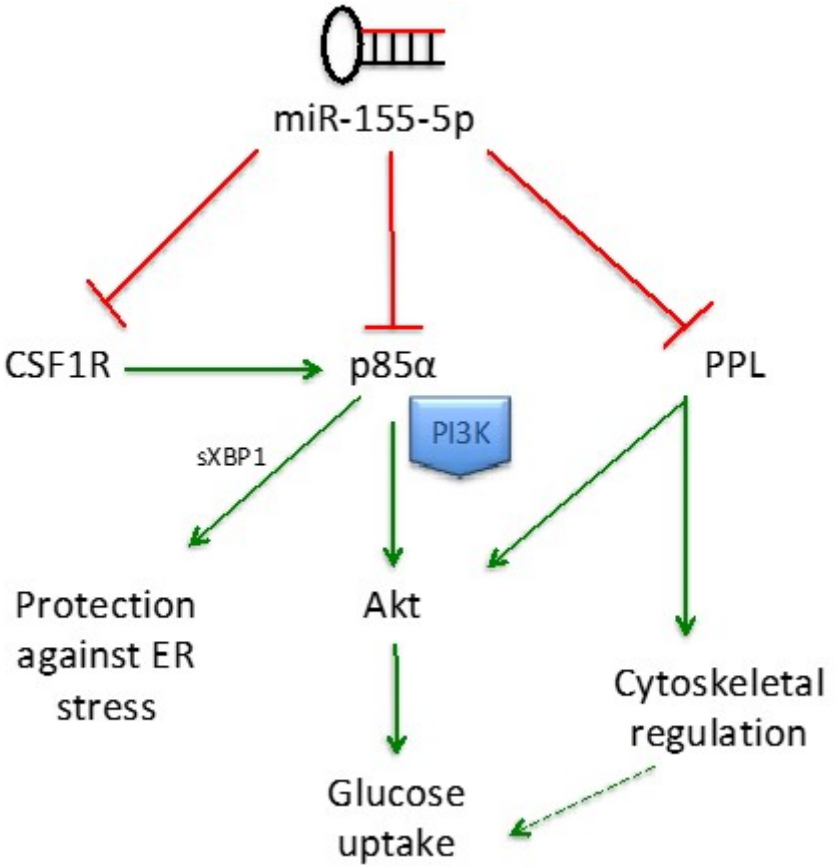

Figure 7.1. Proposed miR-155 directed mechanisms of podocyte insulin resistance. Colony stimulating factor-1 receptor (CSF1R), Phosphoinositide-3-Kinase Regulatory Subunit 1 (PIK3R1 or p85α) and periplakin (PPL) are identified as miR-155 targets of greatest relevance in effecting podocyte insulin signalling. MiR-155 repression of these targets is hypothesised to result in loss of downstream Akt activation and subsequent glucose uptake. Repression of periplakin may result in disturbed cytoskeletal regulation, which may additionally impact the uptake of glucose. Loss of p85α has previously been shown to disrupt the unfolded protein response via an interaction with spliced X-box binding protein-1 (sXBP1), leading to increased podocyte ER stress and apoptosis (157).

7.1 Future Work

Confirmation of miR-155 targeting of the key mRNA targets identified in this thesis may be achieved using luciferase reporter assays, and represents the next logical step in furthering this work. This will be followed by *in vitro* siRNA knockdown of the mRNA targets themselves, to confirm target-mediated effects on podocyte insulin responses.

As noted, miR-155-induced disruptions at the PI3K/Akt signalling node may affect other important downstream pathways not investigated in this work. Examples of downstream effects that could be further explored include changes in protein synthesis and autophagy pathways mediated via mTOR and divergent cell cycle kinetics via FOXO signalling. It would also be interesting to investigate whether the compromise of the unfolded protein response demonstrated by Madhusudhan *et al* could be recapitulated by miR-155-induced repression of p85α, thus representing a further dysregulated pathway that may contribute to the podocytopathy of DN.

A "proof of concept" experiment might involve the development of a podocyte-specific, miR-155 inducible mouse model. The ability to switch miR-155 on and off could be used to determine whether podocyte-specific miR-155 knockout could prevent the development of DN. MiR-155 antagomiRs may also be used to achieve this in *vivo*, however podocyte-specific targeting would be difficult using this technique.

Completion of the podocyte miR-and RNAseq from the db/db mouse model will be performed as soon as one of two limiting factors has been addressed: either there are sufficient numbers of (validated and characterised) GFP-labelled db/db mice to proceed with the miR/RNAseq methods used here, or a single cell sequencing (scSeq) kit capable of miRNA capture becomes available, thereby negating the need for complex labelled mouse models. In recent months, Wang *et al* have reported progress towards achieving simultaneous miR-and mRNAseq from a single cell using human erythroleukaemia and breast cancer cell lines by adopting a "half-cell" genomics approach. They divided single cell lysate material and performed RNAseq using the low input SMARTer library kit, whilst a bespoke adapter ligation method was used to amplify miRNAs (209). A number of technical limitations were noted by the authors, not least the "low throughput" nature of the technique, however it is clear that technology is heading in the right direction. The ability to perform scSeq on whole glomerular tissue would additionally permit simultaneous miRNA profiling of other glomerular cells from the db/db mouse. This data could then be correlated with the urinary miRNA profiling data used in this work to inform on the likely

cellular origins of the urinary miRNAs detected in DKD patients (including miR-155).

7.2 Conclusion

DN is a complex, heterogeneous disease that presents multiple challenges not only in devising efficacious treatments, but also in predicting those patients at greatest risk of developing DN. From the results of this work, I can conclude that insulin resistance in podocytes is associated with a unique microRNA signature, and that glomerular miRNAs are dysregulated very early in the development of DN *in vivo*, and may therefore play crucial roles in initiating DN pathophysiology. MiR-155-5p is identified as a key miRNA capable of inducing podocyte insulin resistance *in vitro* and identifying diabetic patients with DKD by urinary expression. The potential impact of these findings include translation into new urinary biomarkers to risk stratify diabetic patients, and the development of novel therapeutic agents to protect podocytes from becoming insulin resistant, which may be a key causal element in the progression of DN.

References

1. Diabetes.org 2019 [Available from: https://www.diabetes.org.uk/about_us/news/new-stats-people-living-with-diabetes.
2. Diabetes.co.uk. Cost of Diabetes 2019 [Available from: http://www.diabetes.co.uk/cost-of-diabetes.html.
3. Holman RR, Paul SK, Bethel MA, Matthews DR, Neil HA. 10-year follow-up of intensive glucose control in type 2 diabetes. N Engl J Med. 2008;359(15):1577-89.
4. Stratton IM, Adler AI, Neil HA, Matthews DR, Manley SE, Cull CA, et al. Association of glycaemia with macrovascular and microvascular complications of type 2 diabetes (UKPDS 35): prospective observational study. BMJ. 2000;321(7258):405-12.
5. Buse JB, Wexler DJ, Tsapas A, Rossing P, Mingrone G, Mathieu C, et al. 2019 Update to: Management of Hyperglycemia in Type 2 Diabetes, 2018. A Consensus Report by the American Diabetes Association (ADA) and the European Association for the Study of Diabetes (EASD). Diabetes Care. 2019.
6. Hole B, Gilg J, Casula A, Methven S, Castledine C. Chapter 1 UK Renal Replacement Therapy Adult Incidence in 2016: National and Centre-specific Analyses. Nephron. 2018;139 Suppl 1:13-46.
7. Beck-Nielsen H, Groop LC. Metabolic and genetic characterization of prediabetic states. Sequence of events leading to non-insulin-dependent diabetes mellitus. J Clin Invest. 1994;94(5):1714-21.
8. Efendic S, Ostenson CG. Hormonal responses and future treatment of non-insulin-dependent diabetes mellitus (NIDDM). J Intern Med. 1993;234(2):127-38.
9. Holman RR. Assessing the potential for alpha-glucosidase inhibitors in prediabetic states. Diabetes Res Clin Pract. 1998;40 Suppl:S21-5.
10. Weyer C, Bogardus C, Mott DM, Pratley RE. The natural history of insulin secretory dysfunction and insulin resistance in the pathogenesis of type 2 diabetes mellitus. J Clin Invest. 1999;104(6):787-94.
11. Kim JW, Yoon KH. Glucolipotoxicity in Pancreatic β-Cells. Diabetes Metab J. 2011;35(5):444-50.
12. Sako Y, Grill VE. A 48-hour lipid infusion in the rat time-dependently inhibits glucose-induced insulin secretion and B cell oxidation through a process likely coupled to fatty acid oxidation. Endocrinology. 1990;127(4):1580-9.
13. Hull RL, Westermark GT, Westermark P, Kahn SE. Islet amyloid: a critical entity in the pathogenesis of type 2 diabetes. J Clin Endocrinol Metab. 2004;89(8):3629-43.
14. Røder ME, Dinesen B, Hartling SG, Houssa P, Vestergaard H, Sodoyez-Goffaux F, et al. Intact proinsulin and beta-cell function in lean and obese subjects with and without type 2 diabetes. Diabetes Care. 1999;22(4):609-14.
15. Carter JS, Pugh JA, Monterrosa A. Non-insulin-dependent diabetes mellitus in minorities in the United States. Ann Intern Med. 1996;125(3):221-32.

16. Barnett AH, Eff C, Leslie RD, Pyke DA. Diabetes in identical twins. A study of 200 pairs. Diabetologia. 1981;20(2):87-93.
17. Manolio TA, Collins FS, Cox NJ, Goldstein DB, Hindorff LA, Hunter DJ, et al. Finding the missing heritability of complex diseases. Nature. 2009;461(7265):747-53.
18. Florez JC. Clinical review: the genetics of type 2 diabetes: a realistic appraisal in 2008. J Clin Endocrinol Metab. 2008;93(12):4633-42.
19. Holt RIG CC, Flyvbjerg A et al. Obesity and diabetes. Hauner H, editor. Oxford: Wiley-Blackwell; 2010.
20. Chan JM, Rimm EB, Colditz GA, Stampfer MJ, Willett WC. Obesity, fat distribution, and weight gain as risk factors for clinical diabetes in men. Diabetes Care. 1994;17(9):961-9.
21. Boden G, Chen X. Effects of fat on glucose uptake and utilization in patients with non-insulin-dependent diabetes. J Clin Invest. 1995;96(3):1261-8.
22. Kadowaki T, Yamauchi T, Kubota N, Hara K, Ueki K, Tobe K. Adiponectin and adiponectin receptors in insulin resistance, diabetes, and the metabolic syndrome. J Clin Invest. 2006;116(7):1784-92.
23. Schmidt MI, Duncan BB, Sharrett AR, Lindberg G, Savage PJ, Offenbacher S, et al. Markers of inflammation and prediction of diabetes mellitus in adults (Atherosclerosis Risk in Communities study): a cohort study. Lancet. 1999;353(9165):1649-52.
24. Hotamisligil GS, Shargill NS, Spiegelman BM. Adipose expression of tumor necrosis factor-alpha: direct role in obesity-linked insulin resistance. Science. 1993;259(5091):87-91.
25. Pradhan AD, Manson JE, Rifai N, Buring JE, Ridker PM. C-reactive protein, interleukin 6, and risk of developing type 2 diabetes mellitus. JAMA. 2001;286(3):327-34.
26. Lumeng CN, Bodzin JL, Saltiel AR. Obesity induces a phenotypic switch in adipose tissue macrophage polarization. J Clin Invest. 2007;117(1):175-84.
27. Obstfeld AE, Sugaru E, Thearle M, Francisco AM, Gayet C, Ginsberg HN, et al. C-C chemokine receptor 2 (CCR2) regulates the hepatic recruitment of myeloid cells that promote obesity-induced hepatic steatosis. Diabetes. 2010;59(4):916-25.
28. Hirosumi J, Tuncman G, Chang L, Görgün CZ, Uysal KT, Maeda K, et al. A central role for JNK in obesity and insulin resistance. Nature. 2002;420(6913):333-6.
29. Carpentier A, Mittelman SD, Lamarche B, Bergman RN, Giacca A, Lewis GF. Acute enhancement of insulin secretion by FFA in humans is lost with prolonged FFA elevation. Am J Physiol. 1999;276(6):E1055-66.
30. Sun K, Kusminski CM, Scherer PE. Adipose tissue remodeling and obesity. J Clin Invest. 2011;121(6):2094-101.
31. Hovind P, Tarnow L, Rossing P, Jensen BR, Graae M, Torp I, et al. Predictors for the development of microalbuminuria and macroalbuminuria in patients with type 1 diabetes: inception cohort study. BMJ. 2004;328(7448):1105.
32. Tsai WC, Wu HY, Peng YS, Ko MJ, Wu MS, Hung KY, et al. Risk Factors for Development and Progression of Chronic Kidney Disease: A Systematic Review and Exploratory Meta-Analysis. Medicine (Baltimore). 2016;95(11):e3013.
33. Rossing K, Christensen PK, Hovind P, Tarnow L, Rossing P, Parving HH. Progression of nephropathy in type 2 diabetic patients. Kidney Int. 2004;66(4):1596-605.

34. Thakar CV, Christianson A, Himmelfarb J, Leonard AC. Acute kidney injury episodes and chronic kidney disease risk in diabetes mellitus. Clin J Am Soc Nephrol. 2011;6(11):2567-72.
35. Foundation NK. KDOQI Clinical Practice Guideline for Diabetes and CKD: 2012 Update. Am J Kidney Dis. 2012;60(5):850-86.
36. He F, Xia X, Wu XF, Yu XQ, Huang FX. Diabetic retinopathy in predicting diabetic nephropathy in patients with type 2 diabetes and renal disease: a meta-analysis. Diabetologia. 2013;56(3):457-66.
37. Association AD. Diagnosis and classification of diabetes mellitus. Diabetes Care. 2014;37 Suppl 1:S81-90.
38. Klimontov VV, Korbut AI. Albuminuric and non-albuminuric patterns of chronic kidney disease in type 2 diabetes. Diabetes Metab Syndr. 2019;13(1):474-9.
39. Bentata Y, Karimi I, Benabdellah N, El Alaoui F, Haddiya I, Abouqal R. Albuminuria in type 2 diabetes mellitus: from remission to progression. Ren Fail. 2016;38(3):481-3.
40. Boronat M, García-Cantón C, Quevedo V, Lorenzo DL, López-Ríos L, Batista F, et al. Non-albuminuric renal disease among subjects with advanced stages of chronic kidney failure related to type 2 diabetes mellitus. Ren Fail. 2014;36(2):166-70.
41. Ito H, Takeuchi Y, Ishida H, Antoku S, Abe M, Mifune M, et al. High frequencies of diabetic micro- and macroangiopathies in patients with type 2 diabetes mellitus with decreased estimated glomerular filtration rate and normoalbuminuria. Nephrol Dial Transplant. 2010;25(4):1161-7.
42. Ekinci EI, Jerums G, Skene A, Crammer P, Power D, Cheong KY, et al. Renal structure in normoalbuminuric and albuminuric patients with type 2 diabetes and impaired renal function. Diabetes Care. 2013;36(11):3620-6.
43. Said SM, Nasr SH. Silent diabetic nephropathy. Kidney Int. 2016;90(1):24-6.
44. Tervaert TW, Mooyaart AL, Amann K, Cohen AH, Cook HT, Drachenberg CB, et al. Pathologic classification of diabetic nephropathy. J Am Soc Nephrol. 2010;21(4):556-63.
45. Mottl AK, Gasim A, Schober FP, Hu Y, Dunnon AK, Hogan SL, et al. Segmental Sclerosis and Extracapillary Hypercellularity Predict Diabetic ESRD. J Am Soc Nephrol. 2018;29(2):694-703.
46. Hong D, Zheng T, Jia-qing S, Jian W, Zhi-hong L, Lei-shi L. Nodular glomerular lesion: a later stage of diabetic nephropathy? Diabetes Res Clin Pract. 2007;78(2):189-95.
47. Caramori ML, Kim Y, Huang C, Fish AJ, Rich SS, Miller ME, et al. Cellular basis of diabetic nephropathy: 1. Study design and renal structural-functional relationships in patients with long-standing type 1 diabetes. Diabetes. 2002;51(2):506-13.
48. Qi C, Mao X, Zhang Z, Wu H. Classification and Differential Diagnosis of Diabetic Nephropathy. J Diabetes Res. 2017;2017:8637138.
49. Brenner BM, Cooper ME, de Zeeuw D, Keane WF, Mitch WE, Parving HH, et al. Effects of losartan on renal and cardiovascular outcomes in patients with type 2 diabetes and nephropathy. N Engl J Med. 2001;345(12):861-9.
50. Parving HH, Lehnert H, Bröchner-Mortensen J, Gomis R, Andersen S, Arner P, et al. The effect of irbesartan on the development of diabetic nephropathy in patients with type 2 diabetes. N Engl J Med. 2001;345(12):870-8.

51. Eijkelkamp WB, Zhang Z, Remuzzi G, Parving HH, Cooper ME, Keane WF, et al. Albuminuria is a target for renoprotective therapy independent from blood pressure in patients with type 2 diabetic nephropathy: post hoc analysis from the Reduction of Endpoints in NIDDM with the Angiotensin II Antagonist Losartan (RENAAL) trial. J Am Soc Nephrol. 2007;18(5):1540-6.
52. Pergola PE, Raskin P, Toto RD, Meyer CJ, Huff JW, Grossman EB, et al. Bardoxolone methyl and kidney function in CKD with type 2 diabetes. N Engl J Med. 2011;365(4):327-36.
53. Williams ME, Bolton WK, Khalifah RG, Degenhardt TP, Schotzinger RJ, McGill JB. Effects of pyridoxamine in combined phase 2 studies of patients with type 1 and type 2 diabetes and overt nephropathy. Am J Nephrol. 2007;27(6):605-14.
54. Perkovic V, Jardine MJ, Neal B, Bompoint S, Heerspink HJL, Charytan DM, et al. Canagliflozin and Renal Outcomes in Type 2 Diabetes and Nephropathy. N Engl J Med. 2019;380(24):2295-306.
55. Tanaka S, Sugiura Y, Saito H, Sugahara M, Higashijima Y, Yamaguchi J, et al. Sodium-glucose cotransporter 2 inhibition normalizes glucose metabolism and suppresses oxidative stress in the kidneys of diabetic mice. Kidney Int. 2018;94(5):912-25.
56. Shin SJ, Chung S, Kim SJ, Lee EM, Yoo YH, Kim JW, et al. Effect of Sodium-Glucose Co-Transporter 2 Inhibitor, Dapagliflozin, on Renal Renin-Angiotensin System in an Animal Model of Type 2 Diabetes. PLoS One. 2016;11(11):e0165703.
57. Wang Y, Xu L, Yuan L, Li D, Zhang Y, Zheng R, et al. Sodium-glucose co-transporter-2 inhibitors suppress atrial natriuretic peptide secretion in patients with newly diagnosed Type 2 diabetes. Diabet Med. 2016;33(12):1732-6.
58. Garvey WT, Van Gaal L, Leiter LA, Vijapurkar U, List J, Cuddihy R, et al. Effects of canagliflozin versus glimepiride on adipokines and inflammatory biomarkers in type 2 diabetes. Metabolism. 2018;85:32-7.
59. Vallon V, Gerasimova M, Rose MA, Masuda T, Satriano J, Mayoux E, et al. SGLT2 inhibitor empagliflozin reduces renal growth and albuminuria in proportion to hyperglycemia and prevents glomerular hyperfiltration in diabetic Akita mice. Am J Physiol Renal Physiol. 2014;306(2):F194-204.
60. Yin W, Xu S, Wang Z, Liu H, Peng L, Fang Q, et al. Recombinant human GLP-1(rhGLP-1) alleviating renal tubulointestitial injury in diabetic STZ-induced rats. Biochem Biophys Res Commun. 2018;495(1):793-800.
61. Hendarto H, Inoguchi T, Maeda Y, Ikeda N, Zheng J, Takei R, et al. GLP-1 analog liraglutide protects against oxidative stress and albuminuria in streptozotocin-induced diabetic rats via protein kinase A-mediated inhibition of renal NAD(P)H oxidases. Metabolism. 2012;61(10):1422-34.
62. Drucker DJ. The Ascending GLP-1 Road From Clinical Safety to Reduction of Cardiovascular Complications. Diabetes. 2018;67(9):1710-9.
63. Mann JFE, Ørsted DD, Buse JB. Liraglutide and Renal Outcomes in Type 2 Diabetes. N Engl J Med. 2017;377(22):2197-8.
64. de Vos LC, Hettige TS, Cooper ME. New Glucose-Lowering Agents for Diabetic Kidney Disease. Adv Chronic Kidney Dis. 2018;25(2):149-57.
65. Tuttle KR, Lakshmanan MC, Rayner B, Busch RS, Zimmermann AG, Woodward DB, et al. Dulaglutide versus insulin glargine in patients with type 2 diabetes and moderate-to-severe chronic kidney disease (AWARD-7): a multicentre, open-label, randomised trial. Lancet Diabetes Endocrinol. 2018;6(8):605-17.

66. Moellmann J, Klinkhammer BM, Onstein J, Stöhr R, Jankowski V, Jankowski J, et al. Glucagon-Like Peptide 1 and Its Cleavage Products Are Renoprotective in Murine Diabetic Nephropathy. Diabetes. 2018;67(11):2410-9.
67. Kanasaki K, Shi S, Kanasaki M, He J, Nagai T, Nakamura Y, et al. Linagliptin-mediated DPP-4 inhibition ameliorates kidney fibrosis in streptozotocin-induced diabetic mice by inhibiting endothelial-to-mesenchymal transition in a therapeutic regimen. Diabetes. 2014;63(6):2120-31.
68. Groop PH, Cooper ME, Perkovic V, Emser A, Woerle HJ, von Eynatten M. Linagliptin lowers albuminuria on top of recommended standard treatment in patients with type 2 diabetes and renal dysfunction. Diabetes Care. 2013;36(11):3460-8.
69. Rosenstock J, Perkovic V, Johansen OE, Cooper ME, Kahn SE, Marx N, et al. Effect of Linagliptin vs Placebo on Major Cardiovascular Events in Adults With Type 2 Diabetes and High Cardiovascular and Renal Risk: The CARMELINA Randomized Clinical Trial. JAMA. 2019;321(1):69-79.
70. Scirica BM, Bhatt DL, Braunwald E, Steg PG, Davidson J, Hirshberg B, et al. Saxagliptin and cardiovascular outcomes in patients with type 2 diabetes mellitus. N Engl J Med. 2013;369(14):1317-26.
71. Anguiano L, Riera M, Pascual J, Soler MJ. Endothelin Blockade in Diabetic Kidney Disease. J Clin Med. 2015;4(6):1171-92.
72. Mann JF, Green D, Jamerson K, Ruilope LM, Kuranoff SJ, Littke T, et al. Avosentan for overt diabetic nephropathy. J Am Soc Nephrol. 2010;21(3):527-35.
73. Heerspink HJL, Parving HH, Andress DL, Bakris G, Correa-Rotter R, Hou FF, et al. Atrasentan and renal events in patients with type 2 diabetes and chronic kidney disease (SONAR): a double-blind, randomised, placebo-controlled trial. Lancet. 2019;393(10184):1937-47.
74. Sato A, Hayashi K, Naruse M, Saruta T. Effectiveness of aldosterone blockade in patients with diabetic nephropathy. Hypertension. 2003;41(1):64-8.
75. Bakris GL, Agarwal R, Chan JC, Cooper ME, Gansevoort RT, Haller H, et al. Effect of Finerenone on Albuminuria in Patients With Diabetic Nephropathy: A Randomized Clinical Trial. JAMA. 2015;314(9):884-94.
76. Bakris GL, Agarwal R, Anker SD, Pitt B, Ruilope LM, Nowack C, et al. Design and Baseline Characteristics of the Finerenone in Reducing Kidney Failure and Disease Progression in Diabetic Kidney Disease Trial. Am J Nephrol. 2019;50(5):333-44.
77. Pichler R, Afkarian M, Dieter BP, Tuttle KR. Immunity and inflammation in diabetic kidney disease: translating mechanisms to biomarkers and treatment targets. Am J Physiol Renal Physiol. 2017;312(4):F716-F31.
78. Brosius FC, Tuttle KR, Kretzler M. JAK inhibition in the treatment of diabetic kidney disease. Diabetologia. 2016;59(8):1624-7.
79. Ridker PM, Libby P, MacFadyen JG, Thuren T, Ballantyne C, Fonseca F, et al. Modulation of the interleukin-6 signalling pathway and incidence rates of atherosclerotic events and all-cause mortality: analyses from the Canakinumab Anti-Inflammatory Thrombosis Outcomes Study (CANTOS). Eur Heart J. 2018;39(38):3499-507.
80. de Zeeuw D, Akizawa T, Audhya P, Bakris GL, Chin M, Christ-Schmidt H, et al. Bardoxolone methyl in type 2 diabetes and stage 4 chronic kidney disease. N Engl J Med. 2013;369(26):2492-503.
81. Chin MP, Wrolstad D, Bakris GL, Chertow GM, de Zeeuw D, Goldsberry A, et al. Risk factors for heart failure in patients with type 2 diabetes mellitus and

stage 4 chronic kidney disease treated with bardoxolone methyl. J Card Fail. 2014;20(12):953-8.
82. Taniguchi CM, Emanuelli B, Kahn CR. Critical nodes in signalling pathways: insights into insulin action. Nat Rev Mol Cell Biol. 2006;7(2):85-96.
83. Saltiel AR, Kahn CR. Insulin signalling and the regulation of glucose and lipid metabolism. Nature. 2001;414(6865):799-806.
84. White MF. IRS proteins and the common path to diabetes. Am J Physiol Endocrinol Metab. 2002;283(3):E413-22.
85. Sarbassov DD, Guertin DA, Ali SM, Sabatini DM. Phosphorylation and regulation of Akt/PKB by the rictor-mTOR complex. Science. 2005;307(5712):1098-101.
86. Cantley LC. The phosphoinositide 3-kinase pathway. Science. 2002;296(5573):1655-7.
87. Torii S, Yamamoto T, Tsuchiya Y, Nishida E. ERK MAP kinase in G cell cycle progression and cancer. Cancer Sci. 2006;97(8):697-702.
88. Rodriguez-Viciana P, Warne PH, Dhand R, Vanhaesebroeck B, Gout I, Fry MJ, et al. Phosphatidylinositol-3-OH kinase as a direct target of Ras. Nature. 1994;370(6490):527-32.
89. Chiang SH, Baumann CA, Kanzaki M, Thurmond DC, Watson RT, Neudauer CL, et al. Insulin-stimulated GLUT4 translocation requires the CAP-dependent activation of TC10. Nature. 2001;410(6831):944-8.
90. Chiang SH, Hwang J, Legendre M, Zhang M, Kimura A, Saltiel AR. TCGAP, a multidomain Rho GTPase-activating protein involved in insulin-stimulated glucose transport. EMBO J. 2003;22(11):2679-91.
91. Marlais M, Coward RJ. Paediatrics, insulin resistance and the kidney. Pediatr Nephrol. 2015;30(8):1217-24.
92. Mogensen CE, Christensen NJ, Gundersen HJ. The acute effect of insulin on heart rate, blood pressure, plasma noradrenaline and urinary albumin excretion. The role of changes in blood glucose. Diabetologia. 1980;18(6):453-7.
93. Hegedüs L, Christensen NJ, Mogensen CE, Gundersen HJ. Oral glucose increases urinary albumin excretion in normal subjects but not in insulin-dependent diabetics. Scand J Clin Lab Invest. 1980;40(5):479-82.
94. Pilz S, Rutters F, Nijpels G, Stehouwer CD, Højlund K, Nolan JJ, et al. Insulin sensitivity and albuminuria: the RISC study. Diabetes Care. 2014;37(6):1597-603.
95. Juutilainen A, Lehto S, Rönnemaa T, Pyörälä K, Laakso M. Proteinuria and metabolic syndrome as predictors of cardiovascular death in non-diabetic and type 2 diabetic men and women. Diabetologia. 2006;49(1):56-65.
96. Andersen AR, Christiansen JS, Andersen JK, Kreiner S, Deckert T. Diabetic nephropathy in Type 1 (insulin-dependent) diabetes: an epidemiological study. Diabetologia. 1983;25(6):496-501.
97. Ahlqvist E, Storm P, Käräjämäki A, Martinell M, Dorkhan M, Carlsson A, et al. Novel subgroups of adult-onset diabetes and their association with outcomes: a data-driven cluster analysis of six variables. Lancet Diabetes Endocrinol. 2018;6(5):361-9.
98. Hadjadj S, Péan F, Gallois Y, Passa P, Aubert R, Weekers L, et al. Different patterns of insulin resistance in relatives of type 1 diabetic patients with retinopathy or nephropathy: the Genesis France-Belgium Study. Diabetes Care. 2004;27(11):2661-8.
99. Hale LJ, Coward RJ. Insulin signalling to the kidney in health and disease. Clin Sci (Lond). 2013;124(6):351-70.

100. Brenner BM, Hostetter TH, Humes HD. Glomerular permselectivity: barrier function based on discrimination of molecular size and charge. Am J Physiol. 1978;234(6):F455-60.
101. Rowe DJ, Dawnay A, Watts GF. Microalbuminuria in diabetes mellitus: review and recommendations for the measurement of albumin in urine. Ann Clin Biochem. 1990;27 (Pt 4):297-312.
102. Salmon AH, Neal CR, Harper SJ. New aspects of glomerular filtration barrier structure and function: five layers (at least) not three. Curr Opin Nephrol Hypertens. 2009;18(3):197-205.
103. Daehn I, Casalena G, Zhang T, Shi S, Fenninger F, Barasch N, et al. Endothelial mitochondrial oxidative stress determines podocyte depletion in segmental glomerulosclerosis. J Clin Invest. 2014;124(4):1608-21.
104. Eremina V, Baelde HJ, Quaggin SE. Role of the VEGF--a signaling pathway in the glomerulus: evidence for crosstalk between components of the glomerular filtration barrier. Nephron Physiol. 2007;106(2):p32-7.
105. Wang L, Zhang T, Fang M, Shen N, Wang D, Teng J, et al. Podocytes protect glomerular endothelial cells from hypoxic injury via deSUMOylation of HIF-1α signaling. Int J Biochem Cell Biol. 2015;58:17-27.
106. Haraldsson B, Nyström J, Deen WM. Properties of the glomerular barrier and mechanisms of proteinuria. Physiol Rev. 2008;88(2):451-87.
107. F. J. The Ultrastructure of the Normal Human Glomerulus. Copenhagen, Denmark: Munksgaard; 1966.
108. Sugio S, Kashima A, Mochizuki S, Noda M, Kobayashi K. Crystal structure of human serum albumin at 2.5 A resolution. Protein Eng. 1999;12(6):439-46.
109. Chappell D, Jacob M, Paul O, Rehm M, Welsch U, Stoeckelhuber M, et al. The glycocalyx of the human umbilical vein endothelial cell: an impressive structure ex vivo but not in culture. Circ Res. 2009;104(11):1313-7.
110. Potter DR, Damiano ER. The hydrodynamically relevant endothelial cell glycocalyx observed in vivo is absent in vitro. Circ Res. 2008;102(7):770-6.
111. Satchell S. The role of the glomerular endothelium in albumin handling. Nat Rev Nephrol. 2013;9(12):717-25.
112. Singh A, Satchell SC, Neal CR, McKenzie EA, Tooke JE, Mathieson PW. Glomerular endothelial glycocalyx constitutes a barrier to protein permeability. J Am Soc Nephrol. 2007;18(11):2885-93.
113. Yoshioka T, Ichikawa I, Fogo A. Reactive oxygen metabolites cause massive, reversible proteinuria and glomerular sieving defect without apparent ultrastructural abnormality. J Am Soc Nephrol. 1991;2(4):902-12.
114. Fridén V, Oveland E, Tenstad O, Ebefors K, Nyström J, Nilsson UA, et al. The glomerular endothelial cell coat is essential for glomerular filtration. Kidney Int. 2011;79(12):1322-30.
115. Slater SC, Ramnath RD, Uttridge K, Saleem MA, Cahill PA, Mathieson PW, et al. Chronic exposure to laminar shear stress induces Kruppel-like factor 2 in glomerular endothelial cells and modulates interactions with co-cultured podocytes. Int J Biochem Cell Biol. 2012;44(9):1482-90.
116. Williams ME. Diabetic nephropathy: the proteinuria hypothesis. Am J Nephrol. 2005;25(2):77-94.
117. Suh JH, Miner JH. The glomerular basement membrane as a barrier to albumin. Nat Rev Nephrol. 2013;9(8):470-7.
118. Aoki S, Saito-Hakoda A, Yoshikawa T, Shimizu K, Kisu K, Suzuki S, et al. The reduction of heparan sulphate in the glomerular basement membrane does

not augment urinary albumin excretion. Nephrol Dial Transplant. 2018;33(1):26-33.
119. Miner JH. The glomerular basement membrane. Exp Cell Res. 2012;318(9):973-8.
120. Salem RM, Todd JN, Sandholm N, Cole JB, Chen WM, Andrews D, et al. Genome-Wide Association Study of Diabetic Kidney Disease Highlights Biology Involved in Glomerular Basement Membrane Collagen. J Am Soc Nephrol. 2019;30(10):2000-16.
121. Saleem MA, Zavadil J, Bailly M, McGee K, Witherden IR, Pavenstadt H, et al. The molecular and functional phenotype of glomerular podocytes reveals key features of contractile smooth muscle cells. Am J Physiol Renal Physiol. 2008;295(4):F959-70.
122. Grahammer F, Schell C, Huber TB. The podocyte slit diaphragm--from a thin grey line to a complex signalling hub. Nat Rev Nephrol. 2013;9(10):587-98.
123. Ryan GB, Rodewald R, Karnovsky MJ. An ultrastructural study of the glomerular slit diaphragm in aminonucleoside nephrosis. Lab Invest. 1975;33(5):461-8.
124. Ranganathan S. Pathology of Podocytopathies Causing Nephrotic Syndrome in Children. Front Pediatr. 2016;4:32.
125. Ruotsalainen V, Patrakka J, Tissari P, Reponen P, Hess M, Kestilä M, et al. Role of nephrin in cell junction formation in human nephrogenesis. Am J Pathol. 2000;157(6):1905-16.
126. Kestilä M, Lenkkeri U, Männikkö M, Lamerdin J, McCready P, Putaala H, et al. Positionally cloned gene for a novel glomerular protein--nephrin--is mutated in congenital nephrotic syndrome. Mol Cell. 1998;1(4):575-82.
127. Martin CE, Jones N. Nephrin Signaling in the Podocyte: An Updated View of Signal Regulation at the Slit Diaphragm and Beyond. Front Endocrinol (Lausanne). 2018;9:302.
128. Möller CC, Flesche J, Reiser J. Sensitizing the Slit Diaphragm with TRPC6 ion channels. J Am Soc Nephrol. 2009;20(5):950-3.
129. Reiser J, Polu KR, Möller CC, Kenlan P, Altintas MM, Wei C, et al. TRPC6 is a glomerular slit diaphragm-associated channel required for normal renal function. Nat Genet. 2005;37(7):739-44.
130. Faul C, Asanuma K, Yanagida-Asanuma E, Kim K, Mundel P. Actin up: regulation of podocyte structure and function by components of the actin cytoskeleton. Trends Cell Biol. 2007;17(9):428-37.
131. Asanuma K, Yanagida-Asanuma E, Faul C, Tomino Y, Kim K, Mundel P. Synaptopodin orchestrates actin organization and cell motility via regulation of RhoA signalling. Nat Cell Biol. 2006;8(5):485-91.
132. Yu H, Kistler A, Faridi MH, Meyer JO, Tryniszewska B, Mehta D, et al. Synaptopodin Limits TRPC6 Podocyte Surface Expression and Attenuates Proteinuria. J Am Soc Nephrol. 2016;27(11):3308-19.
133. Lennon R, Randles MJ, Humphries MJ. The importance of podocyte adhesion for a healthy glomerulus. Front Endocrinol (Lausanne). 2014;5:160.
134. Pagtalunan ME, Miller PL, Jumping-Eagle S, Nelson RG, Myers BD, Rennke HG, et al. Podocyte loss and progressive glomerular injury in type II diabetes. J Clin Invest. 1997;99(2):342-8.
135. Petermann AT, Pippin J, Krofft R, Blonski M, Griffin S, Durvasula R, et al. Viable podocytes detach in experimental diabetic nephropathy: potential mechanism underlying glomerulosclerosis. Nephron Exp Nephrol. 2004;98(4):e114-23.

136. Lin JS, Susztak K. Podocytes: the Weakest Link in Diabetic Kidney Disease? Curr Diab Rep. 2016;16(5):45.
137. Dessapt C, Baradez MO, Hayward A, Dei Cas A, Thomas SM, Viberti G, et al. Mechanical forces and TGFbeta1 reduce podocyte adhesion through alpha3beta1 integrin downregulation. Nephrol Dial Transplant. 2009;24(9):2645-55.
138. Matsusaka T, Sandgren E, Shintani A, Kon V, Pastan I, Fogo AB, et al. Podocyte injury damages other podocytes. J Am Soc Nephrol. 2011;22(7):1275-85.
139. Steffes MW, Schmidt D, McCrery R, Basgen JM, Group IDNS. Glomerular cell number in normal subjects and in type 1 diabetic patients. Kidney Int. 2001;59(6):2104-13.
140. Weil EJ, Lemley KV, Mason CC, Yee B, Jones LI, Blouch K, et al. Podocyte detachment and reduced glomerular capillary endothelial fenestration promote kidney disease in type 2 diabetic nephropathy. Kidney Int. 2012;82(9):1010-7.
141. Meyer TW, Bennett PH, Nelson RG. Podocyte number predicts long-term urinary albumin excretion in Pima Indians with Type II diabetes and microalbuminuria. Diabetologia. 1999;42(11):1341-4.
142. Dimke H, Maezawa Y, Quaggin SE. Crosstalk in glomerular injury and repair. Curr Opin Nephrol Hypertens. 2015;24(3):231-8.
143. Yu D, Petermann A, Kunter U, Rong S, Shankland SJ, Floege J. Urinary podocyte loss is a more specific marker of ongoing glomerular damage than proteinuria. J Am Soc Nephrol. 2005;16(6):1733-41.
144. Petrica L, Ursoniu S, Gadalean F, Vlad A, Gluhovschi G, Dumitrascu V, et al. Urinary podocyte-associated mRNA levels correlate with proximal tubule dysfunction in early diabetic nephropathy of type 2 diabetes mellitus. Diabetol Metab Syndr. 2017;9:31.
145. Mima A, Ohshiro Y, Kitada M, Matsumoto M, Geraldes P, Li C, et al. Glomerular-specific protein kinase C-β-induced insulin receptor substrate-1 dysfunction and insulin resistance in rat models of diabetes and obesity. Kidney Int. 2011;79(8):883-96.
146. Tejada T, Catanuto P, Ijaz A, Santos JV, Xia X, Sanchez P, et al. Failure to phosphorylate AKT in podocytes from mice with early diabetic nephropathy promotes cell death. Kidney Int. 2008;73(12):1385-93.
147. Coward RJ, Welsh GI, Yang J, Tasman C, Lennon R, Koziell A, et al. The human glomerular podocyte is a novel target for insulin action. Diabetes. 2005;54(11):3095-102.
148. Welsh GI, Hale LJ, Eremina V, Jeansson M, Maezawa Y, Lennon R, et al. Insulin signaling to the glomerular podocyte is critical for normal kidney function. Cell Metab. 2010;12(4):329-40.
149. Coward RJ, Welsh GI, Koziell A, Hussain S, Lennon R, Ni L, et al. Nephrin is critical for the action of insulin on human glomerular podocytes. Diabetes. 2007;56(4):1127-35.
150. Kim EY, Anderson M, Dryer SE. Insulin increases surface expression of TRPC6 channels in podocytes: role of NADPH oxidases and reactive oxygen species. Am J Physiol Renal Physiol. 2012;302(3):F298-307.
151. Kim EY, Dryer SE. Effects of insulin and high glucose on mobilization of slo1 BKCa channels in podocytes. J Cell Physiol. 2011;226(9):2307-15.
152. Bosch JP, Lew S, Glabman S, Lauer A. Renal hemodynamic changes in humans. Response to protein loading in normal and diseased kidneys. Am J Med. 1986;81(5):809-15.

153. Perlstein TS, Gerhard-Herman M, Hollenberg NK, Williams GH, Thomas A. Insulin induces renal vasodilation, increases plasma renin activity, and sensitizes the renal vasculature to angiotensin receptor blockade in healthy subjects. J Am Soc Nephrol. 2007;18(3):944-51.
154. Tuttle KR, Puhlman ME, Cooney SK, Short RA. Effects of amino acids and glucagon on renal hemodynamics in type 1 diabetes. Am J Physiol Renal Physiol. 2002;282(1):F103-12.
155. Hale LJ, Hurcombe J, Lay A, Santamaría B, Valverde AM, Saleem MA, et al. Insulin directly stimulates VEGF-A production in the glomerular podocyte. Am J Physiol Renal Physiol. 2013;305(2):F182-8.
156. Ising C, Koehler S, Brähler S, Merkwirth C, Höhne M, Baris OR, et al. Inhibition of insulin/IGF-1 receptor signaling protects from mitochondria-mediated kidney failure. EMBO Mol Med. 2015;7(3):275-87.
157. Madhusudhan T, Wang H, Dong W, Ghosh S, Bock F, Thangapandi VR, et al. Defective podocyte insulin signalling through p85-XBP1 promotes ATF6-dependent maladaptive ER-stress response in diabetic nephropathy. Nat Commun. 2015;6:6496.
158. Santamaria B, Marquez E, Lay A, Carew RM, González-Rodríguez Á, Welsh GI, et al. IRS2 and PTEN are key molecules in controlling insulin sensitivity in podocytes. Biochim Biophys Acta. 2015;1853(12):3224-34.
159. Canaud G, Bienaimé F, Viau A, Treins C, Baron W, Nguyen C, et al. AKT2 is essential to maintain podocyte viability and function during chronic kidney disease. Nat Med. 2013;19(10):1288-96.
160. Cho H, Mu J, Kim JK, Thorvaldsen JL, Chu Q, Crenshaw EB, et al. Insulin resistance and a diabetes mellitus-like syndrome in mice lacking the protein kinase Akt2 (PKB beta). Science. 2001;292(5522):1728-31.
161. Lay AC, Coward RJM. The Evolving Importance of Insulin Signaling in Podocyte Health and Disease. Front Endocrinol (Lausanne). 2018;9:693.
162. Lay AC, Hurcombe JA, Betin VMS, Barrington F, Rollason R, Ni L, et al. Prolonged exposure of mouse and human podocytes to insulin induces insulin resistance through lysosomal and proteasomal degradation of the insulin receptor. Diabetologia. 2017;60(11):2299-311.
163. Drapeau N, Lizotte F, Denhez B, Guay A, Kennedy CR, Geraldes P. Expression of SHP-1 induced by hyperglycemia prevents insulin actions in podocytes. Am J Physiol Endocrinol Metab. 2013;304(11):E1188-98.
164. Lizotte F, Denhez B, Guay A, Gévry N, Côté AM, Geraldes P. Persistent Insulin Resistance in Podocytes Caused by Epigenetic Changes of SHP-1 in Diabetes. Diabetes. 2016;65(12):3705-17.
165. Mitrofanova A, Sosa MA, Fornoni A. Lipid mediators of insulin signaling in diabetic kidney disease. Am J Physiol Renal Physiol. 2019;317(5):F1241-F52.
166. Mitrofanova A, Mallela SK, Ducasa GM, Yoo TH, Rosenfeld-Gur E, Zelnik ID, et al. SMPDL3b modulates insulin receptor signaling in diabetic kidney disease. Nat Commun. 2019;10(1):2692.
167. Hyvönen ME, Saurus P, Wasik A, Heikkilä E, Havana M, Trokovic R, et al. Lipid phosphatase SHIP2 downregulates insulin signalling in podocytes. Mol Cell Endocrinol. 2010;328(1-2):70-9.
168. Du P, Fan B, Han H, Zhen J, Shang J, Wang X, et al. NOD2 promotes renal injury by exacerbating inflammation and podocyte insulin resistance in diabetic nephropathy. Kidney Int. 2013;84(2):265-76.
169. Doublier S, Salvidio G, Lupia E, Ruotsalainen V, Verzola D, Deferrari G, et al. Nephrin expression is reduced in human diabetic nephropathy: evidence for

a distinct role for glycated albumin and angiotensin II. Diabetes. 2003;52(4):1023-30.
170. Kelly DJ, Aaltonen P, Cox AJ, Rumble JR, Langham R, Panagiotopoulos S, et al. Expression of the slit-diaphragm protein, nephrin, in experimental diabetic nephropathy: differing effects of anti-proteinuric therapies. Nephrol Dial Transplant. 2002;17(7):1327-32.
171. Langham RG, Kelly DJ, Cox AJ, Thomson NM, Holthöfer H, Zaoui P, et al. Proteinuria and the expression of the podocyte slit diaphragm protein, nephrin, in diabetic nephropathy: effects of angiotensin converting enzyme inhibition. Diabetologia. 2002;45(11):1572-6.
172. Lin CL, Wang FS, Hsu YC, Chen CN, Tseng MJ, Saleem MA, et al. Modulation of notch-1 signaling alleviates vascular endothelial growth factor-mediated diabetic nephropathy. Diabetes. 2010;59(8):1915-25.
173. Menne J, Meier M, Park JK, Boehne M, Kirsch T, Lindschau C, et al. Nephrin loss in experimental diabetic nephropathy is prevented by deletion of protein kinase C alpha signaling in-vivo. Kidney Int. 2006;70(8):1456-62.
174. Lin CL, Lee PH, Hsu YC, Lei CC, Ko JY, Chuang PC, et al. MicroRNA-29a promotion of nephrin acetylation ameliorates hyperglycemia-induced podocyte dysfunction. J Am Soc Nephrol. 2014;25(8):1698-709.
175. Huber TB, Hartleben B, Kim J, Schmidts M, Schermer B, Keil A, et al. Nephrin and CD2AP associate with phosphoinositide 3-OH kinase and stimulate AKT-dependent signaling. Mol Cell Biol. 2003;23(14):4917-28.
176. Piwkowska A, Rogacka D, Audzeyenka I, Kasztan M, Angielski S, Jankowski M. Insulin increases glomerular filtration barrier permeability through PKGIα-dependent mobilization of BKCa channels in cultured rat podocytes. Biochim Biophys Acta. 2015;1852(8):1599-609.
177. Gödel M, Hartleben B, Herbach N, Liu S, Zschiedrich S, Lu S, et al. Role of mTOR in podocyte function and diabetic nephropathy in humans and mice. J Clin Invest. 2011;121(6):2197-209.
178. Lamming DW, Ye L, Katajisto P, Goncalves MD, Saitoh M, Stevens DM, et al. Rapamycin-induced insulin resistance is mediated by mTORC2 loss and uncoupled from longevity. Science. 2012;335(6076):1638-43.
179. Lennon R, Pons D, Sabin MA, Wei C, Shield JP, Coward RJ, et al. Saturated fatty acids induce insulin resistance in human podocytes: implications for diabetic nephropathy. Nephrol Dial Transplant. 2009;24(11):3288-96.
180. Wasik AA, Dumont V, Tienari J, Nyman TA, Fogarty CL, Forsblom C, et al. Septin 7 reduces nonmuscle myosin IIA activity in the SNAP23 complex and hinders GLUT4 storage vesicle docking and fusion. Exp Cell Res. 2017;350(2):336-48.
181. Imano E, Kanda T, Nakatani Y, Nishida T, Arai K, Motomura M, et al. Effect of troglitazone on microalbuminuria in patients with incipient diabetic nephropathy. Diabetes Care. 1998;21(12):2135-9.
182. Nakamura T, Ushiyama C, Osada S, Hara M, Shimada N, Koide H. Pioglitazone reduces urinary podocyte excretion in type 2 diabetes patients with microalbuminuria. Metabolism. 2001;50(10):1193-6.
183. Isshiki K, Haneda M, Koya D, Maeda S, Sugimoto T, Kikkawa R. Thiazolidinedione compounds ameliorate glomerular dysfunction independent of their insulin-sensitizing action in diabetic rats. Diabetes. 2000;49(6):1022-32.
184. Ma LJ, Marcantoni C, Linton MF, Fazio S, Fogo AB. Peroxisome proliferator-activated receptor-gamma agonist troglitazone protects against nondiabetic glomerulosclerosis in rats. Kidney Int. 2001;59(5):1899-910.

185. Lennon R, Welsh GI, Singh A, Satchell SC, Coward RJ, Tavaré JM, et al. Rosiglitazone enhances glucose uptake in glomerular podocytes using the glucose transporter GLUT1. Diabetologia. 2009;52(9):1944-52.
186. Nissen SE, Wolski K. Effect of rosiglitazone on the risk of myocardial infarction and death from cardiovascular causes. N Engl J Med. 2007;356(24):2457-71.
187. Xiao T, Guan X, Nie L, Wang S, Sun L, He T, et al. Rapamycin promotes podocyte autophagy and ameliorates renal injury in diabetic mice. Mol Cell Biochem. 2014;394(1-2):145-54.
188. Lloberas N, Cruzado JM, Franquesa M, Herrero-Fresneda I, Torras J, Alperovich G, et al. Mammalian target of rapamycin pathway blockade slows progression of diabetic kidney disease in rats. J Am Soc Nephrol. 2006;17(5):1395-404.
189. Inoki K, Mori H, Wang J, Suzuki T, Hong S, Yoshida S, et al. mTORC1 activation in podocytes is a critical step in the development of diabetic nephropathy in mice. J Clin Invest. 2011;121(6):2181-96.
190. Sarbassov DD, Ali SM, Sengupta S, Sheen JH, Hsu PP, Bagley AF, et al. Prolonged rapamycin treatment inhibits mTORC2 assembly and Akt/PKB. Mol Cell. 2006;22(2):159-68.
191. Cha JJ, Hyun YY, Lee MH, Kim JE, Nam DH, Song HK, et al. Renal protective effects of toll-like receptor 4 signaling blockade in type 2 diabetic mice. Endocrinology. 2013;154(6):2144-55.
192. Ahmadian M, Suh JM, Hah N, Liddle C, Atkins AR, Downes M, et al. PPARγ signaling and metabolism: the good, the bad and the future. Nat Med. 2013;19(5):557-66.
193. Huang SS, Ding DF, Chen S, Dong CL, Ye XL, Yuan YG, et al. Resveratrol protects podocytes against apoptosis via stimulation of autophagy in a mouse model of diabetic nephropathy. Sci Rep. 2017;7:45692.
194. Li B, Xiao X, Miao Y, Guo L, Zhen J, Li X, et al. Resveratrol alleviates obesity-associated podocyte injury in ovariectomized obese rats. Exp Ther Med. 2020;19(1):123-30.
195. Qin X, Jiang M, Zhao Y, Gong J, Su H, Yuan F, et al. Berberine protects against diabetic kidney disease via promoting PGC-1α-regulated mitochondrial energy homeostasis. Br J Pharmacol. 2019.
196. Lehtonen S. SHIPping out diabetes-Metformin, an old friend among new SHIP2 inhibitors. Acta Physiol (Oxf). 2020;228(1):e13349.
197. Rogacka D, Audzeyenka I, Rychłowski M, Rachubik P, Szrejder M, Angielski S, et al. Metformin overcomes high glucose-induced insulin resistance of podocytes by pleiotropic effects on SIRT1 and AMPK. Biochim Biophys Acta Mol Basis Dis. 2018;1864(1):115-25.
198. Lee RC, Feinbaum RL, Ambros V. The C. elegans heterochronic gene lin-4 encodes small RNAs with antisense complementarity to lin-14. Cell. 1993;75(5):843-54.
199. Friedman RC, Farh KK, Burge CB, Bartel DP. Most mammalian mRNAs are conserved targets of microRNAs. Genome Res. 2009;19(1):92-105.
200. Kozomara A, Griffiths-Jones S. miRBase: annotating high confidence microRNAs using deep sequencing data. Nucleic Acids Res. 2014;42(Database issue):D68-73.
201. Lorenzen JM, Thum T. Circulating and urinary microRNAs in kidney disease. Clin J Am Soc Nephrol. 2012;7(9):1528-33.

202. Yekta S, Shih IH, Bartel DP. MicroRNA-directed cleavage of HOXB8 mRNA. Science. 2004;304(5670):594-6.
203. Huntzinger E, Izaurralde E. Gene silencing by microRNAs: contributions of translational repression and mRNA decay. Nat Rev Genet. 2011;12(2):99-110.
204. Xu W, San Lucas A, Wang Z, Liu Y. Identifying microRNA targets in different gene regions. BMC Bioinformatics. 2014;15 Suppl 7:S4.
205. Dharap A, Pokrzywa C, Murali S, Pandi G, Vemuganti R. MicroRNA miR-324-3p induces promoter-mediated expression of RelA gene. PLoS One. 2013;8(11):e79467.
206. Vasudevan S. Posttranscriptional upregulation by microRNAs. Wiley Interdiscip Rev RNA. 2012;3(3):311-30.
207. Landgraf P, Rusu M, Sheridan R, Sewer A, Iovino N, Aravin A, et al. A mammalian microRNA expression atlas based on small RNA library sequencing. Cell. 2007;129(7):1401-14.
208. Ludwig N, Leidinger P, Becker K, Backes C, Fehlmann T, Pallasch C, et al. Distribution of miRNA expression across human tissues. Nucleic Acids Res. 2016;44(8):3865-77.
209. Wang N, Zheng J, Chen Z, Liu Y, Dura B, Kwak M, et al. Single-cell microRNA-mRNA co-sequencing reveals non-genetic heterogeneity and mechanisms of microRNA regulation. Nat Commun. 2019;10(1):95.
210. Brancati G, Großhans H. An interplay of miRNA abundance and target site architecture determines miRNA activity and specificity. Nucleic Acids Res. 2018;46(7):3259-69.
211. Bartel DP, Chen CZ. Micromanagers of gene expression: the potentially widespread influence of metazoan microRNAs. Nat Rev Genet. 2004;5(5):396-400.
212. Simpson K, Wonnacott A, Fraser DJ, Bowen T. MicroRNAs in Diabetic Nephropathy: From Biomarkers to Therapy. Curr Diab Rep. 2016;16(3):35.
213. O'Brien J, Hayder H, Zayed Y, Peng C. Overview of MicroRNA Biogenesis, Mechanisms of Actions, and Circulation. Front Endocrinol (Lausanne). 2018;9:402.
214. Han J, Lee Y, Yeom KH, Nam JW, Heo I, Rhee JK, et al. Molecular basis for the recognition of primary microRNAs by the Drosha-DGCR8 complex. Cell. 2006;125(5):887-901.
215. Khvorova A, Reynolds A, Jayasena SD. Functional siRNAs and miRNAs exhibit strand bias. Cell. 2003;115(2):209-16.
216. Nagalakshmi VK, Ren Q, Pugh MM, Valerius MT, McMahon AP, Yu J. Dicer regulates the development of nephrogenic and ureteric compartments in the mammalian kidney. Kidney Int. 2011;79(3):317-30.
217. Pastorelli LM, Wells S, Fray M, Smith A, Hough T, Harfe BD, et al. Genetic analyses reveal a requirement for Dicer1 in the mouse urogenital tract. Mamm Genome. 2009;20(3):140-51.
218. Sequeira-Lopez ML, Weatherford ET, Borges GR, Monteagudo MC, Pentz ES, Harfe BD, et al. The microRNA-processing enzyme dicer maintains juxtaglomerular cells. J Am Soc Nephrol. 2010;21(3):460-7.
219. Mladinov D, Liu Y, Mattson DL, Liang M. MicroRNAs contribute to the maintenance of cell-type-specific physiological characteristics: miR-192 targets Na+/K+-ATPase β1. Nucleic Acids Res. 2013;41(2):1273-83.
220. Chau BN, Xin C, Hartner J, Ren S, Castano AP, Linn G, et al. MicroRNA-21 promotes fibrosis of the kidney by silencing metabolic pathways. Sci Transl Med. 2012;4(121):121ra18.

221. Szeto CC, Ching-Ha KB, Ka-Bik L, Mac-Moune LF, Cheung-Lung CP, Gang W, et al. Micro-RNA expression in the urinary sediment of patients with chronic kidney diseases. Dis Markers. 2012;33(3):137-44.
222. Zhong X, Chung AC, Chen HY, Meng XM, Lan HY. Smad3-mediated upregulation of miR-21 promotes renal fibrosis. J Am Soc Nephrol. 2011;22(9):1668-81.
223. Lin L, Gan H, Zhang H, Tang W, Sun Y, Tang X, et al. MicroRNA-21 inhibits SMAD7 expression through a target sequence in the 3' untranslated region and inhibits proliferation of renal tubular epithelial cells. Mol Med Rep. 2014;10(2):707-12.
224. Brennan EP, Nolan KA, Börgeson E, Gough OS, McEvoy CM, Docherty NG, et al. Lipoxins attenuate renal fibrosis by inducing let-7c and suppressing TGFβR1. J Am Soc Nephrol. 2013;24(4):627-37.
225. Gebeshuber CA, Kornauth C, Dong L, Sierig R, Seibler J, Reiss M, et al. Focal segmental glomerulosclerosis is induced by microRNA-193a and its downregulation of WT1. Nat Med. 2013;19(4):481-7.
226. Wu J, Zheng C, Fan Y, Zeng C, Chen Z, Qin W, et al. Downregulation of microRNA-30 facilitates podocyte injury and is prevented by glucocorticoids. J Am Soc Nephrol. 2014;25(1):92-104.
227. Wu J, Zheng C, Wang X, Yun S, Zhao Y, Liu L, et al. MicroRNA-30 family members regulate calcium/calcineurin signaling in podocytes. J Clin Invest. 2015;125(11):4091-106.
228. Sun H, Li QW, Lv XY, Ai JZ, Yang QT, Duan JJ, et al. MicroRNA-17 post-transcriptionally regulates polycystic kidney disease-2 gene and promotes cell proliferation. Mol Biol Rep. 2010;37(6):2951-8.
229. Patel V, Williams D, Hajarnis S, Hunter R, Pontoglio M, Somlo S, et al. miR-17~92 miRNA cluster promotes kidney cyst growth in polycystic kidney disease. Proc Natl Acad Sci U S A. 2013;110(26):10765-70.
230. Serino G, Sallustio F, Cox SN, Pesce F, Schena FP. Abnormal miR-148b expression promotes aberrant glycosylation of IgA1 in IgA nephropathy. J Am Soc Nephrol. 2012;23(5):814-24.
231. Bao H, Chen H, Zhu X, Zhang M, Yao G, Yu Y, et al. MiR-223 downregulation promotes glomerular endothelial cell activation by upregulating importin α4 and α5 in IgA nephropathy. Kidney Int. 2014;85(3):624-35.
232. Lan YF, Chen HH, Lai PF, Cheng CF, Huang YT, Lee YC, et al. MicroRNA-494 reduces ATF3 expression and promotes AKI. J Am Soc Nephrol. 2012;23(12):2012-23.
233. Lorenzen JM, Kaucsar T, Schauerte C, Schmitt R, Rong S, Hübner A, et al. MicroRNA-24 antagonism prevents renal ischemia reperfusion injury. J Am Soc Nephrol. 2014;25(12):2717-29.
234. Qingjuan L, Xiaojuan F, Wei Z, Chao W, Pengpeng K, Hongbo L, et al. miR-148a-3p overexpression contributes to glomerular cell proliferation by targeting PTEN in lupus nephritis. Am J Physiol Cell Physiol. 2016;310(6):C470-8.
235. Yao F, Sun L, Fang W, Wang H, Yao D, Cui R, et al. Hsa-miR-371-5p inhibits human mesangial cell proliferation and promotes apoptosis in lupus nephritis by directly targeting hypoxia-inducible factor 1α. Mol Med Rep. 2016;14(6):5693-8.

236. Beltrami C, Simpson K, Jesky M, Wonnacott A, Carrington C, Holmans P, et al. Association of Elevated Urinary miR-126, miR-155, and miR-29b with Diabetic Kidney Disease. Am J Pathol. 2018;188(9):1982-92.
237. Krupa A, Jenkins R, Luo DD, Lewis A, Phillips A, Fraser D. Loss of MicroRNA-192 promotes fibrogenesis in diabetic nephropathy. J Am Soc Nephrol. 2010;21(3):438-47.
238. Jenkins RH, Martin J, Phillips AO, Bowen T, Fraser DJ. Pleiotropy of microRNA-192 in the kidney. Biochem Soc Trans. 2012;40(4):762-7.
239. Deshpande SD, Putta S, Wang M, Lai JY, Bitzer M, Nelson RG, et al. Transforming growth factor-β-induced cross talk between p53 and a microRNA in the pathogenesis of diabetic nephropathy. Diabetes. 2013;62(9):3151-62.
240. Putta S, Lanting L, Sun G, Lawson G, Kato M, Natarajan R. Inhibiting microRNA-192 ameliorates renal fibrosis in diabetic nephropathy. J Am Soc Nephrol. 2012;23(3):458-69.
241. Wang Q, Wang Y, Minto AW, Wang J, Shi Q, Li X, et al. MicroRNA-377 is up-regulated and can lead to increased fibronectin production in diabetic nephropathy. FASEB J. 2008;22(12):4126-35.
242. Wang B, Komers R, Carew R, Winbanks CE, Xu B, Herman-Edelstein M, et al. Suppression of microRNA-29 expression by TGF-β1 promotes collagen expression and renal fibrosis. J Am Soc Nephrol. 2012;23(2):252-65.
243. Chen HY, Zhong X, Huang XR, Meng XM, You Y, Chung AC, et al. MicroRNA-29b inhibits diabetic nephropathy in db/db mice. Mol Ther. 2014;22(4):842-53.
244. McClelland AD, Herman-Edelstein M, Komers R, Jha JC, Winbanks CE, Hagiwara S, et al. miR-21 promotes renal fibrosis in diabetic nephropathy by targeting PTEN and SMAD7. Clin Sci (Lond). 2015;129(12):1237-49.
245. Li A, Peng R, Sun Y, Liu H, Peng H, Zhang Z. LincRNA 1700020I14Rik alleviates cell proliferation and fibrosis in diabetic nephropathy via miR-34a-5p/Sirt1/HIF-1α signaling. Cell Death Dis. 2018;9(5):461.
246. Wang B, Jha JC, Hagiwara S, McClelland AD, Jandeleit-Dahm K, Thomas MC, et al. Transforming growth factor-β1-mediated renal fibrosis is dependent on the regulation of transforming growth factor receptor 1 expression by let-7b. Kidney Int. 2014;85(2):352-61.
247. Fu Y, Zhang Y, Wang Z, Wang L, Wei X, Zhang B, et al. Regulation of NADPH oxidase activity is associated with miRNA-25-mediated NOX4 expression in experimental diabetic nephropathy. Am J Nephrol. 2010;32(6):581-9.
248. Liu Y, Li H, Liu J, Han P, Li X, Bai H, et al. Variations in MicroRNA-25 Expression Influence the Severity of Diabetic Kidney Disease. J Am Soc Nephrol. 2017;28(12):3627-38.
249. Harvey SJ, Jarad G, Cunningham J, Goldberg S, Schermer B, Harfe BD, et al. Podocyte-specific deletion of dicer alters cytoskeletal dynamics and causes glomerular disease. J Am Soc Nephrol. 2008;19(11):2150-8.
250. Ho J, Ng KH, Rosen S, Dostal A, Gregory RI, Kreidberg JA. Podocyte-specific loss of functional microRNAs leads to rapid glomerular and tubular injury. J Am Soc Nephrol. 2008;19(11):2069-75.
251. Shi S, Yu L, Chiu C, Sun Y, Chen J, Khitrov G, et al. Podocyte-selective deletion of dicer induces proteinuria and glomerulosclerosis. J Am Soc Nephrol. 2008;19(11):2159-69.

252. Zhdanova O, Srivastava S, Di L, Li Z, Tchelebi L, Dworkin S, et al. The inducible deletion of Drosha and microRNAs in mature podocytes results in a collapsing glomerulopathy. Kidney Int. 2011;80(7):719-30.
253. Boerries M, Grahammer F, Eiselein S, Buck M, Meyer C, Goedel M, et al. Molecular fingerprinting of the podocyte reveals novel gene and protein regulatory networks. Kidney Int. 2013;83(6):1052-64.
254. Henique C, Bollée G, Loyer X, Grahammer F, Dhaun N, Camus M, et al. Genetic and pharmacological inhibition of microRNA-92a maintains podocyte cell cycle quiescence and limits crescentic glomerulonephritis. Nat Commun. 2017;8(1):1829.
255. Long J, Wang Y, Wang W, Chang BH, Danesh FR. Identification of microRNA-93 as a novel regulator of vascular endothelial growth factor in hyperglycemic conditions. J Biol Chem. 2010;285(30):23457-65.
256. Shi S, Yu L, Zhang T, Qi H, Xavier S, Ju W, et al. Smad2-dependent downregulation of miR-30 is required for TGF-β-induced apoptosis in podocytes. PLoS One. 2013;8(9):e75572.
257. Long J, Wang Y, Wang W, Chang BH, Danesh FR. MicroRNA-29c is a signature microRNA under high glucose conditions that targets Sprouty homolog 1, and its in vivo knockdown prevents progression of diabetic nephropathy. J Biol Chem. 2011;286(13):11837-48.
258. Lin X, Zhen X, Huang H, Wu H, You Y, Guo P, et al. Role of MiR-155 Signal Pathway in Regulating Podocyte Injury Induced by TGF-β1. Cell Physiol Biochem. 2017;42(4):1469-80.
259. Lin X, You Y, Wang J, Qin Y, Huang P, Yang F. MicroRNA-155 deficiency promotes nephrin acetylation and attenuates renal damage in hyperglycemia-induced nephropathy. Inflammation. 2015;38(2):546-54.
260. Li M, Armelloni S, Zennaro C, Wei C, Corbelli A, Ikehata M, et al. BDNF repairs podocyte damage by microRNA-mediated increase of actin polymerization. J Pathol. 2015;235(5):731-44.
261. Xu Y, Zhang J, Fan L, He X. miR-423-5p suppresses high-glucose-induced podocyte injury by targeting Nox4. Biochem Biophys Res Commun. 2018;505(2):339-45.
262. Bai X, Geng J, Li X, Wan J, Liu J, Zhou Z, et al. Long Noncoding RNA LINC01619 Regulates MicroRNA-27a/Forkhead Box Protein O1 and Endoplasmic Reticulum Stress-Mediated Podocyte Injury in Diabetic Nephropathy. Antioxid Redox Signal. 2018;29(4):355-76.
263. Trajkovski M, Hausser J, Soutschek J, Bhat B, Akin A, Zavolan M, et al. MicroRNAs 103 and 107 regulate insulin sensitivity. Nature. 2011;474(7353):649-53.
264. Yang WM, Jeong HJ, Park SY, Lee W. Induction of miR-29a by saturated fatty acids impairs insulin signaling and glucose uptake through translational repression of IRS-1 in myocytes. FEBS Lett. 2014;588(13):2170-6.
265. Massart J, Sjögren RJO, Lundell LS, Mudry JM, Franck N, O'Gorman DJ, et al. Altered miR-29 Expression in Type 2 Diabetes Influences Glucose and Lipid Metabolism in Skeletal Muscle. Diabetes. 2017;66(7):1807-18.
266. Sun X, Lin J, Zhang Y, Kang S, Belkin N, Wara AK, et al. MicroRNA-181b Improves Glucose Homeostasis and Insulin Sensitivity by Regulating Endothelial Function in White Adipose Tissue. Circ Res. 2016;118(5):810-21.
267. Ying W, Riopel M, Bandyopadhyay G, Dong Y, Birmingham A, Seo JB, et al. Adipose Tissue Macrophage-Derived Exosomal miRNAs Can Modulate In Vivo and In Vitro Insulin Sensitivity. Cell. 2017;171(2):372-84.e12.

268. Shao Y, Ren H, Lv C, Ma X, Wu C, Wang Q. Changes of serum Mir-217 and the correlation with the severity in type 2 diabetes patients with different stages of diabetic kidney disease. Endocrine. 2017;55(1):130-8.
269. Sun J, Li ZP, Zhang RQ, Zhang HM. Repression of miR-217 protects against high glucose-induced podocyte injury and insulin resistance by restoring PTEN-mediated autophagy pathway. Biochem Biophys Res Commun. 2017;483(1):318-24.
270. Ding XQ, Gu TT, Wang W, Song L, Chen TY, Xue QC, et al. Curcumin protects against fructose-induced podocyte insulin signaling impairment through upregulation of miR-206. Mol Nutr Food Res. 2015;59(12):2355-70.
271. Wonnacott A, Bowen T, Fraser DJ. MicroRNAs as biomarkers in chronic kidney disease. Curr Opin Nephrol Hypertens. 2017;26(6):460-6.
272. Cheng Y, Wang X, Yang J, Duan X, Yao Y, Shi X, et al. A translational study of urine miRNAs in acute myocardial infarction. J Mol Cell Cardiol. 2012;53(5):668-76.
273. Beltrami C, Clayton A, Newbury LJ, Corish P, Jenkins RH, Phillips AO, et al. Stabilization of Urinary MicroRNAs by Association with Exosomes and Argonaute 2 Protein. Noncoding RNA. 2015;1(2):151-66.
274. Newbury LJ, Wonnacott A, Simpson K, Bowen T, Fraser D. Assessment of Urinary MicroRNAs by Quantitative Polymerase Chain Reaction in Diabetic Nephropathy Patients. Methods Mol Biol. 2020;2067:277-85.
275. Cheng N, Xu Y, Luo Y, Zhu L, Zhang Y, Huang K, et al. Specific and relative detection of urinary microRNA signatures in bladder cancer for point-of-care diagnostics. Chem Commun (Camb). 2017;53(30):4222-5.
276. Nakamura T, Ushiyama C, Suzuki S, Hara M, Shimada N, Ebihara I, et al. Urinary excretion of podocytes in patients with diabetic nephropathy. Nephrol Dial Transplant. 2000;15(9):1379-83.
277. Hergenreider E, Heydt S, Tréguer K, Boettger T, Horrevoets AJ, Zeiher AM, et al. Atheroprotective communication between endothelial cells and smooth muscle cells through miRNAs. Nat Cell Biol. 2012;14(3):249-56.
278. Simonson B, Das S. MicroRNA Therapeutics: the Next Magic Bullet? Mini Rev Med Chem. 2015;15(6):467-74.
279. Hanna J, Hossain GS, Kocerha J. The Potential for microRNA Therapeutics and Clinical Research. Front Genet. 2019;10:478.
280. Lithwick-Yanai G, Dromi N, Shtabsky A, Morgenstern S, Strenov Y, Feinmesser M, et al. Multicentre validation of a microRNA-based assay for diagnosing indeterminate thyroid nodules utilising fine needle aspirate smears. J Clin Pathol. 2017;70(6):500-7.
281. Lanford RE, Hildebrandt-Eriksen ES, Petri A, Persson R, Lindow M, Munk ME, et al. Therapeutic silencing of microRNA-122 in primates with chronic hepatitis C virus infection. Science. 2010;327(5962):198-201.
282. Gomez IG, MacKenna DA, Johnson BG, Kaimal V, Roach AM, Ren S, et al. Anti-microRNA-21 oligonucleotides prevent Alport nephropathy progression by stimulating metabolic pathways. J Clin Invest. 2015;125(1):141-56.
283. Wang B, Yao K, Huuskes BM, Shen HH, Zhuang J, Godson C, et al. Mesenchymal Stem Cells Deliver Exogenous MicroRNA-let7c via Exosomes to Attenuate Renal Fibrosis. Mol Ther. 2016;24(7):1290-301.
284. Ni L, Saleem M, Mathieson PW. Podocyte culture: tricks of the trade. Nephrology (Carlton). 2012;17(6):525-31.
285. Agilent Technologies U. Agilent bioanalyser 2019 [Available from: https://www.agilent.com/en/product/automated-

electrophoresis/bioanalyzer-systems/bioanalyzer-rna-kits-reagents/bioanalyzer-small-rna-analysis-228257 - productdetails.
286. Ye J, Coulouris G, Zaretskaya I, Cutcutache I, Rozen S, Madden TL. Primer-BLAST: a tool to design target-specific primers for polymerase chain reaction. BMC Bioinformatics. 2012;13:134.
287. Livak KJ, Schmittgen TD. Analysis of relative gene expression data using real-time quantitative PCR and the 2(-Delta Delta C(T)) Method. Methods. 2001;25(4):402-8.
288. Illumina. Illumina TruSeq small RNA Library Prep Reference guide 2016 [Available from: https://support.illumina.com/content/dam/illumina-support/documents/documentation/chemistry_documentation/samplepreps_truseq/truseqsmallrna/truseq-small-rna-library-prep-kit-reference-guide-15004197-02.pdf.
289. Takemoto M, Asker N, Gerhardt H, Lundkvist A, Johansson BR, Saito Y, et al. A new method for large scale isolation of kidney glomeruli from mice. Am J Pathol. 2002;161(3):799-805.
290. Hunt SE, McLaren W, Gil L, Thormann A, Schuilenburg H, Sheppard D, et al. Ensembl variation resources. Database (Oxford). 2018;2018.
291. Dobin A, Davis CA, Schlesinger F, Drenkow J, Zaleski C, Jha S, et al. STAR: ultrafast universal RNA-seq aligner. Bioinformatics. 2013;29(1):15-21.
292. Liao Y, Smyth GK, Shi W. featureCounts: an efficient general purpose program for assigning sequence reads to genomic features. Bioinformatics. 2014;30(7):923-30.
293. Love MI, Huber W, Anders S. Moderated estimation of fold change and dispersion for RNA-seq data with DESeq2. Genome Biol. 2014;15(12):550.
294. Vlachos IS, Zagganas K, Paraskevopoulou MD, Georgakilas G, Karagkouni D, Vergoulis T, et al. DIANA-miRPath v3.0: deciphering microRNA function with experimental support. Nucleic Acids Res. 2015;43(W1):W460-6.
295. Agarwal V, Bell GW, Nam JW, Bartel DP. Predicting effective microRNA target sites in mammalian mRNAs. Elife. 2015;4.
296. Wong N, Wang X. miRDB: an online resource for microRNA target prediction and functional annotations. Nucleic Acids Res. 2015;43(Database issue):D146-52.
297. Chou CH, Shrestha S, Yang CD, Chang NW, Lin YL, Liao KW, et al. miRTarBase update 2018: a resource for experimentally validated microRNA-target interactions. Nucleic Acids Res. 2018;46(D1):D296-D302.
298. Peterson SM, Thompson JA, Ufkin ML, Sathyanarayana P, Liaw L, Congdon CB. Common features of microRNA target prediction tools. Front Genet. 2014;5:23.
299. Wolf G, Chen S, Ziyadeh FN. From the periphery of the glomerular capillary wall toward the center of disease: podocyte injury comes of age in diabetic nephropathy. Diabetes. 2005;54(6):1626-34.
300. Ryu HS, Park SY, Ma D, Zhang J, Lee W. The induction of microRNA targeting IRS-1 is involved in the development of insulin resistance under conditions of mitochondrial dysfunction in hepatocytes. PLoS One. 2011;6(3):e17343.
301. Shoelson SE, Lee J, Goldfine AB. Inflammation and insulin resistance. J Clin Invest. 2006;116(7):1793-801.
302. Suárez Y, Fernández-Hernando C, Pober JS, Sessa WC. Dicer dependent microRNAs regulate gene expression and functions in human endothelial cells. Circ Res. 2007;100(8):1164-73.

303. Jovanović I, Zivković M, Jovanović J, Djurić T, Stanković A. The co-inertia approach in identification of specific microRNA in early and advanced atherosclerosis plaque. Med Hypotheses. 2014;83(1):11-5.
304. Garofalo M, Quintavalle C, Romano G, Croce CM, Condorelli G. miR221/222 in cancer: their role in tumor progression and response to therapy. Curr Mol Med. 2012;12(1):27-33.
305. Li Y, Zhao L, Shi B, Ma S, Xu Z, Ge Y, et al. Functions of miR-146a and miR-222 in Tumor-associated Macrophages in Breast Cancer. Sci Rep. 2015;5:18648.
306. Shi Z, Zhao C, Guo X, Ding H, Cui Y, Shen R, et al. Differential expression of microRNAs in omental adipose tissue from gestational diabetes mellitus subjects reveals miR-222 as a regulator of ERα expression in estrogen-induced insulin resistance. Endocrinology. 2014;155(5):1982-90.
307. Zhou L, Jiang F, Chen X, Liu Z, Ouyang Y, Zhao W, et al. Downregulation of miR-221/222 by a microRNA sponge promotes apoptosis in oral squamous cell carcinoma cells through upregulation of PTEN. Oncol Lett. 2016;12(6):4419-26.
308. Wong QW, Ching AK, Chan AW, Choy KW, To KF, Lai PB, et al. MiR-222 overexpression confers cell migratory advantages in hepatocellular carcinoma through enhancing AKT signaling. Clin Cancer Res. 2010;16(3):867-75.
309. Ono K, Igata M, Kondo T, Kitano S, Takaki Y, Hanatani S, et al. Identification of microRNA that represses IRS-1 expression in liver. PLoS One. 2018;13(1):e0191553.
310. Thai TH, Calado DP, Casola S, Ansel KM, Xiao C, Xue Y, et al. Regulation of the germinal center response by microRNA-155. Science. 2007;316(5824):604-8.
311. Rodriguez A, Vigorito E, Clare S, Warren MV, Couttet P, Soond DR, et al. Requirement of bic/microRNA-155 for normal immune function. Science. 2007;316(5824):608-11.
312. Kroesen BJ, Teteloshvili N, Smigielska-Czepiel K, Brouwer E, Boots AM, van den Berg A, et al. Immuno-miRs: critical regulators of T-cell development, function and ageing. Immunology. 2015;144(1):1-10.
313. Blüml S, Bonelli M, Niederreiter B, Puchner A, Mayr G, Hayer S, et al. Essential role of microRNA-155 in the pathogenesis of autoimmune arthritis in mice. Arthritis Rheum. 2011;63(5):1281-8.
314. Xin Q, Li J, Dang J, Bian X, Shan S, Yuan J, et al. miR-155 Deficiency Ameliorates Autoimmune Inflammation of Systemic Lupus Erythematosus by Targeting S1pr1 in Faslpr/lpr Mice. J Immunol. 2015;194(11):5437-45.
315. Chen Z, Ma T, Huang C, Hu T, Li J. The pivotal role of microRNA-155 in the control of cancer. J Cell Physiol. 2014;229(5):545-50.
316. Roehle A, Hoefig KP, Repsilber D, Thorns C, Ziepert M, Wesche KO, et al. MicroRNA signatures characterize diffuse large B-cell lymphomas and follicular lymphomas. Br J Haematol. 2008;142(5):732-44.
317. Miller AM, Gilchrist DS, Nijjar J, Araldi E, Ramirez CM, Lavery CA, et al. MiR-155 has a protective role in the development of non-alcoholic hepatosteatosis in mice. PLoS One. 2013;8(8):e72324.
318. Kim S, Lee E, Jung J, Lee JW, Kim HJ, Kim J, et al. microRNA-155 positively regulates glucose metabolism via PIK3R1-FOXO3a-cMYC axis in breast cancer. Oncogene. 2018;37(22):2982-91.
319. Cui B, Chen L, Zhang S, Mraz M, Fecteau JF, Yu J, et al. MicroRNA-155 influences B-cell receptor signaling and associates with aggressive disease in chronic lymphocytic leukemia. Blood. 2014;124(4):546-54.

320. Kong W, Yang H, He L, Zhao JJ, Coppola D, Dalton WS, et al. MicroRNA-155 is regulated by the transforming growth factor beta/Smad pathway and contributes to epithelial cell plasticity by targeting RhoA. Mol Cell Biol. 2008;28(22):6773-84.
321. Zhang Y, Mei H, Chang X, Chen F, Zhu Y, Han X. Adipocyte-derived microvesicles from obese mice induce M1 macrophage phenotype through secreted miR-155. J Mol Cell Biol. 2016;8(6):505-17.
322. Boldin MP, Taganov KD, Rao DS, Yang L, Zhao JL, Kalwani M, et al. miR-146a is a significant brake on autoimmunity, myeloproliferation, and cancer in mice. J Exp Med. 2011;208(6):1189-201.
323. Alidoust M, Hamzehzadeh L, Rivandi M, Pasdar A. Polymorphisms in non-coding RNAs and risk of colorectal cancer: A systematic review and meta-analysis. Crit Rev Oncol Hematol. 2018;132:100-10.
324. Long JP, Dong LF, Chen FF, Fan YF. miR-146a-5p targets interleukin-1 receptor-associated kinase 1 to inhibit the growth, migration, and invasion of breast cancer cells. Oncol Lett. 2019;17(2):1573-80.
325. Salazar-Ruales C, Arguello JV, López-Cortés A, Cabrera-Andrade A, García-Cárdenas JM, Guevara-Ramírez P, et al. Salivary MicroRNAs for Early Detection of Head and Neck Squamous Cell Carcinoma: A Case-Control Study in the High Altitude Mestizo Ecuadorian Population. Biomed Res Int. 2018;2018:9792730.
326. Zhuang P, Muraleedharan CK, Xu S. Intraocular Delivery of miR-146 Inhibits Diabetes-Induced Retinal Functional Defects in Diabetic Rat Model. Invest Ophthalmol Vis Sci. 2017;58(3):1646-55.
327. Lee HW, Khan SQ, Khaliqdina S, Altintas MM, Grahammer F, Zhao JL, et al. Absence of miR-146a in Podocytes Increases Risk of Diabetic Glomerulopathy via Up-regulation of ErbB4 and Notch-1. J Biol Chem. 2017;292(2):732-47.
328. Wu D, Xi QY, Cheng X, Dong T, Zhu XT, Shu G, et al. miR-146a-5p inhibits TNF-α-induced adipogenesis via targeting insulin receptor in primary porcine adipocytes. J Lipid Res. 2016;57(8):1360-72.
329. Ohana R, Weiman-Kelman B, Raviv S, Tamm ER, Pasmanik-Chor M, Rinon A, et al. MicroRNAs are essential for differentiation of the retinal pigmented epithelium and maturation of adjacent photoreceptors. Development. 2015;142(14):2487-98.
330. Courboulin A, Paulin R, Giguère NJ, Saksouk N, Perreault T, Meloche J, et al. Role for miR-204 in human pulmonary arterial hypertension. J Exp Med. 2011;208(3):535-48.
331. He H, Chen K, Wang F, Zhao L, Wan X, Wang L, et al. miR-204-5p promotes the adipogenic differentiation of human adipose-derived mesenchymal stem cells by modulating DVL3 expression and suppressing Wnt/β-catenin signaling. Int J Mol Med. 2015;35(6):1587-95.
332. Lin YC, Lin JF, Tsai TF, Chou KY, Chen HE, Hwang TI. Tumor suppressor miRNA-204-5p promotes apoptosis by targeting BCL2 in prostate cancer cells. Asian J Surg. 2017;40(5):396-406.
333. Sacconi A, Biagioni F, Canu V, Mori F, Di Benedetto A, Lorenzon L, et al. miR-204 targets Bcl-2 expression and enhances responsiveness of gastric cancer. Cell Death Dis. 2012;3:e423.
334. Imam JS, Plyler JR, Bansal H, Prajapati S, Bansal S, Rebeles J, et al. Genomic loss of tumor suppressor miRNA-204 promotes cancer cell migration and invasion by activating AKT/mTOR/Rac1 signaling and actin reorganization. PLoS One. 2012;7(12):e52397.

335. Civelek M, Hagopian R, Pan C, Che N, Yang WP, Kayne PS, et al. Genetic regulation of human adipose microRNA expression and its consequences for metabolic traits. Hum Mol Genet. 2013;22(15):3023-37.
336. Han X, Li Q, Wang C, Li Y. MicroRNA-204-3p Attenuates High Glucose-Induced MPC5 Podocytes Apoptosis by Targeting Braykinin B2 Receptor. Exp Clin Endocrinol Diabetes. 2018.
337. Xu JW, Wang TX, You L, Zheng LF, Shu H, Zhang TP, et al. Insulin-like growth factor 1 receptor (IGF-1R) as a target of MiR-497 and plasma IGF-1R levels associated with TNM stage of pancreatic cancer. PLoS One. 2014;9(3):e92847.
338. Yan JJ, Zhang YN, Liao JZ, Ke KP, Chang Y, Li PY, et al. MiR-497 suppresses angiogenesis and metastasis of hepatocellular carcinoma by inhibiting VEGFA and AEG-1. Oncotarget. 2015;6(30):29527-42.
339. Wang W, Ren F, Wu Q, Jiang D, Li H, Shi H. MicroRNA-497 suppresses angiogenesis by targeting vascular endothelial growth factor A through the PI3K/AKT and MAPK/ERK pathways in ovarian cancer. Oncol Rep. 2014;32(5):2127-33.
340. Wang L, Li B, Li L, Wang T. MicroRNA-497 suppresses proliferation and induces apoptosis in prostate cancer cells. Asian Pac J Cancer Prev. 2013;14(6):3499-502.
341. Wang L, Jiang CF, Li DM, Ge X, Shi ZM, Li CY, et al. MicroRNA-497 inhibits tumor growth and increases chemosensitivity to 5-fluorouracil treatment by targeting KSR1. Oncotarget. 2016;7(3):2660-71.
342. Guo ST, Jiang CC, Wang GP, Li YP, Wang CY, Guo XY, et al. MicroRNA-497 targets insulin-like growth factor 1 receptor and has a tumour suppressive role in human colorectal cancer. Oncogene. 2013;32(15):1910-20.
343. Xu Y, Chen J, Gao C, Zhu D, Xu X, Wu C, et al. MicroRNA-497 inhibits tumor growth through targeting insulin receptor substrate 1 in colorectal cancer. Oncol Lett. 2017;14(6):6379-86.
344. Wang X, Wang M, Li H, Lan X, Liu L, Li J, et al. Upregulation of miR-497 induces hepatic insulin resistance in E3 rats with HFD-MetS by targeting insulin receptor. Mol Cell Endocrinol. 2015;416:57-69.
345. Chen JS, Liang LL, Xu HX, Chen F, Shen SL, Chen W, et al. miR-338-3p inhibits epithelial-mesenchymal transition and metastasis in hepatocellular carcinoma cells. Oncotarget. 2017;8(42):71418-29.
346. Huang N, Wu Z, Lin L, Zhou M, Wang L, Ma H, et al. MiR-338-3p inhibits epithelial-mesenchymal transition in gastric cancer cells by targeting ZEB2 and MACC1/Met/Akt signaling. Oncotarget. 2015;6(17):15222-34.
347. Chen JT, Yao KH, Hua L, Zhang LP, Wang CY, Zhang JJ. MiR-338-3p inhibits the proliferation and migration of gastric cancer cells by targeting ADAM17. Int J Clin Exp Pathol. 2015;8(9):10922-8.
348. Zhang X, Wang C, Li H, Niu X, Liu X, Pei D, et al. miR-338-3p inhibits the invasion of renal cell carcinoma by downregulation of ALK5. Oncotarget. 2017;8(38):64106-13.
349. Zhuang Y, Dai J, Wang Y, Zhang H, Li X, Wang C, et al. MiR-338* suppresses fibrotic pathogenesis in pulmonary fibrosis through targeting LPA1. Am J Transl Res. 2016;8(7):3197-205.
350. Zhang P, Shao G, Lin X, Liu Y, Yang Z. MiR-338-3p inhibits the growth and invasion of non-small cell lung cancer cells by targeting IRS2. Am J Cancer Res. 2017;7(1):53-63.

351. Chen X, Pan M, Han L, Lu H, Hao X, Dong Q. miR-338-3p suppresses neuroblastoma proliferation, invasion and migration through targeting PREX2a. FEBS Lett. 2013;587(22):3729-37.
352. Dou L, Wang S, Sun L, Huang X, Zhang Y, Shen T, et al. Mir-338-3p Mediates Tnf-A-Induced Hepatic Insulin Resistance by Targeting PP4r1 to Regulate PP4 Expression. Cell Physiol Biochem. 2017;41(6):2419-31.
353. Magee GM, Bilous RW, Cardwell CR, Hunter SJ, Kee F, Fogarty DG. Is hyperfiltration associated with the future risk of developing diabetic nephropathy? A meta-analysis. Diabetologia. 2009;52(4):691-7.
354. Gaudet AD, Fonken LK, Gushchina LV, Aubrecht TG, Maurya SK, Periasamy M, et al. miR-155 Deletion in Female Mice Prevents Diet-Induced Obesity. Sci Rep. 2016;6:22862.
355. Lin X, Qin Y, Jia J, Lin T, Chen L, Zeng H, et al. MiR-155 Enhances Insulin Sensitivity by Coordinated Regulation of Multiple Genes in Mice. PLoS Genet. 2016;12(10):e1006308.
356. Bhatt K, Lanting LL, Jia Y, Yadav S, Reddy MA, Magilnick N, et al. Anti-Inflammatory Role of MicroRNA-146a in the Pathogenesis of Diabetic Nephropathy. J Am Soc Nephrol. 2016;27(8):2277-88.
357. Mann M, Mehta A, Zhao JL, Lee K, Marinov GK, Garcia-Flores Y, et al. An NF-κB-microRNA regulatory network tunes macrophage inflammatory responses. Nat Commun. 2017;8(1):851.
358. Han Y, Li Y, Jiang Y. The Prognostic Value of Plasma MicroRNA-155 and MicroRNA-146a Level in Severe Sepsis and Sepsis-Induced Acute Lung Injury Patients. Clin Lab. 2016;62(12):2355-60.
359. Huang Y, Liu Y, Li L, Su B, Yang L, Fan W, et al. Involvement of inflammation-related miR-155 and miR-146a in diabetic nephropathy: implications for glomerular endothelial injury. BMC Nephrol. 2014;15:142.
360. Chartoumpekis DV, Zaravinos A, Ziros PG, Iskrenova RP, Psyrogiannis AI, Kyriazopoulou VE, et al. Differential expression of microRNAs in adipose tissue after long-term high-fat diet-induced obesity in mice. PLoS One. 2012;7(4):e34872.
361. Kwak SJ, Paeng J, Kim DH, Lee SH, Nam BY, Kang HY, et al. Local kallikrein-kinin system is involved in podocyte apoptosis under diabetic conditions. Apoptosis. 2011;16(5):478-90.
362. Lang H, Xiang Y, Lin N, Ai Z, You Z, Xiao J, et al. Identification of a Panel of MiRNAs as Positive Regulators of Insulin Release in Pancreatic B-Cells. Cell Physiol Biochem. 2018;48(1):185-93.
363. Liu B, Shyr Y, Cai J, Liu Q. Interplay between miRNAs and host genes and their role in cancer. Brief Funct Genomics. 2018;18(4):255-66.
364. van Eekelen M, Runtuwene V, Masselink W, den Hertog J. Pair-wise regulation of convergence and extension cell movements by four phosphatases via RhoA. PLoS One. 2012;7(4):e35913.
365. Reedijk M, Liu X, van der Geer P, Letwin K, Waterfield MD, Hunter T, et al. Tyr721 regulates specific binding of the CSF-1 receptor kinase insert to PI 3'-kinase SH2 domains: a model for SH2-mediated receptor-target interactions. EMBO J. 1992;11(4):1365-72.
366. Zhang S, Hulver MW, McMillan RP, Cline MA, Gilbert ER. The pivotal role of pyruvate dehydrogenase kinases in metabolic flexibility. Nutr Metab (Lond). 2014;11(1):10.

367. Liu D, Li S, Cui Y, Tong H, Yan Y. Podocan affects C2C12 myogenic differentiation by enhancing Wnt/β-catenin signaling. J Cell Physiol. 2019;234(7):11130-9.
368. Rui L, Yuan M, Frantz D, Shoelson S, White MF. SOCS-1 and SOCS-3 block insulin signaling by ubiquitin-mediated degradation of IRS1 and IRS2. J Biol Chem. 2002;277(44):42394-8.
369. Baran CP, Tridandapani S, Helgason CD, Humphries RK, Krystal G, Marsh CB. The inositol 5'-phosphatase SHIP-1 and the Src kinase Lyn negatively regulate macrophage colony-stimulating factor-induced Akt activity. J Biol Chem. 2003;278(40):38628-36.
370. Nio Y, Okawara M, Okuda S, Matsuo T, Furuyama N. Podocan Is Expressed in Blood and Adipose Tissue and Correlates Negatively With the Induction of Diabetic Nephropathy. J Endocr Soc. 2017;1(7):772-86.
371. Thomson DW, Bracken CP, Szubert JM, Goodall GJ. On measuring miRNAs after transient transfection of mimics or antisense inhibitors. PLoS One. 2013;8(1):e55214.
372. Hendrickson DG, Hogan DJ, McCullough HL, Myers JW, Herschlag D, Ferrell JE, et al. Concordant regulation of translation and mRNA abundance for hundreds of targets of a human microRNA. PLoS Biol. 2009;7(11):e1000238.
373. Guo H, Ingolia NT, Weissman JS, Bartel DP. Mammalian microRNAs predominantly act to decrease target mRNA levels. Nature. 2010;466(7308):835-40.
374. Selbach M, Schwanhäusser B, Thierfelder N, Fang Z, Khanin R, Rajewsky N. Widespread changes in protein synthesis induced by microRNAs. Nature. 2008;455(7209):58-63.
375. Fridrich A, Hazan Y, Moran Y. Too Many False Targets for MicroRNAs: Challenges and Pitfalls in Prediction of miRNA Targets and Their Gene Ontology in Model and Non-model Organisms. Bioessays. 2019;41(4):e1800169.
376. Engelman JA. Targeting PI3K signalling in cancer: opportunities, challenges and limitations. Nat Rev Cancer. 2009;9(8):550-62.
377. Huang X, Shen Y, Liu M, Bi C, Jiang C, Iqbal J, et al. Quantitative proteomics reveals that miR-155 regulates the PI3K-AKT pathway in diffuse large B-cell lymphoma. Am J Pathol. 2012;181(1):26-33.
378. Thauvin-Robinet C, Auclair M, Duplomb L, Caron-Debarle M, Avila M, St-Onge J, et al. PIK3R1 mutations cause syndromic insulin resistance with lipoatrophy. Am J Hum Genet. 2013;93(1):141-9.
379. Mauvais-Jarvis F, Ueki K, Fruman DA, Hirshman MF, Sakamoto K, Goodyear LJ, et al. Reduced expression of the murine p85alpha subunit of phosphoinositide 3-kinase improves insulin signaling and ameliorates diabetes. J Clin Invest. 2002;109(1):141-9.
380. Brachmann SM, Ueki K, Engelman JA, Kahn RC, Cantley LC. Phosphoinositide 3-kinase catalytic subunit deletion and regulatory subunit deletion have opposite effects on insulin sensitivity in mice. Mol Cell Biol. 2005;25(5):1596-607.
381. Duroux-Richard I, Robin M, Peillex C, Apparailly F. MicroRNAs: Fine Tuners of Monocyte Heterogeneity. Front Immunol. 2019;10:2145.
382. Rajman M, Schratt G. MicroRNAs in neural development: from master regulators to fine-tuners. Development. 2017;144(13):2310-22.
383. Garner KL, Betin VMS, Pinto V, Graham M, Abgueguen E, Barnes M, et al. Enhanced insulin receptor, but not PI3K, signalling protects podocytes from ER stress. Sci Rep. 2018;8(1):3902.

384. Menke J, Rabacal WA, Byrne KT, Iwata Y, Schwartz MM, Stanley ER, et al. Circulating CSF-1 promotes monocyte and macrophage phenotypes that enhance lupus nephritis. J Am Soc Nephrol. 2009;20(12):2581-92.
385. Theurich S, Tsaousidou E, Hanssen R, Lempradl AM, Mauer J, Timper K, et al. IL-6/Stat3-Dependent Induction of a Distinct, Obesity-Associated NK Cell Subpopulation Deteriorates Energy and Glucose Homeostasis. Cell Metab. 2017;26(1):171-84.e6.
386. Brosius FC, Alpers CE, Bottinger EP, Breyer MD, Coffman TM, Gurley SB, et al. Mouse models of diabetic nephropathy. J Am Soc Nephrol. 2009;20(12):2503-12.
387. Zhao HJ, Wang S, Cheng H, Zhang MZ, Takahashi T, Fogo AB, et al. Endothelial nitric oxide synthase deficiency produces accelerated nephropathy in diabetic mice. J Am Soc Nephrol. 2006;17(10):2664-9.
388. Hudkins KL, Pichaiwong W, Wietecha T, Kowalewska J, Banas MC, Spencer MW, et al. BTBR Ob/Ob mutant mice model progressive diabetic nephropathy. J Am Soc Nephrol. 2010;21(9):1533-42.
389. Breyer MD, Böttinger E, Brosius FC, Coffman TM, Harris RC, Heilig CW, et al. Mouse models of diabetic nephropathy. J Am Soc Nephrol. 2005;16(1):27-45.
390. Mallipattu SK, Gallagher EJ, LeRoith D, Liu R, Mehrotra A, Horne SJ, et al. Diabetic nephropathy in a nonobese mouse model of type 2 diabetes mellitus. Am J Physiol Renal Physiol. 2014;306(9):F1008-17.
391. Okazaki M, Saito Y, Udaka Y, Maruyama M, Murakami H, Ota S, et al. Diabetic nephropathy in KK and KK-Ay mice. Exp Anim. 2002;51(2):191-6.
392. Melez KA, Harrison LC, Gilliam JN, Steinberg AD. Diabetes is associated with autoimmunity in the New Zealand obese (NZO) mouse. Diabetes. 1980;29(10):835-40.
393. Jefferson JA, Shankland SJ, Pichler RH. Proteinuria in diabetic kidney disease: a mechanistic viewpoint. Kidney Int. 2008;74(1):22-36.
394. Østergaard MV, Pinto V, Stevenson K, Worm J, Fink LN, Coward RJ. DBA2J db/db mice are susceptible to early albuminuria and glomerulosclerosis that correlate with systemic insulin resistance. Am J Physiol Renal Physiol. 2017;312(2):F312-F21.
395. Hartleben B, Gödel M, Meyer-Schwesinger C, Liu S, Ulrich T, Köbler S, et al. Autophagy influences glomerular disease susceptibility and maintains podocyte homeostasis in aging mice. J Clin Invest. 2010;120(4):1084-96.
396. Fu J, Wei C, Lee K, Zhang W, He W, Chuang P, et al. Comparison of Glomerular and Podocyte mRNA Profiles in Streptozotocin-Induced Diabetes. J Am Soc Nephrol. 2016;27(4):1006-14.
397. Croce AC, Bottiroli G. Autofluorescence spectroscopy and imaging: a tool for biomedical research and diagnosis. Eur J Histochem. 2014;58(4):2461.
398. Baker MA, Davis SJ, Liu P, Pan X, Williams AM, Iczkowski KA, et al. Tissue-Specific MicroRNA Expression Patterns in Four Types of Kidney Disease. J Am Soc Nephrol. 2017;28(10):2985-92.
399. Raabe CA, Tang TH, Brosius J, Rozhdestvensky TS. Biases in small RNA deep sequencing data. Nucleic Acids Res. 2014;42(3):1414-26.
400. Kann M, Ettou S, Jung YL, Lenz MO, Taglienti ME, Park PJ, et al. Genome-Wide Analysis of Wilms' Tumor 1-Controlled Gene Expression in Podocytes Reveals Key Regulatory Mechanisms. J Am Soc Nephrol. 2015;26(9):2097-104.
401. Markel P, Shu P, Ebeling C, Carlson GA, Nagle DL, Smutko JS, et al. Theoretical and empirical issues for marker-assisted breeding of congenic mouse strains. Nat Genet. 1997;17(3):280-4.

402. Karaiskos N, Rahmatollahi M, Boltengagen A, Liu H, Hoehne M, Rinschen M, et al. A Single-Cell Transcriptome Atlas of the Mouse Glomerulus. J Am Soc Nephrol. 2018;29(8):2060-8.
403. Fu J, Akat KM, Sun Z, Zhang W, Schlondorff D, Liu Z, et al. Single-Cell RNA Profiling of Glomerular Cells Shows Dynamic Changes in Experimental Diabetic Kidney Disease. J Am Soc Nephrol. 2019;30(4):533-45.
404. Lu Y, Ye Y, Yang Q, Shi S. Single-cell RNA-sequence analysis of mouse glomerular mesangial cells uncovers mesangial cell essential genes. Kidney Int. 2017;92(2):504-13.
405. AlJanahi AA, Danielsen M, Dunbar CE. An Introduction to the Analysis of Single-Cell RNA-Sequencing Data. Mol Ther Methods Clin Dev. 2018;10:189-96.
406. Yeri A, Courtright A, Danielson K, Hutchins E, Alsop E, Carlson E, et al. Evaluation of commercially available small RNASeq library preparation kits using low input RNA. BMC Genomics. 2018;19(1):331.
407. Dard-Dascot C, Naquin D, d'Aubenton-Carafa Y, Alix K, Thermes C, van Dijk E. Systematic comparison of small RNA library preparation protocols for next-generation sequencing. BMC Genomics. 2018;19(1):118.
408. Quail MA, Otto TD, Gu Y, Harris SR, Skelly TF, McQuillan JA, et al. Optimal enzymes for amplifying sequencing libraries. Nat Methods. 2011;9(1):10-1.
409. Coenen-Stass AML, Magen I, Brooks T, Ben-Dov IZ, Greensmith L, Hornstein E, et al. Evaluation of methodologies for microRNA biomarker detection by next generation sequencing. RNA Biol. 2018;15(8):1133-45.
410. Trionfini P, Benigni A. MicroRNAs as Master Regulators of Glomerular Function in Health and Disease. J Am Soc Nephrol. 2017;28(6):1686-96.
411. Vickers KC, Palmisano BT, Shoucri BM, Shamburek RD, Remaley AT. MicroRNAs are transported in plasma and delivered to recipient cells by high-density lipoproteins. Nat Cell Biol. 2011;13(4):423-33.
412. Zhang Y, Liu D, Chen X, Li J, Li L, Bian Z, et al. Secreted monocytic miR-150 enhances targeted endothelial cell migration. Mol Cell. 2010;39(1):133-44.
413. Chang YJ, Li YS, Wu CC, Wang KC, Huang TC, Chen Z, et al. Extracellular MicroRNA-92a Mediates Endothelial Cell-Macrophage Communication. Arterioscler Thromb Vasc Biol. 2019;39(12):2492-504.
414. Valadi H, Ekström K, Bossios A, Sjöstrand M, Lee JJ, Lötvall JO. Exosome-mediated transfer of mRNAs and microRNAs is a novel mechanism of genetic exchange between cells. Nat Cell Biol. 2007;9(6):654-9.
415. Gallego Romero I, Pai AA, Tung J, Gilad Y. RNA-seq: impact of RNA degradation on transcript quantification. BMC Biol. 2014;12:42.
416. Lopez JP, Diallo A, Cruceanu C, Fiori LM, Laboissiere S, Guillet I, et al. Biomarker discovery: quantification of microRNAs and other small non-coding RNAs using next generation sequencing. BMC Med Genomics. 2015;8:35.
417. Wang X, Shen E, Wang Y, Li J, Cheng D, Chen Y, et al. Cross talk between miR-214 and PTEN attenuates glomerular hypertrophy under diabetic conditions. Sci Rep. 2016;6:31506.
418. Liu H, Wang X, Liu S, Li H, Yuan X, Feng B, et al. Effects and mechanism of miR-23b on glucose-mediated epithelial-to-mesenchymal transition in diabetic nephropathy. Int J Biochem Cell Biol. 2016;70:149-60.
419. Chen X, Zhao L, Xing Y, Lin B. Down-regulation of microRNA-21 reduces inflammation and podocyte apoptosis in diabetic nephropathy by relieving the repression of TIMP3 expression. Biomed Pharmacother. 2018;108:7-14.

420. Badal SS, Wang Y, Long J, Corcoran DL, Chang BH, Truong LD, et al. miR-93 regulates Msk2-mediated chromatin remodelling in diabetic nephropathy. Nat Commun. 2016;7:12076.
421. Zha F, Bai L, Tang B, Li J, Wang Y, Zheng P, et al. MicroRNA-503 contributes to podocyte injury via targeting E2F3 in diabetic nephropathy. J Cell Biochem. 2019;120(8):12574-81.
422. Duan YR, Chen BP, Chen F, Yang SX, Zhu CY, Ma YL, et al. Exosomal microRNA-16-5p from human urine-derived stem cells ameliorates diabetic nephropathy through protection of podocyte. J Cell Mol Med. 2019.
423. Zhang X, Yang Z, Heng Y, Miao C. MicroRNA-181 exerts an inhibitory role during renal fibrosis by targeting early growth response factor-1 and attenuating the expression of profibrotic markers. Mol Med Rep. 2019;19(4):3305-13.
424. Liu M, Liu L, Bai M, Zhang L, Ma F, Yang X, et al. Hypoxia-induced activation of Twist/miR-214/E-cadherin axis promotes renal tubular epithelial cell mesenchymal transition and renal fibrosis. Biochem Biophys Res Commun. 2018;495(3):2324-30.
425. Wang W, Tang S, Li H, Liu R, Su Y, Shen L, et al. MicroRNA-21a-5p promotes fibrosis in spinal fibroblasts after mechanical trauma. Exp Cell Res. 2018;370(1):24-30.
426. Wang G, Kwan BC, Lai FM, Chow KM, Li PK, Szeto CC. Urinary miR-21, miR-29, and miR-93: novel biomarkers of fibrosis. Am J Nephrol. 2012;36(5):412-8.
427. Xu H, Sun F, Li X, Sun L. Down-regulation of miR-23a inhibits high glucose-induced EMT and renal fibrogenesis by up-regulation of SnoN. Hum Cell. 2018;31(1):22-32.
428. Wang Y, Le Y, Xue JY, Zheng ZJ, Xue YM. Let-7d miRNA prevents TGF-β1-induced EMT and renal fibrogenesis through regulation of HMGA2 expression. Biochem Biophys Res Commun. 2016;479(4):676-82.
429. Liu S, Wang Y, Li W, Yu S, Wen Z, Chen Z, et al. miR-221-5p acts as an oncogene and predicts worse survival in patients of renal cell cancer. Biomed Pharmacother. 2019;119:109406.
430. Slaby O, Redova M, Poprach A, Nekvindova J, Iliev R, Radova L, et al. Identification of MicroRNAs associated with early relapse after nephrectomy in renal cell carcinoma patients. Genes Chromosomes Cancer. 2012;51(7):707-16.
431. Yu Z, Ni L, Chen D, Zhang Q, Su Z, Wang Y, et al. Identification of miR-7 as an oncogene in renal cell carcinoma. J Mol Histol. 2013;44(6):669-77.
432. Quan J, Li Y, Pan X, Lai Y, He T, Lin C, et al. Oncogenic miR-425-5p is associated with cellular migration, proliferation and apoptosis in renal cell carcinoma. Oncol Lett. 2018;16(2):2175-84.
433. Xiong F, Liu K, Zhang F, Sha K, Wang X, Guo X, et al. MiR-204 inhibits the proliferation and invasion of renal cell carcinoma by inhibiting RAB22A expression. Oncol Rep. 2016;35(5):3000-8.
434. Zhai W, Ma J, Zhu R, Xu C, Zhang J, Chen Y, et al. MiR-532-5p suppresses renal cancer cell proliferation by disrupting the ETS1-mediated positive feedback loop with the KRAS-NAP1L1/P-ERK axis. Br J Cancer. 2018;119(5):591-604.
435. Wang X, Wang T, Chen C, Wu Z, Bai P, Li S, et al. Serum exosomal miR-210 as a potential biomarker for clear cell renal cell carcinoma. J Cell Biochem. 2018.
436. Fedorko M, Juracek J, Stanik M, Svoboda M, Poprach A, Buchler T, et al. Detection of let-7 miRNAs in urine supernatant as potential diagnostic approach

in non-metastatic clear-cell renal cell carcinoma. Biochem Med (Zagreb). 2017;27(2):411-7.
437. Du M, Giridhar KV, Tian Y, Tschannen MR, Zhu J, Huang CC, et al. Plasma exosomal miRNAs-based prognosis in metastatic kidney cancer. Oncotarget. 2017;8(38):63703-14.
438. Leiter EH, Coleman DL, Hummel KP. The influence of genetic background on the expression of mutations at the diabetes locus in the mouse. III. Effect of H-2 haplotype and sex. Diabetes. 1981;30(12):1029-34.
439. Hinder LM, Park M, Rumora AE, Hur J, Eichinger F, Pennathur S, et al. Comparative RNA-Seq transcriptome analyses reveal distinct metabolic pathways in diabetic nerve and kidney disease. J Cell Mol Med. 2017;21(9):2140-52.
440. Brownlee M. The pathobiology of diabetic complications: a unifying mechanism. Diabetes. 2005;54(6):1615-25.
441. Sharma K. Mitochondrial hormesis and diabetic complications. Diabetes. 2015;64(3):663-72.
442. Sivaskandarajah GA, Jeansson M, Maezawa Y, Eremina V, Baelde HJ, Quaggin SE. Vegfa protects the glomerular microvasculature in diabetes. Diabetes. 2012;61(11):2958-66.
443. Chen X, Xu X, Pan B, Zeng K, Xu M, Liu X, et al. miR-150-5p suppresses tumor progression by targeting VEGFA in colorectal cancer. Aging (Albany NY). 2018;10(11):3421-37.
444. van den Heuvel AP, de Vries-Smits AM, van Weeren PC, Dijkers PF, de Bruyn KM, Riedl JA, et al. Binding of protein kinase B to the plakin family member periplakin. J Cell Sci. 2002;115(Pt 20):3957-66.
445. Suzuki A, Horiuchi A, Ashida T, Miyamoto T, Kashima H, Nikaido T, et al. Cyclin A2 confers cisplatin resistance to endometrial carcinoma cells via up-regulation of an Akt-binding protein, periplakin. J Cell Mol Med. 2010;14(9):2305-17.
446. Khalil R, Koop K, Kreutz R, Spaink HP, Hogendoorn PC, Bruijn JA, et al. Increased dynamin expression precedes proteinuria in glomerular disease. J Pathol. 2019;247(2):177-85.
447. Nigi L, Grieco GE, Ventriglia G, Brusco N, Mancarella F, Formichi C, et al. MicroRNAs as Regulators of Insulin Signaling: Research Updates and Potential Therapeutic Perspectives in Type 2 Diabetes. Int J Mol Sci. 2018;19(12).
448. Craici IM, Wagner SJ, Bailey KR, Fitz-Gibbon PD, Wood-Wentz CM, Turner ST, et al. Podocyturia predates proteinuria and clinical features of preeclampsia: longitudinal prospective study. Hypertension. 2013;61(6):1289-96.
449. Cunard R, Sharma K. The endoplasmic reticulum stress response and diabetic kidney disease. Am J Physiol Renal Physiol. 2011;300(5):F1054-61.
450. Besnard V, Dagher R, Madjer T, Joannes A, Jaillet M, Kolb M, et al. Identification of periplakin as a major regulator of lung injury and repair in mice. JCI Insight. 2018;3(5).

Appendix

The American Journal of Pathology, Vol. 188, No. 9, September 2018

ELSEVIER

The American Journal of
PATHOLOGY

ajp.amjpathol.org

BIOMARKERS, GENOMICS, PROTEOMICS, AND GENE REGULATION

Association of Elevated Urinary miR-126, miR-155, and miR-29b with Diabetic Kidney Disease

Cristina Beltrami,* Kate Simpson,*† Mark Jesky,‡ Alexa Wonnacott,* Christopher Carrington,* Peter Holmans,§ Lucy Newbury,*† Robert Jenkins,* Thomas Ashdown,* Colin Dayan,¶ Simon Satchell,‖ Peter Corish,** Paul Cockwell,‡ Donald Fraser,*† and Timothy Bowen*†

From the Wales Kidney Research Unit, Division of Infection and Immunity, the MRC Centre for Neuropsychiatric Genetics and Genomics,§ Division of Psychological Medicine and Clinical Neurosciences, and the Diabetes Research Group,¶ Division of Infection and Immunity, School of Medicine, College of Biomedical and Life Sciences, and the Cardiff Institute of Tissue Engineering and Repair,† Cardiff University, Cardiff; the Department of Renal Medicine,‡ Queen Elizabeth Hospital Birmingham, Birmingham; Bristol Renal,‖ Bristol Medical School, University of Bristol, Bristol; and the BBI Group,** The Courtyard, Cardiff, United Kingdom*

Accepted for publication June 11, 2018.

Address correspondence to Timothy Bowen, Ph.D., Wales Kidney Research Unit, Division of Infection and Immunity, School of Medicine, College of Biomedical and Life Sciences, Cardiff University, Heath Park Campus, Cardiff CF14 4XN, United Kingdom. E-mail: bowent@cf.ac.uk.

Effective diabetic kidney disease (DKD) biomarkers remain elusive, and urinary miRNAs represent a potential source of novel noninvasive disease sentinels. We profiled 754 miRNAs in pooled urine samples from DKD patients ($n = 20$), detecting significantly increased miR-126, miR-155, and miR-29b compared with controls ($n = 20$). These results were confirmed in an independent cohort of 89 DKD patients, 62 diabetic patients without DKD, and 41 controls: miR-126 (2.8-fold increase; $P < 0.0001$), miR-155 (1.8-fold increase; $P < 0.001$), and miR-29b (4.6-fold increase; $P = 0.024$). Combined receiver operating characteristic curve analysis resulted in an area under the curve of 0.8. A relative quantification threshold equivalent to 80% sensitivity for each miRNA gave a positive signal for 48% of DKD patients compared with 3.6% of diabetic patients without DKD. Laser-capture microdissection of renal biopsy specimens, followed by quantitative RT-PCR, detected miR-155 in glomeruli and proximal and distal tubules, whereas miR-126 and miR-29b were most abundant in glomerular extracts. Subsequent experiments showed miR-126 and miR-29b enrichment in glomerular endothelial cells (GEnCs) compared with podocytes, proximal tubular epithelial cells, and fibroblasts. Significantly increased miR-126 and miR-29b were detected in GEnC conditioned medium in response to tumor necrosis factor-α and transforming growth factor-β1, respectively. Our data reveal an altered urinary miRNA profile associated with DKD and link these variations to miRNA release from GEnCs. *(Am J Pathol 2018, 188: 1982–1992; https://doi.org/10.1016/j.ajpath.2018.06.006)*

Recent estimates suggest that 1 in 12 of the global population experiences diabetes mellitus, and approximately 40% of those affected will go on to develop diabetic kidney disease (DKD).[1] DKD is the leading cause of end-stage renal disease, and predisposing factors include genetic causes, ethnicity, hyperglycemia, insulin resistance, intraglomerular hypertension, and hyperfiltration.[2,3]

Supported by the National Institute for Health Research Invention for Innovation (i4i) Programme grant II-LA-0712-20003 (T.B. is the principal investigator for the grant) and the Kidney Research UK Project grant awards RP44/2014 (T.B.) and IN4/2013 (S.S.). The JABBS Foundation funded collection of the Renal Impairment in Secondary Care cohort (P.Coc.). The Wales Kidney Research Unit is funded by core support from Health and Care Research Wales (D.F.).

D.F. and T.B. contributed equally to this work as senior authors.

Disclosures: C.D. is an advisor for Novo Nordisk and provides services to Sanofi Genzyme and AstraZeneca (2015 to 2017); S.S. received travel support from Boehringer Ingelheim and UCB UK grant support (2013 to 2015); P.Cor. serves as a consultant for Life Sciences Bridging Fund Wales Consultancy (2015 to 2017); P.Coc. received funding from JABBS Foundation (2014 to 2015); T.B. and D.F. are inventors for patent WO/2017/129977 Chronic Kidney Disease Diagnostic.

The views expressed in this article are those of the authors and not necessarily those of the National Health Service, the National Institute for Health Research, or the Department of Health (United Kingdom).

https://doi.org/10.1016/j.ajpath.2018.06.006

Hyperglycemia results in numerous deleterious consequences, including up-regulated cytokine synthesis, renin-angiotensin system activation, generation of advanced glycation end products and reactive oxygen species, and increased protein kinase C activity.[4,5] Nitric oxide and NF-κB pathway–driven loss of endothelial and vascular modulation have been implicated in insulin resistance, and early DKD may be associated with insulin signaling defects specific to the podocyte.[6] These insults result in loss of glomerular filtration rate and ultimately renal failure from mesangial hyperexpansion, nodular glomerulosclerosis, and tubulointerstitial fibrosis.[7]

Detection of urinary microalbuminuria currently forms the basis of DKD progression monitoring, varying from normal mean albuminuria values of approximately 10 mg/day to a diagnosis of microalbuminuria at 30 to 300 mg/day and macroalbuminuria >300 mg/day.[8] Prognosis is complicated, because not all microalbuminuric patients progress to overt nephropathy. Several novel biomarkers have been assessed for utility in DKD, but none are being used as routine clinical markers, and they may lack specificity and sensitivity to predict individual DKD patient outcomes. In light of the above, novel markers that can discriminate etiology, progression, and/or response to treatment remain highly desirable.

miRNAs are ubiquitously expressed short noncoding RNAs that regulate the expression of most protein coding genes in the human genome, and detection of miR-192, miR-194, miR-215, miR-216, miR-146a, miR-204, and miR-886 is elevated in the kidney.[9] Urinary miRNAs represent a highly promising novel source of noninvasive biomarkers that are stabilized via argonaute 2 protein/exosome association and are rapidly and precisely detected by quantitative RT-PCR (RT-qPCR).[10]

Reports have suggested a role for miRNAs in the pathology of DKD,[11,12] including previous work from this laboratory showing decreased miR-192 in biopsy specimens from late-stage DKD patients with diminished renal function.[13] However, comparatively little is known about the abundance of urinary miRNAs in DKD patients.

We hypothesized that alterations in urinary miRNA profiles would be associated with DKD. Candidate DKD biomarkers were identified by comparing miRNA profiles in urine samples from a patient discovery cohort with those from unaffected controls. Selected candidates were then measured in a larger independent cohort. Subsequently, laser-capture microdissection (LCM) of renal biopsy specimens and *in vitro* cell culture were used to investigate the sources of our candidate urinary miRNA DKD biomarkers with respect to nephron domain and cell type.

Materials and Methods

Study Participants

DKD was defined in accordance with the National Kidney Foundation Kidney Disease Outcomes Quality Initiative Clinical Practice Guidelines and Clinical Practice Recommendations for Diabetes and Chronic Kidney Disease (CKD).[14] Accordingly, CKD should be attributable to diabetes in the presence of macroalbuminuria (in the absence of urinary infection), in the presence of microalbuminuria with concomitant diabetic retinopathy, or in type 1 diabetes of at least 10 years' duration.[14] The initial profiling study cohort

Table 1 Demographic and Clinical Parameters of Patients Recruited from Two Centers

	Patients (n = 151)		
Feature	Diabetic (n = 62)	DKD (n = 89)	Controls (n = 41)
Male sex, n (%)	37 (58)	55 (62)	18 (44)
Nonwhite, n (%)	13 (21)	33 (37)	
Age in years, means ± SD	52 ± 16.1	62 ± 13.6	55 ± 15.4
eGFR, mL/minute per 1.73 m^2			
Means ± SD	78 ± 16.3	30 ± 20.9	
Median (IQR)	84 (72–90)	22 (17–38)	
CKD stage, n (%)			
No CKD/CKD G1 (eGFR ≥ 90 mL/minute per 1.73 m^2)	23 (37)	2 (2)	
CKD G2 (eGFR = 60–89 mL/minute per 1.73 m^2)	32 (52)	10 (11)	
CKD G3 (eGFR = 30–59 mL/minute per 1.73 m^2)	5 (8)	17 (19)	
CKD G4 (eGFR = 15–29 mL/minute per 1.73 m^2)	2 (3)	45 (51)	
CKD G5 (eGFR < 15 mL/minute per 1.73 m^2)	0	15 (17)	
ACR, n (%)*			
A1: normal-high normal (ACR < 3 mg/mmol)	54 (87.1)	15 (16.9)	
A2: moderately increased (ACR = 3–30 mg/mmol)	8 (12.9)	25 (28.1)	
A3: severely increased (ACR > 30 mg/mmol)	0 (0)	49 (55.0)	

The two UK centers were as follows: Wales Kidney Research Tissue Bank, Cardiff (University Hospital Wales) and Birmingham (University Hospital Birmingham, Renal Impairment in Secondary Care Study Cohort).

*ACR group cutoffs and nomenclature derived from Kidney Disease: Improving Global Outcomes 2012 recommendations.[14]

ACR, albumin/creatinine ratio; CKD, chronic kidney disease; DKD, diabetic kidney disease; eGFR, estimated glomerular filtration rate; IQR, interquartile range.

of 20 DKD patients and 20 healthy controls was obtained from the Wales Kidney Research Tissue Bank, University Hospital of Wales (Cardiff, UK). The DKD group was predominantly male (85%), and their mean age was 72 years (SD, ±8.7 years). DKD patients were CKD stage 3 to 5 (predialysis), with a mean estimated glomerular filtration rate (eGFR) of 29 mL/minute per 1.73 m^2 (SD, ±8.5 mL/minute per 1.73 m^2) and a mean urinary albumin/creatinine ratio (ACR) of 13.5 mg/mmol (SD, ±14.5 mg/mmol). The control group ($n = 20$) in the profiling cohort was 50% male, and their mean age was 47 years (SD, ±11.0 years); they had no microalbuminuria (ACR, <3 mg/mmol). For further details on ACR categories, see Table 1.

The confirmation cohort was drawn from two secondary care facilities: the Wales Kidney Research Tissue Bank (as above) and the Renal Impairment in Secondary Care study, University Hospital of Birmingham (Birmingham, UK).[15] Eighty-nine patients with DKD, including three patients with type 1 diabetes, and 41 healthy controls were recruited across the two sites. An additional control group of 62 diabetic patients without DKD were recruited from Cardiff, including 17 patients with type 1 diabetes. Ethical approval was granted by the Wales Kidney Research Tissue Bank Governance Committee and the South Birmingham Local Research Ethics Committee, respectively.

Patient demographics and clinical parameters are shown in Table 1. All patients were recruited from specialist nephrology and diabetes care services at the two sites during the period spanning autumn 2010 to autumn 2013. DKD patients from the Renal Impairment in Secondary Care study cohort were predominantly advanced nephropaths, as per Renal Impairment in Secondary Care protocol inclusion criteria: briefly, patients with CKD stages 4 to 5 (predialysis) or CKD stage 3 and accelerated progression and/or proteinuria, as defined by the UK National Institute for Health and Care Excellence 2008 CKD guideline for secondary care review. The diabetic patient control group all had a diagnosis of diabetes by standard American Diabetes Association criteria,[16] but without evidence of DKD (ie, not fulfilling the Kidney Disease Outcomes Quality Initiative criteria).

At the initial clinic visit, renal function was recorded using eGFR, calculated using the modification of diet in renal disease equation.[17] Urine samples were aliquoted for ACR assessment and for RNA extraction (see below). ACR cutoffs for disease severity were defined as per Kidney Disease: Improving Global Outcomes 2012 guidelines.[18]

Urine Collection, RNA Isolation, and RT-qPCR Analysis

Urine samples were collected, and RNA extraction from 350 μL of urine, generation of cDNA from equal volumes of RNA extracts, and RT-qPCR were then performed, as described in detail elsewhere.[10] TaqMan assays (Thermo Fisher Scientific, Paisley, UK) used in this study were as follows: hsa-miR-29b-3p (identification number 000413), hsa-miR-126-3p (identification number 002228), hsa-miR-155-5p (identification number 002623), and hsa-miR-191-5p (identification number 002299). Relative quantities were calculated using the $2^{-\Delta\Delta Ct}$ method, and miRNA expression was normalized to hsa-miR-191-5p.[10]

miRNA Profiling by TaqManArray Human MicroRNA Cards

Urinary miRNAs were reverse transcribed using the Megaplex Primer Pools (Human Pools A version 2.1 and B version 3.0; Thermo Fisher Scientific) with a predefined pool of 381 reverse transcription primers for each Megaplex Primer Pool. A fixed volume of 3 μL of RNA solution was used as input in each reverse transcription reaction, and reverse transcription reactions were performed according to the manufacturer's recommendations. Reverse transcription reaction products were amplified using Megaplex PreAmp Primers (Primers A version 2.1 and B version 3.0; Thermo Fisher Scientific), the samples were then diluted to a final volume of 100 μL, and control subject and DKD patient products were pooled as follows.

To exclude the possibility that sex, age, and eGFR status had extreme effects on miRNA expression profiles, the following pooling strategy was followed: control pool 1, urine samples from 5 females of average age 44.8 years; control pool 2, 5 females, with average age of 57.6 years; control pool 3, 5 males, with average age of 35.2 years; and control pool 4, 5 males, with average of 53.2 years. The following patient pool (PPs) were used: PP1, urine samples from five CKD3 patients with an eGFR between 43.3 and 36 mL/minute per 1.73 m^2; PP2, five stage 3 patients, with an eGFR from 35 to 31 mL/minute per 1.73 m^2; PP3, five stage 4/5 patients, with an eGFR from 27.3 to 23 mL/minute per 1.73 m^2; and PP4, five stage 4/5 patients, with eGFR from 22 to 12.9 mL/minute per 1.73 m^2.

TaqManArray Human MicroRNA Cards A version 2.1 and B version 3.0 (Thermo Fisher Scientific) were used to quantify 754 human miRNAs. Each array included 377 test miRNAs, three endogenous controls, and a negative control. Quantitative PCR was performed on an Applied Biosystems 7900HT thermocycler (Thermo Fisher Scientific) using the manufacturer's recommended program.

LCM from Renal Biopsy Samples

Glomeruli and proximal tubular and distal tubular profiles were microdissected from sections (6 μm thick) obtained from five formalin-fixed, paraffin-embedded archived renal biopsy samples from unaffected individuals using the Arcturus Pixcell IIe infrared laser enabled LCM system (Thermo Fisher Scientific).

Cell Culture

Human conditionally immortalized glomerular endothelial cell (GEnC) and human podocyte cell lines were propagated

at 33°C, as described previously.[19,20] After 5 (GEnC) and 14 (podocyte) days, cells were transferred to 37°C incubation to inactivate the SV40 T antigen and permit differentiation, before experimental use. Where stated, GEnCs were growth arrested for 24 hours and then treated with 10 ng/mL tumor necrosis factor (TNF)-α or 1 ng/mL transforming growth factor (TGF)-β1 at either 5 mmol/L normoglycemic or 25 mmol/L hyperglycemic D-glucose concentrations for 24 hours. Proximal tubular epithelial cell line HK-2[21] and fibroblast[22] cultures were maintained as described elsewhere. Cells and culture medium obtained from each well were used for RNA extraction, as described above.

Statistical Analysis

miRNA profiling data were analyzed using Thermo Fisher Scientific's DataAssist Software version 3.01, NormFinder Software version 0.953 (*http://moma.dk/normfinder-software*, last accessed February 21, 2018), and GraphPad Prism 6 version 6.0d (GraphPad Software, La Jolla, CA). Pearson correlation coefficients were used to detect clusters of similarity in miRNA threshold cycle values between each pool group in patients and between each pool group in controls. To identify a suitable reference gene for the normalization of miRNA expression in this study, the NormFinder algorithm was applied to the expression data obtained from the Human TaqMan miRNA Arrays. Analysis comparing miRNA levels between subjects with DKD and controls was performed using GraphPad Prism 6 version 6.0d. $P < 0.05$ was considered statistically significant. miRNA profiling data sets can be found in Gene Expression Omnibus (*https://www.ncbi.nlm.nih.gov/geo*; accession number GSE114477).

Results

Altered Urinary miRNA Detection in DKD Patients

To select candidate miRNAs that may act as DKD biomarkers, data from unbiased expression profiling of 754 miRNAs in urine samples from 20 DKD patients and 20 unaffected controls were compared. Analyses were performed on four patient and four control pools, each composed of urine samples from five individuals, as recommended by Zhang and Gant.[23] Samples were pooled before profiling to minimize the contribution of subject-to-subject variation and to make substantive features easier to find, and thereby identify biomarkers common across individuals.[24] Previous analysis suggested that 40 individuals might optimally be pooled across eight arrays,[23] which was our chosen pooling approach.

miRNAs for which statistically significant fold-change increases were detected in patient urine compared with control samples (12 data points) and the corresponding down-regulated miRNAs (35 data points) are shown in Figure 1A. The fold-change data for these 47 miRNAs are summarized in Figure 1B, and the 8 miRNAs exhibiting greater than fivefold change were subsequently selected as potential candidate biomarkers for further analysis.

Specific RT-qPCR assays were then used to analyze these miRNAs in each component urine sample pooled for profiling analysis. Statistically significant differences in miRNA detection between DKD patient and control urine samples were replicated for miR-126 (4.3-fold increase; $P = 0.0087$), miR-155 (22.9-fold increase; $P = 0.0024$), and miR-29b (4.9-fold increase; $P = 0.0002$) (Figure 1, C–E).

Elevated Urinary miR-126, miR-155, and miR-29b Detection in an Independent DKD Patient Cohort

To test the above findings, miR-126, miR-155, and miR-29b were quantified in samples from an independent cohort of patients with established DKD from the Renal Impairment in Secondary Care study.[15] Samples from 89 patients meeting the criteria established in the UK National Institute for Health and Care Excellence 2008 criteria were available. An additional cohort of 62 patients with diabetes mellitus, but without proteinuria or other evidence of DKD, were included, as were samples from 41 individuals without evidence of diabetes or DKD (Table 1). Diabetes patients without DKD were included as a third group in this analysis to identify DKD-specific miRNA detection changes and not purely hyperglycemia-driven effects from our profiling comparison of DKD patients with control individuals.

Significant differences were again seen between DKD patients and controls for miR-126 (2.8-fold increase; $P < 0.0001$) (Figure 2A), miR-155 (1.8-fold increase; $P < 0.001$) (Figure 2B), and miR-29b (4.6-fold increase; $P = 0.024$) (Figure 2C). Comparison of DKD patients with diabetic patients without DKD was statistically significant for miR-126 (3.1-fold increase; $P < 0.0001$) and miR-155 (1.6-fold increase; $P = 0.024$), with a trend to increased miR-29b (4.1-fold increase; $P = 0.121$) (Figure 2, A–C).

RT-qPCR data for all three miRNAs were used to compare DKD patients and diabetic patients without DKD in the combined receiver operating characteristic curve analysis shown in Figure 2D, giving an area under the curve of 0.80. To analyze the contributions of each miRNA to the above receiver operating characteristic curve, individual specificity and likelihood ratios were calculated for relative expression values equivalent to a sensitivity of 80%.[26,27] Data displayed in Table 2 illustrate the magnitude of corresponding specificity values was miR-126 > miR-155 > miR-29b, and that combined miRNA data resulted in a ≥6.5% increase in specificity and likelihood ratio compared with individual miRNAs. These relative expression data were then used as consecutive threshold values to discriminate between DKD and diabetic patients without DKD (Table 3) from the independent cohort. The discriminatory order was miR-29b (DKD/diabetic patients without DKD = 5.62) > miR-126 (DKD/diabetic patients without

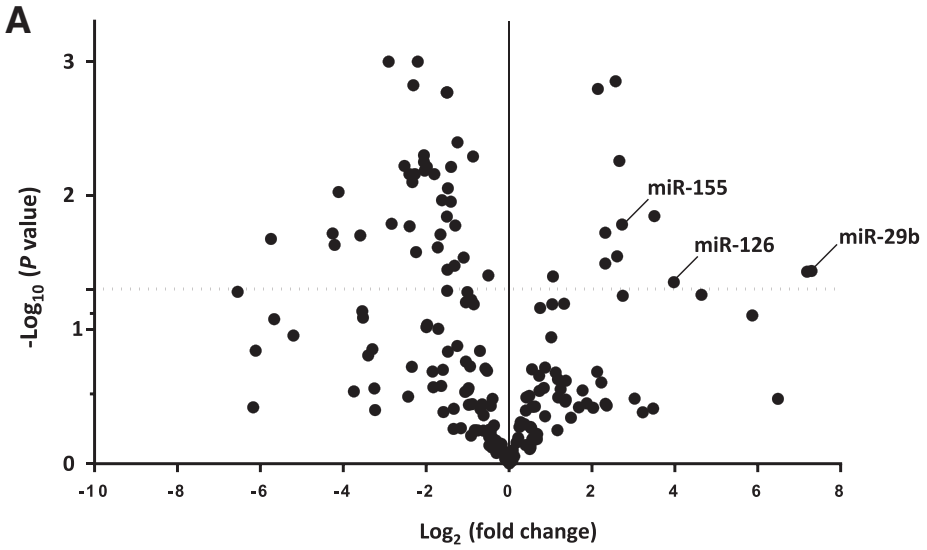
A
miR-155
miR-126
miR-29b
-Log10 (P value)
Log2 (fold change)

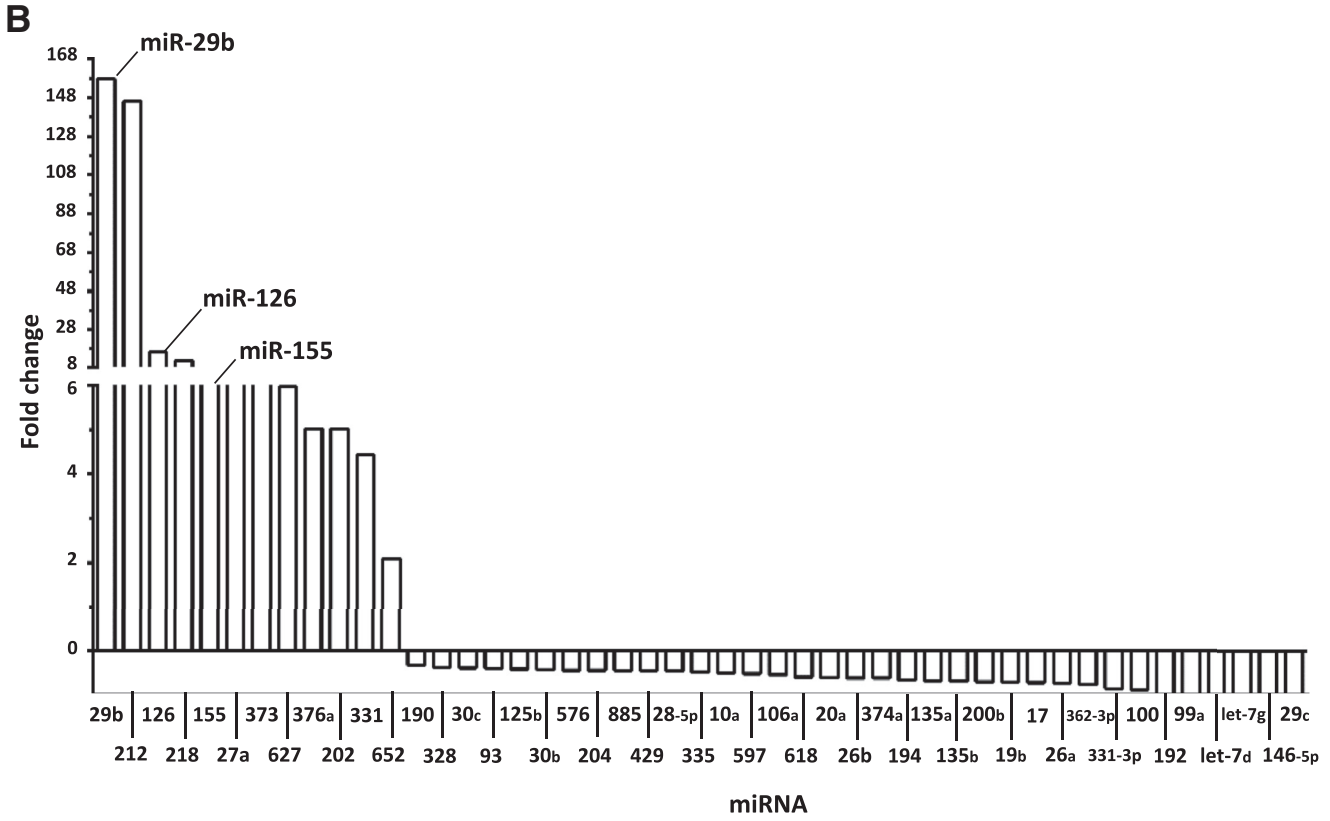
B
miR-29b
miR-126
miR-155
Fold change
29b 126 155 373 376a 331 190 30c 125b 576 885 28-5p 10a 106a 20a 374a 135a 200b 17 362-3p 100 99a let-7g 29c
212 218 27a 627 202 652 328 93 30b 204 429 335 597 618 26b 194 135b 19b 26a 331-3p 192 let-7d 146-5p
miRNA

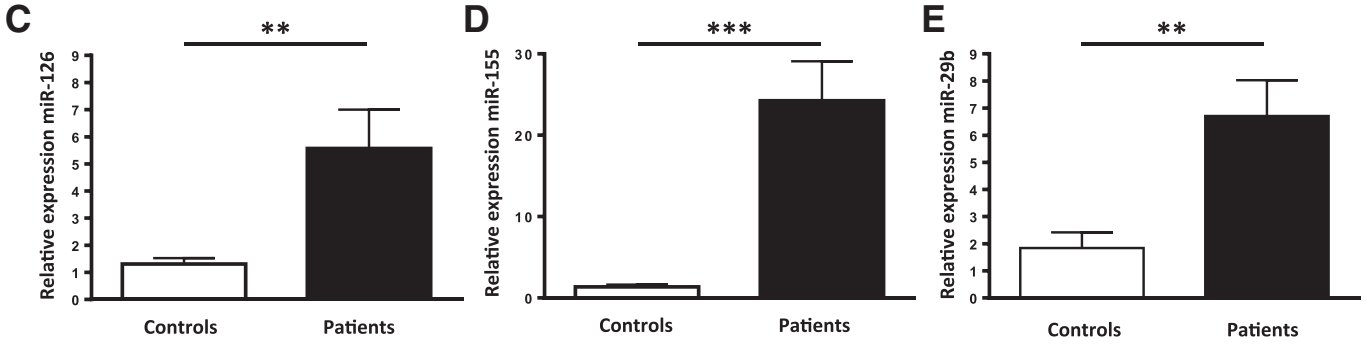
C
**
Relative expression miR-126
Controls
Patients
D
***
Relative expression miR-155
Controls
Patients
E
**
Relative expression miR-29b
Controls
Patients

DKD = 3.48) > miR-155 (DKD/diabetic patients without DKD = 2.23), and relative expression values exceeding all three thresholds were obtained for 48.0% of DKD patients compared with 3.6% of diabetic patients without DKD (Table 3).

LCM Shows Increased Glomerular Abundance of miR-126 and miR-29b That Is Replicated in GEnC Culture

Previous reports have linked changes in miRNA expression to DKD pathology, but have focused on whole tissue studies. For example, association of decreased miR-192 expression with disease progression in DKD biopsy specimens by *in situ* hybridization has been reported.[13]

Herein, LCM was used to isolate glomeruli and proximal and distal tubules (Figure 3A) from histologically normal formalin-fixed, paraffin-embedded renal biopsy samples, and miR-126, miR-155, and miR-29b expression was analyzed by RT-qPCR. In Figure 3B, a typical CD10-stained formalin-fixed, paraffin-embedded biopsy section is seen before and after LCM to isolate glomeruli and proximal and distal renal tubules. miR-126, miR-155, and miR-29b were detected in extracts from all three nephron regions (Figure 3, C–E). Increased glomerular abundances were observed for miR-126 (Figure 3C) and miR-29b (Figure 3E), whereas miR-155 was most abundant in the distal tubule (Figure 3D).

Conclusions regarding nephron region–specific miRNA expression from the above analyses are inherently limited, however, because tissue extracts are subject to trace contamination by cells from other nephron domains. Therefore, cellular miRNA localization within each nephron region was subsequently investigated by RT-qPCR analysis of podocyte and endothelial cell (GEnC) cultures from the glomerulus, renal proximal tubular epithelial cells, and fibroblasts. Detection of miR-126 was significantly higher in GEnCs compared with other cell types (Figure 3F). Most miR-155 was detected in proximal tubular epithelial cells and least miR-155 was detected in GEnCs (Figure 3G), whereas miR-29b was most abundant in GEnCs (Figure 3H).

GEnC Release of miR-126 and miR-29b in an *in Vitro* Model of Hyperglycemia Is Driven by TNF-α and TGF-β1, Respectively

The above data localized the majority of miR-126 and miR-29b expression to the GEnC. Stimuli by which miRNAs are released into the glomerular ultrafiltrate, and hence the urine, were investigated next. Data from animal models of diabetes show increased glomerular and proximal tubular epithelial cell TNF-α expression, and renoprotective effects of TGF-β inhibitors have also been reported.[28,29] GEnC expression of our candidate miRNAs was thus analyzed *in vitro* in response to TNF-α and TGF-β1 in normoglycemia and hyperglycemia (Figure 4).

The presence of TNF-α led to significantly increased miR-126 detection in GEnC conditioned medium at 5 and 25 mmol/L D-glucose (Figure 4B), a pattern also seen for miR-29b after TGF-β1 addition (Figure 4D). These cytokines did not increase GEnC expression of miR-126 (Figure 4A) or miR-29b (Figure 4C), a pattern consistent with increased release, but not expression, of miRNAs.

No significant changes in miR-155 were detected in response to elevated D-glucose with either cytokine, and data for TNF-α are shown (Figure 4, E and F). Similarly, changes in miR-126 after TGF-β1 addition, and for miR-29b in the presence of TNF-α, were not observed (data not shown). Elevated D-glucose alone did not change miRNA expression in GEnCs or conditioned medium (Figure 4).

Discussion

DKD is the leading cause of kidney failure, requiring renal replacement therapy worldwide, but effective methods to identify and halt progression of disease-specific pathophysiological changes remain elusive. Current effective interventions, such as control of blood glucose and blood pressure, are challenging to achieve, costly, and time intensive. Existing tests track DKD from diabetic diagnosis to kidney failure, but do not allow accurate prognosis for the individual patient. In addition, the absence of treatment response biomarkers hinders development of emerging DKD therapies. There is, thus, an unmet need for additional DKD biomarkers to target intervention and follow response to therapy.

In this study, urinary miRNA DKD biomarkers were identified. Increased detection of miR-126, miR-155, and miR-29b was observed in the urine of DKD patients in comparison with both unaffected individuals and diabetic patients without DKD. miRNA localization and release studies further suggested specific release of miR-126 and miR-29b from GEnCs. This raised the possibility that

Figure 1 Urinary miRNA detection in urine samples from diabetic kidney disease (DKD) patients and control subjects. **A:** Volcano plot showing the detection profile of the 377 urinary miRNAs in TaqManArray Human MicroRNA Card A in DKD patients and controls. The **dotted horizontal line** represents a *P*-value boundary of 0.05. **B:** Fold change of miRNA detection between DKD patients and controls. DataAssist Softwarewas used to perform relative quantification for sample comparison, to perform *t*-test sample group comparisons, and to produce the graphic output shown. **C–E:** Quantitative RT-PCR (RT-qPCR) analysis shows significant differences in detection of miR-126 (**C**), miR-155 (**D**), and miR-29b (**E**) between patients and control urine in the component urine samples pooled for profiling analyses (**A** and **B**). **C–E:** DKD patients versus controls for miR-126 (**C**), miR-155 (**D**), and miR-29b (**E**). Analysis was performed by unpaired two-tailed *t*-test with Welch's correction. Profiling data analysis using the NormFinder algorithm identified miR-191 as optimal for normalization of RT-qPCR data. Data were normalized to endogenous control miR-191 and are expressed as means ± SEM (**C–E**). $n = 20$ (**A**, DKD patients and controls, four pools of five patients, and **C–E**, each group). $^{**}P < 0.01$, $^{***}P < 0.001$.

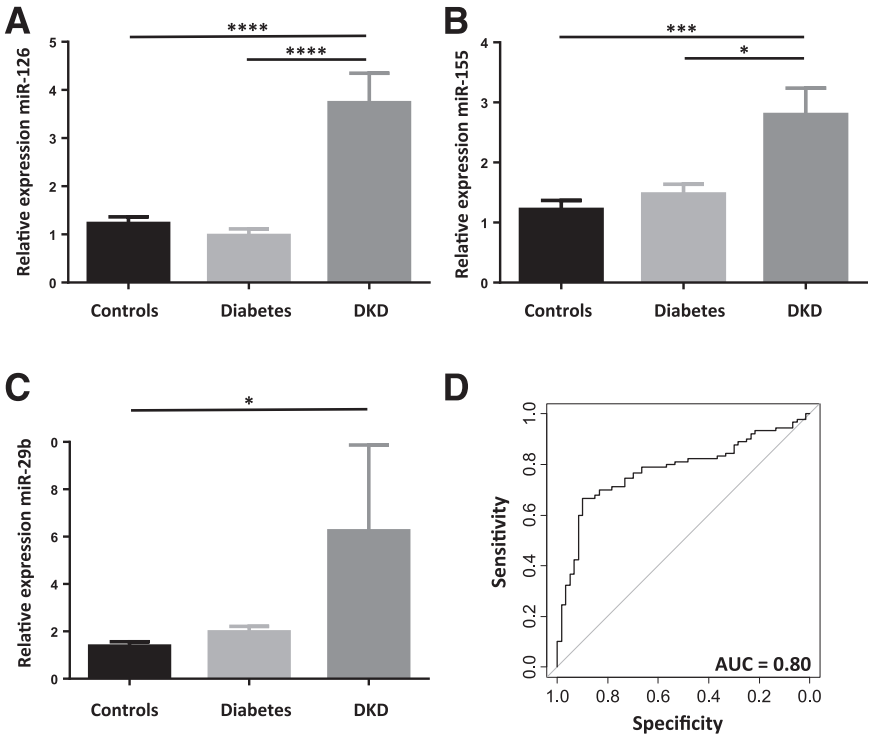

Figure 2 Quantitative RT-PCR detection of selected miRNAs in patients and control subjects. **A**–**C:** Relative expression was significantly different in 89 diabetic kidney disease (DKD) patients compared with 62 diabetic patients without DKD and 41 controls for miR-126 (**A**) and miR-155 (**B**), and significantly different in DKD patients compared with controls for miR-29b (**C**). **A:** DKD patients versus diabetic patients without DKD and controls. **B:** DKD patients and diabetic patients without DKD; DKD patients versus controls. **C:** DKD patients versus controls. Analysis was performed by unpaired one-tailed *t*-test with Welch's correction. Data were normalized to endogenous control miR-191. **D:** Combined receiver operating characteristic curve analysis for miR-126, miR-155, and miR-29b, with an area under the curve (AUC) of 0.80. Data were generated using the pROC package (*http://expasy.org/tools/pROC*)[25] in R-3.2.3. Data are expressed as means ± SEM (**A**–**C**). $n = 89$ (**A**–**C**, DKD patients); $n = 62$ (**A**–**C**, diabetic patients without DKD); $n = 41$ (**A**–**C**, controls). $^{*}P < 0.05$, $^{***}P < 0.001$, and $^{****}P < 0.0001$.

urinary miRNA quantification might provide data on ongoing pathologic processes, and so aid patient stratification and measurement of response to therapy.

Urinary miRNA biomarkers have several potential significant advantages over circulating miRNAs for adoption into existing treatment pathways alongside current biomarkers, including speed and cost of noninvasive sample access.[30] However, few urinary miRNA DKD biomarker data have so far been reported. Previous studies have focused on circulating miRNAs and have generated conflicting data with respect to association of miR-126 with diabetes mellitus and/or DKD. A recent cross-sectional analysis of type 2 diabetes mellitus patients found a negative association with plasma miR-126,[31] and similar findings have been reported for type 1 diabetes mellitus and all complications.[32] By contrast, miR-126 detection did not change in whole blood from type 2 diabetes mellitus patients and control subjects, but decreased in DKD patient samples.[33] Furthermore, no change in plasma miR-126 was observed in a study of pediatric type 1 diabetic patients.[34] These analyses provide inconsistent data for the biomarker utility of circulating miR-126, in contrast to the significant and reproducible increases detected in miR-126, miR-155, and miR-29b in DKD patient urine in the present study.

The DKD-specific alterations in urinary miRNA profiles detected in this study may have functional significance. *In vitro* analyses localized miR-126 and miR-29b principally to the GEnC, with miR-155 expression distributed evenly across the nephron. Glomerular endothelial localization of miR-126 may reflect the role of this transcript in vascular regulation. Targeted mouse miR-126 deletion resulted in vascular abnormalities by removing inhibition of sprouty-related EVH1 domain–containing protein 1 expression, thereby enhancing vascular endothelial growth factor function.[35] A role in DKD pathology for vascular endothelial growth factor-A signaling between GEnCs and podocytes has been proposed.[36] In addition, miR-126 repression of vascular cell adhesion molecule 1 expression in human umbilical vein endothelial cells regulates

Table 2 Sensitivity and Specificity Values, Likelihood Ratios, and RQ Thresholds for miR-126, miR-155, miR-29b, and All Three miRNAs >80% ROC Curve Sensitivity Threshold

Group	Sensitivity, %	Specificity, %	Likelihood ratio	RQ threshold
All three miRNAs	80.21	63.64	2.206	>1.148
miR-126	80.41	57.14	1.876	>0.6762
miR-155	80.61	52.00	1.679	>0.9110
miR-29b	80.61	40.00	1.344	>0.8058

ROC, receiver operating characteristic; RQ, relative expression.

Table 3 DKD and D Patient Numbers and Percentages >80% ROC Curve Sensitivity Threshold for miR-126, miR-155, miR-29b, and All Three miRNAs

Group	miR-126	miR-155	miR-29b	All three miRNAs	Total
Patients >80% sensitivity threshold, *n* (%)					
D	23 (41.8)	30 (54.6)	13 (23.6)	2 (3.6)	55
DKD	80 (81.6)	67 (68.4)	73 (74.5)	47 (48.0)	98

D, diabetic patients without DKD; DKD, diabetic kidney disease; ROC, receiver operating characteristic.

their response to proinflammatory adhesion molecules.[37] miR-126 has also been implicated in the heterogenic inflammatory response of renal microvascular endothelial cells.[38]

Increased expression of miR-155 has been observed in DKD patient renal biopsy specimens, in close correlation with increased serum creatinine.[39] Furthermore, miR-155 deficiency attenuated renal damage and IL-17 expression was down-regulated in streptozotocin-induced DKD mice.[40] Together with miR-126, miR-155 has been implicated in multiple forms of vascular remodeling and associated with cardiovascular disease.[41]

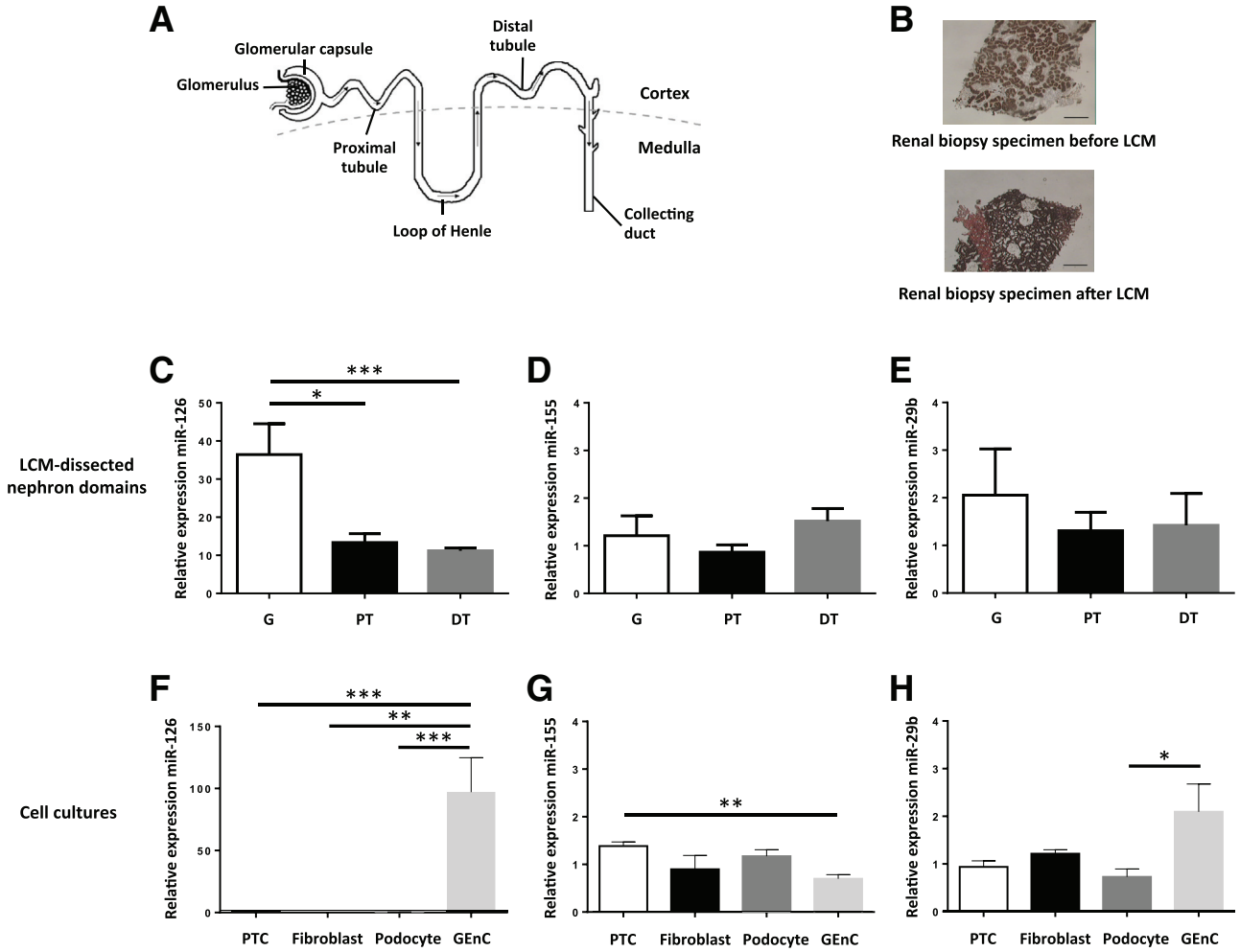

Figure 3 Localization of miRNA expression by laser-capture microdissection (LCM) and cell culture. **A:** Key functional nephron domains include the glomerulus (G), the proximal tubule (PT), and the distal tubule (DT). **B:** A CD10-stained formalin-fixed, paraffin-embedded renal biopsy sample before and after excision of glomeruli by LCM. **C**—**E:** Relative expression of miR-126, miR-155, and miR-29b, respectively, in LCM-isolated Gs, PTs, and DTs from five renal biopsy specimens of healthy individuals. **C:** Statistically significant differences in miRNA expression were observed in G versus PT, and G versus DT. **F**—**H:** Relative expression of miR-126, miR-155, and miR-29b, respectively, in *in vitro* cultured HK-2 renal proximal tubular epithelial cells (PTCs), fibroblasts, podocytes, and conditionally immortalized glomerular endothelial cells (GEnCs). **F:** Statistically significant differences in miRNA expression were observed in GEnCs versus fibroblasts, and GEnCs versus PTCs and podocytes. **G:** PTCs versus GEnCs. **H:** GEnCs versus podocytes. Analysis was performed by one-way analysis of variance with Tukey's multiple comparison test. Data were normalized to endogenous control miR-191 and are presented as means ± SEM (**C**—**H**). $n = 5$ (**C**, biopsy specimens); $n = 4$ (**H**). $^{*}P < 0.05$, $^{**}P < 0.01$, and $^{***}P < 0.001$. Scale bars = 100 μm (**B**).

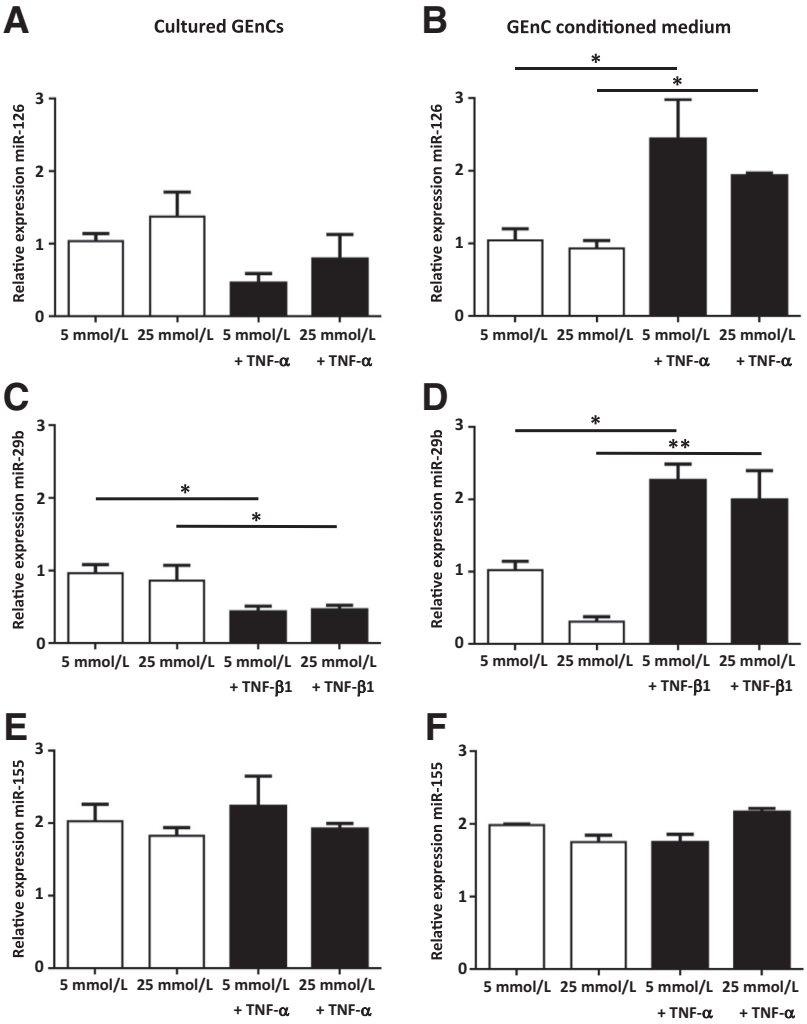

Figure 4 miRNA expression in glomerular endothelial cells (GEnCs) and GEnC conditioned medium in response to hyperglycemia and diabetic kidney disease—related cytokines. After 24 hours of culture in 5 or 25 mmol/L D-glucose, relative expression in GEnCs and GEnC conditioned medium, respectively, of miR-126 in response to 10 ng/mL tumor necrosis factor (TNF)-α (**A** and **B**), miR-29b in response to 1 ng/mL transforming growth factor (TGF)-β1 (**C** and **D**), and miR-155 in response to 10 ng/mL TNF-α (**E** and **F**), and in untreated cells. **B:** Statistically significant differences in miRNA expression were observed in study of 5 mmol/L D-glucose versus 5 mmol/L D-glucose plus TNF-α, and 25 mmol/L D-glucose versus 25 mmol/L D-glucose plus TNF-α. **C:** Study of 5 mmol/L D-glucose versus 5 mmol/L D-glucose plus TGF-β1, and 25 mmol/L D-glucose versus 25 mmol/L D-glucose plus TGF-β1. **D:** Study of 5 mmol/L D-glucose versus 5 mmol/L D-glucose plus TGF-β1, and 25 mmol/L D-glucose versus 25 mmol/L D-glucose plus TGF-β1. Analysis was performed by one-way analysis of variance with Tukey's multiple comparison test. Data were normalized to endogenous control miR-191 and are presented as means ± SEM (**A**—**F**). $n = 4$ (**D**). $^{*}P < 0.05$, $^{**}P < 0.01$.

Decreased miR-29b has been reported in early and advanced animal models of diabetic renal fibrosis.[42] Chen and colleagues[43] found that loss of renal miR-29b in db/db mice led to increased albuminuria, TGF-β—mediated fibrosis, and immune injury, whereas restored miR-29b expression inhibited renal injury. Indeed, although up-regulated miRNAs were specifically studied, the importance of down-regulated miRNAs cannot be ignored.

miR-29b localized to the glomerular endothelium in this study. Reduction of collagen and laminin synthesis has been reported after forced miR-29b expression in human corneal endothelial cells.[44] In apolipoprotein E knockout mice, miR-29b induced aortic endothelial permeability in response to a high-fat diet and brought about aortic apoptosis by direct targeting of melatonin receptor mt1.[45] In addition, up-regulated miR-29b expression has been observed in human umbilical vein endothelial cells exposed to hyperglycemia.[46]

The cytokine-driven release from GEnCs observed for miR-126 (TNF-α) and miR-29b (TGF-β1) reported herein suggests that these cells may be the principal source of elevated urinary miR-126 and miR-29b detected in DKD. We speculate that this constitutes evidence for disease-related signaling down the nephron that will be interesting to test in future studies. Indeed, there is a reported association of urinary miRNAs with exosomes[10] and exosomal transport, which might facilitate passage of miRNAs through the nephron, for all three candidate biomarker miRNAs.

Exosome-mediated release of miR-126 from $CD34^{+}$ peripheral blood mononuclear cells is proangiogenic, and decreased miR-126 was detected in elevated glucose cell culture and diabetic patients.[47] miR-155 is depleted in urinary exosomes from microalbuminuric type 1 diabetes mellitus patients.[48] Endogenous miR-29b, spontaneously released from beta cells within exosomes, stimulates TNF-α secretion from spleen cells isolated from diabetes-prone nonobese diabetic mice *in vitro*.[49]

In summary, we have used unbiased profiling approaches to identify a urinary miRNA signature associated with DKD and have subsequently confirmed increased miR-126, miR-155, and miR-29b in an independent patient cohort. miR-126 and miR-29b were identified as enriched in GEnCs, and

released from these cells in response to DKD-related cytokines. Urinary miR-126, miR-155, and miR-29b are, therefore, promising DKD biomarkers, and the potential pathologic significance of miR-126 and miR-29b release from GEnCs merits further evaluation.

Acknowledgments

We thank control subjects and patients for the donation of urine samples, including those samples kindly provided by coauthors Dr. Mark D. Jesky and Prof. Paul Cockwell (Queen Elizabeth Hospital Birmingham, Birmingham, UK).

C.B. and K.S. performed experiments, generated and analyzed data, and wrote the manuscript; A.W., C.C., L.N., R.J., and T.A. performed experiments and generated and analyzed data; M.J., P.H., C.D., S.S., P.Cor., and P.Coc. discussed elements of experimental design and/or cohort composition; D.F. and T.B. designed the research; T.B. wrote the manuscript, which was edited by D.F. and then amended and approved by each author.

Supplemental Data

Supplemental material for this article can be found at *https://doi.org/10.1016/j.ajpath.2018.06.006*.

References

1. Jha V, Garcia-Garcia G, Iseki K, Li Z, Naicker S, Plattner B, Saran R, Wang AY, Yang CW: Chronic kidney disease: global dimension and perspectives. Lancet 2013, 382:260–272
2. Cowie CC, Port FK, Wolfe RA, Savage PJ, Moll PP, Hawthorne VM: Disparities in incidence of diabetic end-stage renal disease according to race and type of diabetes. N Engl J Med 1989, 321:1074–1079
3. Regele F, Jelencsics K, Shiffman D, Pare G, McQueen MJ, Mann JF, Oberbauer R: Genome-wide studies to identify risk factors for kidney disease with a focus on patients with diabetes. Nephrol Dial Transplant 2015, 30:26–34
4. Makita Z, Radoff S, Rayfield EJ, Yang Z, Skolnik E, Delaney V, Friedman EA, Cerami A, Viassara H: Advanced glycosylation end products in patients with diabetic nephropathy. N Engl J Med 1991, 325:836–842
5. Schrijvers BF, De Vriese AS, Flyvbjerg A: From hyperglycemia to diabetic kidney disease: the role of metabolic, hemodynamic, intracellular factors and growth factors/cytokines. Endocr Rev 2004, 25: 971–1010
6. Coward RJ, Saleem MA: Podocytes as a target of insulin. Curr Diabetes Rev 2011, 7:22–27
7. Rodriguez-Iturbe B, Johnson RJ, Herrera-Acosta J: Tubulointerstitial damage and progression of renal failure. Kidney Int Suppl 2005, 99: S82–S86
8. Parving H-H, Persson F, Rossing P: Microalbuminuria: a parameter that has changed diabetes care. Diabetes Res Clin Pract 2015, 107:1–8
9. Landgraf P, Rusu M, Sheridan R, Sewer A, Iovino N, Aravin A, et al: A mammalian microRNA expression atlas based on small microRNA sequencing. Cell 2007, 129:1401–1414
10. Beltrami C, Clayton A, Newbury LJ, Corish C, Jenkins RH, Phillips AO, Fraser DJ, Bowen T: Stabilization of urinary microRNAs by association with exosomes and argonaute 2 protein. Noncoding RNA 2015, 1:151–165
11. Trionfini P, Benigni A, Remuzzi G: MicroRNAs in kidney physiology and disease. Nat Rev Nephrol 2015, 11:23–33
12. Simpson K, Wonnacott A, Fraser DJ, Bowen T: MicroRNAs in diabetic nephropathy: from biomarkers to therapy. Curr Diab Rep 2016, 16:35
13. Krupa A, Jenkins R, Luo DD, Lewis A, Phillips AO, Fraser DJ: Loss of MicroRNA-192 promotes fibrogenesis in diabetic nephropathy. J Am Soc Nephrol 2010, 21:438–447
14. KDOQI clinical practice guideline for diabetes and CKD: 2012 update. Am J Kidney Dis 2012, 60:850–886
15. Stringer S, Sharma P, Dutton M, Jesky M, Ng K, Kaur O, Chapple I, Dietrich T, Ferro C, Cockwell P: The natural history of, and risk factors for, progressive chronic kidney disease (CKD): the Renal Impairment in Secondary Care (RIISC) study: rationale and protocol. BMC Nephrol 2013, 14:95
16. American Diabetes Association: Diagnosis and classification of diabetes mellitus. Diabetes Care 2010, 33 Suppl 1:S62–S69
17. Levey AS, Bosch JP, Lewis JB, Greene T, Rogers N, Roth D; Modification of Diet in Renal Disease Study Group: A more accurate method to estimate glomerular filtration rate from serum creatinine: a new prediction equation. Ann Intern Med 1999, 130:461–470
18. Kidney Disease: Improving Global Outcomes (KDIGO) CKD Work Group (2013):: KDIGO 2012 clinical practice guideline for the evaluation and management of chronic kidney disease. Kidney Int Suppl 2013, 3:S1–S150
19. Satchell SC, Tasman CH, Singh A, Ni L, Geelen J, von Rhuland CJ, O'Hare MJ, Saleem MA, van den Heuvel LP, Mathieson PW: Conditionally immortalized human glomerular endothelial cells expressing fenestration in response to VEGF. Kidney Int 2006, 69:1633–1640
20. Saleem MA, O'Hare MJ, Reiser J, Coward RJ, Inward CD, Farren T, Xing CY, Ni L, Mathieson PW, Mundel P: A conditionally immortalized human podocyte cell line demonstrating nephrin and podocin expression. J Am Soc Nephrol 2002, 13:630–638
21. Jenkins RH, Davies LC, Taylor PR, Akiyama H, Cumbers B, Beltrami C, Carrington CP, Phillips AO, Bowen T, Fraser DJ: miR-192 induces G_2/M growth arrest in aristolochic acid nephropathy. Am J Pathol 2014, 184:996–1009
22. Midgley AC, Bowen T, Phillips AO, Steadman R: MicroRNA-7 inhibition rescues loss of epidermal growth factor receptor hyaluronan-dependent differentiation in fibroblasts. Aging Cell 2014, 13:235–244
23. Zhang SD, Gant TW: Effect of pooling samples on the efficiency of comparative studies using microarrays. Bioinformatics 2005, 21: 4378–4383
24. Kendziorski C, Irizarry RA, Chen KS, Haag JD, Gould MN: On the utility of pooling biological samples in microarray experiments. Proc Natl Acad Sci U S A 2005, 102:4252–4257
25. Robin X, Turck N, Hainard A, Tiberti N, Lisacek F, Sanchez JC, Müller M: pROC: an open-source package for R and S+ to analyze and compare ROC curves. BMC Bioinformatics 2011, 12:77
26. Prowle JR, Calzavacca P, Licari E, Ligabo EV, Echeverri JE, Bagshaw SM, Haase-Fielitz A, Haase M, Ostland V, Noiri E, Westerman M, Devarajan P, Bellomo R: Combination of biomarkers for diagnosis of acute kidney injury after cardiopulmonary bypass. Ren Fail 2015, 37:408–416
27. Schley G, Köberle C, Manuilova E, Rutz S, Forster F, Weyand M, Formentini I, Kientsch-Engel R, Kai-Eckardt U, Willam C: Comparison of plasma and urine biomarker performance in acute kidney injury. PLoS One 2015, 10:e0145042
28. Navarro J, Milena F, Mora C, Leon C, Claverie F, Flores C, Garcia J: Tumor necrosis factor-alpha gene expression in diabetic nephropathy: relationship with urinary albumin excretion and effect of angiotensin-converting enzyme inhibition. Kidney Int Suppl 2005, 99:S98–S102
29. Ohga S, Shikata K, Yozai K, Okada S, Ogawa D, Usui H, Wada J, Shikata Y, Makino H: Thiazolidinedione ameliorates renal injury in experimental diabetic rats through anti-inflammatory effects mediated by inhibition of NF-κB activation. Am J Physiol Renal Physiol 2007, 292:F1141–F1150

30. Smith DA, Newbury LJ, Drago G, Bowen T, Redman JE: Electrochemical detection of urinary microRNAs via sulfonamide-bound antisense hybridisation. Sens Actuators B Chem 2017, 253: 335−341
31. Olivieri F, Spazzafumo L, Bonafè M, Recchioni R, Prattichizzo F, Marcheselli M, Micolucci L, Mensà E, Giuliani A, Santini G, Gobbi M, Lazzarini R, Boemi M, Testa R, Antonicelli R, Antonio Domenico Procopio AD, Bonfigli AR: miR-21-5p and miR-126a-3p levels in plasma and circulating angiogenic cells: relationship with type 2 diabetes complications. Oncotarget 2015, 6:35372−35382
32. Barutta F, Bruno G, Matullo G, Chaturvedi N, Grimaldi S, Schalkwijk C, Stehouwer CD, Fuller JH, Gruden G: MicroRNA-126 and micro-/macrovascular complications of type 1 diabetes in the EURODIAB prospective complications study. Acta Diabetol 2017, 54:133−139
33. Al-Kafaji G, Al-Mahroos G, Al-Muhtaresh HA, Skrypnyk C, Sabry MA, Ramadan AR: Decreased expression of circulating microRNA-126 in patients with type 2 diabetic nephropathy: a potential blood-based biomarker. Exp Ther Med 2016, 12:815−822
34. Osipova J, Fischer D-C, Dangwal S, Volkmann I, Widera C, Schwarz K, Lorenzen JM, Schreiver C, Jacoby U, Heimhalt M, Thum T, Haffner D: Diabetes-associated MicroRNAs in pediatric patients with type 1 diabetes mellitus: a cross-sectional cohort study. J Clin Endocrinol Metab 2014, 99:E1661−E1665
35. Wang S, Aurora AB, Johnson BA, Qi X, McAnally J, Hill JA, Richardson JA, Bassel-Duby R, Olson EN: The endothelial-specific microRNA miR-126 governs vascular integrity and angiogneneiss. Dev Cell 2008, 15:261−271
36. Brosius FC, Coward RJ: Podocytes, signaling pathways, and vascular factors in diabetic kidney disease. Adv Chronic Kidney Dis 2014, 21: 304−310
37. Harris TA, Yamakuchi M, Ferlito M, Mendell JT, Lowenstein CJ: MicroRNA-126 regulates endothelial expression of vascular cell adhesion molecule 1. Proc Natl Acad Sci U S A 2008, 105:1516−1521
38. Ásgeirsdóttir SA, van Solingen C, Kurniati NF, Zwiers PJ, Heeringa P, van Meurs M, Satchell SC, Saleem MA, Mathieson PW, Banas B, Kamps JA, Rabelink TJ, van Zonneveld AJ, Molema G: MicroRNA-126 contributes to renal microvascular heterogeneity of VCAM-1 protein expression in acute inflammation. Am J Physiol Renal Physiol 2012, 302:F1630−F1639
39. Huang Y, Liu Y, Li L, Su B, Yang L, Fan W, Yin Q, Chen L, Cui T, Zhang J, Lu Y, Cheng J, Fu P, Liu F: Involvement of inflammation-related miR-155 and miR-146a in diabetic nephropathy: implications for glomerular endothelial injury. BMC Nephrol 2014, 15:142
40. Lin X, You Y, Wang J, Qin Y, Huang P, Yang F: MicroRNA-155 deficiency promotes nephrin acetylation and attenuates renal damage in hyperglycemia-induced nephropathy. Inflammation 2015, 38: 546−554
41. Welten SMJ, Goossens EAC, Quax PHA, Nossent AY: The multifactorial nature of microRNAs in vascular remodeling. Cardiovasc Res 2016, 110:6−22
42. Wang B, Komers R, Carew R, Winbanks CE, Xu B, Herman-Edelstein M, Koh P, Thomas M, Jandeleit-Dahm K, Gregorevic P, Cooper ME, Kantharidis P: Suppression of microRNA-29 expression by TGF-β1 promotes collagen expression and renal fibrosis. J Am Soc Nephrol 2012, 23:252−265
43. Chen H-Y, Zhong X, Huang XR, Meng X-M, You Y, Chung ACK, Lan HY: MicroRNA-29b inhibits diabetic nephropathy in db/db mice. Mol Ther 2014, 22:842−853
44. Toyono T, Usui T, Villarreal G, Kallay L, Matthaei M, Vianna LMM, Zhu AY, Kuroda M, Amano S, Jun AS: MicroRNA-29b overexpression decreases extracellular matrix mRNA and protein production in human corneal endothelial cells. Cornea 2016, 35:1466−1470
45. Zhu HQ, Li Q, Dong LY, Zhou Q, Wang H, Wang Y: MicroRNA-29b promotes high-fat diet-stimulated endothelial permeability and apoptosis in apoE knock-out mice by down-regulating MT1 expression. Int J Cardiol 2014, 176:764−770
46. Silambarasan M, Tan JR, Karolina DS, Armugam A, Kaur C, Jeyaseelan K: MicroRNAs in hyperglycemia induced endothelial cell dysfunction. Int J Mol Sci 2016, 17:518
47. Mocharla P, Briand S, Giannotti G, Dörries C, Jakob P, Paneni F, Lüscher T, Landmesser U: AngiomiR-126 expression and secretion from circulating $CD34^+$ and $CD14^+$ PBMCs: role for proangiogenic effects and alterations in type 2 diabetics. Blood 2013, 121: 226−236
48. Barutta F, Tricarico M, Corbelli A, Annaratone L, Pinach S, Grimaldi S, Bruno G, Cimino D, Taverna D, Deregibus MC, Rastaldi MP, Perin PC, Gruden G: Urinary exosomal microRNAs in incipient diabetic nephropathy. PLoS One 2013, 8:e73798
49. Salama A, Fichou N, Allard M, Dubreil L, De Beaurepaire L, Viel A, Jégou D, Bösch S, Bach J-M: MicroRNA-29b modulates innate and antigen-specific immune responses in mouse models of autoimmunity. PLoS One 2014, 9:e106153